

*Dedicated to the 50-th anniversary of
Special Astrophysical Observatory of RAS*

Proceedings

of the International Workshop

Quark Phase Transition in Compact Objects and Multimessenger Astronomy: Neutrino Signals, Supernovae and Gamma-Ray Bursts

Russia

Nizhnij Arkhyz (SAO RAS)

Terskol (BNO INR RAS)

October, 7 - 14, 2015



*Dedicated to the 50-th anniversary of
Special Astrophysical Observatory of RAS*

Proceedings

of the International Workshop on
**Quark Phase Transition in Compact Objects and
Multimessenger Astronomy:
Neutrino Signals, Supernovae and Gamma-Ray Bursts**

Russia
Nizhnij Arkhyz (SAO RAS)
Terskol (BNO INR RAS)
October, 7 – 14, 2015

УДК 524–7 (063)

Q 24

Научное издание

Специальная Астрофизическая Обсерватория Российской Академии наук (САО РАН)

Труды

Международного совещания

**Кварковый фазовый переход в компактных объектах и многоволновая астрономия:
нейтринные сигналы, сверхновые и гамма-всплески**

Ответственные редакторы: В. В. Соколов, В. В. Власюк, В. Б. Петков

Компьютерная верстка: Т. Н. Соколова

Корректор: Т. Н. Соколова

Пятигорск. Издательство «СНЕГ». 2016

На английском языке

Special Astrophysical Observatory of Russian Academy of Sciences (SAO RAS)

Proceedings

of the International Workshop on

**Quark Phase Transition in Compact Objects and Multimessenger Astronomy:
Neutrino Signals, Supernovae and Gamma-Ray Bursts**

ISBN 978–5–903129–85–0

© *Special Astrophysical Observatory
of Russian Academy of Sciences (SAO RAS)*

Content

Preface	5
Alvarez-Castillo D. E. Energetic emissions from deconfinement in compact stars and their relation to the critical end point in the QCD phase diagram	7
Agafonova N. Yu., Ashikhmin V.V., Boliev M.M., Volchenko V.V., Dadykin V.L., Dzaparova I.M., Dobrynina E.A., Enikeev R.I., Kochkarov M.M., Novoseltsev Yu.F., Novoseltseva R.V., Mal'gin A.S., Petkov V.B., Ryazhskaya O.G., Shakiryanova I.R., Yakushev V.F., Yanin A.F. and the LVD Collaboration. The search for coincidences of rare events using LVD and BUST detectors	13
Baryshev Yu.V., Paturel G., Sokolov V.V. Sidereal time analysis as a tool for detection of gravitational and neutrino signals from the core-collapse SN explosions in the inhomogeneous Local Universe	19
Dzhappuev D.D., Petkov V.B., Kudzhaev A.U., Klimenko N.F., Lidvansky A.S., Troitsky S.V. Search for cosmic gamma rays with the Carpet-2 extensive air shower array	30
Fabrika S., Vinokurov A., Atapin K., Sholukhova O. Super-Eddington accretion disks in Ultraluminous X-ray sources	37
Karpov S., Beskin G., Biryukov A., Bondar S., Ivanov E., Katkova E., Perkov A., and Sasyuk V. Mini-MegaTORTORA wide-field monitoring system with sub-second temporal resolution: observation of transient events	43
Kuzminov V.V. Baksan Neutrino Observatory of the INR RAS: current state and prospects	51
Lidvansky A.S. Burst activity of the Crab Nebula and its pulsar at high and ultra-high energies	63
Nadyozhin D.K. Mechanisms of supernova explosion: modern status	69
Novoseltsev Yu.F., Boliev M.M., Dzaparova I.M., Kochkarov M.M., Novoseltseva R.V., Petkov V.B., Volchenko V.I., Volchenko G.V., Yanin A.F. A search for neutrino bursts signal from supernovae at the Baksan Underground Scintillation Telescope	76
Novoseltseva R.V., Boliev M.M., Dzaparova I.M., Kochkarov M.M., Novoseltsev Yu.F., Petkov V.B., Volchenko V.I., Volchenko G.V., Yanin A.F., Agafonova N. Yu., Ashikhmin V. V., Dadykin V. L., Dobrynina E. A., Enikeev R. I., Mal'gin A. S., Ryazhskaya O. G., Shakiryanova I. R., Yakushev V. F., and the LVD Collaboration. Joint analysis of experimental data on the search for neutrino bursts using the BUST and LVD detectors	85
Petkov V.B. Prospects of detecting the QCD phase transition in the Galactic supernova neutrino burst with 20-kton scale liquid scintillation detectors	92
Rudenko V.N. Current status of GW experiment and multi-messenger astronomy	96
Ryazhskaya O.G., Semenov S.V. Interaction of electron neutrino with LSD detector	105
Sokolov Ilya V., Castro-Tirado A.J., Verkhodanov O.V., Zhelenkova O.P., Baryshev Yu.V. Clustering of galaxies around the GRB 021004 sight-line at $z \sim 0.5$	111
Sokolov V.V. On the observed mass distribution of compact stellar remnants in close binary systems and possible interpretations proposed for the time being	121
Spiering Ch. High-Energy Neutrino Astronomy: Where do we stand, where do we go?	133
Verkhodanov O.V., Sokolov V.V., Khabibullina M.L. Correlation between sphere distributions of gamma-ray bursts and CMB fluctuations	142
Vlasyuk V.V., Sokolov V.V. The complex of SAO RAS optical instruments as an instrument for studying transient sources in the Universe	151
Wiktorowicz G. X-ray Binaries and Ultraluminous X-ray Sources	156
Yudin A. On some exotic properties of hybrid stars	162
Yu Y. B., Wu X. F., Huang Y. F., Xu M. Energy Injections in Gamma Ray Bursts	168



Workshop participants

Preface

Now quark-gluon plasma is a new direction both in the high energy physics and in the study of compact objects of the type of neutron star and candidates in black hole (BH) of stellar mass (collapsars). The phase transition in the quark-gluon state is related with the mechanism itself of core-collapse supernovae explosion, because energy of such a transition can be a source of cosmic gamma-ray bursts. Signals of transition of matter to pure quark-gluon plasma can be neutrinos that are observed with modern detectors, including our ones, e.g. Baksan Underground Scintillation Telescope (BUST). Now the equipment of the gravitational detectors LIGO/VIRGO is also customized for signals of such a transition.

The International Workshop on Quark Phase Transition in Compact Objects and Multimessenger Astronomy: Neutrino Signals, Supernovae and Gamma-Ray Bursts (October, 7-14, 2015) was dedicated to Quantum ChromoDynamics (QCD) Phase Transitions and observational signals of these transitions related to formation of compact astrophysical objects. The aim of this workshop is to bring together researchers working on the problems of behavior of matter under critical conditions achievable in such astrophysical objects as “strange” or “hybrid” stars and in laboratories at heavy-ion collisions to discuss fundamental issues and recent developments. Topics included both observations (radio, optical and X-ray astronomy, gamma ray bursts, gravitational waves, neutrino detection, heavy-ion collisions, etc.) and theory (supernova simulations, proto-neutron and neutron stars, equation of state of dense matter, neutron star cooling, unstable modes, nucleosynthesis, explosive transitions, quark-gluon plasma).

The holding of the workshop in locations of two Russia’s unique observatories – Special Astrophysical Observatory of Russian Academy of Science (SAO RAS) and Baksan Neutrino Observatory of Institute of Nuclear Research of Russian Academy of Science (BNO INR RAS) – was determined by character of the most urgent problems of the modern physics and astrophysics included in its program. Solution of observational and theoretical tasks related to these problems demands development of methods combining optical astronomical observations with experiments at neutrino telescopes, installations for registering cosmic rays and modern detectors of gravitational waves.

The scientific program of the workshop covered a wide range of problems of the modern astrophysics including the problem of existence of QCD phase transitions and the matter state at high temperatures and densities. Apparently, such conditions are achievable only in astrophysical objects – collapsars of stellar masses, such as, e.g., neutron stars whose formation is related with collapse and explosion of massive and dense stellar nuclei observed as supernovae and gamma-ray bursts. The first (and the only until now) supernova from which neutrino emission was registered by 4 world’s neutrino observatories (including BNO INR RAS) was the supernova 1987A. So, the detection of neutrinos from SN 1987A established indeed that some supernovae produce some neutrinos.

Considerable time of the workshop was dedicated to discussion of modern possibilities of experimental observation of similar objects and prospects of development of studying in this field. Optical afterglows of transient sources related to gamma-ray bursts and their host galaxies have been observed in SAO RAS during more than 20 years. Sufficient experience of such research was accumulated. Participation of astronomers in programs of the study of localization boxes of neutrino (and, possibly, gravitational) events is already being discussed in detail (e.g., see <https://wikispaces.psu.edu/display/AMON>) at previous international conferences of similar topic. So,

optical astronomers and radio astronomers (with all their telescopes) can join this new international program of synchronous observations of astrophysical objects related with collapse of massive star nuclei.

The workshop included review lectures of leading experts in the workshop topic, original oral presentations and poster sessions. The reports of young researchers were especially welcomed. Participation of leading Russian and foreign researchers will surely contribute to better realization of scientific potential of our observatories (SAO RAS and BNO INR RAS) and to strengthening of international relations. The holding of such a workshop will also promote further development of studying in this field of astrophysics in Russia and education of experienced researchers.

Organizing committee of the workshop

Energetic emissions from deconfinement in compact stars and their relation to the critical end point in the QCD phase diagram

D. E. Alvarez-Castillo

Bogoliubov Laboratory for Theoretical Physics, Joint Institute for Nuclear Research, Joliot-Curie Str. 6, 141980 Dubna, Russia; alvarez@theor.jinr.ru

Abstract In this work we study the case of deconfinement in compact star interiors in the presence of a strong first order phase transition associated to a critical end point in the QCD phase diagram. Neutron stars fulfilling these conditions show a third branch in the mass-radius diagram with the first and second branches being the white dwarfs and neutron stars configurations. The transition to the third branch can be reached by a pure hadronic neutron star through an induced collapse releasing energy that corresponds to a mass-energy difference between the second and third branch configurations. Physical outcomes of this phenomenon that can potentially explain the already detected astrophysical signals are discussed. In particular we present energy estimations for the case of a fast radio burst, seen as a double-peak structure in the object's light curve.

Keywords: Compact Stars, Deconfinement, Fast Radio Bursts, Massive Twins, Energy Bursts

1. Introduction

Neutron stars (NS) are evolved stars being created after the death of a massive star via a supernova explosion or a transition from a white dwarf accretion or dynamical instabilities. Their interiors can reach up to several times the saturation density n_0 , the canonical density inside atomic nuclei. It is quite uncertain what is the state of matter under such high density conditions, therefore research on equation of state (EoS) is currently a very active area. It is important to note that in NS temperature doesn't play a major role in the computation of the EoS, thus it can be neglected. Recent observations have completely changed our understanding of the cold, dense nuclear matter in such compact star interiors.

In this context, accurate mass determination has proved to be of great importance. In particular the observation of the $2M_{\odot}$ pulsars, PSR J0348+0432 [1] and PSR J1614-2230 [2], have strongly constrained the stiffness of the NS EoS. On the contrary, radius measurements are not yet precise enough to test, discard, and select some of the many alternative EoS models. For instance, frequency resolved pulse shape analysis for the nearest millisecond pulsar [3] supports relatively large radii while analysis from X-Ray bursters [4] point out to either moderate or small radii. Promising future radius measurements include upcoming space missions, cf. NICER [5].

Energetic phenomena like fast radio bursts (FRB) – millisecond duration radio bursts from cosmological distances [6] – can be explained by collapse of compact stars into black holes [7]. Under such scheme, the released energy of the process is about 10^{40} erg. This scenario is not to be confused by early NS evolution consisting of hot proton-neutron stars, with deconfinement transition in their interior that could serve as the mechanism triggering the core-collapse supernovae [8], as well as pulsar kicks at birth [9, 10, 11, 12, 13] associated to more energetic emissions.

Neutron stars can suffer a dynamical collapse caused by a deconfinement phase transition in their

cores (possibly leading to a corequake) via spin-down due to continuous electromagnetic emission or by mass accretion. Some early works estimated the energy reservoir for the typical ($\sim 1.4M_{\odot}$) NS mass [14, 15, 16, 17], however here we present a recent EoS model derived in [18] that allows for the formation of a “third family” of compact stars near the maximum mass. Figure 1 shows both gravitational and baryonic masses for compact star configurations with a transition at high masses. We denote the two stars before and after the transition as “high mass twins” because we assume that they bear the same baryonic mass while differing in their mass-energy quantity (binding energy). Although the detailed mechanism is at the moment being developed [19], we can conjecture the following: the deconfinement phase transition occurs via a corequake scenario in which a high-mass hadronic NS collapses into a hybrid compact star disconnected from the former by a gap in the stable configurations (for a recent classification of hybrid stars, see [20]). The instability sets in by the pure hadronic NS after dipole-emission spin-down, or accretion-induced spin-up by matter from a companion.

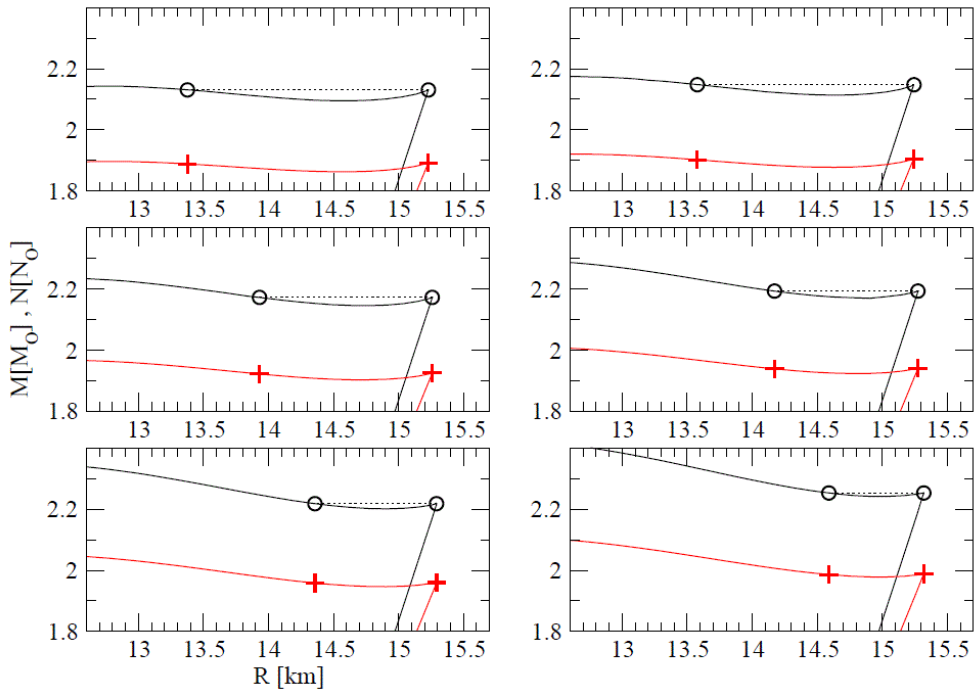


Fig1. Compact star configurations following the instability due to a strong first-order phase transition. Baryonic mass and gravitational mass are given by the black and red curves, respectively. The models are characterized by values of the vector coupling parameter η_4 : 0.0, 1.0, 3.0, 5.0, 7.0, 10.0 starting from the upper left corner down to the bottom right. Notice that the higher the η_4 value the higher the mass at the instability.

For these energy bursts to occur it is important to note that in cold neutron stars the temperatures in their interiors are well below the neutrino opacity temperature ($T_{\nu} \sim 1\text{MeV}$) such that the free streaming scenario applies for neutrino propagation as opposed to the neutrino diffusion mostly suitable for a GRB scenario involving a hot (proto) neutron star ($T_{\nu} < 1\text{MeV}$). A new aspect of this mechanism, going beyond the scenario of Falcke & Rezzolla (a direct collapse of a magnetized NS to a black hole [7]) is the existence of a metastable state between the initial and final states of a supermassive rotating neutron star SURON that could explain a double peak structure of the FRB’s for which recently a case has been made [21]. This metastate in the SURON process corresponds to an object on the third family branch of high

mass hybrid stars, as found recently for microscopically motivated EoS [7, 22].

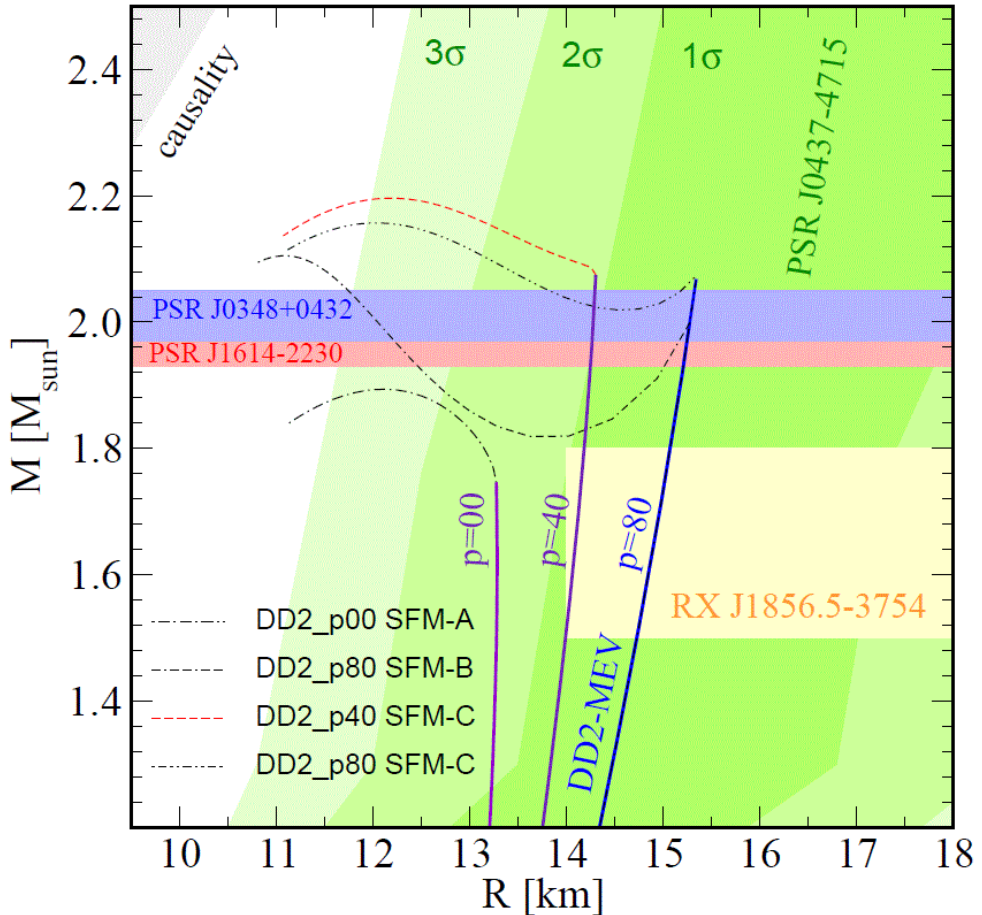


Fig2. String-Flip approach to the high-mass twins [22] and constraints for mass and radius values. The green regions correspond to 1, 2 and 3 σ values as reported in [3]. The vertical bands around $2M_{\odot}$ correspond to the most precisely massive NS measurements [1, 2]. The figure is taken from [22].

2. High-mass twin equation of state

We call neutron star twins those stars with the same mass having different composition and thus different radius. They belong to different branches in the disconnected mass-radius diagram. One of them is pure hadronic whereas the twin star is a hybrid containing quark matter in its core [23, 24, 25, 26, 27]. The case of high mass twins is of great importance because is a consequence of a critical point in the QCD phase diagram [28, 29]. Furthermore, they do not lead to many of the modern issues of compact star physics as discussed in [30]: masquerades [31], the hyperon puzzle [32], and reconfinement [33, 34]. Bayesian studies based on the most reliable observations provide a useful assessment of high mass twins identification [35, 36, 37, 38]. The description of the EoS used here is as follows:

- For hadronic matter we utilize the DD2 (density-dependent relativistic mean field model) EoS

with excluded volume correction (resulting from the internal compositions of nucleons produced by Pauli blocking effects of quarks [39]) that acts at supersaturation densities and provides stiffening to this EoS. For neutron stars this means that the highest mass can be reached at a rather lower interior density values and are characterized by large radii ($\approx 13 - 15$ km, [29]).

- Quark matter is described by a NJL (Nambu–Jona-Lasinio) EoS with multiquark interactions hNJL [40] featuring a coupling strength parameter in the vector channel of the 8-quark interaction η_4 bringing this quark EoS to a sufficient stiffening at high densities in order to support the maximum observed star mass of $2M_\odot$. Alternatively, an equation of state based on the string-flip model [22] captures the same features (excluded volume), but has the advantage of resulting in a broader range of radius difference between the twins (in better agreement with the contrasting either large or short radius observations). The mass-radius diagram for the string-flip compact stars is shown in Figure 2.

3. Results and discussion

The EoS of [18] features the first order phase transitions leading to instability of the NS right after the appearance of a small, dense quark core. When an NS reaches the maximum hadronic mass radial oscillations take over creating an instability (see e.g. [41]), which results into a dynamical collapse. The criterion for unstable configurations is $\partial M/\partial n_c < 0$, where n_c is the central density of the corresponding NS. In Figure 1 the configurations in between circles (maximum hadronic mass NS and its hybrid twin) that have a positive slope are thus forbidden. This is the origin of a gap created by such prohibited configurations in the mass-radius diagram. Figure 3 (left panel) shows the radius change ΔR in the transition, which is between 1 and 1.5 km for some coupling constant values. The available energy ΔE following the transition equals the mass-energy difference $\Delta M c^2$ between the initial and final configurations and is of about 10^{51} erg. See Figure 3 (right panel). The more realistic case of rotation configurations are being currently studied [19].

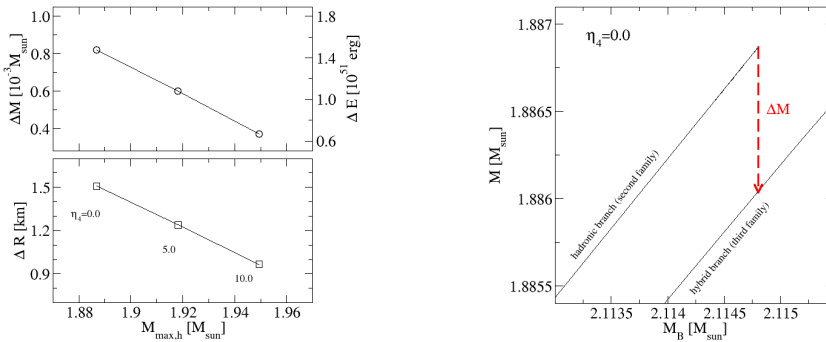


Fig3. Left: Mass difference ΔM (upper panel) and radius difference ΔR (lower panel) resulting from the dynamical NS collapse induced by a deconfinement phase transition for a set of vector coupling parameters $\eta_4 = 0.0, 5.0, 10.0$ of the high-mass twin hNJL models. The corresponding energy release ΔE after the transition is indicated on the right side of the upper panel. Right: Gravitational mass M vs. baryonic mass M_B . $\eta_4 = 0.0$ is the value of the vector coupling in the chosen hNJL model shown here. The red line indicates the energy released in the transition between the maximum hadronic NS and the corresponding hybrid star mass twin. The figures are taken from [42].

We conclude this work by drawing attention to the possibility of energetic emissions produced by a deconfinement phase transition in NS interiors most likely via FRB's, such as the case of the recent

observations of FRB121002 [21] featuring a double peak light curve structure. We identify this double peak signal with the metastable state in the dynamical collapse scenario of a SURON. Furthermore, it is of great importance to mention that the NS EoS presented here can serve as an input to understand scenarios of cosmic ray generation via supernova explosions or NS mergers.

Acknowledgements

D.E. Alvarez-Castillo would like to thank the organizers of *The International Workshop on Quark Phase Transition in Compact Objects and Multimessenger Astronomy: Neutrino Signals, Supernovae and Gamma-Ray Bursts* for their support and hospitality. In particular, he acknowledges interesting and fruitful discussions with Alessandro Drago, Grzegorz Wiktorowicz, Christian Spiering, A.Kh.Khokonov and Igor Iosilevskiy during his stay at SAO and BNO. The author also thanks David Blaschke, Stefan Typel, Mark Kaltenborn and Sanjin Benic for providing the necessary EoS data sets for this work as well as Pawel Haensel, Michal Bejger and Leszek Zdunik for collaboration on the study of the high energy emission mechanism and dynamical collapse. D.E.A.-C. Acknowledges support by the Heisenberg-Landau programme, the Bogoliubov-Infeld programme and by the COST Action MP1304 “NewCompStar”.

References

- [1] Antoniadis, J., Freire, P. C. C., Wex, N., et al. 2013, *Science*, 340, 448
- [2] Demorest, P. B., Pennucci, T., Ransom, S. M., Roberts, M. S. E., & Hessels, J. W. T. 2010, *Nature*, 467, 1081
- [3] Bogdanov, S. 2013, *ApJ*, 762, 96
- [4] Steiner, A. W., Lattimer, J. M., & Brown, E. F. 2010, *ApJ*, 722, 33
- [5] Arzoumanian, Z., Gendreau, K. C., Baker, C. L., et al. 2014, *Proc. SPIE*, 9144, 914420
- [6] Lorimer, D. R., Bailes, M., McLaughlin, M. A., Narkevic, D. J., & Crawford, F. 2007, *Science*, 318, 777
- [7] Falcke, H., & Rezzolla, L. 2014, *A&A*, 562, A137
- [8] Sagert, I., Fischer, T., Hempel, M., Pagliara, G., Schaffner-Bielich, J., Mezzacappa, A., Thielemann, F. K. & Liebendorfer, M. 2009, *Phys. Rev. Lett.*, 102, 081101
- [9] Podsiadlowski, P., Pfahl, E., & Rappaport, S. 2005, *Binary Radio Pulsars*, 328, 327
- [10] Lai, D., Chernoff, D. F., & Cordes, J. M. 2001, *ApJ*, 549, 1111
- [11] Kusenko A. 2005, *Int. J. Mod. Phys. A*, 20, 1148 2001, *ApJ*, 549, 1111
- [12] Berdermann, J., Blaschke, D., Grigorian, H., & Voskresensky, D. N. 2006, *Prog. Part. Nucl. Phys.* 57, 334
- [13] Stasielak, J., Biermann, P. L., & Kusenko, A. 2007, *ApJ*, 654, 290
- [14] Drago, A., & Tambini, U. 1999, *J. Phys. G*, 25, 971
- [15] Berezhiani, Z., Bombaci, I., Drago, A., Frontera, F., & Lavagno, A. 2002, *Nucl. Phys. B Proc. Suppl.*, 113, 268
- [16] Aguilera, D. N., Blaschke, D., & Grigorian, H. 2004, *A&A*, 416, 991
- [17] Zdunik, J. L., Bejger, M., Haensel, P., & Gourgoulhon, E., 2008, *A&A*, 479, 515
- [18] Benic, S., Blaschke, D., Alvarez-Castillo, D. E., Fischer, T., & Typel, S. 2015, *A&A*, 577, A40
- [19] Bejger, M., et al., 2016, in preparation.
- [20] Alford, M. G., Han, S., & Prakash, M., 2013, *Phys. Rev. D* 88, 083013

- [21] Champion, D., 2015, talk at seventh Bonn Workshop on “Formation and Evolution of Neutron Stars”, May 18, 2015
- [22] Alvarez-Castillo, D. E., Kaltenborn, M. A. R., & Blaschke, D. 2015, *J. Phys.: Conf. Ser.* 668 (2016) 012035
- [23] Gerlach, U. H. 1968, *Phys. Rev.*, 172, 1325
- [24] Kampfner, B. 1981, *J. Phys. A*, 14, L47
- [25] Schertler, K., Greiner, C., Schaffner-Bielich, J., & Thoma, M. H. 2000, *Nucl. Phys. A*, 677, 463
- [26] Glendenning, N. K., & Kettner, C. 2000, *A&A*, 353, L9
- [27] Dexheimer, V., Negreiros, R., & Schramm, S. 2015, *Phys. Rev. C*, 91, 055808
- [28] Alvarez-Castillo, D. E., & Blaschke, D. 2015, *PoS CPOD 2014* (2014) 045
- [29] Blaschke, D., Alvarez-Castillo, D. E., & Benic, S. 2013, *PoS CPOD 2013* (2013), 063
- [30] Blaschke, D., & Alvarez-Castillo, D. E. 2015, [arXiv:1503.03834](https://arxiv.org/abs/1503.03834)
- [31] Alford, M., Braby, M., Paris, M., & Reddy, S. 2005, *ApJ*, 629, 969
- [32] Baldo, M., Burgio, G. F., & Schulze, H. -J. 2003, *Superdense QCD Matter and Compact Stars*, D. Blaschke and D. Sedrakian (Eds.), Springer, Heidelberg, 2006, p.113
- [33] Lastowiecki, R., Blaschke, D., Grigorian, H., & Typel, S., 2012, *Acta Phys. Polon. Supp.* 5, 535
- [34] Zdunik, J. L., & Haensel, P. 2013, *A&A*, 551, A61
- [35] Ayriyan, A., Alvarez-Castillo, D. E., Blaschke, D., Grigorian, H., & Sokolowski, M. *Particles and Nuclei*, 46 (5) pp. 854-857 (2015)
- [36] Blaschke, D. B., Grigorian, H. A., Alvarez-Castillo, D. E., & Ayriyan, A. S. 2014, *J. Phys. Conf. Ser.*, 496, 012002
- [37] Alvarez-Castillo, D. E., Ayriyan, A., Blaschke, D., & Grigorian, H. 2015, [arXiv:1506.07755](https://arxiv.org/abs/1506.07755). Conference: C14-09-26
- [38] Ayriyan, A., Alvarez-Castillo, D. E., Blaschke, D., & Grigorian, H. 2015, *J. Phys.: Conf. Ser.* 668 (2016) 012038
- [39] Ropke, G., Blaschke, D., & Schulz, H., 1986, *Phys. Rev. D* 34, 3499
- [40] Benic, S. 2014, *Eur. Phys. J. A*, 50, 111
- [41] Shapiro, S. L., Teukolsky, S. A., *Black Holes, White Dwarfs and Neutron Stars: The Physics of Compact Objects*, 1986, Wiley, New York
- [42] Alvarez-Castillo, D. E., Bejger, M., Blaschke, D., Haensel, P., & Zdunik, L. 2015, [arXiv:1506.08645](https://arxiv.org/abs/1506.08645)

The search for coincidences of rare events using LVD and BUST detectors

N. Yu. Agafonova¹, V. V. Ashikhmin^{1,*}, M. M. Boliev¹, V. V. Volchenko¹,
V. L. Dadykin¹, I. M. Dzaparova¹, E. A. Dobrynina¹, R. I. Enikeev¹,
M. M. Kochkarov¹, Yu. F. Novoseltsev¹, R. V. Novoseltseva¹, A. S. Mal'gin¹,
V. B. Petkov^{1,2}, O. G. Ryazhskaya¹, I. R. Shakiryanova¹, V. F. Yakushev¹,
A. F. Yanin¹ and the LVD Collaboration¹

¹*Russian Academy of Sciences, Institute for Nuclear Research, Moscow, Russia;*

**vole4ka86@mail.ru*

²*Russian Academy of Sciences, Institute of Astronomy, Moscow, Russia*

Abstract The results of the time coincidences of rare events in the LVD and BUST detectors are presented. The rare events could be caused by neutrino interaction in the experimental setup. The distributions of the coincidence number per day for 4-year period are obtained.

Keywords: Underground Physics, Neutrino, Supernovae

1. Introduction

Correct background estimations are very important in the underground physics experiments. The main goal of the experiments is the search for neutrino bursts from collapsing stars, double beta-decay, proton decay, dark matter particles and other extremely rare phenomena. Within the work, research of extremely rare events coincidence will enable us estimating parameters of the search for neutrino bursts. The work is based on data of two experimental large underground detectors: Large Volume Detector (LVD) and Baksan Underground Scintillation Telescope (BUST). The detectors have been operating during the same time since 1992 and because they are situated in different places the background value of pulse coincidences for these detectors is much lower than for each one. Search for event coincidences between LVD and BUST within one second time interval are provided.

2. SN1987A and understanding problems of experimental results

Neutrino bursts from Supernova SN1987A were detected on February 23, 1987. The supernova SN1987A exploded in the Large Magellanic Cloud at a distance of ~50 kpc from the Earth [1]. Four underground detectors (LSD, BUST, Kamiokande, and IMB) were operating at that time and recorded two bursts of neutrino emission at 02:52 and at 07:35 UT [2]. According to standard stellar collapse models developed before the SN1987A phenomenon, the stellar collapse should be accompanied by one neutrino burst. In Figure 1 the time diagram of registered events is presented.

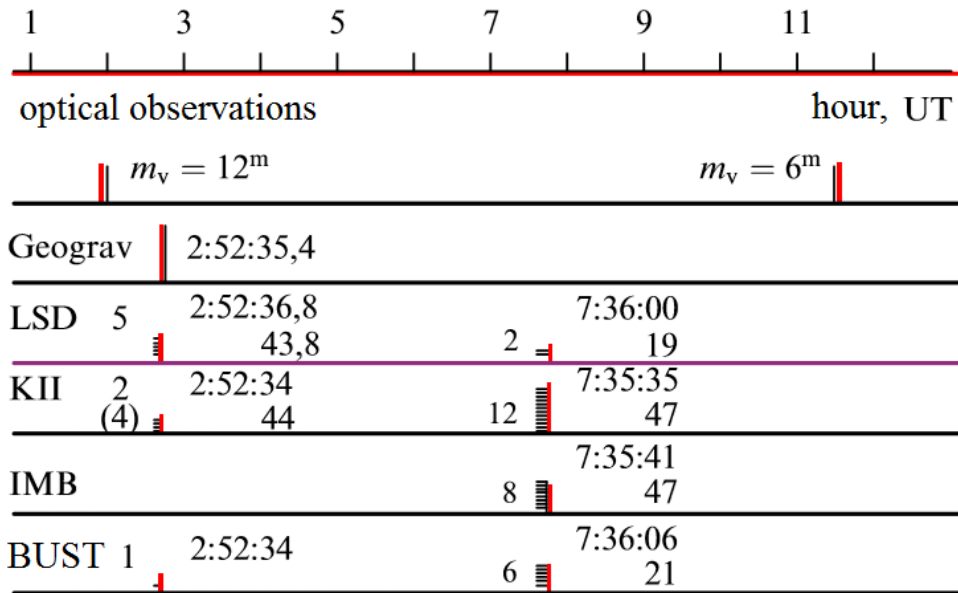


Fig1. Timing diagram of registered events from SN 1987A.

As is shown in the diagram, near 02:52 UT, the most number of events were observed by LSD detector. After that, the search for coincidences in the one-second time window between the single pulses of different pairs of detectors was carried out. The results presented in Figure 2.

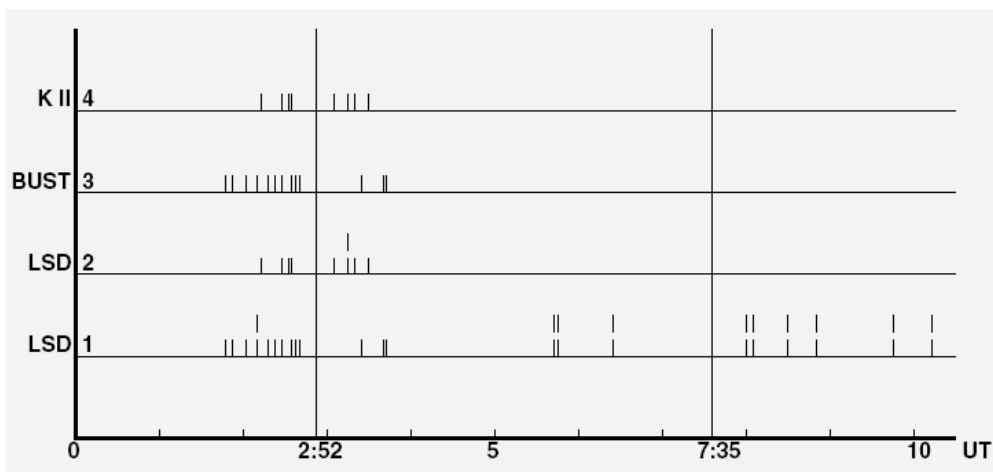


Fig2. The timing diagram of coincidences of the BUST and LSD pulses within 1 s and similar coincidences for the K2 and LSD detectors as well as double pulses in LSD over the period from 0:00 to 10:00 UT on February 23, 1987.

As a result, a statistically significant increase was found in the number of matches between single pulses in the LSD [3] and BUST [4] detectors and in the LSD and Kamiokande detectors around 02:52 UT [5]. Near the 07:35 UT 12 signals were registered by Kamiokande detector, 8 events - by IMB detector, 6 events - by BUST detector and 2 events - by LSD detector. The event detecting principle by

the experimental facilities is based on different physical phenomena: the IMB and Kamiokande registration is based on Cherenkov radiation, LSD and BUST are scintillation detectors. Moreover, only the LSD detector could observe and define all types of neutrinos and antineutrinos, mainly electron neutrinos and antineutrinos. For resolving all problems associated with the understanding of experimental results it is necessary to get answers to some questions. Was neutrino burst detected at 2:52 UT 23, February, 1987? What was type of neutrino detected? How to explain the number of coincidences between single pulses obtained from different detectors pairs? Is the background the number of coincidences? For estimating the background level from single pulses coincidences, searching for coincidences between LVD and BUST events within one second time interval are provided. In the work, the data from 2011 to 2014 were analyzed.

Other objective difficulties of the experimental data processing during the neutrino bursts from SN1987A should be taken into account. In particular, processing of experimental data with two detectors covering a long period of time (about a year) was an almost impossible task because there was no modern computing power. At present time, the joint analysis of data from two different experiments does not look complicated. Moreover, the BUST detector registered neutrino burst from SN1987A and the LSD detector are a prototype of the LVD detector. Search for coincidences of single pulses between the LVD and BUST detectors allows us reconsidering the similar results obtained during SN1987A. In the case of a low counting rate of double coincidences, the experimental results of SN1987A become important.

3. LVD and BUST experiments

Sensitivity of LVD [6] is ten times higher than that of its prototype – the Liquid Scintillator Detector (LSD), which observed five pulses over seven seconds on February 23, 1987 at 02:52 UT (Fig.1). It is located at the LNGS underground laboratory (the Laboratori Nazionali del Gran Sasso, Italy) at a depth of 3650 m.w.e. The LVD detector is an underground iron-scintillator calorimeter with a total mass of 2 kt (1 kt of liquid scintillator and 1 kt of iron). The detector contains 840 independent scintillation counters. Structure of the LVD detector is presented in Fig.3. The structure includes 3 towers. Each tower contains 5 columns, each column consists of 7 portatank levels. Each portatank consists of 8 counters. The modular structure of the LVD and BUST detectors allows us using external counters as an active protection against muons and other background events.

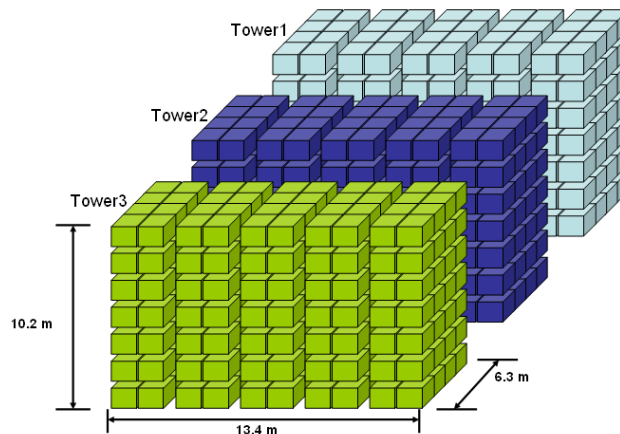


Fig3. Modular structure of the LVD detector.

The BUST detector [4] is located in the North Caucasus, under the mountain Andyrchy at an effective depth of 850 m.w.e. Its size is $17 \times 17 \times 11 \text{ m}^3$ and it consists of four horizontal and four vertical plates with scintillation counters. Five plates are external, while the three lowers of horizontal planes are internal (Fig. 4). The counter size is $0.7 \times 0.7 \times 0.3 \text{ m}^3$. The total number of counters is 3184 and the total scintillator mass is about 0.3 kt. The internal volumes of the counters are filled with liquid scintillator and viewed by the PMT 49B. The operating threshold of the counter is 8 MeV. Identical white spirit based scintillator is used both in LVD and in BUST detectors. In addition to its extremely low cost, the parameters of this scintillator remain virtually stationary under operating conditions during long time [1, 7].

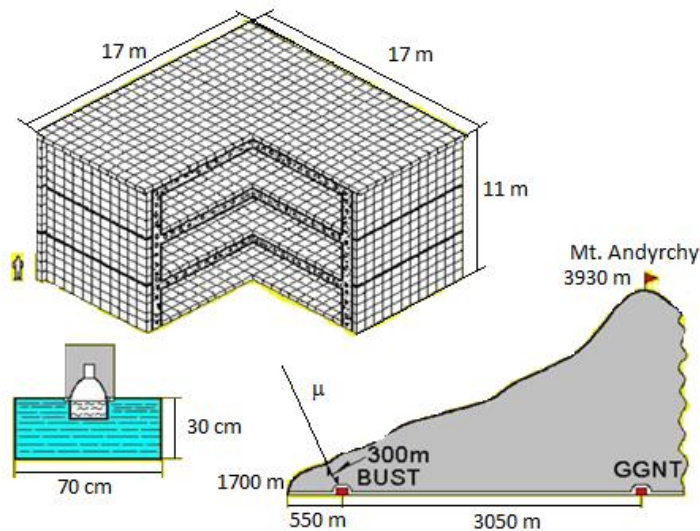


Fig4. Scheme of the BUST detector.

4. Obtained results

In the work, only “neutrino” events in the LVD and BUST detectors are used in analysis. The “neutrino” event is a response of only one inner counter, so far as external counters are used for active defense. The search for coincidences between LVD and BUST “neutrino” events within 1 second time interval was carried out with the 10 MeV energy threshold. The search results allow us to conclude about background origin of found coincidences, i.e., coincidences can be random. Indeed, when looking at the energy spectra of events in LVD and events in BUST, it is possible to see a difference between their forms. In the case of the same origin of “neutrino” events in LVD and BUST their energy spectrum would be identical also. However, in presented energy distributions for 2011-2014 years this is not observed, as is seen in Figs. 5-6. Moreover, the form of the spectrum in LVD and BUST remains constant, indicating different origins of the backgrounds in the experiments.

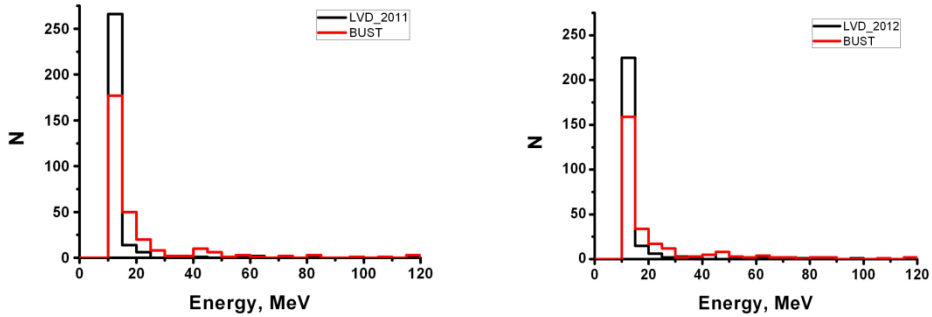


Fig. 5. The energy spectra of events in coincidences for 2011 year (left) and 2012 year (right).

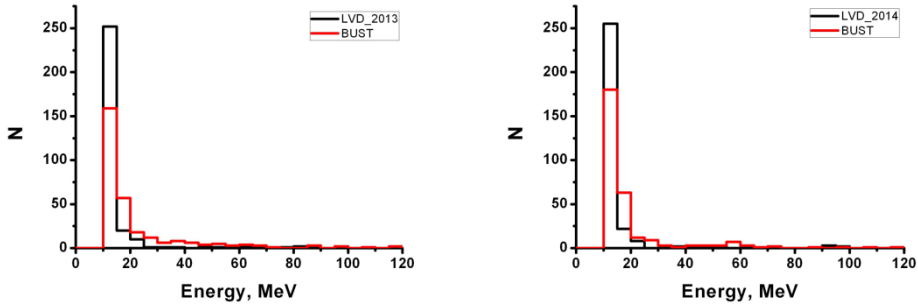


Fig6. The energy spectra of events in coincidences during 2013 (left) and 2014 (right).

To assess the average counting rate the distribution number of coincidences per day were built. Below the data for 2011-2014 are presented. As can be seen from the presented distributions, 5 coincidences per day were recorded only twice during 4 years of readout experimental data. This fact supports the importance of experimental results of SN1987A (see Fig. 2), when 13 coincidences were observed during 2 hours. On average, the counting rate of random coincidences is approximately 1 coincidence per day. The obtained results are presented in Figs. 7-8.

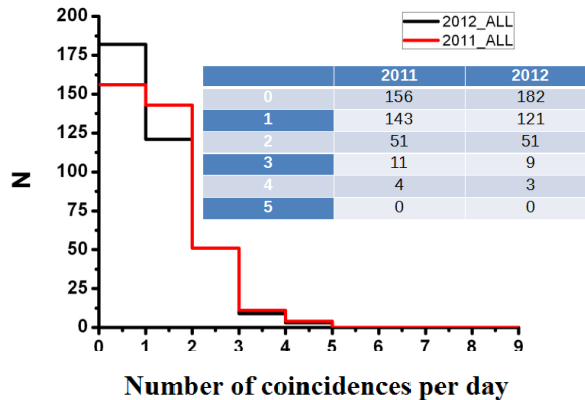


Fig7. The spectra of number of coincidences per day for 2011-2012.

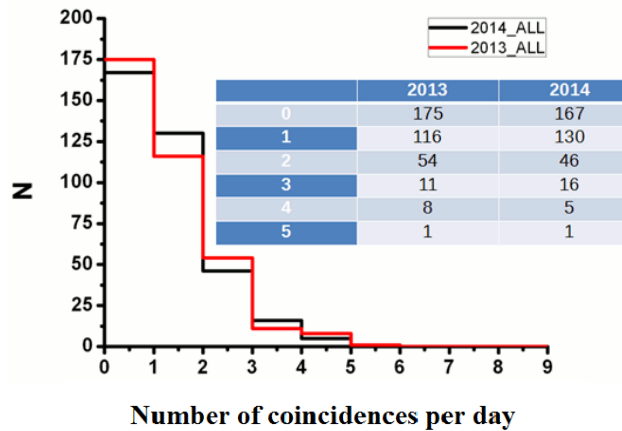


Fig8. The spectra of number of coincidences per day for 2013-2014.

5. Conclusion

The results of neutrino event coincidences registered in the LVD and BUST detectors during 1 second allow us making the following inferences. The counting rate coincidences remained practically unchanged during 4 years of experimental data set, which indicates the stable work of the experiments. In the future, it is planning to carry out the search for coincidences during the whole period of joint work of detectors, i.e. since 1992. Different forms of the energy spectra allow us making a conclusion about different sources of background in the experiments.

The experimental value of the counting rate obtained in the present work demonstrates the importance of experimental results on SN1987A of 23 February 1987. The greatest value of the counting rate of accidental coincidences per day was recorded only 2 times in 4 years and is 5 matches a day. On 23 February 1987 (SN1987A) during 2 hours 13 coincidences were detected. Such large excess in the background level could be due to registration of neutrino interactions in the detectors.

Acknowledgements

This work was supported by the Russian Foundation for Basic Research, project №. 15 -02 -01056_a; the Program for the Support of Leading Scientific School, contract SS-3110.2014.2; and the Presidium of the Russian Academy of Sciences' basic research program Fundamental Properties of Matter and Astrophysics.

References

- [1] Ryazhskaya, O.G., Usp. Fiz. Nauk, 2013, vol. 183, p. 315.
- [2] Ryazhskaya, O.G., Usp. Fiz. Nauk, 2006, vol. 176, p. 1039.
- [3] Badino, G., et al., Nuovo Cimento C, 1984, vol. 7, p. 573.
- [4] Alexeyev, E.N., et al., Proc. 16th Int. Cosmic Ray Conf., Kyoto, 1979, vol. 10, p. 276.
- [5] Dadykin, V.L. and Ryazhskaya O.G., Pis'ma Astron. Zh., 1 2009, vol. 35, p. 427.
- [6] Aglietta, M., et al. (LVD Collab.), Proc. 27th ICRC, Hamburg, 2001, vol. 3, p. 1093.
- [7] Voevodskii, A.V., Dadykin V.L. and Ryazhskaya O.G., Prib. Tekh. Eksp., 1970, vol. 1, p. 85.

Sidereal time analysis as a tool for detection of gravitational and neutrino signals from the core-collapse SN explosions in the inhomogeneous Local Universe

Yu. V. Baryshev ^{1,*}, G. Paturel ², V. V. Sokolov ³

¹*Astronomical Department, Saint Petersburg State University, Saint-Petersburg, Russia;*

**yubaryshevl@mail.ru*

²*CRAL-Observatory de Lyon, Saint-Genis Laval, France*

³*Special Astrophysical Observatory of RAS, Nizhnij Arkhyz, Russia*

Abstract The core-collapse supernova explosion produces both neutrino and gravitational wave (tensor-transversal plus possible scalar-longitudinal) bursts. In the case of GW detectors, which have low angular resolution, the method of sidereal time analysis of output signals was applied for extraction of GW signals from high level noise. This method was suggested by Joseph Weber in 1970 for analysis of signals from his bar detector and later was developed for existing bar and interferometric GW detectors. The same sidereal time approach can be also used for low energy neutrino detectors which have many years of observational time (e.g. Super-Kamiokande, LVD, Baksan). This method is based on: 1) difference between sidereal and mean solar time (which help to delete noises related to day-night solar time), 2) directivity diagram (antenna pattern) of a detector (which chooses a particular sky region in a particular sidereal time), and 3) known position on the sky of spatial inhomogeneities of GW and neutrino sources in the Local Universe (distances less than 100 Mpc), such as the Galactic plane, the Galaxy center, closest galaxies, the Virgo galaxy cluster, the Super-galactic plane, the Great Attractor.

Keywords: Core-Collapse Supernova Explosion, Gravitational Waves, Neutrino Detectors, Methods of Analysis

1. Introduction

Observations of the SN 1987A explosion marked the beginning of both the neutrino and gravitational wave extragalactic astronomy [1 – 5]. From neutrino observations there was evidence for rather complex behavior of a collapsing stellar core during formation of a proto neutron star. Actually it was detected two neutrino bursts of several seconds duration and 4.5 hours' time interval between them.

The first neutrino burst was observed at 2h 52m U.T. on 23 February 1987 by the LSD detector located in the Mont-Blanc laboratory. The second neutrino burst was found at 7h 36m of the same day in the data of Kamiokande, IMB and Baksan. The occurrence of two neutrino bursts, with time distance of about four and half hours, appeared surprising because the most accepted theories predicted that a star should collapse in a very short time, in the range of a few seconds or even less.

The first neutrino burst coincides with the GW burst detected by the room temperature bar detector GEOGRAV in Rome [3, 4] (Fig.1). Also, smaller additional coincident pulses in a period of 2 hours during the rapid evolutionary phase of supernova 1987A were detected by the Weber's bar gravitational antenna in Maryland [5].

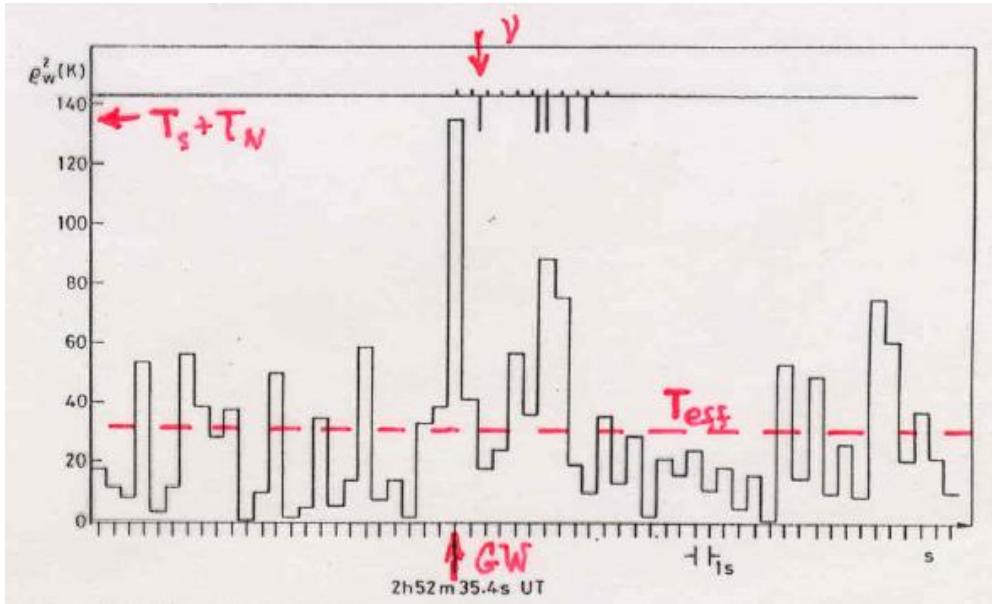


Fig1. Gravitational signal (the continuous curve) from Rome room temperature GEOGRAV detector (signal + noise) and the five neutrino events of the first neutrino burst from Mont Blanc LSD detector at 2h 52m 35s UT [3].

Though the majority of publications on the SN1987A core-collapse observations were dedicated only to analysis of the second neutrino burst (at 7h 36m), there are also attempts to explain the full actually observed phenomena including two neutrino and gravitational busts [5] – [13].

In this report we discuss some problems of theoretical analysis of the massive core-collapse SN explosion and their influence on the strategy of observations which led to discovery of corresponding gravitational and neutrino signals. The method of sidereal time analysis is suggested for detection of gravitational and neutrino signals hidden in the detectors' high level noises.

2. The problem of core-collapse SN explosion

Adam Burrows in his review “Perspectives on Core-Collapse Supernova Theory” [14] emphasized that one of the most important, yet frustrating, astronomical question is “What is the mechanism of core-collapse supernova explosions?” Fifty-year history of CCSN theory, which uses advanced hydrodynamics and shock physics, convection theory, radiative transfer, nuclear physics, neutrino physics, particle physics, statistical physics, thermodynamics and **gravitational physics** have not answered this question definitively. Intriguingly up to now there is no theoretical understanding of how to extract such energy from relativistic collapse of an iron core and produce the observed kinetic energy of an expanding stellar envelope [14] – [15].

2.1. The riddle of “bounce” in the SN gravitational core-collapse

According to the review [14], for all trustworthy models of core-collapse SNe (CCSN) the explosion energy is never higher than a few tenths of Bethe (1 Bethe = 10^{51} ergs), which is not enough to overcome the gravitational binding energy of a “canonical” neutron star of mass $\sim 1.5 M_{\odot}$. Many years theorists have been presented with a stalled accretion shock at a radius near ~ 100 -200 km and have been trying to

revive it (see [14] for a review of the literature). This bounce shock should be the CCSN explosion. However, both simple theory and detailed numerical simulations universally indicate that the neutrino burst and photodissociation of the in-falling nuclei debilitate the shock wave into accretion within ~ 5 milliseconds of bounce. What is more, if the shock is not revived and continues to accrete, all cores will collapse to black holes, which contradicts to observations of NSs in SN remnants.

Rapid rotation with magnetic fields (e.g. [16]) and 3D MGD simulations taking into account different instabilities need to be studied more carefully in future. The true model should explain also such observational properties of the CCSN as two-stage collapse and gravitational signals. However, though many different revival mechanisms were considered, up to now there is no successful model yet, because the problem of CCSN explosion exists at a very fundamental level.

2.2. The long time interval between two neutrino bursts

To overcome the theoretical difficulty of the standard one-pulse neutrino burst from a CCSN explosion, in a number of publications ([11] – [13]) the “two stage collapse” scenario was suggested. The key point in this scenario is the presence of rotation in the stellar core that is about to collapse. This mechanism of the SN explosion is based on the rotational instability and develops through several stages. The inclusion of rotation effects can help to solve the problem of transformation of the original collapse of an iron core to explosion of an SN shell with the energy release on a scale of 10^{51} ergs. The collapse in itself leads to the birth of a neutron star emitting neutrino and gravitational radiation signals of large intensity, whose total energy significantly (by a factor of hundreds) exceeds the SN burst energy.

In the framework of the model [11] – [13] for rotational mechanism of the CCSN explosion there is a two-stage collapse with a phase difference of ~ 5 h and neutrino signal duration of several seconds. This gives an interpretation of the events in underground neutrino signals from the supernova SN 1987A. However within this scenario there are several phenomenological gaps which should be developed and tested in a future theory.

2.3. “Gravitational roots” of the core-collapse SN explosion problem

In the understanding of the physics of core-collapse supernovae explosion the crucial role belongs to a correct description of gravitational interaction because CCSNs are gravitationally powered. The nuclear burning during explosive nucleosynthesis of the outer mantle after explosion might contribute at most $\sim 10\%$ of the blast energy.

A possibility to revive the bounce shock essentially depends on the gravity force acting within a pre-neutron star (pre-NS), where at least post-Newtonian relativistic gravity effects should be taken into account.

In modern theoretical physics there are two alternative descriptions of gravitational interaction. The first description is the Einstein’s geometrical approach - General Relativity Theory (GRT), which is developed in many aspects, but is still really tested in the weak field approximation. GRT is based on curvature of the Riemannian space and has not such physical concepts as gravity force and energy of gravitational field [17].

The second description is the Feynman’s field gravity approach (the field gravity theory – FGT) which is based on consideration of material relativistic quantum physical field in the Minkowski space [18] – [23]. According to the Feynman’s approach the theory of gravitational interaction must be relativistic (gravidynamics – GD) and quantum (quantum gravidynamics – QGD), as well as in the theory of electromagnetic interaction we have electrodynamics (ED) and quantum electrodynamics (QED).

Within FGT all general physical concepts are working as in other theories of fundamental physical interactions, so the gravity force and positive energy density of gravitational field exist inside and outside of a massive body. An important new element of FGT is the principal role of the scalar part ψ of

the symmetric tensor field ψ^{ik} , which is its trace $\psi = \eta_{ik}\psi^{ik}$ and actually presents the repulsive force, which was missed in [17], [18]. The unique role of the scalar field in FGT was discovered in [20] (see also [21] – [23] and references therein).

The CCSN explosion within FGT has an essentially different scenario than in GRT. The post-Newtonian equations of relativistic hydrodynamics in the context of FGT were derived in [24], according to which the gravity force essentially depends on the value and direction of gas flow. This gives a possibility for pulsation of the inner core of a pre-NS star and formation of a jet-like outflow along the rotation axis.

The quantum consideration of the macroscopic limiting high-density quark-gluon bag gives self-gravitating configurations with the preferred mass $6.7 M_{\odot}$ and radius 10 km [21]. So, gravodynamics predicts two peaks in the mass distribution of relativistic compact objects (RCO): $1.4 M_{\odot}$ for neutron stars and $6.7 M_{\odot}$ for quark stars, which can be tested by observations of close binary systems [21].

2.4. Surprises from observations of black hole candidates and possible revival mechanisms in FGT

As was noted above, in the framework of geometrical GRT all cores of massive SNe will collapse to black holes, if the shock is not revived and continues to accrete. However, up to now the problem of “the mechanism of CCSN explosion” is not solved [14], and so the absence of many black holes in remnants of massive SN is a puzzling observational fact.

Other surprising observational facts come from the studies of BH candidates. As was emphasized recently in [25] – [28], the inner 20 gravitational radii around the black hole candidates at the center of luminous Active Galactic Nuclei and stellar mass Black Hole Binaries are now being routinely mapped by X-ray spectral-timing techniques including observations of the iron K_{α} line profiles. An amazing result of such observations is that the estimated radius of the inner edge (R_{in}) of accretion disk around central relativistic compact objects (RCO) is always less than the Schwarzschild radius of corresponding central mass. This points to a suspicion that in the nature there is no Schwarzschild black holes, and this explains why in literature they use now the term “a gravitational radius” (R_g) instead of “the Schwarzschild radius” (R_{Sch}), which relates to each other as:

$$R_g = \frac{GM}{c^2} \quad \text{instead of} \quad R_{Sch} = \frac{2GM}{c^2}$$

The factor “2” is essential, because in the case of the Kerr BH the horizon radius is given by the relation:

$$R_H = R_g (1 + \sqrt{1 - a^2})$$

where $a = J_{bh}/J_{max}$ ($a \leq 1$) is a normalized spin parameter of the Kerr metrics, which is equal to the ratio of angular momentum of a rotating BH to that of maximally rotating (with the velocity of light c) black hole. We should note that the radius of the ergosphere, where the time $dt = 0$, is always equal to the Schwarzschild radius R_{Sch} in the equatorial plane.

From the fitting of the observed Fe K_{α} line profiles it follows that the radius of the inner edge of accretion disc is about $(1.2 - 1.4) R_g$ which demands that BH is rotating with a velocity about $0.998c$. So, according to GRT, the ordinary observed BHs must be maximally rotating ones, because $R_{in} < R_{Sch}$, which is impossible within GRT. For example, in the case of Seyfert 1 galaxy Mrk335 $R_{in} \approx 1.23 R_g$ and the emissivity profile sharply increases to a smaller radius of disk [25].

Another kind of observations of super-massive BH candidates comes from the mm- wavelength VLBI Event Horizon Telescope, which has been designed to answer the crucial questions: Does General

Relativity hold in the strong field regime? Is there an Event Horizon? Can we estimate Black Hole spin by resolving orbits near the Event Horizon? How do Black Holes accrete matter and create powerful jets? [29] – [33].

Event-horizon-scale structure in the super-massive black hole candidate at the Galactic Centre (SgrA*) and M*87 can be achievable directly with the sub-mm EHT in the near future and this will give a possibility to test relativistic and quantum gravity theories at the gravitational radius [32], [33] for the first time. The first results of EHT observations at 1.3mm surprisingly demonstrate that for a RCO in SgrA* there is no light ring expected for BH at radius $5.2R_{Sch}$ [30], [32]. These observations have opened a new page in the study of RCO.

Beside surprising observational data there are several severe paradoxes in the very basis of the theory of black holes (see discussions in [34] – [36]). For example, there is a paradox of the infinite time formation of a black hole (in the coordinates of a distant observer, so for us) and the finite time of BH evaporation – a BH should evaporate before its formation [36].

The situation is so confusing, that even the father of black holes Stephen Hawking claimed in [34] that though there is no escape from a black hole in the classical theory, but in the quantum theory, however, energy and information can escape from a black hole. An explanation of the process requires a theory that successfully merges gravity with other fundamental forces of nature.

Such a way for constructing gravity theory, based on the same principles as other theories of fundamental physical interactions, already exists and it is the Feynman’s Field Gravity Approach (GD and QGD – see [18] – [24] and their references). Within FGT the size of a limited self-gravitating RCO is about the gravitational radius $R_g \approx GM/c^2$, which directly follows from the positive energy density of gravitational field distributed around a massive body. The concept of the gravitational radius in FGT is analogous to the classical radius of electron $R_e = e^2/m_e c^2$. Thus, black holes and singularities are excluded by existence of positive energy density of gravitational field considered in the framework of FGT.

New possibilities for revival mechanisms in the theory of CCSNe are opened by a difference in behavior of the gravity force in GRT and FGT, as we already have discussed in Section 2.3. In the framework of FGT a subsonic inner core and shocked mantle together can execute a long-time coherent harmonic oscillation with a period of ~1 millisecond. Also the core rotation will lead to a jet-like flow due to strong dependence of the gravity force on direction of velocity of particles. All these facts demonstrate that the choice of the certain direction in the physical description of gravitational interaction has important consequences for analysis of the structure and stability of relativistic astrophysical objects.

2.5. A gravitational burst during a CCSN explosion

There is a long-standing problem within the General Relativity Theory (GRT) related to existence and non-localizability of the energy density of gravitational field. It is known as the “pseudo-tensor of energy-momentum” problem [17], which is caused by the geometrical nature of gravity in GRT (see a review in [21]).

However, discovery and observations of a binary system with a pulsar PSR 1913+16 and the loss of its orbital energy via positive energy of gravitational radiation, stopped all discussions about existence of energy density of gravitational field. In fact the Nobel Prize in physics-1993 was given to Hulse & Taylor for discovery of a process of gravitational radiation of positive energy density.

In the case of SN 1987A the puzzling problem in interpretation of a gravitational signal detected by the room temperature GEOGRAV is a too large amount of energy of gravitational wave needed for explanation of the ~30K signal. Indeed, the mass of a progenitor star is about $20 M_{\odot}$, while in the framework of General Relativity Theory the burst of GW should have a form of one-millisecond pulse with the total energy about $2000 c^2 M_{\odot}$ [3] (and even more due to an additional small quantity – the asphericity of core-collapse).

There are attempts to reconsider the value of the cross-section of metallic bar detectors for gravitational waves within GRT by adding quantum mechanics calculations [5], [7] – [10]. Such study is still a controversial subject, though the amplification factor about $10^4 - 10^6$ was claimed.

In the frame of FGT, natural reasons exist for essential increase of sensitivity of the Amaldi-Weber metallic bar detectors and so for explanation of a GW signal from SN 1987A [6]. The first one is the ordinary physical concept of the energy-momentum tensor of gravitational field exists, according to which the GW is localizable and has a positive energy density. Second, the core-collapse can be of pulsating character with a slowly changing frequency, hence at some time when it coincides with a resonance of a bar antenna, the amplification will be high. Also, the cross-section for scalar GW can be much larger due to special features of its interaction with a metallic detector.

3. Sidereal time analysis of gravitational and neutrino signals

The core-collapse of massive stars produces both neutrino and gravitational wave (a tensor plus a possible scalar) bursts. In the case of GW detectors, which have low angular resolution, the method of sidereal time analysis of output signals was applied for extraction of GW signals from a high-level noise. This method was suggested by Joseph Weber (1970) [37] for analysis of signals from his metallic bar detector and later was developed for existing bar and interferometric GW detectors [38] – [42].

The sidereal time approach can be also used for low energy neutrino detectors which have many years of observational time (e.g. LVD [43], Super-Kamiokande [44], Baksan). This method is based on: 1) a difference between sidereal and mean solar time (which helps to delete noises related to the day-night solar time), 2) a directivity diagram (antenna pattern) of a detector (which chooses a particular sky region in a particular sidereal time), and 3) a known position of spatial inhomogeneities of GW and neutrino sources in the Local Universe (distances less than 100 Mpc) on the sky, such as the Galactic plane, the Galaxy center, closest galaxies, the Virgo galaxy cluster, the Super-galactic plane, the Great Attractor.

3.1. Universal time vs. Sidereal Time

The Universal Time (UT) is measured by reference to the Sun direction as seen from the Earth. Because the Earth moves around the Sun, this time is not properly "universal". It is convenient only to define a same time for all inhabitants of the planet. On the opposite, the Sidereal Time (ST) is related to the true Earth rotation and refers to the position of the gamma-point, γ (vernal equinox) in the sky. There is no bright star in this direction, but γ behaves as a virtual star with null declination, obeying the same apparent diurnal motion. More precisely, γ is on the intersection of two planes: the plane of the Sun orbit (ecliptic) and the plane of the terrestrial equator. By convention, γ is in the direction where the Sun crosses the equator from the south to the north (the ascendant node). Because of precession the γ point is not rigorously fixed. Nevertheless, for our purpose this will be perfectly convenient, owing to the small angular resolution of GW and neutrino detectors and to the slow displacement of the γ point.

We should emphasize three characteristics of ST: 1) Contrarily to the UT, the ST is not the same for different places on the Earth, because it takes into account the difference in geographic longitudes of different places. 2) The pace of ST is not identical to the pace of UT. A solar day is longer than a sidereal day (see Figure 2). In other words, the ST runs faster by about 4 minutes per day, i.e. 24h per year. 3) The ST is the hour angle of the gamma point (an angle between the direction of the observer's meridian and the gamma point counted positively towards West (clockwise)).

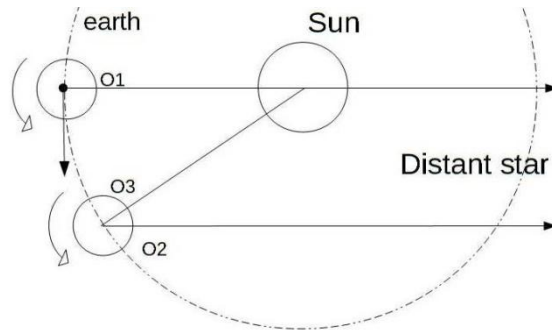


Fig2. Difference in definition of UT and ST. An observer in O1 will see first a distant star in O2 after 24 hours of ST and 4 minutes later the Sun in O3 after 24 hours of UT. This means that one Earth's revolution is equal to $\sim 23\text{h } 56\text{m } 04\text{s}$ of mean solar day.

The merit of the sidereal time analysis can be understood easily. Imagine that many galaxies in a given cluster emit regularly light/neutrino/gw bursts observed with a fixed telescope crossing each day the cluster because of the Earth rotation. If one plots the time of bursts between 0-24h UT, the positions of bursts will be spread all along the axis of time, because they come from an apparent direction that changes regularly due to the displacement of the Earth around the Sun.

If one plots the bursts in sidereal time between 0-24h ST, all the bursts will appear concentrated in the same sidereal time domain. The detection of this emitting region will be easy to identify. Even if some bursts come from some other regions, the cluster will be seen as a bump of events. This means that the ST plot reflects the density of potential sources. This can help to confirm the reality of detection. The summation of all output signals within one Earth's revolution ($\sim 23\text{h } 56\text{m } 04\text{s}$ of mean solar day) during several years of observations will reveal a certain structure at predicted sidereal hours (by using directivity pattern of a detector), so the detection has a statistical sense.

3.2 Calculation of signals within an antenna pattern

For GW detectors, different geometries exist, from a simple bar detector, with only one main axis, to an interferometer with two arms. The orientation with respect to the main direction to the Earth must be taken into account. For instance, in our paper [38], the main axis OX of the detector lies in the local horizontal plane, making an angle Φ_0 with the direction of the north (in the opposite direction of the observer's meridian) and is counted in the direct sense over the range 0- 2π . This axis (OX) together with the zenith axis (OZ) and the third direct axis (OY) define a reference system in which we have to express the sensitivity pattern (lobe antenna) using the proper angles with respect to direction of a source.

The relevant angles for expressing the relative sensitivity pattern of antenna are: the azimuth Φ of the source measured with respect to the OX axis and the zenith distance ζ measured with respect to the OZ axis (see Figure 3).

At each sidereal time and for each latitude, Φ and ζ primarily depend on the equatorial coordinates (α , δ) of a source. However, the detailed expression depends on how the signal acts on the detector (a tensor GW is transversal while a scalar wave is longitudinal). In some cases, a polarization angle has to be used to define the action of the signal [38].

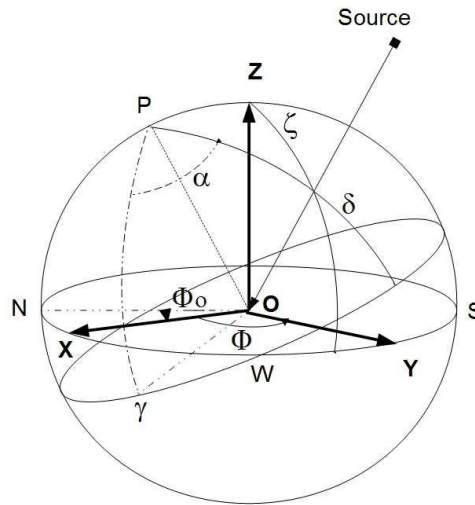


Fig3. Geometry of the system. The antenna pattern must be expressed in the $\{OXYZ\}$ coordinates, OX being often used as the main axis of a GW detector; by expressing the two angles Φ and ζ in function of characteristics of a source (equatorial coordinates and mode of action on a detector).

3.3. Application of ST analysis for GW detectors

Real spatial and projected on the sky galaxy distribution of the Local Universe is very inhomogeneous (see Fig.4 [38]). Many thousands of galaxies can be concentrated in special directions at the sky (the Super-galactic plane, the Virgo cluster, the Great Attractor), and this lead to the expected rate of CCSN events $\sim 1/(3\text{days})$.

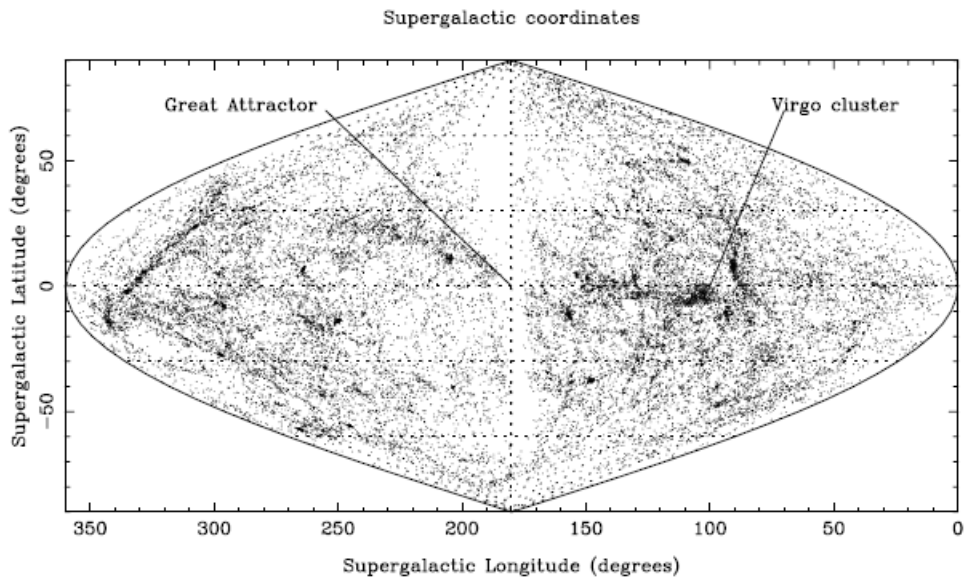


Fig4. Sky distribution of the Local Universe galaxies (distance < 100 Mpc) in the super-galactic coordinates. Interesting observational fact is that the Super-galactic plane is almost orthogonal to the Galactic plane (from [38]).

In order to test the calculation we made the calculation for data produced by the Galactic Center (which is similar to the Galactic Plane), that Weber thought to have detected (Fig.5a [37]). We also made the same for two series of observations by the ROG group in Rome [39]. The result (Fig. 5 b,c) is interesting. Unfortunately, the theoretical GRT prediction does not permit such detection [42].

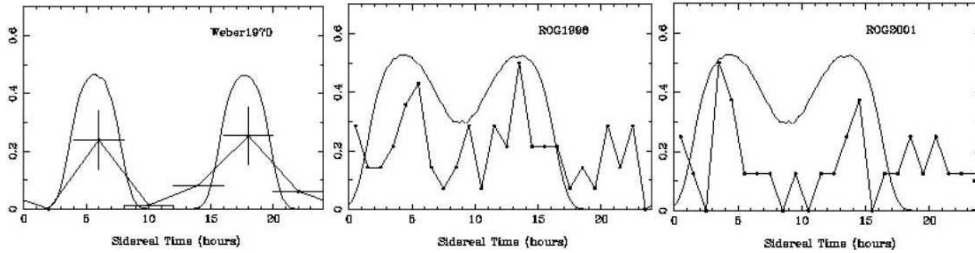


Fig5. a, b, c: Distribution of the relative event counts in sidereal time for bar detectors and sources of tensor (transversal) GW from the Galactic Center/Plane for the cases respectively: 1970 Weber's data (left)[37] and ROG group data from the Explorer detector in 1998 and 2001 (middle and left) [39].

A possibility to explain the GW detections (Fig.5) in principle exists in the framework of FGT, if one takes into account pulsate character of the CCSN explosion and specific properties of generation and detection of the scalar GW.

4. Conclusion

The sidereal time analysis could provide us with a high confidence confirmation of detection of both GW and neutrino coming from SN explosions. The most spectacular result would be the detection of a correlation between GW and neutrino signals as it possibly happened in the case of SN1987A (Fig. 1). The goal of the ST analysis is to get statistical evidence of the extragalactic origin of tiny signals in a large noise.

As explained in this paper, spatial inhomogeneities of GW and neutrino sources in the Local Universe (distances less than 100 Mpc) will produce bumps at given ST hours, for both GW and neutrino events. Each coincidence at the right place (after a proper shift in longitude) would be a strong evidence that the detections are real. To apply the ST analysis to neutrino detection, it is important to determine the directivity diagram of neutrino detectors (LVD, Super-Kamiokande, Baksan). This makes us to dream and gives us a hope to explore the Galactic plane, the Galaxy center, the closest galaxies, the Virgo galaxy cluster, the Super-galactic plane, the Great Attractor by using existing and forthcoming GW and neutrino detectors.

Acknowledgements

YB thanks the Saint-Petersburg State University research project No.6.38.18.2014 for the financial support.

References

- [1] Aglietta, M. et al., Europhys. Letters 3 , 1315 (1987).
- [2] Hirata, K. et al., Phys. Rev. Lett. 58 , 1490 (1987).

- [3] Amaldi, E. et al., *Europhys. Lett.* 3, 1325 (1987)
- [4] Pizzella, G., *Nuovo Cimento B* 102 471 (1989)
- [5] Weber, J., in *Proceedings of the "First Edoardo Amaldi Conference on Gravitational Wave Experiment*, World Scientific, p.416 (1995).
- [6] Baryshev, Yu.V., *Astrophysics*, 40, 377 (1997).
- [7] Srivastava, Y., Widom, A., Pizzella, G.: *Electronic Enhancements in the Detection of Gravitational Waves by Metallic Antennae*, gr-qc/0302024 (2004).
- [8] Sisto, R., Moleti, A., *Int. J. Mod. Phys. D* 13, Iss. 04, 625 (2004).
- [9] Pizzella, G., *Practical Cosmology*.1:287-294, (2008) (Proceedings of the International conference "Problems of Practical Cosmology", 23-27 June 2008, St.-Petersburg, Russia)
- [10] Galeotti, P., Pallottino, G. & Pizzella, G., in *VULCANO WOKSHOP* (2008), *Frontier Objects in Astrophysics and Particle Physics*, May 26-31 (arXiv: 0810.3759)
- [11] Imshennik, V. S., Ryazhskaya, O. G., *Astron. Lett.* 30 14 (2004)
- [12] Nadyozhin, D.K., Imshennik, V.S., *Int.J.Mod.Phys. A*20, 6597-6611 (2005)
- [13] Imshennik, V.S., *Physics - Uspekhi* 53 (11), 1121 (2010)
- [14] Burrows, A., *Rev. Mod. Phys.*, 85, 245 (2013)
- [15] Dolence, J., A. Burrows, W. Zhang, *Ap.J*, 800, id.10 (2015)
- [16] Bisnovatyi-Kogan, G.S., Moiseenko, S.G., Ardeljan, N.V., in *Proc. Frascati Workshop 2013*, *Acta Polytechnica Supplement*, arXiv:1408.2395 (2014)
- [17] Landau, L.D., Lifshitz, E.M., *The Classical Theory of Fields*, Pergamon, Oxford (1971).
- [18] Feynman, R., *Lectures on Gravitation*, California Institute of Technology (1971).
- [19] Feynman, R., Morinigo, F., Wagner, W., *Feynman Lectures on Gravitation*, Addison-Wesley Publ. Comp. (1995).
- [20] Sokolov, V. V., Baryshev, Yu. V., *Gravitation and Relativity Theory*, KGU, vyp.17, 34 (1980).
- [21] Sokolov, V. V., *Int. J. Astron. Astroph. Sp. Sci.*, 2(6), 51 (2015).
- [22] Baryshev, Yu. V., *Practical Cosmology*, 1:276-286, (2008) (Proceedings of the International conference "Problems of Practical Cosmology", 23-27 June 2008, St.-Petersburg, Russia), (arXiv:0809.2323).
- [23] Baryshev, Yu. V., *Practical Cosmology*, 1:347-359 (2008) (Proceedings of the International conference "Problems of Practical Cosmology", 23-27 June 2008, St.-Petersburg, Russia), (arXiv:0809.2328).
- [24] Baryshev, Yu.V., *Vest. Leningrad. Univ. ser.1, vyp.2*, 80 (1988).
- [25] Wilkins, D., arXiv: 1511.01090 (2015)
- [26] Fabian, A., arXiv: 1511.08596 (2015)
- [27] Wilkins, D. et al. *MNRAS*, 454, 4440 (2015)
- [28] King, A., et al., *Ap.J.*,771, 84 (2013)
- [29] Doeleman, S. et al., arXiv: 0906.3899 (2009)
- [30] Doeleman, S. et al., *Nature*, 455, 78 (2008)
- [31] Doeleman, S. et al., *Science*, 338, 355 (2012)
- [32] Falcke, H., Markoff, S., *Class. Quant. Grav.*,30, iss. 24, id. 244003 (2013)

- [33] Johannsen, T. et al., arXiv: 1512.02640 (2015)
- [34] Hawking, S., arXiv:1401.5761 (2014)
- [35] Merali, Z., Nature, 24 January (2014)
- [36] Chowdhury, B., Krauss, L., arXiv: 1409.0187 (2014).
- [37] Weber, J., Phys. Rev. Letters 25, 180 (1970).
- [38] Baryshev, Yu. V., Paturel, G., Astron. Astrophys. 371, 378 (2001).
- [39] Astone, P. et al., Class. Quant. Grav. 19, 5449 (2002).
- [40] Paturel, G., Baryshev, Yu.V., Astron. Astrophys. 398, 377 (2003).
- [41] Paturel, G., Baryshev, Yu.V., ApJ 592, L99 (2003).
- [42] Coccia, E., Dubath, F., Maggiore, M., Phys.Rev.D70:084010 (2004).
- [43] Agafonova, N. et al., Ap. J., 802, 47 (2015).
- [44] Ikeda, M., in Particle and Astroparticle Physics, Gravitation and Cosmology: Predictions, Observations and New Projects - PROCEEDINGS OF THE XXX-TH INTERNATIONAL WORKSHOP ON HIGH ENERGY PHYSICS. Edited by Ryutin R. & Petrov V.. Published by World Scientific Publishing Co. Pte. Ltd., pp. 297-307 (2015)

Search for cosmic gamma rays with the Carpet-2 extensive air shower array

D. D. Dzhappuev^{1,*}, V. B. Petkov¹, A. U. Kudzhaev¹, N. F. Klimenko¹,
A. S. Lidvansky¹, S. V. Troitsky¹

¹*Institute for Nuclear Research, Russian Academy of Sciences; Moscow, Russia;*

**dzhappuev@mail.ru*

Abstract The present-day status of the problem of searching for primary cosmic gamma rays at energies above 100 TeV is discussed, as well as a proposal for a new experiment in this field. It is shown that an increase of the area of the muon detector of the Carpet-2 air shower array up to 410 square meters, to be realized in 2016, will make this array quite competitive with past and existing experiments, especially at modest energies. Some preliminary results of measurements made with smaller area of the muon detector are presented together with estimates of expected results to be obtained with a coming large-area muon detector.

Keywords: Cosmic Rays, Extensive Air Showers, Primary Diffuse Gamma Rays, Muon-poor Showers

1. Introduction

Search for primary gamma rays of energies higher than 100 TeV using the extensive air shower (EAS) method started in 1960s. A lot of experiments were made in this line of research until the present time, different types of detectors and different methods of isolating showers produced by primary gamma rays being used. One can apply the EAS detection method to studies of the diffuse gamma ray emission of cosmic origin, if there is a way of efficient separation of showers produced by primary photons from EAS generated by primary protons and nuclei. Such a separation is possible due to the fact that the showers from primary photons are substantially less abundant with hadrons (and, consequently, muons) than proton showers (the more so in case of showers from nuclei). Thus, by selecting EAS with diminished number of hadrons or muons one can hope to isolate the showers from primary gamma rays. Maze and Zawadski [1] were the first who put forward the idea of searching for high-energy gamma rays by way of detecting muon-poor showers. This seemed to be the simplest way of distinguishing gamma-ray induced showers from ordinary extensive air showers. Following this idea, several groups tried to measure the flux of diffuse gamma ray emission and claimed to obtain some positive results. The experiments at Mt. Chacaltaya [2] and Tien Shan [3], in Yakutsk [4] and Lodz [5] published such results, but they have insufficient statistical significance and were not confirmed later. More careful subsequent experiments (collaborations EAS-TOP [6], CASA-MIA [7] and KASKADE [8] in the energy range $3 \cdot 10^{14} - 5 \cdot 10^{16}$ eV, and Haverah Park [9], AGASA [10]–[12], Yakutsk [13], [14], Pierre Auger [15], [16], and Telescope Array [17] at energies higher than 10^{18} eV) yielded only upper limits on the fluxes of cosmic gamma rays.

2. Present-day Status of the Problem

The upper limits obtained in [6]–[17] are significantly lower than the fluxes measured in early works

[2] – [5] (see Fig. 1). Quite recently, new interesting results have appeared for the energy range $5 \cdot 10^{15} - 2 \cdot 10^{17}$ eV. Archival data of the MSU air shower array were analyzed in [18], [19]. Showers in this experiment were selected according to the low content of muons with energies higher than 10 GeV. For the entire energy range under analysis only upper limits on the cosmic gamma ray flux were obtained, excluding a narrow interval $5 \cdot 10^{16} - 10^{17}$ eV, where muonless showers were recorded, whose number well exceeded the expected number of background events. This allowed authors to estimate the absolute value of the flux of diffuse gamma rays in this energy range. These results are in line with the most recent KASCADE-Grande flux limits at these energies [20].

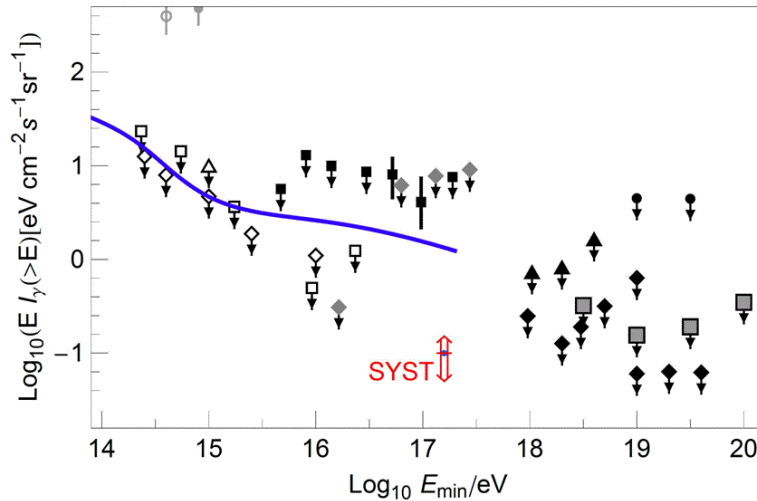


Fig1. Estimates of the integral gamma-ray flux: Detection claims by Tien Shan (gray open circle) and Lodz (gray solid circle), and EAS-MSU (black squares and error bars). Open triangles, squares and diamonds are for EAS-TOP, CASA-MIA, and KASCADE, respectively; gray diamonds: KASCADE-Grande, black triangles: Yakutsk, black diamonds: Pierre Auger, small black circles: AGASA, large squares: Telescope Array. The curve represents an example theoretical prediction [23] for the model in which photons and neutrinos are produced in cosmic-ray collisions with the hot gas surrounding our Galaxy, assuming the best-fit IceCube observed neutrino spectrum.

It should be noted that a new impetus to interest in this problem was given by publications of the IceCube results on detection of high-energy astrophysical neutrinos [21], [22]. Neutrinos produced in decays of charged pions should be accompanied by gamma rays produced in decays of neutral pions. Hence, there is a motivation for new specialized experiments with more precise measurements of the flux of diffuse gamma rays at energies higher than 100 TeV.

The Carpet-2 air shower array of the Baksan Neutrino Observatory includes a large area muon detector that in principle is capable of separating the showers from primary gamma rays with energies higher than 100 TeV. In this paper we present preliminary estimates of sensitivity of the array to the diffuse flux of cosmic gamma rays with the existing muon detector and analyze possible results that can be achieved after a good exposure with the increased area of the muon detector after its modernization (this work is now in progress).

3. Experiment

The Carpet-2 air shower array [24], [25] consists of a surface part (the original Carpet with six external huts) and an underground muon detector (MD). The distance between centers of the Carpet and

MD is 47 m. The Carpet that detects the EAS electron-photon component includes 400 scintillation detectors forming a square (20x20) with a total area of 196 m^2 . The muon detector records the muon component with an energy threshold of 1 GeV. Signals from external huts, each of which contains 9 m^2 of scintillation detectors, are used for determination of shower arrival directions. The accuracy of determination of coordinates of EAS axes hitting the Carpet is no worse than 0.7 m, while the arrival directions of showers are measured with an accuracy of better than $\sim 3^\circ$. The Carpet and MD operate independently of each other and have different dead times of recording electronics. But time markers of events in the MD and Carpet are produced by one and the same clock, so that coincident events are identified within a time interval $\Delta t = 1 \text{ ms}$. The total number of relativistic particles within the Carpet ($N_{r.p.}$) and the number n_μ of muons recorded by the MD are the experimentally measured quantities used to determine the energy of EAS and the total number of muons in it, respectively. The events satisfying the following conditions are included into processing:

1. shower axes are well within the Carpet;
2. zenith angles of showers $\theta < 40^\circ$;
3. $N_{r.p.} \geq 2 \cdot 10^4$.

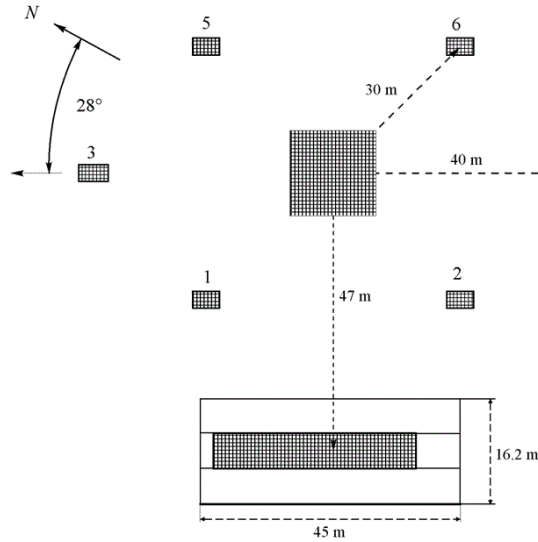


Fig2. The layout of the Carpet-2 air shower array.

3.1. Simulations

For the sensitivity estimates presented here, the CORSIKA code v. 6720 (QGSJET01C, FLUKA 2006) [26] was used for modeling the showers. 5400 showers from primary protons and 6597 showers from primary iron nuclei were simulated within the energy interval (0.316–31.6) PeV, as well as 815 showers from primary gamma rays in the range (0.3–9) PeV. As a result of modeling the following averaged relations were obtained:

$$E_p [\text{GeV}] = 174 \cdot N_{r.p.}^{0.75} \quad (1)$$

$$E_\gamma [\text{GeV}] = 1096 \cdot N_{r.p.}^{0.62} \quad (2)$$

3.2. Preliminary analysis and future prospects

Figure 3 presents the calculated correlation distribution n_μ versus $N_{r.p.}$ for showers from primary protons, iron nuclei and gamma rays, where points with $n_\mu = 0$ are shown as $n_\mu = 0.2$. Though the numbers of simulated proton and gamma-ray showers are not equal, all muon-poor showers with $N_{r.p.} \geq 10^5$ are produced by gamma rays.

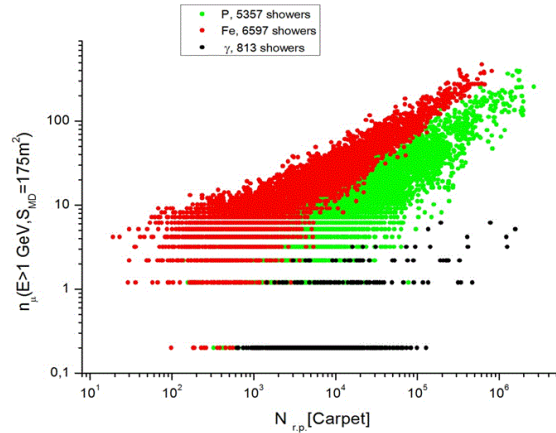


Fig3. The calculated $n_\mu - N_{r.p.}$ dependence (CORSIKA) for EAS induced by protons, iron nuclei and gamma rays.

A similar distribution for experimental data is presented in Fig. 4 together with expectation for gamma rays. To compare the simulations with the data, a subset of 4261 showers recorded during 226 days of work of 175 m² MD was analyzed (the exposure was $5.74 \cdot 10^{13}$ cm² s sr). Experimental muonless events (their number is 1080) are not shown in the figure. Of course, such a number of muonless showers is not necessarily produced by gamma rays, but can be a consequence of fluctuations of the number of muons or of incorrect method of selecting the events. Indeed, as follows from these two distributions the number of muons fluctuates strongly in the interval $N_{r.p.} = 2 \cdot 10^4 \div 10^5$, so that it is impossible to isolate real gamma rays against the background proton showers at currently available statistics of experimental and simulated showers. Only the upper limit on the flux of primary gamma rays can be evaluated, assuming that the detected muonless showers are the background ones. Preliminary constraints on the flux of diffuse gamma rays derived by us are considerably worse as compared to the results obtained earlier in different experiments. In order to improve them we plan to process archival data accumulated for 10 years.

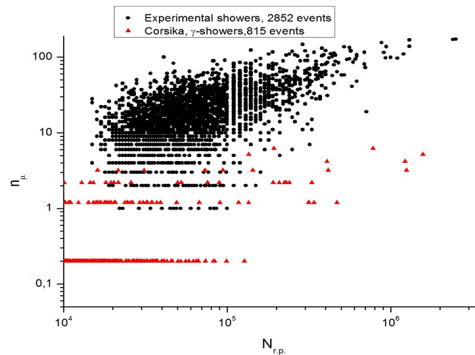


Fig4. Measured and calculated $n_\mu - N_{r.p.}$ dependence (experiment, CORSIKA)

One can diminish relative fluctuations of the number of muons recorded by the MD (thus improving the efficiency of separation of showers) by increasing the muon detector area. This work is now in progress. Next year it is planned to install 235 new scintillation counters with area of 1 m^2 each in tunnels of the MD, thus increasing the MD area up to 410 m^2 . According to further plans, the effective area of the array will be increased up to $6 \cdot 10^3 \text{ m}^2$ (the Carpet-3 array). The area of the MD will be increased in this case up to the maximum possible value of 615 m^2 (total filling of the three MD tunnels).

Commissioning of the 410 m^2 MD will become a crucial step towards gamma-ray astronomy with Carpet-2. Preliminary estimates demonstrate that the background of muonless events from hadronic showers will be reduced drastically in this configuration. Figure 5 demonstrates the estimated sensitivity of the existing array (Carpet-2) and two its modernizations (Carpet-2+ and Carpet-3) as compared to the upper limits obtained by other experiments. One can see that using a new configuration of the Baksan array a significant advance can be achieved at energies below and around 10^{15} eV .

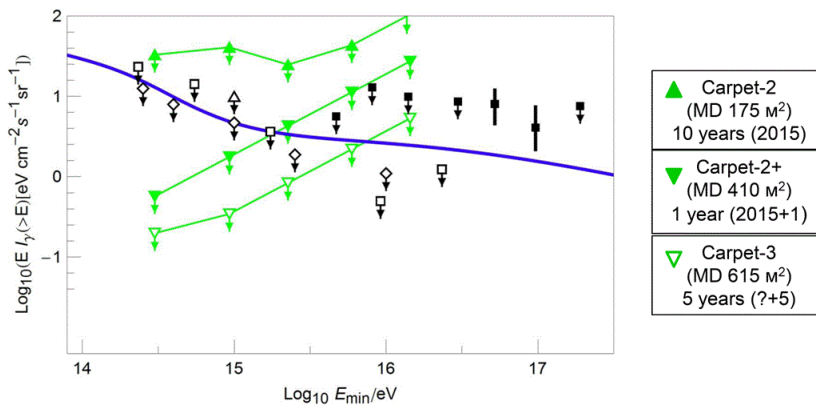


Fig5. The sensitivity of the Carpet-2 and Carpet-3 air shower arrays to the diffuse cosmic photons.

The sensitivity of the upgraded array to point sources will depend on the source's position in the sky. Preliminary estimates give a sensitivity of $\sim 5 \cdot 10^{-13} \text{ cm}^{-2} \text{ s}^{-1}$ for the integral gamma-ray flux of Mrk 501 above 100 TeV (one year of observations with 410 m^2 MD). In more detail, the estimates of sensitivity of Carpet-2+ for gamma rays will be discussed in a forthcoming paper.

4. Conclusions

1. The Carpet air shower array could be quite competitive in gamma-ray astronomy above 100 TeV.
2. To perform this task better, it is highly desirable to increase the area of the Muon Detector as much as possible.
3. The work to reach an area of 410 m^2 next year and 615 m^2 in the future is now in progress.

Acknowledgments

This work was supported in part by the “The fundamental properties of matter and astrophysics” Program for Basic Research of the Presidium of the Russian Academy of Sciences.

The work of DD, VP, AK, and AL is supported by the Russian Foundation for Basic Research, project number 16-02-0687. The work of ST related to testing the EAS-MSU result with different experimental data is supported by the Russian Science Foundation, grant no. 14-12-01340.

References

- [1] Maze, R., Zawadzki, A., On an attempt of detection of primary cosmic photons of very high energy. *Nuovo Cim.* 1960; 17: 625.
- [2] Suga, K., Toyoda, Y., Kamata, K., et al., Diffuse gamma rays with energies greater than 1×10^{14} eV observed in the southern hemisphere. *Astrophys. J.* 1988; 326: 1036-39.
- [3] Nikolsky, S.I., Stamenov, I.N., and Ushev S.Z., γ Quanta with Energy = 10^{15} eV in the Primary Cosmic Radiation. *J. Phys. G* 1987; 13: 883.
- [4] Glushkov, A.V., Efimov, N.N., Efremov, N.N., et al., Estimation of composition of cosmic rays with E_{zero} approximately equals 10^{17} - 10^{18} eV. *Proc. 19th ICRC, La Jolla, 1982*; 2: 186.
- [5] Gawin, J., Maze, R., Wdowczyk, J., and Zawadski, A., Remarks on mu-poor EAS. *Canad. J. Phys.* 1968; 46: 75.
- [6] Aglietta, M., Alessandro, B., Antoni, P., et al. [EAS-TOPcollaboration], A limit to the rate of ultra high energy γ -rays in the primary cosmic radiation. *Astropart. Phys.* 1996; 6:71-5.
- [7] Chantell, M.C., Covault, C.E., Cronin, J.W., et al. [CASA-MIA collaboration], Limits on isotropic diffuse flux of ultrahigh energy γ -radiation. *Phys. Rev. Lett.* 1997; 79: 1805. [astro-ph/9705246].
- [8] Schatz, G., Fessler, F., Antoni, T., et al. [KASCADE collaboration], Search for extremely high energy gamma rays with the KASCADE experiment. *Proc. 28th ICRC, Tsukuba, 2003*; 4: 2293.
- [9] Ave, M., Hinton, J.A., Vasquez, R.A., et al., New constraints from Haverah Park data on the photon and iron fluxes of UHE cosmic rays. *Phys. Rev. Lett.* 2000; 85: 2244. [astro-ph/0007386].
- [10] Shinozaki, K., Chikawa, M., Fukushima, M., et al. [AGASA collaboration], Upper limit on gamma-ray flux above 10^{19} eV estimated by the Akeno Giant Air Shower Array Experiment. *Astrophys. J.* 2002; 571: L117.17.
- [11] Risse, M., Homola, P., Engel, R., et al. Upper limit on the photon fraction in highest-energy cosmic rays from AGASA data. *Phys. Rev. Lett.* 2005; 95: 171102. [astro-ph/0502418].
- [12] Rubtsov, G.I., Dedenko, L.G., Fedorova, G.F., et al., Upper limit on the ultra-high-energy photon flux from AGASA and Yakutsk data. *Phys. Rev. D* 2006; 73: 063009. [astro-ph/0601449].
- [13] Glushkov, A.V., Gorbunov, D.S., Makarov, I.T., et al., Constraining the fraction of primary cosmic ray photons at ultra-high energies from the muon data of the Yakutsk extensive air shower array. *JETP Lett.* 2007; 85: 131. [astro-ph/0701245].
- [14] Glushkov, A.V., Makarov, I.T., Pravdin, M.I., et al., Constraints on the flux of primary cosmic ray photons at energies $E > 10^{18}$ eV from Yakutsk muon data. *Phys. Rev. D* 2010; 82: 041101. [arXiv:0907.0374 [astro-ph/HE]].
- [15] Abraham, J., Abreu, P., Aglietta, M., et al. [Pierre Auger collaboration], Upper limit on the cosmic-ray photon flux above 10^{19} eV using the surface detector of the Pierre Auger Observatory. *Asropart. Phys.* 2008; 29: 243. [arXiv:0712.1147 [astro-ph]].
- [16] Bleve, C., et al. [Pierre Auger collaboration], Updates on the neutrino and photon limits from the Pierre Auger Observatory, In: Aab A, Abreu P, Aglietta M, et al., *The Pierre Auger Observatory: Contributions to the 34th International Cosmic Ray Conference (ICRC 2015)*, arXiv:1509.03732 [astro-ph.HE].
- [17] Rubtsov, G.I., et al. [Telescope Array collaboration], Telescope Array search for photons and neutrinos with the surface detector data, *Proc. 34th International Cosmic Ray Conference (ICRC 2015)*.
- [18] Fomin, Yu.A., Kalmykon, N.N., Kulikov, G.V., Sulakov, V.P., Troitsky, S.V., Estimate of the fraction of primary photons in the cosmic ray flux at energies $\sim 10^{17}$ eV from the EAS-MSU experiment data. *J. Exp. Theor. Phys.* 2013; 117: 1011. [arXiv: 1307.4988 [astro-ph.HE]].
- [19] Fomin, Yu.A., Kalmykon, N.N., Kulikov, G.V., Sulakov, V.P., Troitsky, S.V., Estimate of the cosmic gamma-ray flux at PeV to EeV energies from EAS-MSU experiment data. *JETP Lett.* 2015; 100: 699 [arXiv:

- 1410.2599 [astro-ph.HE]].
- [20] Kang, D. et al., A limit on the diffuse gamma-rays measured with KASCADE-Grande, *J.Phys.Conf.Ser.* 2015; 632: 012013.
 - [21] Aartsen, M.G. et al. [Ice Cube collaboration], First observation of PeV-energy neutrinos with Ice Cube. *Phys. Rev. Lett.* 2013; 111: 021103. [arXiv: 1304.5356 [astro-ph.HE]].
 - [22] Aartsen, M.G. et al. [Ice Cube collaboration], Evidence for High-Energy Extraterrestrial Neutrinos at the IceCube Detector. *Science* 2013; 342: 6161, 1242856. [arXiv: 1311.5238 [astro-ph.HE]].
 - [23] Kalashev, O.E., Troitsky, S.V., IceCube astrophysical neutrinos without a spectral cutoff and $(10^{15}—10^{17})$ eV cosmic gamma radiation. *JETP Lett.* 2015; 100: 761. [arXiv: 1410.2600].
 - [24] Dzhappuev, D.D., Alekseenko, V.V., Volchenko, V.I. et al., Modernization of the Carpet-2 array of the Baksan Neutrino observatory. *Bull. Russ. Acad. Sci. Phys.* 2007; 71: 525-28.
 - [25] Dzhappuev, D.D., Alekseenko, V.V., Lidvansky, A.S., Stenkin, Yu.V., Petkov, V.B., Mikhailova, O.I., Kudzhaev, A.U., Chernyaev, A.B. and Tsyabuk, A.L., Study of EAS hadronic component with hadron energy > 50 GeV. *Proc. 30th ICRC, Merida, 2007, vol. 4, p. 19.*
 - [26] Heck, D. et al., The Air Shower Simulation Program CORSIKA. Report FZKA 6019 (1998), Forschungszentrum, Karlsruhe.

Super-Eddington accretion disks in Ultraluminous X-ray sources

Sergei Fabrika^{1*,2}, Alexander Vinokurov¹, Kirill Atapin^{3,1},
Olga Sholukhova¹

¹*Special Astrophysical Observatory, Nizhnij Arkhyz, Russia; fabrika@sao.ru*

²*Kazan Federal University, Kazan, Russia*

³*Sternberg Astronomical Institute, Moscow State University, Moscow, Russia*

Abstract The origin of Ultraluminous X-ray sources (ULXs) in external galaxies whose X-ray luminosities exceed those of the brightest black holes in our Galaxy hundreds and thousands times is mysterious. The most popular models for the ULXs involve either intermediate mass black holes (IMBHs) or stellar-mass black holes accreting at super-Eddington rates. Here we review the ULX properties, their X-ray spectra indicate the presence of hot winds in their accretion disks supposing the supercritical accretion. However, the strongest evidences come from optical spectroscopy. The spectra of the ULX counterparts are very similar to that of SS433, the only known supercritical accretor in our Galaxy. The spectra are apparently of WNL type (late nitrogen Wolf-Rayet stars) or LBV (luminous blue variables) in their hot state, which are very scarce stellar objects. We find that the spectra do not originate from WNL/LBV type donors but from very hot winds from the accretion disks, whose physical conditions are similar to those in stellar winds from these stars. The results suggest that bona-fide ULXs must constitute a homogeneous class of objects, which most likely have supercritical accretion disks.

Keywords: Ultraluminous X-Ray Sources, Super-Eddington Accretion Disks

1. Introduction

Ultraluminous X-ray sources (ULXs) are X-ray sources with luminosities exceeding the Eddington limit for a typical stellar-mass black hole $\sim 2 \cdot 10^{39} \text{ erg s}^{-1}$. Despite their importance in understanding the origin of supermassive black holes that reside in most of present galaxies, the basic nature of ULXs remains unsolved [1]. The most popular models for the ULXs involve either intermediate mass black holes (IMBH, 10^3 – $10^4 M_\odot$) [2] with standard accretion disks or stellar-mass black holes ($\sim 10 M_\odot$) accreting at super-Eddington rates. The last idea has been suggested [3] by analogy with SS433, the only known super-accretor in the Galaxy [4], and developed in [5], [6]. It was proposed that SS433 supercritical disk's funnel being observed nearly face-on will appear as an extremely bright X-ray source. Both scenarios, however, require a massive donor in a close binary.

Most of ULXs are associated with the star-forming regions and surrounded by nebulae of a complex shape, indicating a dynamical influence of the black hole [7]. They are not distributed throughout galaxies as it would be expected for IMBHs originating from low-metallicity Population III stars. The IMBHs may be produced in a runaway merging in a core of young clusters. In this case, they should stay within the clusters. It has been found [8] that all brightest X-ray sources in Antennae galaxies are located near very young stellar clusters. It was concluded that the sources were ejected in the process of formation of stellar clusters in the dynamical few-body encounters and that the majority of ULXs are massive X-ray binaries with the progenitor masses larger than $50 M_\odot$.

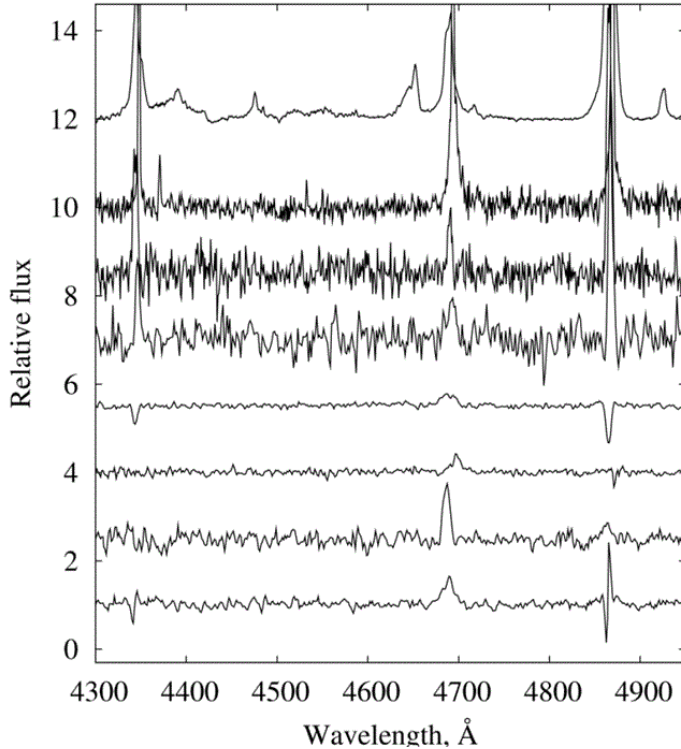


Fig1. Normalized optical spectra of ULX counterparts. From top to bottom: SS 433 (1), NGC 5408 X-1 (2), NGC 4395 X-1 (3), NGC 1313 X-2 (2), NGC 5204 X-1, NGC 4559 X-7, Holmberg IX X-1 and Holmberg II X-1 (1). The numbers in brackets mean optical telescopes: 1 – the Subaru telescope, 2 – VLT (ESO), 3 – the Russian BTA telescope. The spectra are very similar in appearance, they may represent a rare type of massive stars WNL [10] or LBV stars in their hot states [11], [12]. All spectra are also similar to SS 433 [13]. This means that the spectra of the ULX counterparts are formed in hot winds.

X-ray spectra of ULXs often show a high-energy curvature with a downturn between ~ 4 and ~ 7 keV. It was called “an ultraluminous state” [9]. The curvature hints that the ULX accretion disks are not standard. Inner parts of the disks may be covered with a hot outflow or optically thick corona, which Comptonizes the inner disk photons.

2. Results

Spectra of almost all optical counterparts of studied ULXs (with SS433 included) are shown in Fig.1. All spectra were reduced by us. The main features in all spectra are the bright HeII λ 4686, hydrogen H α and H β emission lines. The lines are obviously broad; the widths range from 500 to 1500 km s $^{-1}$.

Calibrated spectra of the ULX optical counterparts taken with the Subaru telescope [14] are given in Fig.2. We conclude that all ULX counterparts ever spectrally observed have the same feature in their spectra, namely, the broad HeII emission line. We also clearly detect the broad H α , H β lines and HeII λ 6678, 5876 lines (Fig.2). There are also some hints on the Bowen CIII/NIIB blend (4640 - 4650 Å). Although the H β line (Figs.1, 2) is affected by nebular emission in spite of our careful extraction, its broad wings are clearly detected. It is obvious that the emission lines are formed in stellar winds or disk winds.

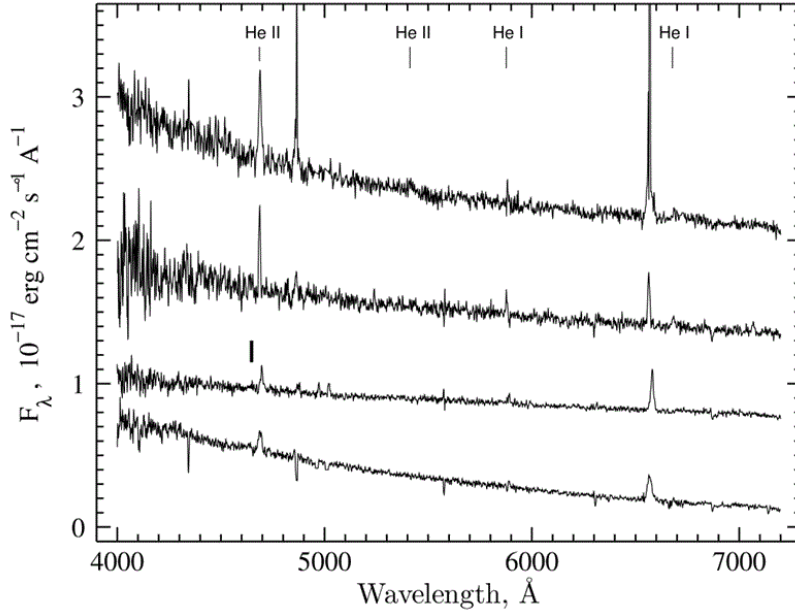


Fig2. Calibrated spectra of the ULX optical counterparts taken with the Subaru telescope [14]. From top to bottom: the ULX in Holmberg II, Holmberg IX, NGC4559, and NGC5204. The two upper spectra were obtained on February 28, while the rest are the summed spectra from three nights. For better visualization we add the flux offsets of 1.8, 1.2 and 0.6 ($10^{-17} \text{ erg/cm}^2 \text{ s} \text{ \AA}^{-1}$) for the Holmberg II, Holmberg IX, and NGC4559 ULXs, respectively. Besides the obvious hydrogen lines we mark HeII lines ($\lambda 4686$ and $\lambda 5412$) and HeI lines ($\lambda 5876$ and $\lambda 6678$). The thick bar indicates the position of the Bowen blend CIII/NIII $\lambda \lambda 4640 - 4650$.

All spectra of the ULXs are surprisingly similar to each other. The optical spectra are also similar to that of SS 433, although the ULX spectra indicate a higher wind temperature. It was suggested in [14] that the ULXs must constitute a homogeneous class of objects, which most likely have supercritical accretion disks.

Among stellar spectra, such a strong HeII line with a nearly normal hydrogen abundance can be found only in stars recently classified as O2–3.5If*/WN5–7 [10]. Hereafter we omit index * which means a stronger ionization as indicated by NIV/NV lines. They are the hottest transition stars, whose classification is based on the H β profile, tracing the increasing wind density (i.e., the mass loss rate) from O2–3.5If, O2–3.5If/WN5–7, and to WN5–7.

We study the spectra of ULX counterparts in the HeII diagram ([15], [14]), where the relation between the line width and equivalent width of the HeII $\lambda 4686$ line is plotted (Fig.3). Here the line width represents the terminal velocity of a stellar wind, while the equivalent width reflects its photosphere temperature and mass loss rate.

In Fig.3, we show the classification diagram of WN stars [15] for LMC and Galactic objects. We supplement the diagram with additional stars recently classified [10]. The diagram plots stars in accordance with their wind velocity (FWHM) and photosphere temperature plus mass loss rate (EW). Three known LBV transitions (LBV–WNL) between their hot and cool states in AGCar, V532 in M33, and HD5980 in SMC are also shown in the figure. Consequent states in each LBV transition are connected by the lines. In their hotter state where the HeII line becomes stronger, the LBVs fit well the classical WNL stars [11].

In the figure, we also present two recently discovered extragalactic black holes NGC300X-1 and IC10X-1 together with the soft ULX transient M101ULX-1. The black holes in NGC300X-1 and IC10 have luminosities $L_X \sim 3 \times 10^{38} \text{ erg s}^{-1}$, almost identical to that of CygX-3, which certainly contains a

WN-type donor star [22]. The comparable luminosities with that of CygX-3, short orbital periods, and the location in the diagram around the WN6–7 region confirm that their optical spectra come from WN donors. The same may be supposed for M101ULX-1 on the basis of its location in the diagram. It has been recently found that this source indeed contains a WN8 type donor [23], although its orbital period is ~ 40 times longer than in CygX-3 and ~ 6 times longer than in two other WR X-ray binaries.

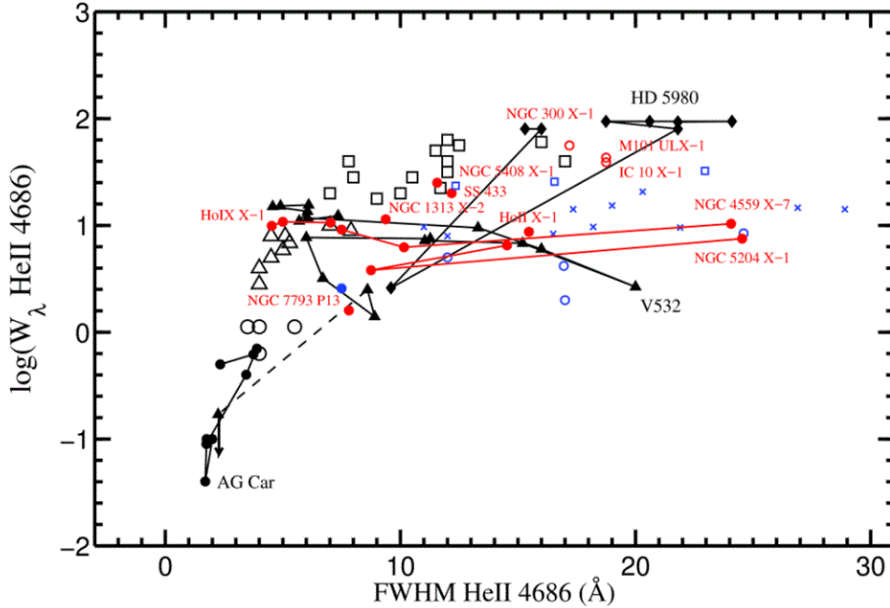


Fig3. Classification diagram of WNL stars in the LMC and our Galaxy [15]. The black open squares, triangles, and circles mark WN8, WN9–10m, and WN11 stars, respectively. The blue filled circle denotes ζ Pup. Other Galactic and LMC stars [10] are O2If and O3If (open blue circles), O2If/WN5, O2.5If/WN6, O3If/WN6, and O3.5If/WN7 (blue crosses), and WN6ha and WN7ha stars (open blue squares). There are three known LBV–WNL transitions (AGCar, V532, and HD5980) in this diagram [11]. Consequent states of each LBV star are connected by the lines. Positions of our four ULX counterparts are also shown (connected by lines to show variability from night to night), together with those of NGC1313X-2, NGC5408X-1, NGC7793P13, SS433, NGC300X-1, M101ULX-1, and IC10X-1 ([13], [16]–[21]).

Thus, the ULX counterparts and SS433 occupy a region at this diagram between O2–3.5If and WN5–7. This is also a region of the “intermediate temperature LBV” V532 and the “LBV excursion” of HD5980. Variability of the HeII lines of our counterparts in three consequent nights is shown by the points connected by the lines. However, their behavior in the HeII diagram is not similar to stars. They exhibit night-to-night variability both in the line width and equivalent width by a factor of 2–3. Variability in the radial velocity of the line is also detected with amplitudes ranging from 100 km s⁻¹ in Holmberg IX to 350 km s⁻¹ in NGC5204.

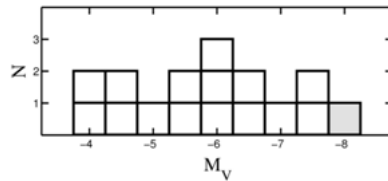


Fig4. Absolute magnitudes of all well-studied ULXs and SS433 (shaded). The data are from [16] with some updates from [25] and [6].

If the ULX counterpart spectra were produced from donor stars, the variable surface gravity at about the same photospheric temperature would be required. Instead, the spectra may be formed in unstable and variable winds formed in accretion disks. This idea agrees with the fact that we do not find any regularities between the EW, FWHM, and radial velocity of the HeII line.

We can exclude the case where these ULXs actually have WNL donors and their stellar winds produce the observed optical spectra. It is difficult to explain the rapid variability of the HeII line-width, because the wind terminal velocity in stars is determined by the surface gravity.

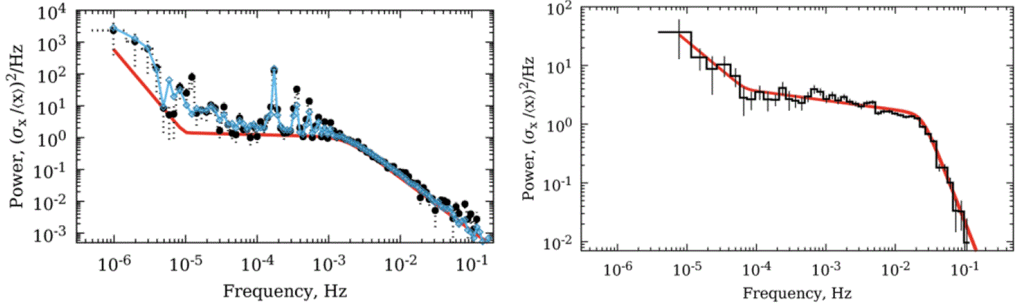


Fig5. Power density spectra of SS433 (left) and the ULX NGC5548 X-1 (right). In SS433 we observe a flat portion [26] which may be considered as alpha-viscosity fluctuations appearing at the spherization radius as was originally proposed [27] for standard disks [24]. The power spectrum of SS433 has been obtained from a single ten-days ASCA observation. The circles and dotted line are the observed power spectra, the red (dark grey) solid line is the initial model of the accretion disk intrinsic variability. The blue (light grey) line and diamonds are the Monte Carlo model, which takes into account the gaps in observations and extra variability added by eclipse occurred during these observations. The power spectrum of SS433 has a flat part stretching from $\sim 10^{-5}$ to $\sim 10^{-3}$ Hz. The power spectrum of NGC5408 X-1 has been obtained by averaging six most long observations from XMM-Newton. A model with two breaks fitting the spectrum is shown by the solid line. This object also has a flat part in the power spectrum.

The total luminosity of a supercritical disk is proportional to the Eddington luminosity with an additional logarithmical factor depending on the original mass accretion rate ([24], [5]), because the excess gas is expelled as a disk wind and the accreted gas is advected with the photon trapping, contributing little to the photon luminosity. However, the UV and optical luminosity in such disks may strongly depend on the original mass accretion rate, because these budgets are mainly produced by the reprocess of the strong irradiation from the wind (the excess gas). Optical spectra of SS433 and the ULX counterpart are nearly the same, but in X-rays they are drastically different because we cannot observe the funnel in SS433 directly. It was found [14] that the mass accretion rates in the ULXs may be by a factor of 1.5–6 smaller and their wind temperatures are by 1.4–4 times higher than those in SS433. In Fig.4 we show the absolute magnitude of all well-studied ULXs together with SS433. Thus, one may interpret that SS433 is intrinsically the same as ULXs but this is an extreme case with a particularly high mass accretion rate, which could explain the presence of its persistent jets [4].

In Fig.5 we present another evidence of the super-Eddington accretion in ULXs. The power density spectrum of SS433 exhibits a flat part in the $10^{-5} - 2 \cdot 10^{-3}$ Hz frequency range [26]. The presence of such a part is related to the abrupt change in the disk structure and the viscous time at the spherization radius. In this place the accretion disk becomes thick, which reduces drastically the time of passage of matter through the disk ([24], [27]). The same picture is observed in the well-studied ULX NGC5408 X-1. We need longer observations of the ULXs to study their power density spectra in more detail.

Acknowledgements

The research was supported by Russian Science Foundation grant N14-50-00043 (observations and

analysis of variability) and Leading Scientific Schools of Russia. SF acknowledges support of the Russian Government Program of Competitive Growth of Kazan Federal University.

References

- [1] H. Feng and R. Soria, *New Astron. Rev.* 55, 166, 2011.
- [2] P. Madau and M.J. Rees, *Astrophys. J.* 551, L27, 2001.
- [3] S. Fabrika and A. Mescheryakov, in *Galaxies and their Constituents at the Highest Angular Resolutions* (IAU Symposium N205, ed. R.T. Schilizzi), 268, 2001.
- [4] S. Fabrika, *ASPRv* 12, 1, 2004.
- [5] J. Poutanen, G. Lipunova, S. Fabrika, A. Butkevich and P. Abolmasov, *MNRAS* 377, 1187, 2007.
- [6] A. Vinokurov, S. Fabrika and K. Atapin, *Astrophys. Bull.* 68, 139, 2013.
- [7] P. Abolmasov, S. Fabrika, O. Sholukhova and V. Afanasiev, *Astrophys. Bull.* 62, 36, 2007.
- [8] J. Poutanen, S. Fabrika, A. Valeev, O. Sholukhova and J. Greiner, *MNRAS* 432, 506, 2013.
- [9] J.C. Gladstone, T.P. Roberts and C. Done, *MNRAS* 397, 1836, 2009.
- [10] P.A. Crowther and N.R. Walborn, *MNRAS* 416, 1311, 2011.
- [11] O.N. Sholukhova, S.N. Fabrika, A.V. Zharova, A.F. Valeev and V.P. Goranskij, *Astrophys. Bull.* 66, 123, 2011.
- [12] O. Sholukhova et al., *MNRAS* 447, 2459, 2015.
- [13] K. Kubota et al., *Astrophys. J.* 709, 1376, 2011.
- [14] S. Fabrika, Y. Ueda, F. Vinokurov, O. Sholukhova and M. Shidatsu, *Nat. Phys.* 11, 551, 2015.
- [15] P. A. Crowther, L. J. Smith, *Astron. Astrophys.* 320, 500, 1997.
- [16] C. Motch, M. W. Pakull, F. Grise, R.Soria, *Astron. Nachr.* 332, 367, 2011.
- [17] T.P. Roberts et al., *Astron. Nachr.* 332, 398, 2011.
- [18] J.M. Silverman, A.V. Filippenko, *Astrophys. J.* 678, L17, 2008.
- [19] P.A. Crowther et al., *MNRAS* 403, L41, 2010.
- [20] K.D. Kuntz et al., *Astrophys. J.* 620, L31, 2005.
- [21] D. Cseh, F. Grise, S. Corbel, P. Kaaret, *Astrophys. J.* 728, L5, 2011.
- [22] M.H. van Kerkwijk, T.R. Geballe, D.L. King, M. van der Klis, J. van Paradijs, *Astron. Astrophys.* 314, 521, 1996.
- [23] J. Liu, J. N. Bregman, Y. Bai, S. Justham, P. Crowther, *Nature*, 503, 500, 2013.
- [24] N.I. Shakura and R.A. Sunyaev, *Astron. Astrophys.* 24, 337, 1973.
- [25] S. Kayaci Avdan et al., *MNRAS* 455, L91, 2016.
- [26] K. Atapin, S. Fabrika, A. Medvedev and A. Vinokurov, *MNRAS* 446, 893, 2015.
- [27] Yu.E. Lyubarskii, *MNRAS* 292, 679, 1997.

Mini–MegaTORTORA wide-field monitoring system with sub–second temporal resolution: observation of transient events

S. Karpov^{1,3,*}, G. Beskin^{1,3}, A. Biryukov⁴, S. Bondar², E. Ivanov², E. Katkova², A. Perkov², and V. Sasyuk³

¹*Special Astrophysical Observatory of Russian Academy of Sciences, Russia;*

^{*}*karpov.sv@gmail.com*

²*Research and Production Corporation “Precision Systems and Instruments”, Russia*

³*Kazan Federal University, Russia*

⁴*Moscow State University, Russia*

Abstract Here we present a summary of first years of operation and first results of a novel 9-channel wide-field optical monitoring system with sub-second temporal resolution, Mini-MegaTORTORA (MMT-9), which is in operation now at Special Astrophysical Observatory on Russian Caucasus. The system is able to observe the sky simultaneously in either wide (~ 900 square degrees) or narrow (~ 100 square degrees) fields of view, either in clear light or with any combination of color (Johnson-Cousins B, V or R) and polarimetric filters installed, with exposure times ranging from 0.1 s to hundreds of seconds. The real-time system data analysis pipeline performs automatic detection of rapid transient events, both near-Earth and extragalactic. The objects routinely detected by MMT include faint meteors and artificial satellites. The pipeline for a longer time scales variability analysis is still in development.

Keywords: Telescopes Instrumentation, Gamma-Ray Burst, Meteorites, Meteors, Meteoroids

1. Introduction

Mini–MegaTORTORA is a novel robotic instrument just commissioned for the Kazan Federal University and developed according to the principles of MegaTORTORA multi–channel and transforming design formulated by us earlier [1] – [4]. It is a successor to the FAVOR [5] – [7] and TORTORA [8] single-objective monitoring instruments we built earlier to detect and characterize fast optical transients of various origins, both cosmological, galactic and near-Earth. The importance of such instruments became evident after discovery and detailed study of the brightest ever optical afterglow of the gamma-ray burst GRB080319B [9], [10].

The Mini-MegaTORTORA (MMT-9) system includes a set of nine individual channels (see Figure 1) installed in pairs on equatorial mounts (see Figure 2). Every channel has a coelostat mirror installed before the Canon EF85/1.2 objective for a rapid (faster than 1 second) adjusting of the objective direction in a limited range (approximately 10 degrees to any direction). This allows us either mosaicking the larger field of view, or pointing all the channels in one direction. In the latter regime, a set of color (Johnson’s B, V or R) and polarimetric (three different directions) filters may be inserted before the objective to maximize the information acquired for the observed region of the sky (performing both three-color photometry and polarimetry).

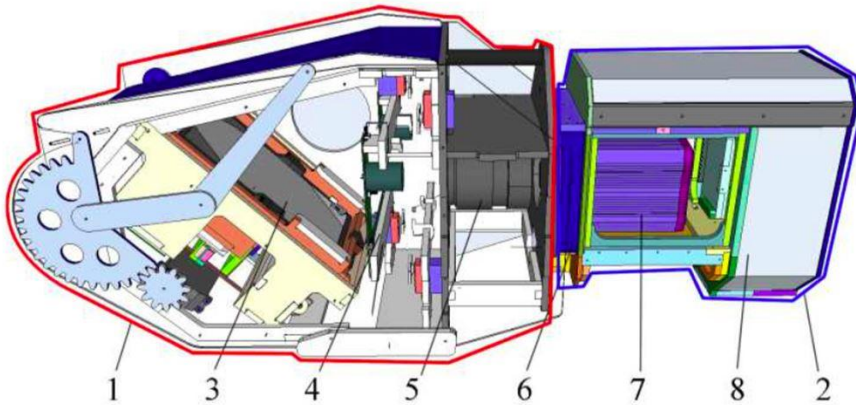


Fig1. Schematic view of a MMT channel. 1 – coelostat unit, 2 – camera unit, 3 – coelostat mirror which can rotate by ~10 degrees around two axes, 4 – installable color and polarimetric filters, 5 – the Canon EF85/1.2 objective, 6 – optical corrector, 7 – the Andor Neo sCMOS detector; 8 – conditioner to keep stable environmental conditions inside the channel.

The channels are equipped with Andor Neo sCMOS detectors having 2560x2160 pixels 6.4 μ m each. The field of view of a channel is roughly 9x11 degrees with an angular resolution of 16'' per pixel. The detector is able to operate with exposure times as small as 0.03 s. In our work we use the 0.1 s exposures providing us with 10 frames per second because on higher frame rates we are unable to process the data in real time.



Fig2. Photo of all 9 channels of MMT installed on 5 mounts in the single cylindrical dome, which is open at that moment. The dome of the Russian 6-m telescope is seen in the background.

Every channel is operated by a dedicated PC which controls its hardware, acquires images from the detector and performs the data processing. The amount of data acquired by a single channel is about 3Tb in 8 hours of observation. The complex as a whole is being controlled by a separate PC.

Initial tests show that the FWHM of stars as seen by MMT channels is around 2 pixels wide. The detection limit in white light for 0.1 s exposure is close to 11 mag, when calibrating to V band magnitudes.

2. Mini–MegaTORTORA operation

Mini–MegaTORTORA started its operation in June 2014, and since then has been routinely monitoring the sky. The observations are governed by a dedicated dynamic scheduler optimized for performing the sky survey. The scheduler selects the next pointing for Mini–MegaTORTORA by simultaneously optimizing the following parameters: distances from the Sun, Moon and the horizon should be maximized, distances from the current pointings of Swift and Fermi satellites should be minimized, and the number of frames already acquired on a given sky position that night should be minimized. In this way a more or less uniform survey of the whole sky hemisphere is being performed while maximizing the probability of observations of gamma-ray bursts. As a non-optimized extension, the scheduler also supports observations of preselected targets given by their coordinates, which may be performed in various regimes supported by Mini–MegaTORTORA (wide-field monitoring of a given region of the sky with or without filters, narrow-field multicolor imaging or polarimetry with lower temporal resolution, etc).

Moreover, the scheduler and central control system supports various types of follow-up observations triggered by external messages and typically corresponding to transient events occurred outside the current Mini–MegaTORTORA field of view. It will try to rapidly re-point and observe the localizations of Swift BAT and XRT triggers in either multi-color or polarimetric mode, typically large error boxes of Fermi GBM in wide-field mode, etc. The large size of Mini–MegaTORTORA field of view in the wide-field regime makes such observations very promising for rapid pin-pointing of possible optical transients corresponding to triggers with bad accuracy of initial localization.

3. Data analysis

The main regime of Mini–MegaTORTORA operation is the wide-field monitoring with high temporal resolution and with no photometric filters installed. In this regime, every channel acquires 10 frames per second, which corresponds to 110 megabytes of data per second. To analyze it, we implemented the real-time fast differential imaging pipeline intended for detection of rapidly varying or moving transient objects – flashes, meteor trails, satellite passes etc. It is analogous to the pipeline of FAVOR and TORTORA cameras [11], [7], and is based on building an iteratively-updated comparison image of a current field of view using the numerically efficient running median algorithm, as well as threshold image using the running similarly constructed median absolute deviation estimate, and then comparison of every new frame with them, extracting candidate transient objects and analyzing lists of these objects from the consecutive frames. Then it filters out noise events, extracts the meteor trails by their generally elongated shape on a single frame, collects the events corresponding to moving objects into focal plane trajectories, etc.

Every 100 frames acquired by a channel are being summed together, yielding “average” frames with 10 s effective exposure and better detection limit. Using these frames, the astrometric calibration is being performed using locally installed ASTROMETRY.NET code [12]. Also the rough photometric calibration is being done. These calibrations, updated every 10 seconds, are used for measuring positions and magnitudes of transients detected by the real-time differential imaging pipeline. The “average” frames are stored permanently (in contrast to “raw” full-resolution data which is typically erased in a day or two after acquisition) and may be used later for studying variability on time scales longer than 10 s.

The Mini–MegaTORTORA typically observes every sky field continuously for 1000 seconds before moving to the next pointing. Before and after observing the field with high temporal resolution, the system acquires deeper “survey” images with 60 seconds exposure in white light in order to study variability of objects down to 14–15 magnitude on even longer time scales; typically, every point of the northern sky is covered by one or more such images every observational night.

As the first step of analysis of these survey data, we implemented the transient detection pipeline

based on comparison of positions of objects detected in our images with Guide Star Catalogue v2.3.2, as well as with Minor Planet Center database. This pipeline routinely detects tens of known asteroids every night, and sometimes – the flares of dwarf novae and other transients.

The full-scale photometric pipeline for survey images is still in preparation, as the precise photometry of these frames turned out to be quite a difficult task due to the large size of point spread function of a Canon objective with extended wings harbouring up to 40% of light. This leads to severe photometric errors in typical stellar fields, significantly crowded even outside the Galaxy plane. Now we are implementing the PSF-fitting code optimized for the accurate measurement of Mini–MegaTORTORA survey images and hope to finish it in 2016.

Below we briefly describe some of the data products of the high temporal resolution pipeline.

3.1. Meteors

The meteors are probably the most frequent astrophysical phenomena flashing in the sky, and easiest to detect in the Mini–MegaTORTORA data stream. The meteor detection is performed in a differential image based on their typically elongated shapes. Then the elongated trails from consecutive frames, having similar directions of elongation, are being merged into a single event. A dedicated analysis subroutine extracts the meteor trail using Hough transformation, detects its extent in every frame, and estimates brightness along the trail, light curve, trajectory, angular velocity and duration. The majority of events are observed in white light (then the brightness is calibrated to V magnitude), while some are being observed in Johnson-Cousins B, V and R photometric filters simultaneously. For such events, the colors are also derived automatically (see Figure 5). All these data are stored in the database and are available online¹.

We are not able to perform any parallactic observations of meteors now (though we are working on installing the second version of Mini–MegaTORTORA which will allow us to measure meteor parallaxes). However, huge amount of meteors measured every night might, in principle, allow detecting the radiants of meteor streams using purely statistical methods. Figure 3 shows the density of intersections of meteor trails from the night corresponding to 2014 Geminids, and the radiant is clearly visible here. Such radiant maps are built automatically and available online for every night.

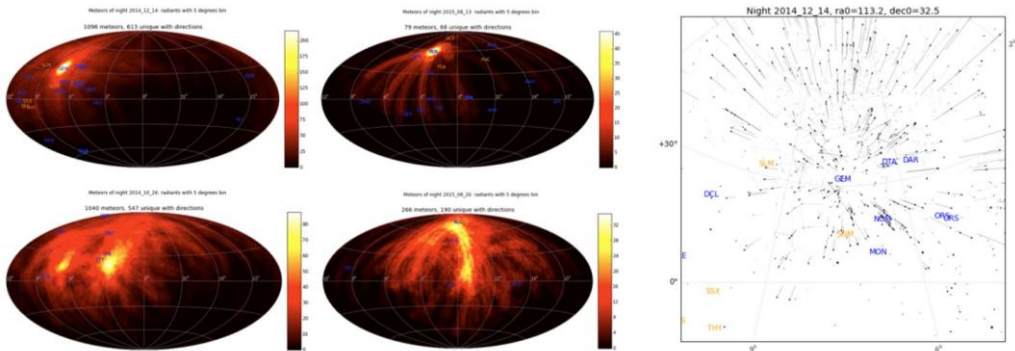


Fig3. Density of intersections of meteor trails from the night corresponding to the peak of 2014 Geminids (left) and meteor trails corresponding to the Geminids shower in the gnomonic projection (right).

¹ The database is published at <http://mmt.favor2.info/meteors> and <http://astroguard.ru/meteors>

The database also contains the full-resolution imaging data, which may be useful for studying the peculiar events like meteors consisting of several particles flying in parallel, or the complex evolution of long lasting tails of brighter meteors due to atmospheric motions (see Figure 4).

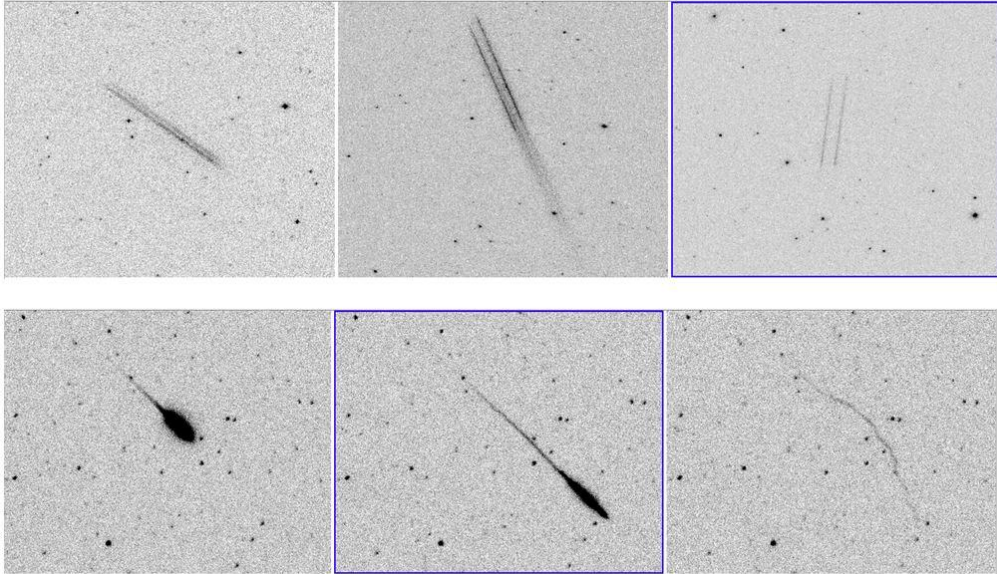


Fig4. Example of multi-particle meteor trails (top) and the complex temporal evolution of a bolide trail in the atmosphere (bottom).

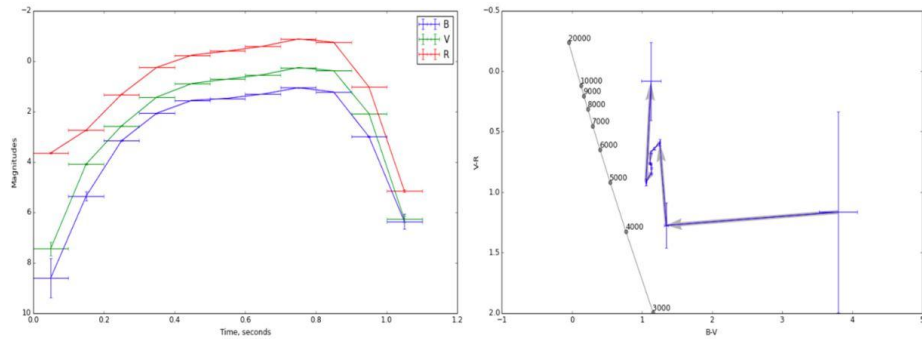


Fig5. Example of a multi-color light curve of a meteor detected by Mini-MegaTORTORA (left) and the corresponding evolution on a two-color diagram (right).

3.2. Satellites

Detection of rapidly moving objects is implemented by comparing the lists of objects detected in consecutive differential frames and extracting those ones which move along (nearly) straight lines with (slowly varying or) constant velocity in the focal plane. This is being done iteratively starting from the third appearance of the object in the frame. After initial detection, the object is being tracked until it fades below the detection limit or leaves the field of view. Afterwards its trajectory and light curve are

stored for a more detailed analysis.

The accuracy of coordinate determination of the real-time transient detection pipeline, which is typically 5-30'', is quite enough for reliable identification of satellites on low and medium-altitude orbits using publicly available orbital elements [13], [14]. We are routinely performing such identification and as a result acquire a large amount of high resolution photometric information on these objects, which we publish online as a fully searchable online database of satellite light curves².

The database includes the following parameters for every satellite track observed: light curves in apparent and standard magnitudes (calibrated to the distance 1000 km and the phase angle 90°), distance and phase angle over time, whether the satellite was inside the penumbra, and a light curve period if it displays a periodicity. For every satellite it also contains the general information and classification of activity taken from public sources (active, inactive, debris etc), as well as variability type estimated by us (periodic variability, variable but aperiodic, non-variable). The number of periodic light curves is up to 20%.

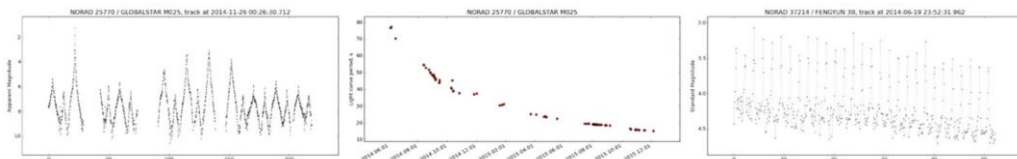


Fig 6. Light curve of a freely rotating inactive satellite detected by Mini-MegaTORTORA (left), its period evolution over time due to interaction with atmosphere and residual technological processes (center) and the rapid variability of an active satellite due to stabilized antenna rotation with 1.8 s period (right).

Periodicity of a satellite light curve may be caused either by rotation of an object as a whole (which is typical for both inactive satellites, upper stages or debris, and active satellites stabilized by rotation), or by some rotating element like an antenna (see Figure 6). The rotation period of inactive objects often changes over time due to some residual technological processes inside the object itself.

3.3. Fast optical flashes

The original aim of Mini-MegaTORTORA differential imaging pipeline is the detection of rapid optical flashes of astrophysical origin, which is being performed by detecting the stellar-like objects visible in several consecutive differential images (to filter out sporadic noise events and cosmic rays) and not changing their position. As of now, we are still in process of calibrating this part of pipeline, as it is being highly contaminated by stellar scintillations and detector noise spikes. We are, however, able to detect a number of rapid flashes caused the rotation of high-altitude slowly moving satellites, which produce short (up to half a second) events with negligible motion. Such flashes are practically indistinguishable from anticipated astrophysical bursts, and may be filtered out only by comparing their positions with predicted ones of known satellites, which is being done using the NORAD database [13].

An example of such an event is shown in Figure 7.

As of now, we did not detect any rapid flash not coincident with such a high-altitude satellite and not having the light curve identical to ones produced by such satellites.

² The database is published at <http://mmt.favor2.info/satellites> and <http://astroguard.ru/satellites>

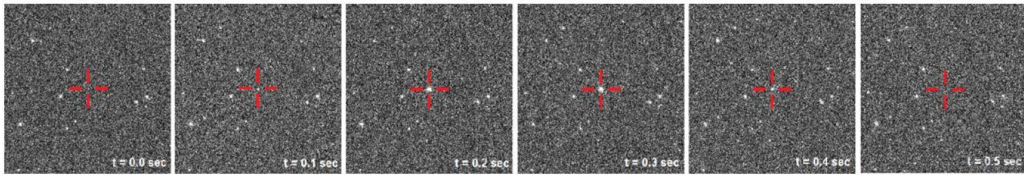


Fig7. Rapid optical flash detected by MMT, with duration less than 0.5 s and peak brightness reaching $\sim 6.5^m$. The flash coincides with the high-altitude passage of MOLNIYA satellite.

4. Conclusions

The Mini–MegaTORTORA (MMT-9) instrument is already operational and shows the performance close to the expected one. We hope it will be useful for studying various phenomena in the sky, both astrophysical and artificial in origin. We expect it to be used for studying faint meteoric streams crossing the Earth orbit, for detecting new comets and asteroids, for finding flashes of flaring stars and novae, studying variable stars of various classes, detecting transits of exoplanets, searching for bright supernovae and optical counterparts of gamma-ray bursts.

The novelty of the MMT is its ability to re-configure itself from a wide-field to narrower-field instrument, which may open new ways of studying the sky, as it may, in principle, autonomously perform thorough study of objects it discovers – to simultaneously acquire three-color photometry and polarimetry of them.

Acknowledgements

This work was supported by the grants of RFBR (No. 09-02-12053, 12-02-00743-A), by the grant of European Union (FP7 grant agreement number 283783, GLORIA project). Mini–MegaTORTORA belongs to Kazan Federal University and the work is performed according to the Russian Government Program of Competitive Growth of Kazan Federal University. Observations on Mini–MegaTORTORA are supported by the Russian Science Foundation grant No. 14-50-00043.

References

- [1] Beskin, G., Bondar, S., Karpov, S., Plokhotnichenko, V., Guarnieri, A., Bartolini, C., Greco, G., Piccioni, A., & Shearer, A. 2010a, *Advances in Astronomy*, 2010
- [2] Beskin, G. M., Karpov, S. V., Plokhotnichenko, V. L., Bondar, S. F., Perkov, A. V., Ivanov, E. A., Katkova, E. V., Sasyuk, V. V., & Shearer, A. 2013, *Physics Uspekhi*, 56, 836
- [3] Beskin, G., Karpov, S., Bondar, S., Perkov, A., Ivanov, E., Katkova, E., Sasyuk, V., Biryukov, A., & Shearer, A. 2014, in *Revista Mexicana de Astronomia y Astrofisica Conference Series*, Vol. 45, *Revista Mexicana de Astronomia y Astrofisica Conference Series*, 20
- [4] Biryukov, A., Beskin, G., Karpov, S., Bondar, S., Ivanov, E., Katkova, E., Perkov, A., & Sasyuk, V. 2015, *Baltic Astronomy*, 24, 100
- [5] Zolotukhin, I., Beskin, G., Biryukov, A., Bondar, S., Hurley, K., Ivanov, E., Karpov, S., Katkova, E., & Pozanenko, A. 2004, *Astronomische Nachrichten*, 325, 675
- [6] Karpov, S., Beskin, G., Biryukov, A., Bondar, S., Hurley, K., Ivanov, E., Katkova, E., Pozanenko, A., & Zolotukhin, I. 2005, *Nuovo Cimento C*, 28, 747
- [7] Karpov, S., Beskin, G., Bondar, S., Guarnieri, A., Bartolini, C., Greco, G., & Piccioni, A. 2010, *Advances in Astronomy*, 2010

- [8] Molinari, E., Bondar, S., Karpov, S., Beskin, G., Biryukov, A., Ivanov, E., Bartolini, C., Greco, G., Guarnieri, A., Piccioni, A., Terra, F., Nanni, D., Chincarini, G., Zerbi, F., Covino, S., Testa, V., Tosti, G., Vitali, F., Antonelli, L., Conconi, P., Malaspina, G., Nicastro, L., & Palazzi, E. 2006, *Nuovo Cimento B*, 121, 1525
- [9] Beskin, G., Karpov, S., Bondar, S., Greco, G., Guarnieri, A., Bartolini, C., & Piccioni, A. 2010b, *ApJ*, 719, L10
- [10] Beskin, G. M., Karpov, S. V., Bondar, S. F., Plokhotnichenko, V. L., Guarnieri, A., Bartolini, C., Greco, G., & Piccioni, A. 2010c, *Physics Uspekhi*, 53, 406
- [11] Beskin, G., Biryukov, A., Bondar, S., Hurley, K., Ivanov, E., Karpov, S., Katkova, E., Pozanenko, A., & Zolotukhin, I. 2004, *Astronomische Nachrichten*, 325, 676
- [12] Lang, D., Hogg, D. W., Mierle, K., Blanton, M., & Roweis, S. 2010, *AJ*, 139, 1782
- [13] US Department of Defence. 2015, Database of satellite orbital parameters, available at <http://www.space-track.org/>
- [14] McCants, M. 2015, Satellite Tracking TLE page, available at <https://www.prismnet.com/~mmccants/tles/index.html>

Baksan Neutrino Observatory of the INR RAS: current state and prospects

V. V. Kuzminov

Baksan Neutrino Observatory of the INR RAS, Neutrino, KBR, Russia; bno_vvk@mail.ru

Abstract An overall view of the Baksan Neutrino Observatory of the INR RAS infrastructure is presented. Ground-based and underground facilities used to study cosmic rays, rare nuclear reactions and decays, to register solar neutrino, to observe various geophysical phenomena are described. Some main results obtained with these facilities and prospects are given.

Keywords: Underground Physics, Neutrino, Supernovae

The Baksan Neutrino Observatory of the Institute for Nuclear Research of the Russian Academy of Sciences (BNO INR RAS) is situated at the foot of the Andyrchy Mountain in the Baksan valley of

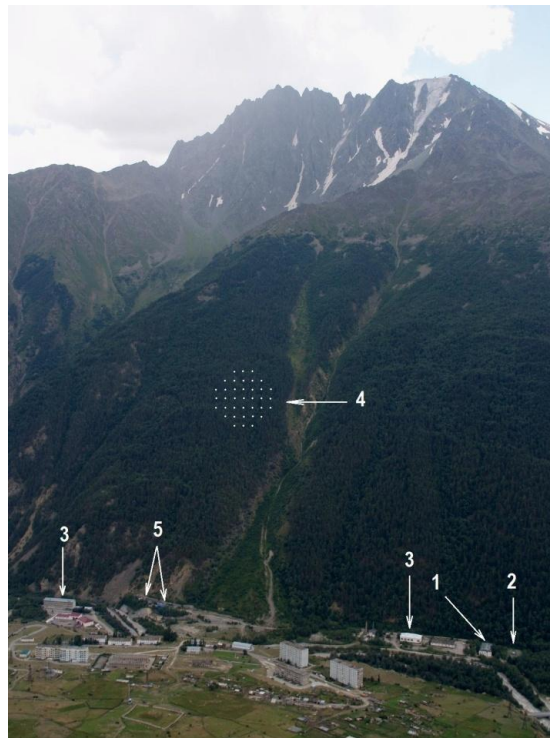


Fig1. The overview of BNO INR RAS and Neutrino village: 1) the “Elling” building with “Carpet” detection facility; 2) the shallow underground hall with “Carpet-2” detection facility; 3) laboratory’s buildings; 4) the schematic view of “Andyrchy”-array at the mountain slope; 5) entrances to the “Main” and “Auxiliary” adits.

Kabardino-Balkarian Republic of the Russian Federation. The Observatory is intended for carrying out investigations in the fields of the cosmic rays physics, neutrino astrophysics and non-accelerator nuclear physics [1], [2]. The Observatory comprises a series of ground-based and underground installations. The overview of BNO INR RAS and Neutrino village is shown in Fig.1.

The ground-based complex of BNO INR RAS

1. “Carpet”

In 1973 the first facility of the Observatory came into operation. It was the ground-based detection facility “Carpet” composed of 400 standard scintillation detectors situated in the experimental hall called “Elling” [3]. Each detector is a rectangular aluminum tank (70 cm·70cm·30cm) filled with liquid scintillator on the base of white spirit (a high purity kerosene fraction of petroleum). Each tank is viewed by PMT (15 cm in diameter) through a viewing port mounted on the central round hole of the larger face of the tank. Analysis of the amplitude distribution of signals and of their delay in arrival to the registering device allows one reconstructing the spatial distribution and direction of particles of an extensive air shower. This ground-based facility of 200 m² shown in Fig.2 is an exact replica of the eight-layer one of the Baksan Underground Scintillation Telescope that came into operation later.



Fig2. The overview of the “Carpet” facility.

The “Carpet” facility was targeted to study primary cosmic rays of $5.7 \cdot 10^9 \div 10^{16}$ eV, mechanisms and characteristics of their interaction with particles of the atmosphere by registering a single secondary component together with EAS generated in such interactions. Six outdoor points, each containing nine scintillation detectors, have been added to the central multiple-unit detector. Four of these points are distributed symmetrically on a circle of 30 m radius, and two points are on a circle of 40 m radius with regard to the “Carpet”’s center. A neutron monitor in a separate compartment of the basic hall is targeted

to register neutrons generated by cosmic rays.

“Carpet” (now “Carpet-2” [4]) performance was significantly improved after coming into operation in 1998 of one section (the middle one) of the three-sectioned large underground Muon Detector facility (MD). The middle section is at ~ 40 m from the “Carpet”’s center. MD is under 2 m layer of the ground (5 m w.e.) which absorbs the soft c.r. component and is composed of 175 scintillator detectors (1 m^2 each and made of plastic scintillator of 5 cm thickness). The continuous registering area of the facility is 175 m^2 ($5 \text{ m} \times 35 \text{ m}$). The threshold energy for muons is 1 GeV. The sensitivity of the facility is 0.006 particles/ m^2 . The creation of “Carpet-3”, the advanced version of “Carpet-2”, is now in progress. It is supposed to be a multipurpose facility registering cosmic rays. Its main purpose would be to study the knee of the c.r. spectrum. “Carpet-3” would register the following components of EASs: 1) electron and photon; 2) muon (with a threshold of 1 GeV); 3) hadron [5].

Analysis of the obtained data allowed one to interpret the presence of multi-jets showers as a result of generation of streams of particles with large transverse momentum, and to evaluate the cross-section of this process in hadron-hadron interactions for the range of energies up to 500 GeV [6]. This experimental result was the first one to confirm quantum chromodynamics predictions and was published before the SPS-collider in CERN had measured this value.

Large counting rate of single muons from cosmic rays ($\sim 4.3 \cdot 10^4 \text{ s}^{-1}$) allows high statistical accuracy even for small time intervals (0.003% for 4 min) and, as a consequence, makes it possible to observe short-time periodic variations (micro-variations). None of these have been found with the “Carpet” array at a confidence level of 0.001%. During this research work a new type of sporadic temporary variations characterized by small time was discovered and attributed to meteorological effects [7]. Their strong correlation with the electric field of atmosphere (such variations occur only during thunderstorms) allowed one to explain this phenomenon and quantitatively describe it [8]. The gigantic increase of cosmic ray intensity during powerful solar burst on September 29, 1989 is one of the most interesting examples of temporary variations in the muon counting rate. Particles of solar origin with energies up to 10^{10} eV were observed for the first time in such an event, and it was the “Carpet” facility that provided the most evident and accurate data at that time [9].

Studying showers of low energy corresponding to primary cosmic rays (c.r.) of 10^{13} eV revealed anisotropy of the latter. The first and second harmonics have been found in the count rate of these showers for sidereal time. C.r. anisotropy for 10^{13} eV was calculated to be $0.05 \pm 0.005\%$ [10].

Air showers of $\geq 10^{14}$ eV are continuously registered and the data are analyzed along several lines: search for point sources of gamma-quanta of the same energy [11]; search for signals from extended gamma-ray sources (mainly in the galactic plane) [12]; search for c.r. anisotropy at these energies [13]; search for x-ray and gamma-ray bursts for known sources [14]. One of the interesting results is the registration of the burst in Crab Nebula, on February 23, 1989. It was the team of scientists of “Carpet” that first published the result [15]. Later it was confirmed by teams of Kolar Gold Mine (India) and EAS Top (LNGS) facilities.

Studying air neutron flux variation involves continuous recording of neutron monitor count rate; the data obtained are sent across internet to www.nmdb.eu-nest-seach.php. Analysis of the parameters of variations presents information used in further studies of characteristics of solar bursts and their effect on the interplanetary magnetic field.

The “Carpet-2” facility allows studying EAS muon component. The dependence of the mean number of muons of $\geq 1 \text{ GeV}$ (N_μ) registered by MD on the total number of EAS particles (N_e) has been found as $N_\mu \sim N_e^\alpha$, where $\alpha = 0.8$. Analysis of the data obtained with MD and “Carpet” allowed scientists to significantly increase the sensitivity of the experiment searching for local sources of ultra high-energy gamma-quanta, to start studying chemical composition of primary cosmic rays of $E \geq 10^{14}$ eV, and to carry out investigation of variations of muons with energies above 1 GeV [16].

2. “Andyrchy”-array

In 1996 the “Andyrchy” array targeted to register EASs with $E_0 \geq 10^{14}$ eV came into operation. It consists of 37 standard detectors of the same type as those of “Carpet-2” (1 m² each, plastic scintillator) evenly spread over the area of 45.000 m² on the slope of the Andyrchy mountain with a maximum gradient of altitude of 150 m and at a distance of 40 m from each other [17]. The central detector of “Andyrchy” is located over BUST, and a vertical thickness of mountain rock separating them is 350 m. It is important to secure the performance of a facility located on the mountain slope during periods of thunderstorm activities. This task has been successfully solved by registering pulses of electromagnetic oscillations generated in lighting discharges. As the increase in amplitude of the pulses with thunderstorm approaching reaches a specified threshold, the electrical network (at the point where the data are collected) automatically disconnects to form short segments, which are switched off from the detector and are re-loaded to the dischargers. The network configuration resumes its functioning after the thunderstorm is over [18].

The following researches are carried out at “Andyrchy”: anisotropy of cosmic rays with $E_0 \geq 10^{14}$ eV [19]; search for gamma-ray bursts with hard energy spectrum [20] and search for evaporating Primordial Black Holes [21].

The “Andyrchy” array and BUST is a complex of two facilities, situated one upon the other. It is used to study the primary cosmic ray spectrum and its composition in the energy region of the knee, a change in the spectral index at about $3 \cdot 10^{15}$ eV [22].

The underground complex of the BNO INR RAS facilities

Schematic view of a longitudinal section of the BNO adit and Andyrchy slope is shown in Fig.3 presenting the locations of different underground laboratories and the dependence of underground muon flux on the distance from the entrance. Descriptions of the laboratories are adduced below.

1. The Baksan Underground Scintillation Telescope

The Baksan Underground Scintillation Telescope (BUST) has come into operation in 1978. It was targeted to solve various tasks in astrophysics, cosmic rays physics and elementary particle physics [23]. BUST is situated in the underground hall of ~ 12.000 m³ at a distance of 550 m from the entrance to the underground horizontal tunnel. The effective thickness of the ground above BUST is 850 g/cm². The telescope is a rectangular building of 11.1 m height and 280 m² base. The blocks of the building are made of low-radioactive concrete. Its four horizontal and four vertical planes are covered with standard scintillation detectors (3180 in total). The total mass of the telescope is 2500 t, that one of the scintillator is 330 t. Signals are taken from each of 3180 standard scintillation detectors and processed in the same way as those of the “Carpet” array. The threshold of integral discriminator corresponds to energy release of 10 MeV in the detector. Signals from individual “A - T” converters, from integral discriminators, and anode signals from a group of detectors from each of 8 layers of the telescope go to the registering devices in the apparatus hall. Analysis of the signals allows one to determine the coordinates of the detectors through which particles have passed and their arrival directions. The information from registering devices together with that of absolute- and relative-time systems goes via a direct channel to DAS (data accumulation system). Every 15 minutes the collected information that has been preliminary processed goes through the optical fiber to the BUST server. About ten diagnostic programs are running simultaneously providing information on the performance of all the systems of the telescope.

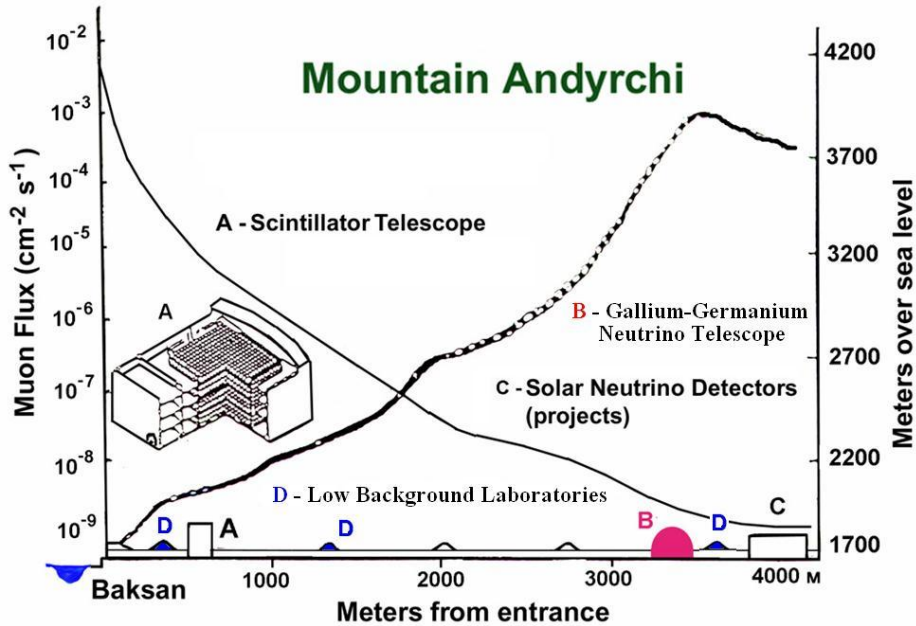


Fig3. Schematic view of a section of the Andyrchi slope along the adit (right scale) and dependence of underground muon flux on the laboratory location depth (left scale).

Though relatively small, the thickness of the mountain rock above the telescope reduces the background caused by c.r. by 3600 times in comparison with that on the surface (the count rate of single muons with $E > 0.2$ TeV is 12 s^{-1}). The reduced c.r. background allows scientists to study problems related to rare processes registration, such as measurement of the muon flux generated by high-energy neutrino; search for neutrino bursts accompanying a star collapse in the Galaxy, and others. At the same time, the residual c. r. intensity in the underground environment allows one to carry out a research into a wide range of tasks of cosmic ray physics: anisotropy of c.r. of $> 10^{12}$ eV, chemical composition of primary c.r. of $10^{12} \div 10^{16}$ eV, interaction of muons of > 1 TeV with matter, and others.

The following are the most important results obtained over the years of research:

- muon flux generated by atmospheric neutrino of cosmic rays in the rock under BUST has been measured to be $I_{\mu}^{\nu} = (2.60 \pm 0.15) \cdot 10^{-13} \text{ cm}^{-2} \text{ s}^{-1} \text{ sr}^{-1}$ [24];
- one of the first limits obtained for the oscillation parameters of atmospheric neutrinos of $\nu_{\mu} \rightarrow \nu_{\tau}$ and $\nu_{\mu} \rightarrow \nu_{e}$ types [25];
- a limit on high-energy neutrino flux from local sources in the galactic plane;
- the best limit, for a time, on the slow and heavy magnetic monopoles $P \leq 5.5 \cdot 10^{-16} \text{ cm}^{-2} \text{ s}^{-1} \text{ sr}^{-1}$ [26];
- the amplitude $(12.3 \pm 2) \cdot 10^{-4}$ and the phase 1.6 ± 0.8 (in sidereal time) of the first harmonic of c.r. anisotropy have been measured [19];
- data accumulated during 34 years (live time 29.8 years) of monitoring the Galaxy in studying neutrino bursts from gravitational stellar collapses gave a limit on the frequency of bursts f to be $f < 0.077 \text{ yr}$ (90% C.L.) [27];
- neutrino flux from SN1987A that collapsed in the Large Magellan Cloud was registered simultaneously with USA, Italy and Japan facilities [28];

- proton stability had been tested in 1981-1983 years and the limit for the half-life of proton was achieved: $T_{1/2} > 0.9 \cdot 10^{31}$ years [29];
- the data obtained in studying of chemical composition of primary c. r. of 10^{13} - 10^{15} eV are in good agreement with the results of direct measurements for lower energies (10^{12} eV) [30];
- the technique to separate hadronic and electromagnetic cascades, based on registration of π - μ -e-decays accompanying the cascade, has been developed and realized in an experiment [31];
- total cross-section of hadronic photoabsorption has been measured for photons with energies up to 10 TeV [32];
- the experimental data on cross-section of γ -N interaction for the range of energies of 40 - 130 GeV have been obtained using the measured value of the nuclear cascades fraction. These data together with those obtained at DESY's HERA collider, confirm the effect of more rapid growth of cross-section of photon-hadron interaction than that of hadron-hadron interactions [33].

A set of preparatory and research works is carrying out at the BNO INR RAS at present time directed to a development of a project of a large liquid scintillator detector with a mass of 5-10 kt which could be built at the ~ 4000 m w.e. depth. The detector is intended for the investigations of the neutrino and antineutrino fluxes from different natural and artificial sources such as decays of the radioactive elements in the Earth, thermo-nuclear reactions in the SUN, super-nova bursts, nuclear reactors and others.

2. Low-background Laboratories

Low-Background Laboratories (LBL) carry out research of extremely rare reactions and decays with energy release up to 4 MeV. For these studies one needs to diminish not only the background caused by cosmic rays but also that one due to the decay of natural radioactive elements always present in the environment. The latter task has been solved by screening the experimental underground facility with a combination of layers of ultrapure shielding materials absorbing radiation, and by making sure that the facility is made of ultrapure material. The researches carried out in the LBL are search for various modes of double beta-decay of a number of isotopes; search for candidate-particles for dark matter of the Universe; test of the law of electrical charge conservation and many others.

There are three underground laboratories, situated at a different depth, where LBL researches are carried out: 1) low-background chamber at a depth of 660 m w.e, 385 m from the entrance to the tunnel, useful area of 100 m^2 , put into operation in 1974 [34]; 2) chamber for precise measurements at 1000 m w.e. depth, 620 m distance from the entrance, useful area is 20 m^2 , put into operation in 1985; 3) deep underground low-background laboratory (DULB-4900) at 4900 m w.e. depth, 3670 m from the entrance, useful area is 200 m^2 , put into operation in 1993, modernized in 2008 [35]. Cosmic ray flux in these three chambers is reduced by $2 \cdot 10^3$, $8 \cdot 10^3$, and 10^7 , respectively.

A number of low-background facilities based on semiconductor, gaseous and scintillation detectors have been designed, made and used over the years in various experiments such as: study of cosmogenic radioactive isotope distribution in the samples of moonrock brought by Automatic Interplanetary Stations Luna-16, Luna-20 and Luna-24; test of the hypothesis of cosmic ray intensity being permanent during the last several hundreds of thousands of years performed by measuring the content of cosmogenic isotope ^{81}Kr in the atmospheric air [36]; investigation of the radioactive purity of industrial metal and a selection of those to be used in the construction of low-background facilities with the lowest possible natural radioactive contamination [37]; the experiments searching for two-neutrino and neutrinoless double-beta-decay of isotopes of ^{76}Ge , ^{100}Mo , ^{150}Nd , ^{136}Xe [38] – [41]; for 2K-capture in ^{78}Kr and ^{124}Xe isotopes [42], as well as other experiments have been carried out.

A possibility of a creation of the new low-background cryogenic laboratory in the existing cavity at the 2620 m distance point of the Main Adit (~ 3000 m w.e.) examines in the BNO at present time.

Investigation of 0.01-4000 eV energy-releases from different rare nuclear processes could be done in the laboratory with cryogenic calorimeters having the best energy resolution in comparison with detectors of the other types.

3. Gallium-Germanium Neutrino Telescope

Gallium-Germanium Neutrino Telescope (GGNT) is targeted to measure solar neutrino flux which carries unique information on thermonuclear reactions in the central regions of the Sun as well as on neutrinos themselves. Since 1986 the experiment has been carried out within the frames of the Soviet American Gallium Experiment (SAGE) [43].

The experiment is based on the reaction (${}^{71}\text{Ga} + \nu_e \rightarrow {}^{71}\text{Ge} + e^-$). The advantage of this reaction is its low threshold of 0.233 MeV. The pp-neutrinos, having energy up to 0.423 MeV and constituting the main portion of solar neutrino flux, can be registered through this reaction. Radioactive isotope, ${}^{71}\text{Ge}$ produced in this reaction undergoes decay by electron capture, with $T_{1/2}=11.4$ days half-life. Registering ${}^{71}\text{Ge}$ decays allows one to determine the number of interacting neutrinos and to calculate the solar neutrino flux.



Fig4. A view of the GGNT hall.

The underground complex of GGNT laboratories is situated at a distance of 3.5 km from the entrance to the tunnel, at a depth of 4700 m w.e. where muon flux is reduced by 10^7 times due to natural mountain rock shielding, and is $(3.0 \pm 0.1) \cdot 10^{-9} \text{ cm}^{-2} \text{ s}^{-1}$. The main hall of this complex is of $60 \cdot 10 \cdot 12 \text{ m}^3$ dimensions. A view of the hall is shown in Fig.4. To reduce the background caused by neutrons and gamma-ray coming from the surrounding natural rocks the hall is encased in concrete of low-radioactivity and steel sheets, of 600 mm and 6 mm thickness, respectively. The flux of neutrons with energies of 1.0-11 MeV in the laboratory is $\leq 2.3 \cdot 10^{-7} \text{ cm}^{-2} \text{ s}^{-1}$. The underground complex of GGNT laboratories includes rooms for: analytical chemistry, ${}^{71}\text{Ge}$ decay registration system, low-background semiconductor Ge-detector and a number of other auxiliary subdivisions. About 50 t of metallic gallium in a melted state is placed into seven chemical reactors. Natural abundance of ${}^{71}\text{Ga}$ isotope in gallium is 39.6%. Given the expected solar neutrino flux of $6 \cdot 10^{10} \text{ cm}^{-2} \text{ s}^{-1}$, there should be produced 25 atoms of ${}^{71}\text{Ge}$ during one month of 50 t metallic gallium exposition in the underground conditions. A unique and effective

technique (90% extraction efficiency achieved and kept over the years) has been developed to extract ^{71}Ge atoms from the 50 t melted metallic gallium target containing $5 \cdot 10^{29}$ of ^{71}Ga atoms. The periodicity of this extraction procedure which is the basic technological process of the telescope is 30 days. The gas GeH_4 is synthesized on the base of the extracted stable Ge-carrier atoms added to the target to extract the generated ^{71}Ge atoms. It constitutes the main component of the gas mixture filled the proportional counter to register ^{71}Ge decays in the underground registration system of GGNT during 4 months, thereby covering ≥ 10 half-life periods of ^{71}Ge . Then, within the period of two months, the background is measured. Data from the proportional counter are transmitted in the on-line mode, via fiber-optic channel, to the local server of the GGNT ground-based laboratory. The whole cycle of operations called a run includes ^{71}Ga -target exposition, extraction of ^{71}Ge , and measurement of ^{71}Ge decays.

The analysis of data obtained in the period of January 1990 - December 2010, yielded $65.1^{+3.7}_{-3.8}$ SNU [44] (1 SNU = 1 interaction per second in the target containing 10^{36} atoms of an active isotope). The result obtained in the SAGE experiment constitutes 51 % from the value of 127.9 ± 8.1 SNU calculated within the frames of the Standard Solar Modal (SSM) BPS08. The SSM value does not take neutrino oscillation into account. This result of SAGE experiment together with the results of other underground experiments registering solar neutrino (Homestake, USA; GALLEX/GNO, LNGS; Kamiokande/SuperK, Japan; SNO, Canada) allows to calculate estimations of :

- pp-neutrino flux that reaches the Earth in the form of electron neutrino (electron flavor), $[(3.4 \pm 0.47) \cdot 10^{10} \text{ cm}^{-2} \text{ s}^{-1}]$ [44];
- total neutrino flux produced in pp-reactions inside the Sun and reaching the Earth in various flavors (electron-, muon- and tau-neutrino) due to oscillation of original electron neutrino, $[(6.0 \pm 0.8) \cdot 10^{10} \text{ cm}^{-2} \text{ s}^{-1}]$ [44].

The experimental value of the total neutrino flux is in good agreement with the one predicted by SSM, $(5.95 \pm 0.06) \cdot 10^{10} \text{ cm}^{-2} \text{ s}^{-1}$.

To test and calibrate the techniques used in the SAGE experiment a ^{51}Cr source of $1.91 \cdot 10^{16} \text{ s}^{-1}$ intensity emitting neutrinos of 747 keV (90%) and 430 keV (10%) was used. In this calibration experiment the ratio of the measured rate of ^{71}Ge production to the expected one caused by a source of given activity has been found to be 0.95 ± 0.12 [45].

Another calibration experiment was made with artificial neutrino ^{37}Ar source emitting 811 keV neutrinos of $1.51 \cdot 10^{16} \text{ s}^{-1}$ intensity. The same ratio of the ^{71}Ge production rates has been found to be $0.79^{+0.09}_{-0.10}$ [46].

The experiment BEST with the two concentric zones Ga-target and 3MCi artificial ^{51}Cr neutrino source is preparing at the BNO INR RAS now [47]. The goals of this experiment are to search for the short-baseline neutrino oscillation and to test of sterile neutrino hypothesis.

4. OGRAN facility

At a distance of 1350 m from the entrance to the main tunnel, the new laboratory is created to accommodate the Optoacoustic GRavitational ANtenna (OGRAN). The OGRAN facility has been constructed using principles of solid-state and laser interferometer gravitational antennae. Acoustic vibrations of solid-state detector (manufactured in the form of cylindrical aluminum bar with a central axial tunnel) induced by gravity wave are registered by optical resonator Fabry-Perot, whose mirrors are mounted on the far ends of the detector. Low noise of such an optical read-out system allows sensitivity of relative deformation to be of 10^{-18} for the detector of 2.5 t without any cooling procedure. This sensitivity is good enough to detect bursts of gravity wave radiation generated in relativistic cataclysms in the center of our Galaxy (~ 10 kpc) and its close vicinity (up to 100 kpc) according to optimistic scenarios. OGRAN is the cooperative project carried out by Institute for Nuclear Research of RAS,

Institute of Laser Physics of SB RAS and Moscow State University (Sternberg Astronomical Institute-SAI MSU).

Construction of the detector was finished in 2011; its installation in the underground laboratory was finished this year. The detector would come into operation in 2016. Measurements of gravity gradient background are supposed to be performed as search for neutrino and gravity events' correlation using simultaneous data of OGRAN and the BUST BNO.

5. Underground complex of Geophysical Facilities

Environmental parameters of the underground laboratory complex are held within stable limits; vibration and acoustic noises are lowered by many times in comparison with those on the surface. Such underground environment provides necessary conditions to carry out various geophysical researches securing their high sensitivity.

There are three underground geophysical laboratories situated at a different distance from the tunnel entrance and supplied with different measuring devices and instruments:

- 1) the laboratory of SAI MSU, at a distance of 530-610 m from the entrance to the tunnel; researches of the Earth strains are carried out with the high-sensitivity wide-band laser interferometer [48];
- 2) the geophysical laboratory No1, at ~1520 m; it is a nearby geophysical complex of the Schmidt Institute of Physics of the Earth RAS having tilt indicators (inclinometers), magnetic variometers, and earthquake detection station at its disposal;
- 3) the geophysical laboratory No2, at ~4000 m; it is a distant geophysical complex IPE RAS having tilt indicators, magnetometers, gravimeters, thermometers as well as earthquake detection stations pertaining to Geophysical Survey RAS.

Data obtained in geophysical experiments allow scientists to monitor seismic activity in the earth crust related to the sleeping volcano Elbrus which is at a distance of about 20 km from the underground geophysical complex of facilities [49].

Various researches at the Baksan Neutrino Observatory INR RAS are carried out in collaborations with Institutions all over Russia and the world. To name some of them, Kabardino-Balkarian State University, Federal South University, Moscow State University, National Research Nuclear University MEPhI, Schmidt Institute of Physics of the Earth RAS, Pushkov Institute of Earth magnetism, ionosphere and radiowaves propagation RAS (IZMIRAN), Polar Geophysical Institute RAS, Geophysical Survey RAS, Institute of Astronomy RAS, JINR, Kharkov National University (Ukraine), Institute of Nuclear Problems (Cosmic Ray Laboratory, Lodz, Poland), international collaborations AMORE, GERDA and EMMA. All these collaborations significantly increase the efficiency of the Baksan complex of ground-based and underground facilities in solving a wide range of problems in modern science.

References

- [1] A.A. Pomansky, "Baksan Neutrino Observatory of INR AS of USSR", *Atomnaya energiya*, v.44, (1978), 376-383. (in Russian)
- [2] V.V. Kuzminov "The Baksan Neutrino Observatory". *Eur. Phys. J. Plus* (2012) 127: 113.
- [3] E.N. Alekseev, V.V. Alekseenko, A.V. Voevodsky et al. "Scintillation detector of 200 m2 area for the cosmic rays registration", *Izvestiya Akademii Nauk SSSR. Seriya Fizicheskaya*, v.38, (1974), 1097-1100. (in Russian)
- [4] D.D. Dzhappuev, V.V. Alekseenko, V.I. Volchenko, et al. "Modernization of the Carpet-2 array of the Baksan Neutrino Observatory", *Bull. Russian Acad. Sci., Phys.*, 71, (2007), 525-527. (in Russian)

- [5] J. Szabelski, for the Carpet-3 collaboration, "Carpet-3 - a new experiment to study primary composition around the knee", *Nuclear Physics B (Proc. Suppl.)* 196 (2009) 371–374. (arXiv:0902.0252 [astro-ph.IM] , 2009.)
- [6] A.E. Chudakov, D.D. Dzhappuev, A.S. Lidvansky, V.A. Tizengauzen, V.P. Sulakov, G. Navarra. "Investigation of EAS with multicore structure". *Proc. of the 16th ICRC, Kyoto*, v.8, (1979), 222-226.
- [7] V.V. Alexeyenko, A.E. Chudakov, V.G. Sborchikov, and V.A. Tizengauzen, "Short perturbation of cosmic ray intensity and electric field in the atmosphere". *Proc. of 19th ICCR, La Jolla*, v.5, (1985), 352-355.
- [8] V.V. Alexeenko, N.S. Khaerdinov, A.S. Lidvansky, V.B. Petkov, "Transient variations of secondary cosmic rays due to atmospheric electric field and evidence for pre-lightning particle acceleration". *Physics Letters A* 301 (2002) 299-306.
- [9] V.V. Alexeenko, A.B. Chernyaev, A.E. Chudakov, N.S. Khaerdinov, A.M. Semenov, A.V. Voevodsky. "29 September 1989 GLE at Baksan Air shower Array (BASA)". *Proc. of the 23th ICRC, Calgary*, v.3, (1993), 163-166.
- [10] V.V. Alexeyenko, A.E. Chudakov, E.N. Gulieva, V.G. Sborshikov "Anisotropy of small EAS (~ 1013 eV)". *Proc. of 17th ICRC, Paris*, v.2, (1981), 146-149.
- [11] V.V. Alexeyenko, A.E. Chudakov, N.S. Khaerdinov, A.S. Lidvansky, G. Navarra, S.S. Ozrokov, V.V. Sklyarov, V.A. Tizengauzen. "A search for gamma-ray point sources with "The Carpet" shower array". *Proc. of 19th ICCR, La Jolla*, v.1, (1985), 91-94.
- [12] V.V. Alexeenko, Yu.M. Andreyev, A.E. Chudakov, A.S. Lidvasky, S.S. Ozrokov, V.V. Sklyarov, V.A. Tizengauzen, S.L. Osborn. "A search for DC and Sporadic emission from point sources with the Baksan EAS Array". *Proc. of the 23th ICRC, Calgary*, v.1, (1993), 440-443.
- [13] V.V. Alexeenko, Yu.M. Andreyev, A.E. Chudakov, A.S. Lidvasky, S.S. Ozrokov, V.V. Sklyarov, V.A. Tizengauzen, S.L. Osborn and A.W. Wolfendale. "An analysis of the Large-Scale anisotropy of cosmic ray in the Baksan Gamma-Ray astronomy experiment". *Proc. of the 23th ICRC, Calgary*, v.1, (1993), 483-485.
- [14] V.V. Alexeenko, Yu.M. Andreyev, A.E. Chudakov, A.S. Lidvansky, S.S. Ozrokov, V.V. Sklyarov, V.A. Tizengauzen, S.L. Osborn. "Studying flux limits for some UHE Gamma-Ray point sources from Baksan EAS Array data". *Proc. of the 22th ICRC, Dublin*, v.1, (1991), 289-292.
- [15] V.V. Alexeenko, Yu.M. Andreyev, A.E. Chudakov, A.S. Lidvasky, S.S. Ozrokov, V.V. Sklyarov, V.A. Tizengauzen, S.L. Osborn. "Burst like event observed by Baksan EAS Array from the Crab Nebule 23 Feb.1989". *Proc. of the 22th ICRC, Dublin*, v.1, (1991), 293-295.
- [16] D.D. Dzhappuev, A.U. Kudzhaev, V.V. Alexeenko, N.F. Klimenko, A.S. Lidvansky, O.I. Mikhailova, V.B. Petkov, Yu. V. Stenkin, A.L Tsybuk and A.B. Chernyaev. "Studying the Muon and Hadron Components of Extensive Air Showers with the Carpet-2 Array". *Bull. of the Russian Academy of Sciences, Physics*, vol. 73, № 5, (2009), 642-644.
- [17] E.N. Alekseev et al., "Air shower array 'Andyrchy' above the Baksan Underground Scintillation telescope", *Bull. Russ.Acad.Sci. Phys* 57, (1993) , 668.
- [18] V.I. Volchenko, G.V. Volchenko, A.N. Zaichenko, V.B. Petkov, V.Ya. Poddubnyi, and A.V. Radchenkov. "The Anti-Lightning Protection System of the Andyrchi Facility". *Instruments and Experimental Techniques.*, vol. 47, No.4, (2004), 35-43.
- [19] V.A. Kozyarivsky, A.S. Lidvansky, V.B. Petkov, and T.I. Tulupova, "Mean Diurnal Variations of Cosmic Ray Intensity as Measured by Andyrchi Air Shower Array ($E \geq 100$ TeV) and Baksan Underground Scintillation Telescope ($E \geq 2.5$ TeV)". arXiv:astro-ph/0406059v1, 2004.
- [20] V.B. Petkov, A.S. Pozanenko, V.M. Loznikov, A.N. Gaponenko, M.V. Andreev, and A.V. Sergeev, "Search for high energy gamma-ray bursts". *Astrophys. Space Sci. Trans.*, 7, (2011), 97-100.
- [21] V.B. Petkov, E.V. Bugaev, P.A. Klimai, M.V. Andreev, V.I. Volchenko, G.V. Volchenko, A.N. Gaponenko, Zh.Sh. Guliev, I.M. Dzaparova, D.V. Smirnov, A.V. Sergeev, A.B. Chernyaev, A.F. Yanin, "Searching for

- Very-High-Energy Gamma-Ray Bursts from Evaporating Primordial Black Holes”, *Astronomy Letters*, v. 34, No. 8, (2008), 509–514. (arXiv:0808.3093v1 [astro-ph], 2008)
- [22] V.B. Petkov, A.G. Bogdanov, M.M. Boliev, S.N. Karpov, V.V. Kindin, R.P. Kokoulin, K.G. Kompaniets, Yu.F. Novoseltsev, R.V. Novoseltseva, A.A. Petrukhin, A.V. Radchenkov, A.V. Shalabaeva, V.I. Volchenko, A.F. Yanin, I.I. Yashin, and A.N. Zaichenko, “A Search for Very High Energy Muons ($E_{\mu} > 100$ TeV) in EAS Around the Knee” *Proc. 28th ICRC, Tsukuba*, v.1, (2003), 57-60.
- [23] E.N. Alexeyev, V.V. Alexeyenko, Yu.M. Andreyev, V.N. Bakatanov, A.V. Butkevich, A.E. Chudakov, M.D. Galperin, A.A. Gitelson, V.I. Gurentsov, A.E. Danshin, V.A. Dogujaev, V.L. Dadikin, Ya.S. Elensky, V.A. Kozyarivsky, I.M. Kogai, N.F. Klimenko, A.A. Kiryushin, Yu.N. Konovalov, B.A. Makoev, V.Ya. Markov, Yu.Ya. Markov, Yu.V. Malovichko, N.A. Metlinsky, A.R. Mishelev, S.P. Miksheyev, Yu.F. Novoseltsev, V.G. Sborshikov, V.V. Sklyarov, V.I. Stepanov, Yu.V. Stenkin, Yu.R. Sulla-Petrovsky, T.I. Tulupova, A.V. Voevodsky, V.I. Volchenko, V.N. Zakideshev. “Baksan underground scintillation telescope”. *Proc. of 16th ICRC, Kyoto*, v.10, (1979), 276-281.
- [24] M.M. Boliev, A.V. Butkevich, A.E. Chudakov, B.A. Makoev, S.P. Mikheev, V.N. Zakideshev. “ ν -flax as measured by Baksan underground telescope”. *Proc. of 17th ICRC, Paris*, v.7, (1981), 106-109.
- [25] M.M. Boliev, A.V. Butkevich, V.N. Zakidyshev, B.A. Makoev, S.P. Mikheev, A.E. Chudakov. “Limitations on parameters of neutrino Oscillations According To Data Of The Baksan Underground Telescope”. *Yad.Fiz.* 34 (1981) 1418-1421. (in Russian).
- [26] Yu.F. Novoseltsev, M.M. Boliev, A.V. Butkevich, S.P. Mikheev and V.B. Petkov, "A search for massive magnetic monopoles at the Baksan Underground Scintillation Telescope (BUST)", *Nuclear Physics B (Proc. Suppl.)*, v.151, N1, (2006), 337-340.
- [27] R.V. Novoseltseva, M.M. Boliev, V.I. Volchenko, G.V. Volchenko, I.M. Dzaparova, M.M. Kochkarov, Yu.F. Novoseltsev, V.B. Petkov, P.S. Striganov, A. F. Yanin, " Update for 2010 of the results of the search for neutrino bursts from core collapse supernovae at the Baksan Underground Scintillation Telescope". *Proc. of 32nd International Cosmic Ray Conference (Beijing, China, August 11-18, 2011)*, v. 4, (2011), 152.
- [28] E.N. Alexeyev, L.N. Alexeyeva, I.V. Krivosheina, V.I. Volchenko. “Detection of Neutrino Sygnal from SN1987A, using the INR Baksan underground scintillation telescope”. *Proc. of the 2nd Int. Sym. UP-87, M.*, (1988), 85-93.
- [29] E.N. Alexeyev, V.N. Bakatanov, A.V. Butkevich, A.E. Chudakov, A.A. Gitelson, A.E. Danshin, G.P. Keidan, A.A. Kiryushin, A.V. Voevodsky, and B.E. Shtern. “Lower limit on the proton lifetime according to date from the Baksan underground scintillation telescope”. *JETP Lett.*, v. 33, No 12, (1981), 651-653.
- [30] V.N. Bakatanov, S.N. Boziev, A.E. Chudakov, Yu.F. Novosel'tsev, M.V. Novosel'tseva, A.V. Voevodsky “Primary cosmic ray composition at the $E=(10-1000)$ Tev per nucleon from simultaneous recording of underground induced cascades and accompanying multimuons”. *Proc. of 22 ICRC, Dublin*, v. 2, (1991), 17-20.
- [31] V.N. Bakatanov, Yu.F. Novosel'tsev, R.V. Novosel'tseva, Yu.V. Sten'kin, A.E. Chudakov. “Intensity of π - μ -e-decays at different depths according to Baksan underground scintillation telescop data”. *Izvestiya Akademii Nauk SSSR Seriya fizicheskaya*, v.49, No7, (1985), 1369-1372. (in Russian)
- [32] V.N. Bakatanov, Yu.F. Novosel'tsev, R.V. Novosel'tseva, A.M. Semenov, Yu.V. Sten'kin, A.E. Chudakov. “Cross section of photo-nuclear interaction at 0.9-10 TeV” *Pis'ma Zh.Eksp. Teor.Fiz.*, v.48, 1988, pp. 121-123. (in Russian)
- [33] Yu.F. Novoseltsev, G.M. Vereshkov. “Estimation of charm production cross section in diffractive hadronic interactions at high energies $\sqrt{s} > 1.8$ TeV”. *Nuclear Physics B, (Proc.Suppl)* v. 151, (2006), 209-212,
- [34] E.L. Kovalchuk, V.V. Kuzminov, A.A. Pomansky, G.T. Zatsepin. “Deep underground laboratory for low-radioactivity measurements”. *Proc. of the Int. Conf. on Low-Radioactivity Measurements and Applications, The High Tatras, Czechoslovakia, October 6-10, 1975. Comenius University, Bratislava, Slovenske Pedagogicke Nakladatel'ctvo*, (1977), 23-27.

- [35] Ju.M. Gavriljuk, A.M. Gangapshev, A.M. Gezhaev, V.V. Kazalov, V.V. Kuzminov, S.I. Panasenko, S.S. Ratkevich, S.P. Yakimenko. “Working characteristics of the New Low-Background Laboratory (DULB-4900, Baksan Neutrino Observatory)” arXiv: 1204.6424 [physics.ins-det] 01 May 2012 Nuclear Instruments and Methods in Physics Research A 729 (2013) 576–580.
- [36] V.V. Kuzminov, A.A. Pomansky. “ ^{81}Kr production rate in the atmosphere”. Proc. of the 18th Int. Cosmic Ray Conf., India, Bangalore, v.2, (1983), 357-360.
- [37] E.N. Kovalchuk, A.A. Pomansky, A.A. Smolnikov, A.H. Temmoev. “The radioactive contamination of different materials”. Proc. of the 3th Int. Conf. "The Natural Radiation Environment", Houston, USA, 1978, v.1, (1980), 661-666.
- [38] C.E. Aalseth, F.T. Avignone, R.L. Brodzinski, J.I. Collar, E. Garcia, D. Gonzales, F. Hasenbalg, W.K. Hensley, I.V. Kirpichnikov, A.A. Klimenko, H.S. Miley, A. Morales, J. Morales, A. Ortis de Solorzano, S.B. Osetrov, V.S. Pogosov, J. Puimeton, J.H. Reeves, C. Saenz, A. Salinas, M.L. Sarsa, A.A. Smolnikov, A.S. Starostin, A.G. Tamanyan, A.A. Vasenko, S.I. Vasiliev, A. Villar. “Recent Results from the IGEX Double-beta Decay Experiment”. Nucl. Phys. B (Proc.Suppl.), 48, (1996), 223-225.
- [39] A.A. Klimenko, S.B. Osetrov, A.A. Pomansky, A.A. Smolnikov, S.I. Vasilyev. “Observation of the excess of events in the experiment on the search for a two-neutrino double beta decay of ^{100}Mo ”. Pis'ma Zh.Eksp. Teor.Fiz., 51, No.11, (1990), 550-553. (in Russian)
- [40] A.A. Klimenko, S.B. Osetrov, A.A. Pomansky, A.A. Smolnikov, S.I. Vasilyev. “Search for a two-neutrino mode of double beta decay of the isotope ^{150}Nd ”. Pis'ma Zh.Eksp. Teor.Fiz., 58, No.3, (1993), 177-179. (in Russian)
- [41] Ju.M. Gavriljuk, A.M. Gangapshev, V.V. Kazalov, V.V. Kuzminov, S.I. Panasenko, S.S. Ratkevich, D.A. Zhantudueva, S.P. Yakimenko. “Results of a search for 2β -decay of ^{136}Xe with high pressure copper proportional counters in Baksan Neutrino Observatory INR RAS”. arXiv:1112.0859v2 [nucl-ex] 20 Dec 2011
- [42] Yu. M. Gavriljuk, A. M. Gangapshev, V. V. Kazalov, V. V. Kuzminov, S. I. Panasenko and S. S. Ratkevich. “Indications of $2\nu 2K$ capture in ^{78}Kr ” Phys. Rev. C 87, 035501 (2013)
- [43] J.N. Abdurashitov et al. (SAGE Collaboration), “Measurement of the solar neutrino capture rate with gallium metal”. Phys. Rev. C 60 055801 (1999); astro-ph/9907113
- [44] V.N. Gavrin “Contribution of Gallium experiments to the understanding of solar physics and neutrino physics”. Physics of Atomic Nuclei, v.76, N10,(2013), 1238-1243.
- [45] J.N. Abdurashitov et al. (SAGE Collaboration). “Measurement of the response of a gallium metal solar neutrino experiment to neutrinos from a ^{51}Cr source”. Phys. Rev. C 59 2246 (1999)
- [46] J.N. Abdurashitov et al. “Measurement of the response of a Ga solar neutrino experiment to neutrinos from a ^{37}Ar source”. Phys. Rev. C 73 045805 (2006)
- [47] V. Gavrin, B. Cleveland, S. Danshin, S. Elliott, V. Gorbachev, T. Ibragimova, A. Kalikhov, T. Knodel, Yu. Kozlova, Yu. Malyskin, V. Matveev, I. Mirmov, J. Nico, R.G.H. Robertson, A. Shikhin, D. Sinclair, E. Veretenkin, J. Wilkerson. “Current status of new SAGE project with ^{51}Cr neutrino source”. Phys. Part. Nucl. 46 (2015) 131-137
- [48] V.K. Milyukov, V.N. Rudenko, B.S. Klyachko, A.M. Kart, A.V. Myasnikov. “Wide-Band Laser Interferometer for Monitoring the Earth Strains”. In: Solid State Laser (Laser Optics'98). Proceedings of the International Society for Optical Engineering (SPIE). v.368, (1998), 116-121.
- [49] A.L. Sobisevich, V.K. Milyukov, A.V. Kozyreva, O.V. Rudenko, L.Ye. Sobisevich. “On a Resonant Properties of Magmatic Structures of the Elbrus Volcano”. In: Nonlinear Acoustic at the Beginning of the 21st Century (Proceedings of the 16th International Symposium on Nonlinear Acoustic, Moscow, 2002). v.1, Moscow: MSU, (2002), 269-274.

Burst activity of the Crab Nebula and its pulsar at high and ultra-high energies

A. S. Lidvansky

Institute for Nuclear Research, Russian Academy of Sciences, Moscow; lidvansk@lebedev.ru

Abstract Characteristics of the flares of gamma rays detected from the Crab Nebula by the AGILE and Fermi-LAT satellite instruments are compared with those of a gamma ray burst recorded by several air shower arrays on February 23, 1989 and with one recent observation made by ARGO-YBJ array. It is demonstrated that though pulsar-periodicity and energy spectra of emissions at 100 MeV (satellite gamma ray telescopes) and 100 TeV (EAS arrays) are different, their time structures seem to be similar. Moreover, may be the difference between “flares” and “waves” recently found in the Crab Nebula emission by AGILE team also exists at ultra-high energies.

Keywords: Crab Nebula, Gamma Ray Astronomy, Cosmic Rays, Extensive Air Showers

1. Introduction

Gamma-ray flares from the Crab Nebula were discovered in a few-hundred-MeV energy range by the AGILE [1] and Fermi LAT [2] satellite telescopes. Since then, both the telescopes continue recording such flares approximately once in a year, the strongest of them (super-flare) having been detected in April 2011 [7], [8]. The energy spectra of additional emission during the flares were measured to be different from those of the Nebula, however, “the mechanism driving the flares, their impulsive nature, the 12-month recurrence time, and the location, remain unknown” [12]. For all that, based on multi-wavelength campaign to study the Crab using Keck, Hubble Space Telescope (HST), and Chandra X-ray Observatory, the authors of [12] suggested the so-called “inner knot” to be just the emitting region for the flares. In addition, the analysis made by the AGILE collaboration for the September-October 2007 event has found a fine structure in the flare’s time behavior [10]. They have demonstrated that there is a difference between shorter “flares” and longer “waves” in the Crab Nebula emission during this flare.

After sensational discovery of gamma ray flares by AGILE and Fermi LAT it was recalled [3] that one event of this type (though at much higher energies) had been discovered many years ago by several EAS arrays [4], [5], [6].

2. Gamma-Ray Emission Burst on February 23, 1989

The first announcement about this burst was made during the International Workshop on Gamma-Ray Astronomy in Crimea in 1989 [4]. An increase of intensity of extensive air showers (EAS) was detected by the Carpet air shower array of the Baksan Neutrino Observatory on February 23, 1989. After this communication the group at Kolar Gold Fields (KGF) in India confirmed this result of Baksan and published a paper [5] on simultaneous detection of a gamma-ray burst in the Crab Nebula at ultra high-energies independently by two EAS arrays. Final publication [6] by the Baksan and Durham University teams summarized the data of all arrays that could observe the source on this day. It was demonstrated that with different significance the burst was detected by all air shower arrays located in the longitude range from India to Italy (KGF, Tien Shan, Baksan and EAS TOP). The arrays located to

the east and west from this interval (at that time OHYA MINE and Akeno SPICA in Japan and HEGRA at La Palma, Canary Islands, were in operation) showed no excess from the source direction. Thus, the total duration of the observed effect was no longer than about 7 hours. One can speak also about a possible decay of intensity whose maximum probably fell on observations with the KGF array. Figures 1 and 2 taken from paper [6] demonstrate the most remarkable features of the burst as detected by the Baksan Carpet air shower array.

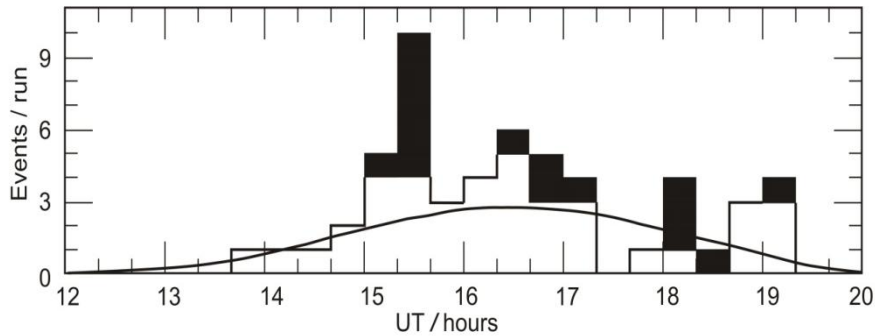


Fig1. The number of events within the Crab cell per 20 min run for 23 February 1989. The smooth curve represents the expected background. The blacked events are from the 9th bin in Fig. 2.

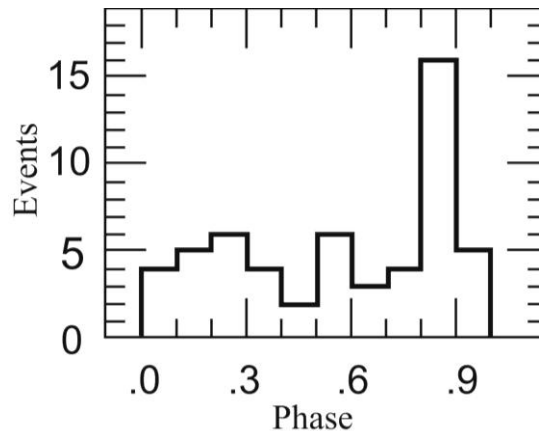


Fig2. The relative phase distribution of the 55 events within the Crab cell after barycentring the arrival times and applying the values of the pulsar period and its derivative according to the Jodrell Bank Crab ephemeris.

It is clearly seen that the Baksan array data demonstrate an obvious dependence of the effect on the pulsar phase: events from a single phase bin can produce the entire observed excess of intensity (the KGF group also found some phase irregularity, though not so well pronounced). Summarizing, one can state that with a rather high probability (the combined probability of random coincidences was estimated in [6] as $1.25 \cdot 10^{-7}$) a gamma-ray burst from the Crab Nebula was detected on February 23, 1989 in the energy range $10^{14} - 10^{15}$ eV, and excess emission in this burst is somehow connected with the pulsar's activity.

3. Different or Similar Types of Flares at Different Energies?

3.1. Temporal Structure

In [3] attention was attracted to the fact that three-pulse temporal structure in the event of February 23, 1989 might be reproduced at least in one of the AGILE flare events (September 2007). A bit later it has been discovered [10] that in addition to flares there exists another type of intensity increase called waves. And exactly during the September 2007 three short flares (F1, F2, and F3) were identified together with two waves W1 and W2 (see Fig. 3).

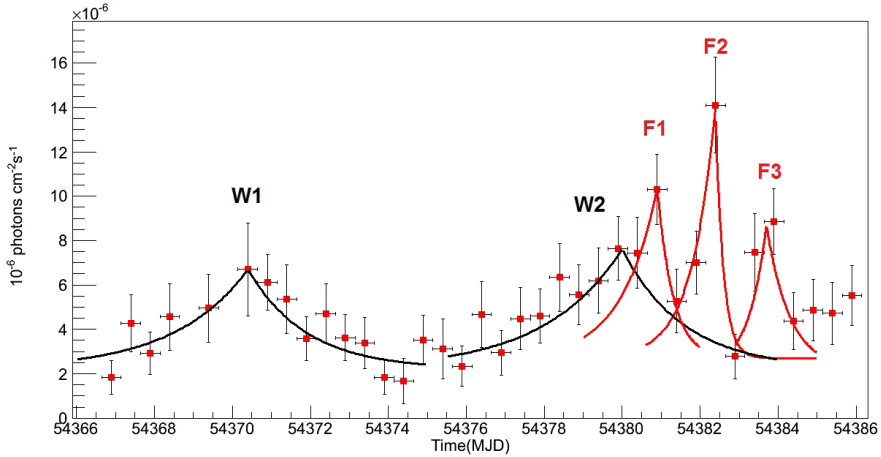


Fig3. The difference between flares and waves in the Crab Nebula gamma-ray emission according to Striani et al. [10]. The three-flare structure of the event is similar to three bunches of narrow-phase emission constituting almost all excess counts in Fig. 1.

Similarity of the temporal structures for events of Fig. 1 and Fig. 2 is obvious. In one case three bunches shorter than one hour are repeated with a period slightly longer than one hour. The other event includes three flares with duration of about one day, and they are repeated with a period a bit longer than one day. So, a sort of a stable pattern with a scale factor is observed at drastically different energies of gamma rays. It should be noted that the fine temporal structure was also reported by the Fermi LAT team for the March 2013 flare: “The light curve shows three sharp spikes (MJD 56357.1, 56357.9, 56360.1) on top of a strongly increased flux level.” [15]. Here, the period between the spikes is not so constant, but its duration, nevertheless, is close to that of Fig. 3 event.

The results of AGILE and Fermi LAT stimulated other groups to search for possible Crab flares, and one of them at first seemed to be successful. The ARGO-YBJ array after processing the data for Crab direction has found [9] an enhancement for the period September 19-26, 2010, which is shown in Fig. 4 for a 10-day period of averaging. The same event is presented in Fig. 5 with averaging over 2 days. This result was obtained at energies (about 1 TeV) intermediate between two region considered above. Nevertheless, there is a temptation to think that ratio of durations (several hours for 1989 event and about a week in this case) gives some evidence in favor of existence of the same “flares and waves” dichotomy at ultra-high energies. However, in the next publication [11] of ARGO-YBJ this piece of data was partially disavowed, though another interesting fact was presented: a correlation between Fermi and ARG-YBJ Crab intensities: “Even if the ARGO-YBJ rate variations are consistent with statistical fluctuations, the Fermi and ARGO-YBJ data seems to follow a similar trend. The ARGO-YBJ rate appears higher in the “hot” Fermi periods.” [11].

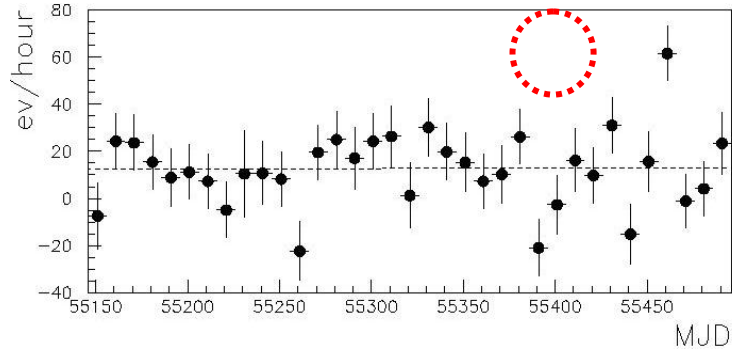


Fig4. The Crab light curve obtained in September 2010 by the ARGO-YBJ array with 10-day bins. The flare recorded by satellite gamma-ray telescopes took place on September 8-22. The point in red dashed circle is for September 19-26, 2010. Its significance is 5.4 standard deviations.

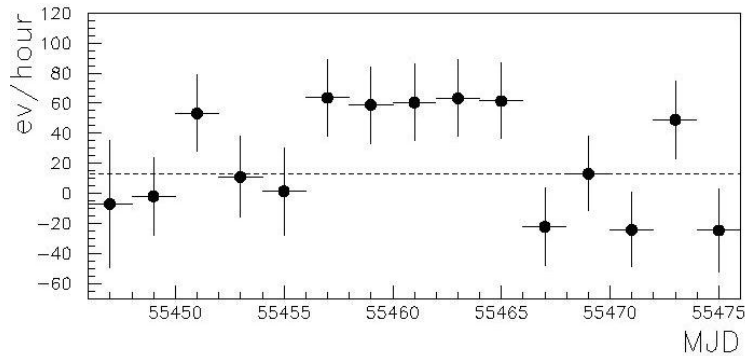


Fig5. The same data as in Fig. 4, but for the 2-day bin. The average rate in 8 days is 61 ± 13 ev/h, which is 4.8 times larger than the average rate in 3 years: 12.8 ± 1.3 ev/h.

3.2. Energy Spectra

It is commonly believed that the energy spectrum of the Crab Nebula is formed by synchrotron emission below 1 GeV and by inverse Compton radiation at higher energies. As far as flaring radiation is concerned, it is presumed to be associated with the synchrotron component. Spectral behavior of the flares appeared to be rather different: according to Fermi LAT, the flare in 2009 February exhibited only a flux increase with no spectral change. On the contrary, the flares in 2010 September and 2011 April had fluxes strongly correlated with the spectral index. In the March 2013 flare “the spectrum of the synchrotron nebula hardens as the flux increases” [15]. At the same time, according to an analysis made in [15], within the measurement accuracy the spectrum of the pulsar did not change in the entire analysis window with respect to the all-time average, and only synchrotron component of the Crab Nebula is rapidly variable.

For the ultra-high energy bursts at the moment no information on spectra is available.

3.3. Pulsar Periodicity

The Crab pulsar emission has a very complicated energy dependence. In the radio waveband in addition to the main pulse (MP) and interpulse (IP) there are a precursor of the MP, low-frequency component (LFC) and two high-frequency components (HFC1 and HFC2), as well as giant radio pulses

that randomly appear on different phases. At higher energies the Crab light curve becomes more regular and the gamma-ray domain has only two pulses P1 and P2. The amplitudes of these two pulses depend on energy. For example, the P2 pulse is twice larger in amplitude than P1 at energy less than 10 MeV (COMPTEL), but already at energy > 30 MeV (EGRET) the situation is opposite. At the energy exceeding 100 GeV (the data of Cherenkov telescopes VERITAS and MAGIC) the pulse P2 becomes dominant again. There are also some indications to the possible appearance of a new pulse P3. So, it would be not surprising if at still higher energy only a single pulse survives, as it takes place in Fig. 2.

4. Discussion and Conclusion

Interpretation of gamma-ray flares as produced by synchrotron radiation of accelerated electrons in compact regions of intensified magnetic field (plasma instabilities) requires the energy of such electrons as high as 10^{15} eV (for example, [10]). If these electrons do really exist, one can recall the idea of Atoyan and Aharonian [16] that Crab Nebula wisps probably have sufficient amount of matter to make bremsstrahlung radiation effective. If so, 1000 TeV electrons can easily produce 100 TeV gamma rays. Even without this hypothesis accelerated particles can produce simultaneously multi-TeV emission via inverse Compton effect and hundred-MeV - GeV emission through synchrotron radiation [17]. When explaining two sets of data discussed in this paper, the problem is that at ultra-high energies the pulsar periodicity takes place, while it is not observed in hundred-MeV flares. As possible explanation one can suggest that at lower energies an observer receives gamma rays from a larger quasi-spherical surface of the pulsar-wind driven shock, so that the phase is randomized because of path differences.

Nevertheless, many details of the mechanisms of flare generation (like, for example, triple scaled temporal structure and distinction between flares and waves) are unclear as before, and the Crab Nebula still remains an enigmatic “astrophysical chimera” [13]. One can hope, however, that the above juxtaposition of data at different energies will be useful for construction of a realistic model of the source internal mechanism.

Acknowledgments

The work is partially supported by the Russian Foundation for Basic Research, grant no. 16-02-00687.

References

- [1] Tavani, M. et al. Discovery of Powerful Gamma-Ray Flares from the Crab Nebula. *Science* 2011; 331: Issue 6018, 736-39. doi: 10.1126/science.1200083
- [2] Abdo, A.A. et al. Gamma-Ray Flares from the Crab Nebula. *Science* 2011; 331: 739-42. doi: 10.1126/science.1199705
- [3] Lidvansky, A.S. On the burst activity of the Crab Nebula and pulsar at high and ultra-high energies. *Journal of Physics: Conference Series* 2013; 409: 012114. doi:10.1088/1742-6596/409/1/012114
- [4] Alexeenko, V.V., Lidvansky, A.S. and Tizengauzen, V.A., “A Search for $> 10^{14}$ eV Gamma Rays from Point Sources at Baksan Air Shower Array in 1984-1988”: *Proc. of Int. Workshop on Very High Energy Gamma Ray Astronomy (Crimea, USSR)*, 17-21 April, 1989. Ed. by A.A. Stepanyan, D.J. Fegan and M.F. Cawley, p. 187.
- [5] Acharya, B.S., Rao, M.V.S., Sivaprasad, K., Sreekantan, B.V. and Vishwanath, P.R. First simultaneous detection of PeV energy burst from the Crab Nebula. *Nature* 1990; 347: 364-5. doi:10.1038/347364a0
- [6] Alexeenko, V.V., Andreyev, Yu.M., Chudakov, A.E., Elensky, Ya.S., Lidvansky, A.S., Ozrokov, S.Kh., Stenkin, Yu.V., Tizengauzen, V.A., Graham, L.J., Osborne, J.L. and Wolfendale, A.W. The ultra-high energy gamma-ray burst from the Crab Nebula observed by the Baksan EAS array. 1992 *J. Phys. G: Nucl. Part.*

Phys.; 18: L83-L88.

- [7] Buehler, R. et al. Gamma-ray Activity in the Crab Nebula: The Exceptional Flare of 2011 April. *The Astrophysical Journal* 2012; 749: 26. doi: 10.1088/0004-637X/749/1/26
- [8] Striani, E. et al. The Crab Nebula Super-Flare in 2011 April: Extremely Fast Particle Acceleration and Gamma-Ray Emission. *The Astrophysical Journal Letters*, 2011; 741: L5. doi:10.1088/2041-8205/741/1/L5
- [9] Vernetto, S. et al. "Study of the Crab Nebula flux variability with the ARGO-YBJ detector": Proc. of 32nd ICRC, Beijing, 2011.
- [10] Striani, E. et al. Variable gamma-ray emission from the Crab Nebula: Short flares and long "waves", *Astrophys. Journ.* 2013; 765: 52. doi: 10.1088/0004-637X/765/1/52
- [11] Bartoli, B. et al. Crab Nebula: Five-Year Observation with ARGO-YBJ. *The Astrophysical Journal* 2015; 798: 119.
- [12] Rudy, A. et al. Characterization of the Inner Knot of the Crab: The Site of the Gamma-ray Flares? *The Astrophysical Journal* 2015; 811: 24. doi: 10.1088/0004-637X/811/1/24
- [13] Hester, J.J. The Crab Nebula: An Astrophysical Chimera. *Annu. Rev. Astron. Astrophys.* 2008; 46: 127–55. doi: 10.1146/annurev.astro.45.051806.110608
- [14] Bühler, R. and Blandford, R. The surprising Crab pulsar and its nebula: a review. *Rep. Prog. Phys.* 2014; 77: 066901. doi: 10.1088/0034-4885/77/6/066901
- [15] Mayer, M. et al. Rapid Gamma-ray Flux Variability during the 2013 March Crab Nebula Flare. *The Astrophysical Journal Letters* 2013; 775: L37. doi: 10.1088/2041-8205/775/2/L37
- [16] Atoyan, A.M. & Aharonian, F.A. On the mechanisms of gamma radiation in the Crab Nebula. *Mon. Not. Roy. Astron Soc.* 1996; 278: 525.
- [17] Bednarek, W. & Idec, W. On the variability of the GeV and multi-TeV gamma-ray emission from the Crab nebula. *Mon. Not. Roy. Astron Soc.* 2011; 414: 2229.

Mechanisms of supernova explosion: modern status

D. K. Nadyozhin

Alikhanov ITEP, Moscow, Russia; nadezhin@itep.ru

Abstract The mechanisms of explosion of different type supernovae (SNe) are discussed. At least four mechanisms are under detailed inspection of scientific community for core-collapse SNe. They are the instability of standing accreting shock front that results in the large scale 3-dimensional hydrodynamic flows, the phase transition from nuclear to quark matter, the magnetic-rotational expulsion of supernova envelope, and rotational fission of collapsing stellar core into a pair of proto neutron stars. The mechanism of explosion of cosmological SNe (of Type Ia) is physically understood as the thermonuclear explosion of carbon-oxygen-helium matter. However there exists a serious problem with modeling of the structure and propagation of unstable thermonuclear flame that is crucial for numerical agreement with observations.

Keywords: Supernovae, Supernova Remnants

1. Introduction

Physically, there are two fundamental types of SNe: the thermonuclear SNe represented by Type Ia SNe (SN Ia) and the core-collapse SNe, respectively. The core-collapse SNe are subdivided into several subtypes depending on the amount of hydrogen hanging around the stellar core just before it begins to collapse such as Type IIP, II_n, II_b, Ib, and Ic SNe. The progenitors of Type IIP and II_n SNe have plenty of hydrogen in their envelopes, typically as much as $(10 - 15) M_{\odot}$. SNe II_n have also some hydrogen in an extended atmosphere formed by stellar wind on the top of their dense hydrogen enriched envelopes. The progenitors of Type IIL SNe have much less hydrogen, about $(0.1 - 1) M_{\odot}$ whereas the spectra of Type II_b SNe show only traces of hydrogen during the first few days after the explosion, then these SNe become similar to SNe Ib. Types Ib and Ic progenitors virtually have no hydrogen left. Type Ic differs from Ib by lack of helium. The Type Ic progenitors are believed to have lost not only all hydrogen but also a fair amount of helium during their evolution.

2. Thermonuclear SNe (Type Ia)

The type Ia SNe are believed to arise in close binary stellar systems from explosive carbon burning either in a degenerate carbon-oxygen (CO) white dwarf as soon as due to accretion it's mass increases to a certain value close to *Chandrasekhar mass* ($M \approx 1.4 M_{\odot}$) or in the process of mergence of two white dwarf binary components. The explosion energy $E_{\text{exp}} \approx 10^{51}$ erg comes from the thermonuclear burning of ^{12}C and ^{16}O mixture into ^{56}Ni that has the maximum binding energy among nuclei with equal numbers of neutrons and protons. The white dwarf turns out to be totally disrupted in the explosion — no stellar remnant is left! The total energy of electromagnetic radiation $E_{\text{rad}} \approx 6 \times 10^{49}$ erg is mostly supplied by the $^{56}\text{Ni} \rightarrow ^{56}\text{Co} \rightarrow ^{56}\text{Fe}$ beta-decays. The hydrodynamic modeling of the SN Ia light curves shows that only a small fraction of explosion energy is transformed into radiation: $E_{\text{rad}} / E_{\text{exp}} \approx 0.06$. This is by a factor of 2 less than the ratio of the energy released per $^{56}\text{Ni} \rightarrow ^{56}\text{Fe}$ beta decay (5.5 MeV) to the energy produced per synthesized ^{56}Ni (47 MeV) during the thermonuclear burning of the mixture of equal C and O mass fractions. This happens because a portion of beta decay energy is expended on the hydrodynamic

expansion of supernova debris. Hence, almost all E_{exp} resides in the kinetic energy of the envelope expanding with the mean velocity $\approx 8\,000$ km/s. Comparison of the SN Ia models with observations shows that about $(0.6 - 1) M_{\odot}$ of ^{56}Ni is produced per SN Ia outburst.

The ignition of thermonuclear fuel and propagation of the flame in degenerate stellar matter is a fundamental problem still to be solved to understand the basic mechanism of SN Ia explosions and finally to calibrate SN Ia as standard candles for observational cosmology. From the beginning the thermonuclear flame propagates by means of a sub-sonic deflagration being governed by the electron thermal conduction. The burning front proves to be extremely thin and fraught with a number of instabilities such as Rayleigh–Taylor, Kelvin–Helmholtz and Landau–Darries ones. Since the Reynolds number typically is of the order of 10^{14} , the front gets a strongly wrinkled structure and the burning becomes of turbulent nature. Owing to the growth of surface area covered by the front the rate of combustion considerably increases. As a result, after a time the deflagration can develop into a super-sonic detonation that is driven by a shock wave which heats matter up to the ignition. The transition from the deflagration to detonation is required in order to achieve the compliance between theoretically predicted chemical compositions of the SN Ia ejecta and that observed in the SN Ia spectra. However, for a group of discovered recently sub luminous SNe Ia the deflagration alone seems to be adequate [1]. There is also a problem with understanding how and where the nuclear fuel actually begins to burn. The flame may flare up not necessarily in the very centre but either in an off center bubble or in separate little spots randomly distributed around. An extensive study of turbulent burning in degenerate matter of white dwarfs is under way. The current results and further references can be found in [1-9].

3. Core-collapse SNe

The iron stellar cores begin to collapse owing to the loss of dynamical stability. Due to the photo-disintegration of iron into free nucleons and α -particles the adiabatic index γ becomes less than the critical value $4/3$. Hence, the gradient of pressure cannot withstand the force of gravity any more. An inner core with a mass of $(0.6 - 0.8) M_{\odot}$ around the stellar center begins to contract almost in a free fall regime. In a few hundredths of second the central density reaches the nuclear density and the contraction slows down. The outermost layers, being still in a state close to free fall, collide with the decelerated inner core. Thereby a nearly standing accreting shock wave (SAS) forms at the boundary of the inner core and the outer envelope. The key question for the core-collapse supernova mechanism is to verify whether such a standing shock becomes finally transformed into an outgoing blast wave that would expel the supernova envelope.

The SN outburst of core-collapse SNe is triggered by the gravitational collapse of the “iron” core of a mass $M_{\text{Fe}}=(1.2-2) M_{\odot}$ into a neutron star. About $(10-15)\% M_{\text{Fe}}c^2$ is radiated in the form of neutrinos and antineutrinos of all flavors (e, μ, τ):

$$E_{\nu\bar{\nu}} = (3-5) \times 10^{53} \text{ erg.}$$

The explosion energy (kinetic energy of the envelope expansion) according to observations:

$$E_{\text{exp}} = (0.5-2) \times 10^{51} \text{ erg.}$$

It comes from the shock wave created at the boundary between a new-born neutron star and the envelope to be expelled. So, for succesful explosion it is enough to transport in stellar envelope less than 1% of total neutrino energy $E_{\nu\bar{\nu}}$:

$$E_{\text{exp}}/E_{\nu\bar{\nu}} \sim 10^{-3} - 10^{-2}.$$

Figure 1 clearly demonstrates the formation of the SAS for the case of spherically symmetrical collapse of a $2 M_{\odot}$ iron-oxygen stellar core [10]. At 0.123 s after the beginning of braking of the inner

core contraction, nearly $1.8 M_{\odot}$ is encircled by the SAS front.

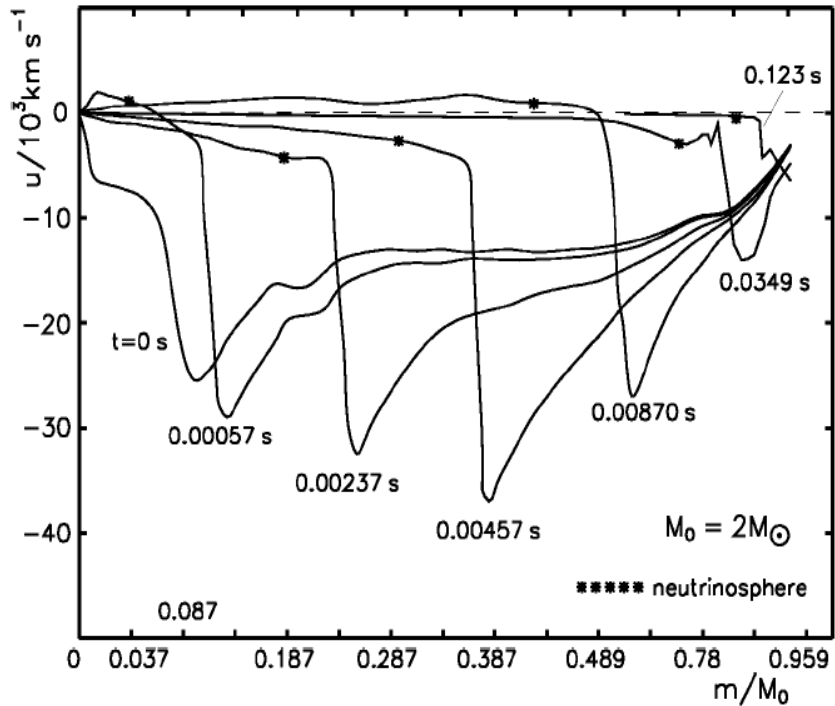


Fig1. The velocity versus the relative mass m/M_0 at different times (Adapted from [10])

Figure 2 shows the characteristic features of the hydrodynamic flow in the region around the neutrinosphere and SAS wave.

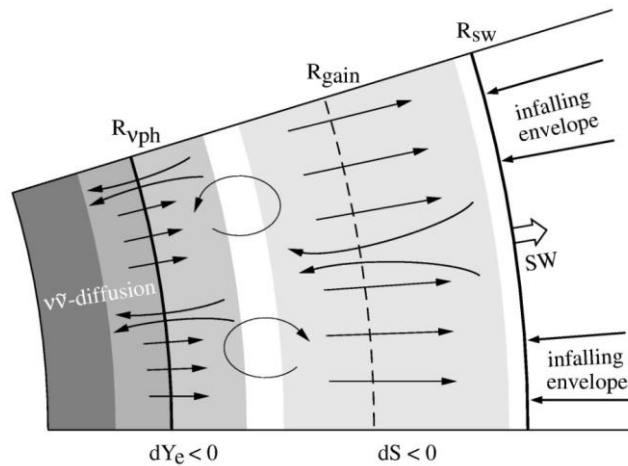


Fig2. The layout of hydrodynamic flow in the interval between the shock wave (R_{SW}) and the neutrinosphere (R_{vph}). Two regions of convective instability are shaded in light gray. At radii $r > R_{gain}$ the heating of matter by the neutrino flux from the neutrinosphere exceeds the cooling by the local neutrino losses.

The large scale convective currents are expected to evolve due to negative gradients of both the entropy ($dS < 0$, entropy-driven convection) that appears in the region just below the SW and of the electron fraction ($dY_e < 0$, lepton-driven convection) nearby the neutrinosphere. These currents transport some energy to the SW in addition to that supplied by the neutrino flux from the neutrinosphere. There was suggested that this effect can force the SW to propagate outside. However, an extensive modeling of the core-collapse SNe during last three decades has demonstrated that neither the convection nor the heating due to the neutrino flux (at $r > R_{\text{gain}}$, Fig. 2) can increase the explosion energy to the value that would be large enough to explain the observations. Nevertheless in case of spherically symmetric collapse, the SW finally throws an envelope out. This happens when with time the rate of mass accretion from the envelope considerably decreases and the excessive pressure like an over-compressed elastic spring pushes the SW outward forcing it to propagate through a steep density gradient. Unfortunately, this effect (called a hydrodynamic bounce) can produce only a low energy explosion with E_{exp} being at least one or even two orders of magnitude less than its standard value of 10^{51} erg. Although such a weak explosion seems to be adequate for some sub luminous Type II SNe like the historical Crab nebula SN 1054 (see [11] and discussion therein), the problem how to get the more energetic explosions remains to be far from a satisfactory solution, at least in the framework of spherically symmetric models.

Therefore, it is plausible to assume that the solution can be found by addressing to substantially non-spherical effects such as, for instance, magneto-rotational mechanism [12–14] and rotational fission of the collapsing core into a binary system of proto-neutron stars that evolves losing angular momentum and energy through the gravitational waves with subsequent explosion of a low-mass ($\approx 0.1M_{\odot}$) component [15–18].

During the last years it became clear that the spherically symmetrical SN models can, nevertheless, explode due to the phase transition from nuclear to quark matter if the transition occurs *after* the SAS formation. Figure 3 shows an example of detailed hydrodynamic calculations [19] (see also [20]). The formation of SAS completed at 240.5 ms (thick black solid line). Then the phase transition appeared at radius about 8 km and initiated further gravitational contraction of stellar interiors that produced new shock wave propagating outwards. At 256.3 ms this shock wave reaches SAS pushing it far off the accreting envelope and thereby triggering the supernova explosion. A very important result of calculations in [19] is also the prediction of a narrow (~ 1 ms) peak of electron antineutrino flux with mean square antineutrino energy up to 35 MeV. The peak occurs at 256–257 ms. Such a peak can be observed by modern neutrino detectors for the SN in our Galaxy.

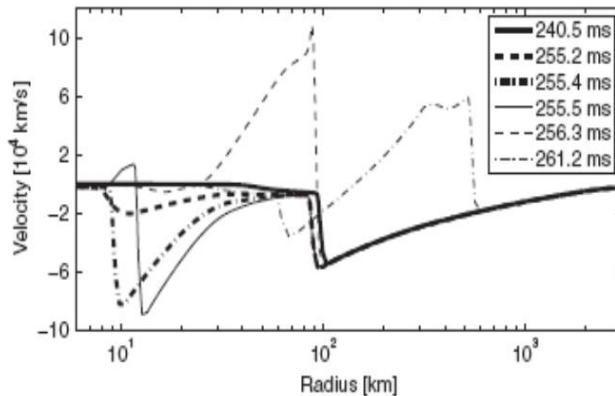


Fig3. The supernova explosion induced by the phase transition from nuclear to quark matter inside a spherically symmetrical stellar core [19].

Another possibility to obtain the SN explosion for initially spherically symmetrical presupernova model is connected with the SAS instability (SASI) with regard to 2D and 3D perturbations. The instability strengthens the convective currents in the gain region under the SAS front (Fig. 2) allowing them to penetrate into the accreting flow and to transport there more energy thereby facilitating the expulsion of the supernova envelope. The SASI is under careful examination by scientific community already many years [21–26].

3.1. The supernova 1987A in the Large Magellanic Cloud

The most outstanding issues of the SN 1987A are

- (i) the detection of extragalactic neutrinos,
- (ii) the discovery of radioactive nuclides (^{56}Ni , ^{56}Co , ^{57}Co , ^{44}Ti) in the SN ejecta,
- (iii) the recognition of the decisive significance of large-scale mixing just before or in the process of the explosion and of nonspherical effects.

Theoretical deciphering of the SN 1987A neutrino signal is not yet completed. The rotational fragmentation model is the only one that combines two, separated by 4.7 hours, neutrino signals in one self consistent scenario [15–18]. Recent observations of the intrinsic dusty ejecta of SN 1987A in the infrared line (1.644 μm [SiII]+[Fe II]) [27] showed that the dust, screening central point source, has the shape of a prolate ellipsoid laying in the plain perpendicular to the axis of rotation – exactly as the rotational fragmentation model predicts.

The crucial point here is the long-awaited discovery of a stellar remnant (a neutron star or a black hole) which emergence out of the supernova debris is expected in the near future. At present, only upper limits on the optical and X-ray luminosities of the SN 1987A central point source are available [28].

4. Conclusion

For lack of space, several important topics were not discussed in this extremely short review. Among them is the connection of SNe with gamma-ray bursts, the onset of a neutrino-driven wind that presumably should blow from a nascent hot neutron star, and the nucleosynthesis in SNe (in particular, the neutrino-induced nucleosynthesis and r-process in a core-collapse SNe). To make up this deficiency we refer the reader to the excellent reviews [29 – 33].

Acknowledgements

I am very grateful to the Organizing Committee for excellent organization of the SAO & BNO Workshop and heartfelt hospitality.

References

- [1] Phillips, M.M., Li, W., Frieman, J.A. et al., “The Peculiar SN 2005hk: Do Some Type Ia Supernovae Explode as Deflagrations?”, *Pub. Astron. Soc. Pacific*, 2007. V. 119, P. 360–402. (astro-ph/0611295v2).
- [2] Röpke, F.K., Hillebrandt, W., “Three-dimensional Modeling of Type Ia Supernova Explosions in Origin of Matter and Evolution of Galaxies”, S.Kubono et al. (eds), *AIP* 2006. P. 190–195.
- [3] Woosley, S.E., Kasen, D., Blinnikov, S.I., Sorokina, E.I., “Type Ia Supernova Light Curves”, *Astrophys. J.*, 2007. V. 662, P. 487–503.
- [4] Röpke, F.K., Hillebrandt, W., Schmidt, W. et al. , “A Three-Dimensional Deflagration Model for Type Ia Supernovae Compared with Observations”, *Astrophys. J.*, 2007. V. 668, P. 1132–1139.

- [5] Lisewski, A.M., Hillebrandt, W., Woosley, S.E. et al., “Distributed Burning in Type Ia Supernovae: a Statistical Approach”, *Astrophys. J.*, 2000. V. 537, P. 405–413.
- [6] Hillebrandt, W., Niemeyer, J.C., “Type Ia Supernova Explosion models”, *Ann. Rev. Astron. Astrophys.*, 2000. V. 38, P. 191–230.
- [7] Hillebrandt, W., Sim, S.A., Röpke, F.K., “Off-center explosions of Chandrasekhar-mass white dwarfs: an explanation of super-bright type Ia supernovae?”, *Astron. Astrophys.*, 2007. V. 465, P. L17–L20.
- [8] Mazzali, P.A., Röpke, F.K., Benetti, S., Hillebrandt, W., “A Common Explosion Mechanism for Type Ia Supernovae”, *Science*, 2007. V. 315, P. 825–828.
- [9] Sim, S.A., Sauer, D.N., Röpke, F.K., Hillebrandt, W., “Light curves for off-centre ignition models of Type Ia supernovae”, *Month. Not. R. Astron. Soc.*, 2007. V. 378, P. 2–12.
- [10] Nadyozhin, D.K., “The gravitational collapse of iron-oxygen stars with masses of $2 M_{\odot}$ and $10 M_{\odot}$ II”, *Ap&SS*, 1977. V. 51, P. 283.
- [11] Kitaura, F.S., Janka, H.-Th., Hillebrandt, W., “Explosions of O-Ne-Mg cores, the Crab supernova, and subluminescent type II-P supernovae”, *Astron. Astrophys.*, 2006. V. 450, P. 345–350.
- [12] Bisnovaty-Kogan, G.S., “The Explosion of a Rotating Star As a Supernova Mechanism”, *Astron. Zh.*, 1970. V. 47, P. 813–815. (*Sov. Astron.*, 1970. V. 14, P. 652).
- [13] Ardeljan, N.V., Bisnovaty-Kogan, G.S., Moiseenko, S.G., “Magnetorotational supernovae”, *Month. Not. R. Astron. Soc.*, 2005. V. 359, P. 333–344.
- [14] Moiseenko, S.G., Bisnovaty-Kogan, G.S., “Magnetorotational supernovae. Magnetorotational instability. Jet formation”, *Astrophys. Space Sci.*, 2007. V. 311, P. 191–195.
- [15] Imshennik, V.S., “Scenario for a supernova explosion in the gravitational collapse of a massive stellar core”, *Sov. Astron. Lett.*, 1992. V. 18, P. 194–198.
- [16] Imshennik, V.S., Ryazhskaya, O.G., “A Rotating Collapsar and Possible Interpretation of the LSD Neutrino Signal from SN 1987A”, *Astron. Lett.*, 2004. V. 30, P. 14–31. (astro-ph/0401613).
- [17] Ryazhskaya, O.G., “Neutrinos from stellar core collapses: present status of experiments”, *Physics – Uspekhi*, 2006. V. 49 (10), P. 1017–1027.
- [18] Imshennik, V.S., “Rotational explosion mechanism for collapsing supernovae and the two-stage neutrino signal from supernova 1987A in the Large Magellanic Cloud”, *Physics – Uspekhi*, 2010. V. 53, P. 1081–1092.
- [19] Sagert, I., T. Fischer, T. Hempel, M. et al., “Signals of the QCD Phase Transition in Core-Collapse Supernovae”, *PRL*, 2009. V. 102, 081101.
- [20] Krivoruchenko, M.I. et al., “Nuclear matter at high density: phase transitions, multi-quark states, and supernova outbursts”, *Yadernaya Fizika*, 2011. V. 74, P. 1–42.
- [21] Blondin, J.M., Mezzacappa, A., DeMarino, C., “Stability of standing accretion shocks, with an eye toward core-collapse supernovae”, *ApJ*, 2003. V. 584, P. 971–980.
- [22] Imshennik, V.S. and Litvinova, I.Yu., “Neutrino Crown of a Protoneutron Star and Analysis of Its Convective Instability”, *Physics of Atomic Nuclei*, 2006. V. 69, P. 636–657.
- [23] Yamasaki, T. and Yamada, S., “Stability of accretion flows with stalled shocks in core-collapse supernovae”, *ApJ*, 2007. V. 656, P. 1019–1037.
- [24] Scheck, L. et al., “Multidimensional supernova simulations with approximative neutrino transport II. Convection and the advective-acoustic cycle in the supernova core”, *A&A*, 2008. V. 477, P. 931–952.
- [25] Marek, A. and Janka, H.-Th., “Delayed neutrino-driven supernova explosions aided by the standing accretion-shock instability”, *ApJ*, 2009, V. 694, P. 664–696.

- [26] Fernandez, R., “Three-dimensional simulations of SASI- and convection-dominated core-collapse supernovae”, *MNRAS*, 2015, V. 452, P. 2071-2086.
- [27] Kjær, K., Leibundgut, B., Fransson, C. et al., “The 3-D structure of SN 1987A’s inner ejecta”, *A&A*, 2010, V. 517, A51.
- [28] Graves, G.J.M., Challis, P.M., Chevalier, R.A. et al., “Limits from the Hubble Space Telescope on a Point Source in SN 1987A”, *ApJ*, 2005. V. 629, P. 944–959. (astro-ph/055066).
- [29] Wallerstein, G., Iben, I. Jr., Parker, P. et al. “Synthesis of the elements in stars: forty years of progress”, *Rev. Mod. Phys.*, 1997. V. 69. P. 995–1081.
- [30] Woosley, S.E., Heger, A., Weaver, T.A. “The evolution and explosion of massive stars”, *Rev. Mod. Phys.*, 2002. V. 74. P. 1015–1071.
- [31] Woosley, S.E., Heger, A. “Supernovae, Gamma-Ray Bursts, and Stellar Rotation”, *Proceed. IAU Symp.* No. 215, 2004. P. 601–612. (astro-ph/0301373).
- [32] Blinnikov, S. “Supernovae and gamma-ray bursts”, *Surveys High Energy Phys.*, 2006. V. 20, 89–124.
- [33] Thielemann, F.-K., Fröhlich, C., Hirschi, R. et al. “Production of intermediate-mass and heavy nuclei”, *Progr. Particle Nuclear Phys.*, 2007. V. 59. P. 74–93.

A search for neutrino bursts signal from supernovae at the Baksan Underground Scintillation Telescope

Yu. F. Novoseltsev ^{1,*}, M. M. Boliev ¹, I. M. Dzaparova ^{1,2}, M. M. Kochkarov ¹,
R. V. Novoseltseva ¹, V. B. Petkov ^{1,2}, V. I. Volchenko ¹, G. V. Volchenko ¹,
A. F. Yanin ¹

¹*Institute for Nuclear Research of the Russian Academy of Sciences, 60th October Anniversary Prospect, 7a, 117312 Moscow, Russia; *novoseltsev@inr.ru*

²*Institute of Astronomy of the Russian Academy of Sciences, 48 Pyatnitskaya St., 119017, Moscow, Russia*

Abstract The current status of the experiment on recording neutrino bursts from core collapse stars is presented. The actual observational time is 29.76 years. The upper bound of the mean frequency of core collapse supernovae in our Galaxy is $f_{\text{col}} < 0.077 \text{ year}^{-1}$ (90% CL).

Keywords: Supernova, Neutrino Bursts

1. Introduction

The detection of neutrinos from the supernova SN1987A [1] – [4] experimentally proved the critical role of neutrinos in the explosion of massive stars, as was suggested more than 50 years ago [5] – [7].

Neutrinos are especially important, because they reveal physical conditions in the star core at the instant of collapse. The SN1987A event helped to establish some aspects of the theory, namely the total energy radiated, the neutrinos temperatures and the duration of neutrino burst [8], [9].

At present, the standard paradigm of SN explosion mechanism is the “delayed explosion scenario” or “neutrino mechanism”, which was suggested first by Wilson [10] and Bethe [11]. In this scenario, one of the key parameters is a neutrino energy deposition behind the stalled shock. This energy deposition can revive the shock energy (which the shock wave lost during propagation through the outer iron core) and leads finally to the SN explosion.

In recent years a substantial progress has been achieved in two-dimensional (2D) and three-dimensional (3D) hydrodynamic simulations of SN progenitor evolution. These simulations found out considerable deviations from spherical symmetry [12] – [14]. In particular, the lepton-number emission self-sustained asymmetry (LESA) phenomenon is identified [15]. It means that the observed neutrino flux depends on the observer position.

On the other hand, results obtained in 3D simulations pointed out that energy of the shock wave is insufficient for a successful SN explosion. However in the recent work by T. Melson et al. [16] it has been shown that strangeness contributions to neutrino-nucleon scattering with an axial-vector coupling of $g_a^s = -0.2$ are sufficient to turn a non-exploding 3D simulation (in which $g_a = 1.26$ was used for the standard isovector form factor) to a successful explosion. This result indicates that an accurate knowledge of neutrino-nucleon interaction rates, in particular also for neutral current scattering, is of crucial importance for assessing the viability of the neutrino driven explosion mechanism.

The supernova neutrino detection will be crucial to test the explosion mechanism and thus to compare current supernova models with experimental data.

Several neutrino detectors have been observing the Galaxy in the last decades to search for stellar collapses, namely Super-Kamiokande [17], Baksan [18], [19], MACRO [20], LVD [21], [22], AMANDA [23], SNO [24]. At present, the new generation detectors, which are capable to record effectively the neutrino burst from the next SN, are added to the facilities listed above: IceCube [25],

Borexino [26], [27], KamLAND [28] and some others.

The Baksan Underground Scintillation Telescope operates under the program of search for neutrino bursts since the mid-1980. In this paper we present the current status of the experiment and some results related to investigation of background events and stability of the facility operation. Section 2 is a brief description of the facility. Section 3 is devoted to the method of neutrino burst detection. Discussion and Conclusion are presented in Section 4.

2. The facility

The Baksan Underground Scintillation Telescope (BUST) is located in the Northern Caucasus (Russia) in an underground laboratory at the effective depth $8.5 \cdot 10^4 \text{ g} \cdot \text{cm}^{-2}$ (850 m of w.e.) [29]. The facility has the size $17 \times 17 \times 11 \text{ m}^3$ and consists of four horizontal scintillation planes and four vertical ones (Fig.1).

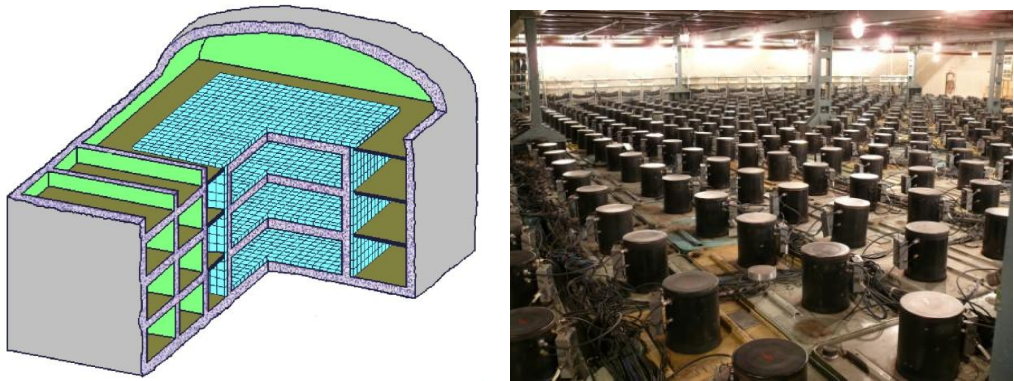


Fig1. The Baksan Underground Scintillation Telescope, Right –the upper plane of the BUST

Five planes of them are external planes and three lower horizontal planes are internal ones. The upper horizontal plane consists of 576 (24×24) liquid scintillator counters of the standard type, three lower planes have 400 (20×20) counters each. The vertical planes have (15×24) and (15×22) counters. Each counter is $0.7 \times 0.7 \times 0.3 \text{ m}^3$ in size, filled with an organic $\text{C}_n\text{H}_{2n+2}$ ($n \approx 9$) scintillator, and viewed by one photomultiplier with a photocathode diameter of 15 cm. The distance between neighboring horizontal scintillation layers is 3.6 m. The angular resolution of the facility is 2° , time resolution is 5 ns.

Information from each counter is transmitted over three channels: an anode channel (which serves to trigger formation and amplitude measurements up to 2.5 GeV), a pulse channel with the operation threshold 8 MeV and 10 MeV for the horizontal and vertical planes, respectively (at first this threshold was equal to 12.5 MeV; the most probable energy deposition of a muon in a counter is $50 \text{ MeV} \equiv 1$ relativistic particle) and a logarithmic channel with the threshold $s_0 = 0.5 \text{ GeV}$. The signal from the fifth dynode of PM tube FEU-49 goes to a logarithmic channel (LC) where it is converted into a pulse whose length t is proportional to logarithm of the signal amplitude [30].

The BUST is a multipurpose detector. The physical experiments began in 1978. Since that time, the parameters of scintillation counters and data acquisition system were permanently improved. One of the current tasks is the search for neutrino bursts. The facility has been operating almost continuously under the program of search for neutrino bursts since the mid-1980. The total time of Galactic observation accounts for 90% of the calendar time.

3. The method of neutrino burst detection

The BUST consists of 3184 standard autonomous counters. The total scintillator mass is 330 t, and the mass enclosed in three lower horizontal layers (1200 standard counters) is 130 tons. The majority of the events recorded with the Baksan telescope from a supernova explosion will be produced in inverse beta decay reactions



If the mean antineutrino energy $E_{\bar{\nu}_e} = 12 - 15 \text{ MeV}$ [31], [32], the pass of e^+ (produced in reaction (1)) will be included, as a rule, in the volume of one counter. In such a case the signal from a supernova (SN) explosion will appear as a series of events from singly triggered counters (one and only one counter from 3184 operates; below we call such an event “a single event” or “1 from 3200” event) during the neutrino burst.

The search for a neutrino burst consists in the recording of single events bunch within a time interval of $\tau = 20 \text{ s}$ (according to the modern collapse models the burst duration does not exceed 20 s). The expected number of neutrino interactions detected during an interval of duration δt from the beginning of the collapse can be expressed as:

$$N_{ev}^H = N_H \int_0^{\delta t} dt \int_0^\infty dE \times F(E, t) \times \sigma(E) \eta_1(E), \quad (2)$$

here N_H is the number of free protons, $F(E, t)$ is the flux of electron antineutrinos, $\sigma(E)$ is the IBD cross section and $\eta_1(E)$ is the detection efficiency of e^+ in reaction (1) ($\eta_1 \approx 0.7$ if the positron energy $E_e = 10 \text{ MeV}$ and $\eta_1 = 0.9$, if $E_e = 20 \text{ MeV}$). The symbol “H” in the left side indicates that the hydrogen is the target.

If one assumes the distance from the SN is 10 kpc and the total energy irradiated in neutrinos is

$$\varepsilon_{tot} = 3 \times 10^{53} \text{ erg} \quad (3)$$

the expected number of single events from reaction (1) (we assume the total energy of the $\bar{\nu}_e$ flux is equal to $(1/6\varepsilon_{tot})$) will be

$$N_{ev}^H \cong 35 \quad (4)$$

Flavor oscillations are unavoidable, of course. However, in recent years it was recognized that the expected neutrino signal depends strongly on the oscillation scenario (see e.g. [33] - [36]). In the absence of a quantitatively reliable prediction of the flavor-dependent fluxes and spectra it is difficult to estimate the oscillation impact on ν_e - and $\bar{\nu}_e$ fluxes arriving to the Earth.

Therefore we do not discuss the effects of flavor oscillations in this paper.

Background events are radioactivity and cosmic ray muons if only one counter from 3184 hit. The total count rate from background events is $f = 0.02 \text{ s}^{-1}$ in internal planes (three lower horizontal layers) and $\approx 1.5 \text{ s}^{-1}$ in external ones. Therefore three lower horizontal layers are used as a target (the estimation (4) has been calculated for three internal planes). The trigger is the operation of any counter pulse channel (with the threshold 8 MeV).

In Fig.2 we show how the counter operation threshold changed with time ($12.5 \rightarrow 10 \rightarrow 8 \text{ MeV}$) and the corresponding total count rate of single events in the three internal planes (1200 counters, the target mass is 130t).

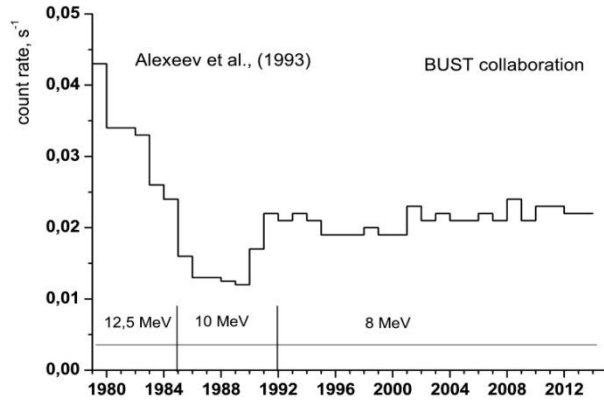


Fig2. The mean count rate of single events in the three telescope internal planes (1200 counters) vs the counter operation threshold

The energy spectra of single events (i.e. background events) in three lower horizontal planes are presented in Fig.3. The planes have the numbers 6, 7 and 8 (the numeration is from the bottom upwards). The exposure time is 322 days in 2014 year. The spectra have been measured by linear amplitude channels which have the threshold of 6 MeV and the energy resolution of 60 KeV.

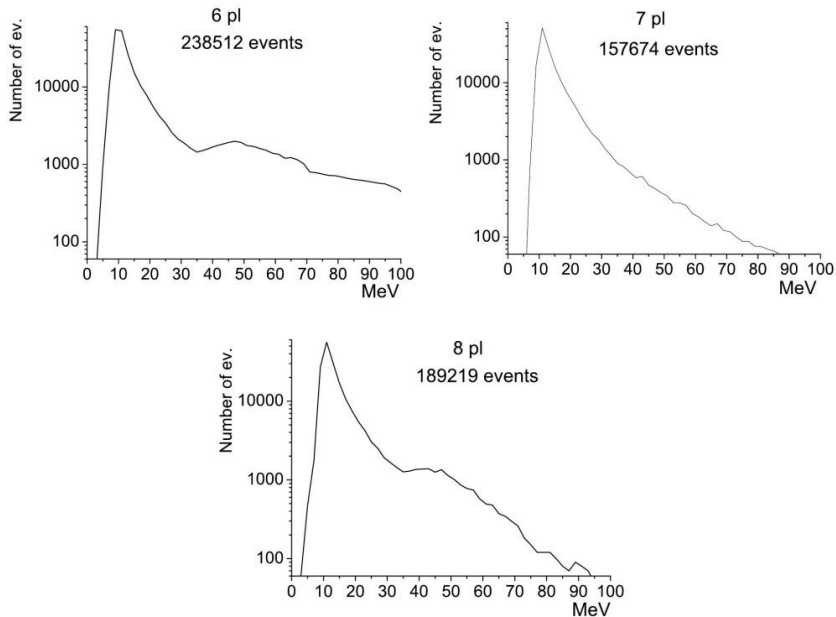


Fig3. Energy spectra of events "1 from 3200" in the 6-th, 7-th and 8-th planes. The exposure time is 322 days (2014 y). The energy bin width is 2 MeV. The total numbers of events are shown in each panel.

The peak in the region of 10 - 15 MeV is due to decays of cosmogenic isotopes (^{12}B , ^{12}N , ^8B , ^8Li etc.), which are generated in inelastic interactions of muons with nuclei of ^{12}C into scintillator and nuclei of surrounding matter. We estimate the rate of cosmogenic isotopes generation on the base of results obtained in [37]. In reality, we observe the summary decay curve from all isotopes which is truncated at

the left side with the operation threshold of counters (8 MeV). The rest single events are muons which pass the external planes without recording (through a slit between counters or brushing counters so that energy deposition is less than 8 MeV).

The expected number of background events during the exposure time is $\approx 190\,000$. This value should be compared with the experimental events number.

Background events can imitate the expected signal (k single events within the sliding time interval τ) with a count rate

$$p(k) = f \times \exp(-f\tau) \frac{(f\tau)^{k-1}}{(k-1)!} \quad (5)$$

The treatment of experimental data (background events over a period 2001 - 2014 y; $T_{\text{actual}} = 11.98$ years) is shown by squares in Fig.4 in comparison with the expected distribution according to the expression (5) calculated at $f = 0.02 \text{ s}^{-1}$. Note there is no normalization in Fig.4.

Background events are to create clusters with $k = 8$ with the rate 0.138 y^{-1} (and $6.9 \cdot 10^{-3} \text{ y}^{-1}$ if $k = 9$). The expected number of clusters with $k = 8$ during the time interval $T_{\text{actual}} = 11.98 \text{ y}$ is 1.65 that we observe in the experiment (2 events). Clusters with $k \geq 9$ should be considered as a neutrino burst signal.

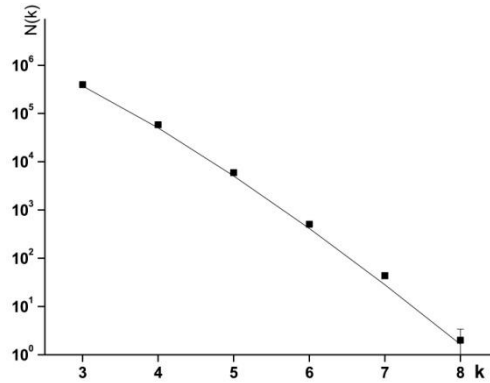
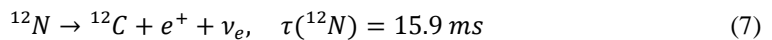
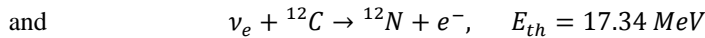
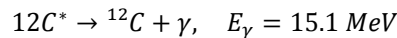
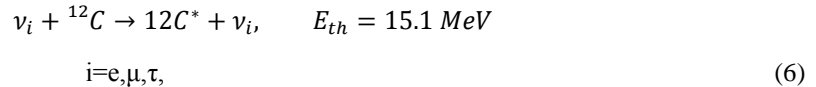


Fig4. Number of bunches with k single events within time interval of $\tau = 20\text{s}$. Squares are experimental data, the curve is the expected number according to expression (5).

3.1. Reactions on Carbon nuclei

There are models which predict the mean neutrino energy from SN is $\overline{E_\nu} = 30 - 40 \text{ MeV}$ [38], [39]. In such case the reactions on Carbon nuclei of the scintillator become effective and neutrinos can be detected in the BUST through interactions:



τ is a lifetime of the nucleus ^{12}N .

Reaction (6) allows us measuring the total neutrino flux with the energy $E_\nu > 15.1 \text{ MeV}$.

If the mean energy $\overline{E}_\nu = 30 \text{ MeV}$ the expected number of events for reactions (6) and (7) can be estimated (under conditions (3)) by the formulae

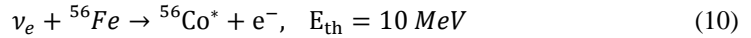
$$N_{ev2}^C = 16 \times \eta_2 \quad (E_\nu = 15 \text{ MeV}) \quad (8)$$

$$N_{ev3}^C = 30 \times \eta_3 \quad (E_\nu = 30 \text{ MeV}) \quad (9)$$

The radiation length for our scintillator is 47 g/cm^2 therefore $\eta_2 \approx 0.3$. In reaction (7) BUST can detect both e^- with energy ($E_\nu - 17 \text{ MeV}$) and e^+ , if the energy deposition from these particles is greater than 8 MeV. In the latter case, reaction (7) will have the distinctive signature: two signals separated by the 1 - 45 ms time interval (dead time of the BUST is 1 ms).

In reaction (7) the sum of energies ($E_{e^+} + E_\nu$) is 17.3 MeV therefore $\eta_3 \approx 0.7$.

The low part of the overlap between horizontal scintillation planes is the 8 mm iron layer. This can be used as the target in the reaction



(cobalt emerges in the excited state).

Under conditions (3) the expected number of events from reaction (10) (neutrinos arrive from above) is

$$N_{ev}^{\text{Fe}} = 6.3 \times \eta_{\text{Fe}} \quad (20 \text{ MeV}) \quad (11)$$

$\eta_{Fe}(20\text{MeV}) \approx 0.3$ is the detection efficiency of e^- with the energy 20 MeV produced into the 8 mm iron layer.

It should be noticed, if $\overline{E}_{\nu e} = 30 - 40 \text{ MeV}$ a noticeable percentage of neutrino reactions will cause triggering two adjacent counters.

4. Discussion and Conclusion

The Baksan Underground Scintillation Telescope operates under the program of search for neutrino bursts since June 30, 1980. The counting rate of single events was stable over the period of observation and its behavior is Poissonian.

One can see from expression (4) that the “radius of sensitivity” of the Baksan telescope is $\approx 20 \text{ kpc}$. This region includes $\approx 95\%$ stars of our Galaxy. For more distant SNe, the cluster-signal will have the number of recorded neutrino events $k < 9$ (if we do not hope for an exotic mechanism with large neutrino energies). In this case, one should investigate the correlations with others detectors.

Over the period of June 30, 1980 to December 31, 2014, the actual observation time was 29.76 years [18], [40]. This is the longest observation time of our Galaxy with neutrino at the same facility.

No candidate for the core collapse has been detected during the observation period. This leads to an upper bound on the mean frequency of gravitational collapses in the Galaxy

$$f_{\text{col}} < 0.077 \text{ y}^{-1}, \quad 90\% \text{ CL} \quad (12)$$

Recent estimations of the Galactic core-collapse SN rate give roughly the value $\approx 2\text{-}5$ events per century (see e.g. [41]).

The results of two-dimensional (2D) [42] – [44] and 3D [12], [13], [45], [14] hydrodynamical simulations of SN progenitors evolution found out considerable deviations from spherical symmetry and imply that SN explosions are multi-dimensional.

In particular, the lepton-number emission self-sustained asymmetry (LESA) phenomenon is identified in 3D simulations [36], [15], i.e. the observed neutrino flux depends on the observer position. The dependence ν_e - and $\bar{\nu}_e$ fluxes arriving to the Earth according the oscillation scenario only complicates the interpretation.

The result obtained in [16] can be an important step on a path leading to conversion of the “delayed explosion scenario” from a standard paradigm to the generally used one.

References

- [1] K. Hirata, T. Kajita, M. Koshiba, et al. “Observation of a neutrino burst from the supernova SN1987A”, *Phys.Rev.Lett.*, v.58, p. 1490, 1987
- [2] R.M. Bionta, G. Blewitt, C.B. Bratton, et al. (IMB collaboration), “Observation of a neutrino burst in coincidence with supernova 1987A in the large magellanic cloud”, *Phys.Rev.Lett.*, v. 58, p. 1494, 1987
- [3] E.N. Alekseev, L.N. Alekseeva, I.V. Krivosheina and V.I. Volchenko, “Detection of the neutrino signal from SN, 1987A using the INR Baksan underground scintillation telescope”, *JETPL*, v. 45, p. 589, 1987
- [4] M. Aglietta, G. Badino, G. Bologna, et.al “On the event observed in the Mont Blanc Underground Neutrino observatory during the occurrence of Supernova 1987A”, *Europhys.Lett.*, v. 3, p. 1315, 1987
- [5] G. Gamow and M. Shoenberg, “The Possible Role of Neutrinos in Stellar Evolution”, *Phys.Rev.*, v.58, p.1117, 1940
- [6] Ya.B. Zeldovich and O.Kh. Guseinov, “Neutronization of matter during collapse and the neutrino spectrum”, *Dokl.Akad. Nauk SSSR*, v. 162, p.791, 1965
- [7] S.A. Colgate and R.H. White, “The hydrodynamic behavior of supernovae explosions”, *Astrophys.J.*, v. 143, p. 626, 1966
- [8] T.J. Loredo, D.Q. Lamb, “Bayesian Analysis of Neutrinos from Supernova SN1987A”, *Phys.Rev.D*, v. 65, p. 063002, 2002
- [9] G. Pagliaroli, F. Vissani, M.L. Costantini, A. Ianni, “Improved analysis of SN1987A antineutrino events”, *Astropart.Phys.*, v. 31, p.163, 2009
- [10] J. R. Wilson, “Supernovae and post-collapse behavior”, in: *Numerical Astrophysics, Proc. Symposium in honour of James R. Wilson, held at the University of Illinois Urbana Champaign, October, 1982*. Ed. by J.M. Centrella, J. M. Le Blanc and R. L. Bowers (Boston: Jones and Bartlett Publ., 1985) p. 422.
- [11] H. A. Bethe and J. R. Wilson, “Revival of a stalled supernova shock by neutrino heating”, *Astrophys. J.* v. 295, p. 14, 1985
- [12] F. Hanke, A. Marek, B. Muller, H.-Th. Janka, “Is strong SASI activity the key to successful neutrino-driven supernova explosions?” *Astrophys. J.* v. 755, p. 138, 2012
- [13] T. Takiwaki, K. Kotake and Y. Suwa, “Three-dimensional hydrodynamic core-collapse supernova simulations for an 11.2 Msun star with spectral neutrino transport”, *Astrophys. J.* v. 749, p. 98, 2012
- [14] C.D. Ott, E. Abdkimalov, P. Moesta, R. Haas, S. Drasco, E. O'Connor, C. Reisswig, C. Meakin and E. Schnetter, “General-Relativistic Simulations of Three-Dimensional Core-Collapse Supernovae”, *Supernovae*, *Astrophys. J.* v.768, p. 115, 2013
- [15] I. Tamborra, F. Hanke, H. Janka, B. Muller, G. Raffelt, A. Marek, “Self-sustained asymmetry of lepton-number emission: a new phenomenon during the supernova shock-accretion phase in three dimensions”, *Astrophys. J.*, v. 792, p. 96, 2014; \arXiv:1402.5418 (2014)
- [16] T. Melson, H-T. Janka, R. Bollig et al., “Neutrino-driven explosion of a 20 solar-mass star in three dimensions enabled by strange-quark contributions to neutrino-nucleon scattering”, \arXiv:1504.07631 (2015)

- [17] M. Ikeda, A. Takeda, Y. Fukuda et al., (Super-Kamiokande Collaboration) “Search for Supernova neutrino bursts at Super-Kamiokande”, *Astrophys.J.*, v. 669, p.519, 2007
- [18] E.N. Alekseev, L.N. Alekseeva, V.I. Volchenko, et al., “Upper bound on the collapse rate of massive stars in the Milky Way given by neutrino observations with the Baksan underground telescope”, *Zh. Eksp.Teor.Fiz.*, v. 104, p.2897, 1993
- [19] R.V. Novoseltseva, M.M. Boliev, I.M. Dzaparova, et al. “The Search for Neutrino Bursts from Core Collapse Supernovae at the Baksan Underground Scintillation Telescope”, *Proc. 31th ICRC, Lodz (2009)*
- [20] M. Ambrosio et al. (MACRO Collaboration) “Search for stellar gravitational collapses with the MACRO detector”, *Eur.Phys.J.C*, v. 37, p. 265, 2004
- [21] M. Aglietta et al. (LVD Collaboration), “The most powerful scintillator supernovae detector: LVD”, *Nuovo Cimento A*, v.105, p.1793, 1992
- [22] N.Yu. Agafonova, M. Aglietta, P. Antonioli et al. (LVD collaboration), “Study of the effect of neutrino oscillations on the supernova neutrino signal in the LVD detector”, *Astropart.Phys.*, v. 27, p. 254, 2007
- [23] J. Ahrens et al. (AMANDA Collaboration), “Search for supernova neutrino bursts with the AMANDA detector”, *Astropart.Phys.*, v. 16,, p. 345, 2002
- [24] B. Aharmim, S.N. Ahmed, A.E. Anthony, et al. “Low Multiplicity Burst Search at the Sudbury Neutrino Observatory”, *Astrophys.J.*, v. 728, p. 83, 2011
- [25] Lund, A. Marek, C. Lunardini, H.-T. Janka and G. Raffelt, “Fast time variations of supernova neutrino fluxes and their detectability”, *Phys. Rev. D*, v. 82, p. 063007, 2010
- [26] G. Bellini et al.(Borexino Collaboration), “First real time detection of ^7Be solar neutrinos by Borexino” *Phys. Lett. B*, v. 658 (4), p. 101, 2007
- [27] G. Bellini, “Novel results on low energy neutrino physics” Talk at TAUP 2011 conference, Munich, 5-9 Sept. 2011,
- [28] K. Eguchi et al. (KamLAND Collaboration), “First Results from KamLAND: Evidence for Reactor Antineutrino Disappearance”, *Phys. Rev. Lett.* , v. 90, p. 021802, 2003
- [29] E.N. Alexeyev, V.V. Alexeyenko, Yu.M. Andreyev, V.N. Bakatanov, et al. “Baksan underground scintillation telescope”, *Proc. of 16 ICRC, Kyoto*, v. 10, p. 276, 1979
- [30] V.M. Achkasov, V.N. Bakatanov, Yu. F. Novoseltsev, et al. “An investigation of the energy spectrum and inelastic muon interaction at the Baksan Underground scintillation telescope” *Bull. Russ. Acad.Sci.Phys.*, v 50, p.2224, 1986
- [31] V.S. Imshennik, D.K. Nadezhin “Final stages of star evolution and supernova explosions”, *Itogi Nauki i Tehniki, ser. Astronomy*, v. 21, p. 63, 1982
- [32] W. Hillebrandt, P. Hoflich, “The supernova 1987A in the Large Magellanic Cloud”, *Rep.Prog.Phys.* v. 52, p. 1421, 1989
- [33] J. Pantaleone, “Neutrino oscillations at high densities”, *Phys. Lett. B*, v. 287, p. 128, 1992
- [34] R.F. Sawyer, “Speed-up of neutrino transformations in a supernova environment”, *Phys. Rev. D* v.72, p.045003, 2005
- [35] H. Duan, G.M. Fuller, J. Carlson, Y.-Z. Qian, “Simulation of Coherent Non-Linear Neutrino Flavor Transformation in the Supernova Environment I: Correlated Neutrino Trajectories”, *Phys. Rev. D*, v. 74, p. 105014, 2006
- [36] I. Tamborra, G. Raffelt, F. Hanke, H.-T. Janka and B. Muller, “Neutrino emission characteristics and detection opportunities based on three-dimensional supernova simulations”, *Phys. Rev. D*, v. 90, p. 045032, 2014; arXiv: 1406.0006 (2014)

- [37] G. Bellini et al.(Borexino Collaboration), “Cosmogenic Backgrounds in Borexino at 3800 m water-equivalent depth”, arXiv: 1304.7381v2 (2013)
- [38] V.S. Imshennik “Explosion Mechanism in Supernovae Collapse”, *Space Sci.Rev.* v. 74, p. 325, 1995
- [39] V. Bajkov, V.M. Suslin, V.M. Chechetkin, V. Bychkov, L. Stenflo, “Radiation of a neutrino mechanism for type II supernovae”, *Russ. Astronom. journal*, v. 84 (4), p. 308, 2007
- [40] R.V. Novoseltseva, M.M. Boliev, G.M. Vereshkov, et al., “The Search for Neutrino Bursts from Collapsing Core Supernovae at the Baksan Underground Scintillation Telescope”, *Bull. Russ. Acad.Sci.Phys.*, v. 75, p. 419, 2011
- [41] S.M. Adams, C.S. Kochanek, J.F. Beacom, M.R. Vagins, K.Z. Stanek, “Observing the Next Galactic Supernova”, *Astrophys.J.*, v. 778, p. 164 , 2013
- [42] T.D. Brandt, A. Burrows, C.D. Ott and E. Livne, “Results from core-collapse simulations with multi-dimensional, multiangle neutrino transport”, *Astrophys. J.* v. 728, v. 8, 2011
- [43] B. Muller, H.-Th. Janka, A. Marek, “A New Multi-Dimensional General Relativistic Neutrino Hydrodynamics Code for Core-Collapse Supernovae II. Relativistic Explosion Models of Core-Collapse Supernovae”, *Astrophys. J.*, v. 756, p. 84, 2012
- [44] B. Muller, H.-T. Janka, A. Heger, “New two-dimensional models of supernova explosions by the neutrino-heating mechanism: evidence for different instability regimes in collapsing stellar cores”, *Astrophys. J.*, v. 761, p. 72, 2012
- [45] A. Burrows, J. Dolence, J. Murphy, “An Investigation into the Character of Pre-Explosion Core-Collapse Supernova Shock Motion”, *Astrophys. J.* ,v. 759, p.5, 2012

Joint analysis of experimental data on the search for neutrino bursts using the BUST and LVD detectors

R. V. Novoseltseva¹, M. M. Boliev¹, I. M. Dzaparova^{1,2}, M. M. Kochkarov¹, Yu. F. Novoseltsev^{1,*}, V. B. Petkov^{1,2}, V. I. Volchenko¹, G. V. Volchenko¹, A. F. Yanin¹, N. Yu. Agafonova¹, V. V. Ashikhmin¹, V. L. Dadykin¹, E. A. Dobrynina¹, R. I. Enikeev¹, A. S. Mal'gin¹, O. G. Ryazhskaya¹, I. R. Shakiryanova¹, V. F. Yakushev¹, and the LVD Collaboration¹

¹*Institute for Nuclear Research of the Russian Academy of Sciences, 60th October Anniversary Prospect, 7a, 117312 Moscow, Russia*

²*Institute of Astronomy of the Russian Academy of Sciences, 48 Pyatnitskaya St., 119017, Moscow, Russia*

**novoseltsev@inr.ru*

Abstract Preliminary results of joint analysis of data of the INR's Baksan Underground Scintillation Telescope (BUST) and the Gran Sasso Large Volume Detector (LVD) are presented. The results can be explained by random pulse coincidences in the BUST and LVD detectors.

Keywords: Supernova, Neutrino Bursts

1. Introduction

The neutrino burst from a supernova (SN) is a very rare and transient event. To record it, several long-time experiments with a high percent of live time are needed.

A joint analysis of data of different facilities, operating in the search for neutrino bursts regime, will allow us to make the search with a greater sensitivity and increase reliability of detected neutrino signals. For the task of supernovae search, this is especially important in cases when the observation of SN is performed under "uncomfortable" conditions, for example, a shading of optical flare by galactic dust or in the case of non-canonical optical luminosity of an SN.

With that end in view, we attempt to carry out a joint analysis of data of the BUST and LVD detectors. In this paper we use the data of both facilities over the period of 2012 - 2014.

Section 2 is a brief description of the BUST and LVD detectors. Section 3 is devoted to the method of neutrino burst detection. In Section 4 the algorithm of the search for temporal coincidences of "single events" clusters in both facilities is presented. Section 5 is the conclusion.

2. The BUST and LVD detectors

The Baksan Underground Scintillation Telescope (BUST) is located in the Northern Caucasus (Russia) in the underground laboratory at the effective depth $8.5 \cdot 10^4 \text{ g} \cdot \text{cm}^{-2}$ (850 m of w.e.) [1]. The facility has the size $17 \times 17 \times 11 \text{ m}^3$ and consists of four horizontal scintillation planes and four vertical ones (Fig. 1).

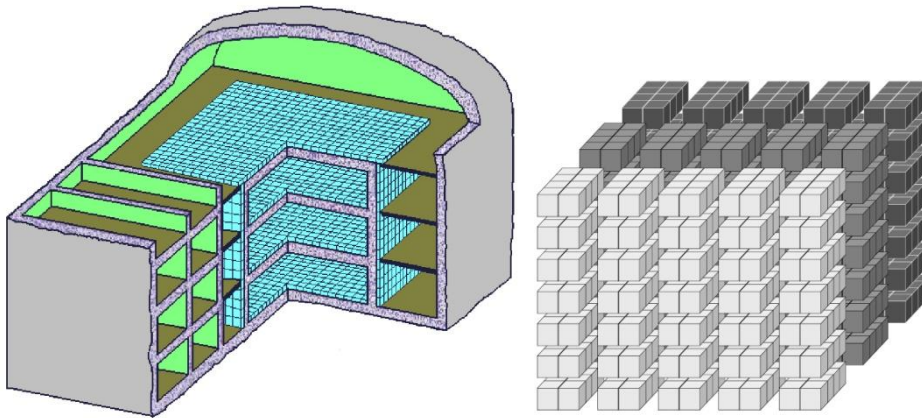


Fig1. Left – the Baksan Underground Scintillation Telescope, Right –the Large Volume Detector (schematic views)

Five planes of them are external planes and three lower horizontal planes are internal ones. The upper horizontal plane consists of 576 (24×24) liquid scintillator counters of the standard type, three lower planes have 400 (20×20) counters each. The vertical planes have (15×24) and (15×22) counters. Each counter is $0.7 \times 0.7 \times 0.3 \text{ m}^3$ in size, filled with the organic $\text{C}_n\text{H}_{2n+2}$ ($n \approx 9$) scintillator, and viewed by one photomultiplier (FEU 49B) with a photocathode diameter of 15 cm. The distance between neighboring horizontal scintillation layers is 3.6 m. The angular resolution of the facility is 2° , the time resolution is 5 ns.

Information from each counter is transmitted over three channels: an anode channel (which serves for triggering formation and amplitude measurements up to 2.5 GeV), a pulse channel with the operation threshold 8 MeV and 10 MeV for the horizontal and vertical planes, respectively (at first this threshold was equal to 12.5 MeV; the most probable energy deposition of a muon in a counter is $50 \text{ MeV} \equiv 1$ relativistic particle) and a logarithmic channel with the threshold $s_0 = 0.5 \text{ GeV}$. A signal from the fifth dynode of PM tube FEU-49 goes to the logarithmic channel where it is converted into a pulse whose length t is proportional to logarithm of the signal amplitude.

The BUST is a multipurpose detector. One of the current tasks is the search for neutrino bursts. The facility has been operating almost continuously under the program of search for neutrino bursts since the mid-1980. The total time of Galactic observation accounts for 90% of the calendar time.

The Large Volume Detector (LVD) is located at the LNGS underground laboratory (the Laboratori Nazionali del Gran Sasso, Italy) at a depth of 3600 m w.e.[2]. The LVD detector is an underground iron scintillator calorimeter with a total mass of 2 kt (1 kt of liquid scintillator and 1 kt of iron). LVD consists of an array of 840 scintillator counters (Fig. 1). The whole array is divided into three identical towers with independent high voltage power supply, trigger and data acquisition. In turn, each tower consists of 35 modules hosting a cluster of 8 counters. Each counter ($1.5 \times 1 \times 1 \text{ m}^3$ in size) is filled with liquid scintillator having a mass of 1200 kg, and is monitored by three FEU 49B or FEU 125 photomultipliers. The operating threshold of the counter is 5 MeV. The total time of Galactic observation accounts for $\approx 99\%$ of the calendar time [3].

Identical hydrocarbon-based scintillators are used in the BUST and LVD detectors.

3. The method of neutrino burst detection

The BUST consists of 3184 standard autonomous counters. The total scintillator mass is 330 t, and the mass enclosed in three lower horizontal layers (1200 standard counters) is 130 tons. The majority of

events recorded with the Baksan telescope from a supernova explosion will be produced in inverse beta decay reactions



If the mean antineutrino energy is around 15 MeV [4], [5], the pass of e^+ (produced in reaction (1)) will be included, as a rule, in the volume of one counter. In such a case the signal from a supernova explosion will appear as a series of events from singly triggered counters (a single counter of 3184 operates; below we call such an event “the single event” or “1 from 3200”) during a neutrino burst.

Background events are radioactivity and cosmic ray muons if only one counter from 3184 hit. The total count rate from background events is $f = 0.02 \text{ s}^{-1}$ in internal planes (three lower horizontal layers) and $\approx 1.5 \text{ s}^{-1}$ in external ones. Therefore three lower horizontal layers are used as a target. The trigger is an operation of any counter pulse channel (with the threshold 8 MeV).

In Fig.2 we show how the counter operation threshold changed with time (12.5 \rightarrow 10 \rightarrow 8 MeV) and the corresponding total count rate of single events in the three internal planes (1200 counters, the target mass is 130t).

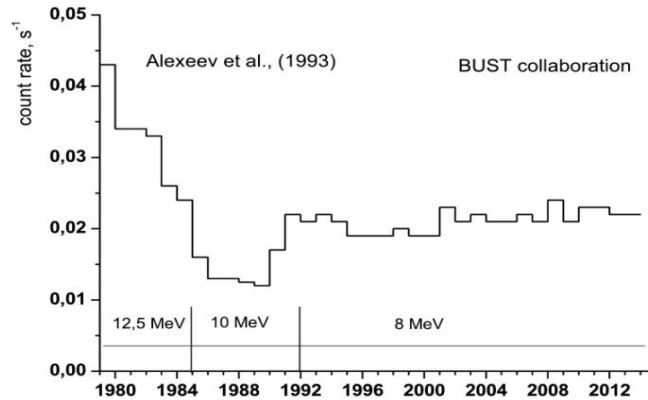


Fig2. The mean count rate of single events in the three telescope internal planes (1200 counters) vs the counter operation threshold.

Background events can imitate the expected signal (k single events within sliding time interval τ) with a count rate [6]

$$p(k) = f \times \exp(-f\tau) \frac{(f\tau)^{k-1}}{(k-1)!} \quad (2)$$

The processing of experimental data (background events over a period 2001 - 2014 y; $T_{\text{actual}} = 11.98$ years) is shown by squares in Fig.4 in comparison with the expected distribution according to expression (2) calculated at $f = 0.02 \text{ s}^{-1}$. Note there is no normalization in Fig.3.

Background events are to create clusters with $k = 8$ with the rate $= 0,138 \text{ y}^{-1}$ (and $= 6.9 \cdot 10^{-3} \text{ y}^{-1}$ if $k = 9$). The expected number of clusters with $k = 8$ during the time interval $T_{\text{actual}} = 11.98 \text{ y}$ is 1.65 what we observe in the experiment (2 events). Clusters with $k \geq 9$ should be considered as a neutrino burst signal.

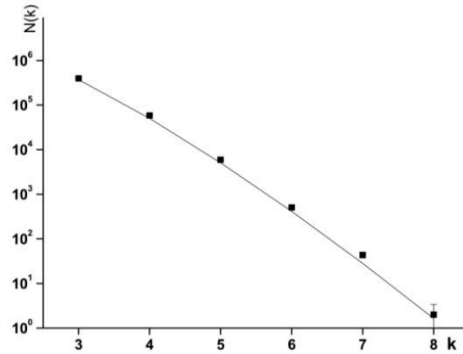


Fig3. The BUST; the number of bunches with k single events within time interval of $\tau = 20$ s. Squares are experimental data, the curve is the expected number according to the expression (2)

The search for a neutrino burst in the LVD detector consists also in the recording of a single- event cluster within a time interval of $\tau = 20$ s (in the case of the LVD detector, “the single event” is “1 from 840” event). In order to reduce the count rate from background events, the counters of internal part of the facility were selected. A total of 360 counters in the LVD detector were selected for further analysis. The count rate of single events in the array of 360 counters selected for analysis in the LVD is 0.4 s^{-1} . It is shown in Fig.4.

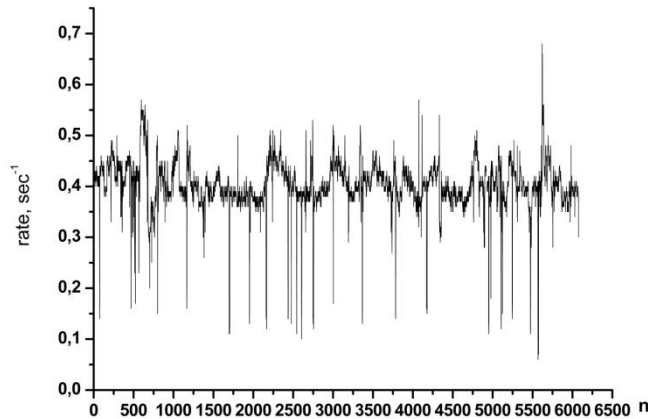


Fig4. The LVD; the count rate of single events in the array of 360 counters vs the RUN number; (data of 2012 – 2014 years, the number of RUNs 6074)

4. The joint analysis of the BUST and LVD data

We carried out a search for coincidence of clusters of single events in both facilities (BUST and LVD). It should be noticed, we treat background events certainly and the present analysis is of methodical character. The search for the clusters coincidence has been performed for two variants:

- 1) search for clusters in LVD, which coincide with clusters in the BUST and the “inverse” task
- 2) search for clusters in BUST, which coincide with clusters in the LVD.

In the first variant we proceed from the fact that, for a real neutrino burst, an LVD cluster begins

earlier than that at the BUST. It is related with a larger target mass in the LVD (430 t instead of 130 t in the BUST) and a smaller value of the detection threshold (5 MeV instead of 8 MeV at the BUST). It will lead to that the number of recorded neutrino events in LVD, k_{LVD} , will be 4-5 times greater than the event number in BUST:

$$k_{LVD} \approx (4 - 5) * k_{BUST} \quad (3)$$

Therefore the search algorithm was the following.

For each cluster in BUST, which has a fixed number of events, k_{BUST} , and starts at t_{BUST} , we search (20 s) for clusters in LVD which start in the interval from $(t_{BUST} - 10 \text{ s})$ up to t_{BUST} . Among the latter the cluster with the maximal multiplicity k_{LVD} is compared with the one in BUST at t_{BUST} . As a result of such processing, the distributions of LVD clusters on the multiplicity, k_{LVD} , were obtained for a given number of events in the cluster in BUST (Fig.5). Some parameters of these distributions are shown in Table1.

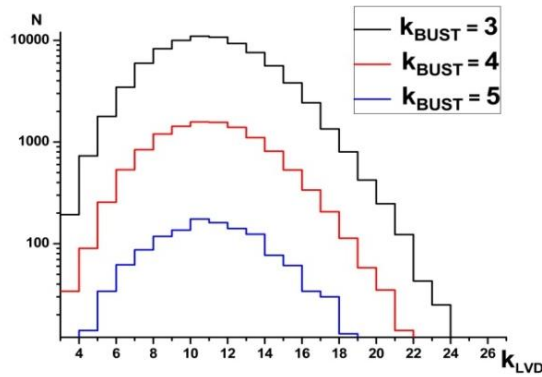


Fig5. Distributions of LVD clusters on the multiplicity, k_{LVD} , for the fixed number of events in the BUST cluster

As one can see from the table, the mean and most probable number of events in the LVD clusters does not change when the multiplicity of BUST clusters grows, as it would be if the events in the clusters are background events. It is clear also that the value of \bar{k} does not practically change at the occurrence of even several of real neutrino bursts. I.e. the parameter \bar{k} is not sensitive to presence of neutrino bursts, however it is an indicator of stable operation of the facility.

Table1. $N(k_{BUST})$ - the number of clusters registered for BUST; \bar{k}_{LVD} - the mean number of events in LVD clusters; k_{peak} - the number of events at which the peak in the distribution is observed (due to poor statistics, no peak is observed at $k_{BUST} = 6$ and 7)

k_{BUST}	$N(k_{BUST})$	\bar{k}_{LVD}	k_{peak}
3	83909pt	9.71	10
4	12126	9.70	10
5	1273	9.63	10
6	90	9.08	
7	8	8.63	

It should be noted that although the cluster in the LVD, in case of a real neutrino signal, always starts earlier cluster in BUST, this advance does not certainly exceed of 10 seconds. Therefore, the proposed algorithm provides a search for correlations for all models of the collapse of the star core.

The “inverse” task consisted in the search for clusters in the BUST that began less than 10 s later than the LVD clusters. Such coincidences were sought in three ranges of LVD cluster multiplicity: 6–8, 12–14 and 18–20 events in a cluster. The obtained multiplicity distributions of BUST clusters are presented in Table 2. As in the former case, the mean number of events in BUST clusters, k , remains the same as the multiplicity of LVD clusters grows. This indicates to stable operation of BUST.

Table2. Multiplicity distributions of the BUST clusters that coincided in time with LVD clusters with fixed multiplicity

k_{LVD}	2	3	4	5	6	\bar{k}_{BUST}
6 - 8	89912	6440	329	8	0	2.07
12 - 14	58848	4055	201	8	0	2.07
18 - 20	2178	168	11	0	0	2.08

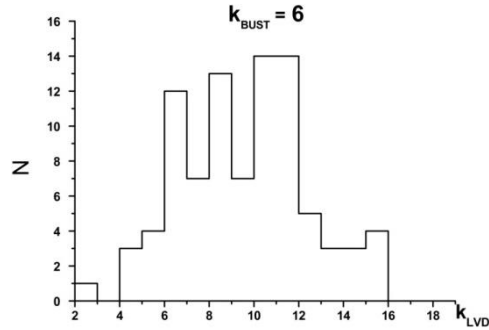


Fig6. The multiplicity distribution of LVD clusters which coincide with BUST clusters at $k_{BUST} = 6$

In Fig.6, the multiplicity distribution of LVD clusters which coincide with BUST clusters at $k_{BUST} = 6$ is shown. If we assume that any of 90 BUST clusters with $k_{BUST} = 6$ (see Table 1) is the signal from a real neutrino burst (from some distant source) then the corresponding cluster in LVD must have (according to estimation (3)) $\approx 25 - 30$ events. The distribution in Fig.A3 terminates at the multiplicity $k_{LVD} = 15$. It does imply that none of 90 BUST clusters with $k_{BUST} = 6$ can be considered as a candidate for the neutrino burst signal.

5. Conclusion

We have presented the first results of the joint analysis of the BUST and LVD data on the search for neutrino bursts.

We have performed the search for coincidence of clusters of single events in the BUST and LVD detectors over the period of 2012 – 2014. The obtained results point out to the stable operation of the

facilities and can be explained by random coincidences of background events.

The joint analysis of data of different facilities can be especially useful for the recording of neutrino bursts from distant sources (e.g. in Magellanic Clouds).

References

- [1] E.N. Alexeyev, V.V. Alexeyenko, Yu.M. Andreyev, et al. "Baksan underground scintillation telescope", Proc. of 16 ICRC, Kyoto, v. 10, p. 276, 1979
- [2] M. Aglietta, et al. (LVD Collaboration), Proc. 27th Int. CosmicRay Conf., Hamburg, 2001, v. 3, p. 1093
- [3] N.Yu. Agafonova a, M. Aglietta, P. Antonioli, et al. (LVD collaboration), "On-line recognition of supernova neutrino bursts in the LVD", Astropart.Phys., v. 28, p. 516, 2008
- [4] V.S. Imshennik, D.K. Nadezhin, "Final stages of star evolution and supernova explosions", Itogi Nauki i Tehniki, ser. Astronomy, v. 21, p. 63, 1982
- [5] W. Hillebrandt, P. Hoflich, "The supernova 1987A in the Large Magellanic Cloud", Rep.Prog.Phys. v.52, p. 1421, 1989
- [6] R.V. Novoseltseva, M.M. Boliev, G.M. Vereshkov, et al., "The Search for Neutrino Bursts from Collapsing Core Supernovae at the Baksan Underground Scintillation Telescope", Bull. Russ. Acad.Sci.Phys., v. 75, p. 419, 2011
- [7] E.N. Alekseev, L.N. Alekseeva, V.I. Volchenko, et al. "Upper bound on the collapse rate of massive stars in the Milky Way given by neutrino observations with the Baksan underground telescope", Zh. Eksp. Teor.Fiz., v. 104, p.2897, 1993

Prospects of detecting the QCD phase transition in the Galactic supernova neutrino burst with 20-kton scale liquid scintillation detectors

V. B. Petkov^{1,2,*}

¹*Institute for Nuclear Research of the Russian Academy of Sciences, 60th October Anniversary Prospect, 7a, 117312 Moscow, Russia*

²*Institute of Astronomy of the Russian Academy of Sciences, 48 Pyatnitskaya St., 119017, Moscow, Russia*

*vpetkov@inr.ru

Abstract. The supernova explosion in the Galaxy is a rare event; that is why the comprehensive study of the next one has absolute priority for the low-energy neutrino astronomy. Because the detailed explosion mechanism has not been unambiguously identified yet and the surrounding matter envelope is opaque for photons, the neutrinos only can give information about physical conditions, dynamics of the collapse, and the SN mechanism. Furthermore, neutrinos could potentially reveal new physics (e.g. QCD phase transition) operating deep in the stellar core.

Keywords: Supernova, Neutrino Bursts

1. Introduction

Observing a high-statistics neutrino signal from supernova explosions in the Galaxy is the major goal of the low-energy neutrino astronomy. The prospects for detecting all flavors of neutrinos and antineutrinos from a core-collapse supernova (ccSN) in operating and forthcoming large liquid scintillation detectors (LLSDs) are widely discussed now. The new-generation large liquid scintillation detectors must have the capability to distinguish the various detection channels. Large statistics must be collected to study spectra and time profiles of all neutrino flavors, thereto the new detectors should have enough large target mass. The peculiarities in the neutrino signal from the ccSNe can also be detected in the forthcoming LLSD.

The QCD phase transition during the postbounce evolution of core-collapse supernovae can be observable as the second peak in a neutrino signal that is accompanied by significant changes in energy of emitted neutrinos [1]. In contrast to the first neutronization burst, this second neutrino burst is dominated by emission of antineutrinos. This circumstance is useful for detection of this peak due to the high cross section of inverse beta decay reaction [2].

2. Next-generation detectors

2.1. The proposed LLSD

The large liquid scintillation neutrino detectors, such as JUNO [3, 4], RENO-50 [5] and LENA [6], are under consideration now. The proposed LLSDs are being planned for a variety of physics reasons. These include determination of the neutrino mass hierarchy, precision measurement of neutrino parameters, detection of supernova neutrinos, solar neutrinos, geoneutrinos, sterile neutrinos, atmospheric neutrinos, nucleon decay, and many other exotic searches.

JUNO will have an inner volume of 20 kton and RENO-50 is being designed to have an inner volume of 18 kton. LENA will have a much larger target mass of liquid scintillator, 50 kton. At low energies, the

variety of detection channels available in liquid scintillator will allow us making the energy- and flavor-resolved analysis of a neutrino burst emitted by a galactic supernova. Due to target mass and background conditions, LENA will also be sensitive to the faint signal of the Diffuse Supernova Neutrino Background.

2.2. Baksan Large Volume Scintillation Detector (BLVSD)

One of the proposed LLSDs is the Baksan Large Volume Scintillation Detector (BLVSD). This detector will be installed at the Baksan Neutrino Observatory (BNO) of the Institute for Nuclear Research, Russian Academy of Sciences, at a depth of 4800 m.w.e. (Fig. 1).

A large volume detector filled with liquid scintillator at the Baksan Neutrino Observatory has been discussed for a long time [7], [8], [9], [10], [11]. The main research activities of BLVSD are neutrino geophysics and neutrino astrophysics. At present R&D work aimed at creation of a new-generation detector using an extra-pure scintillator of 5 – 20 kiloton mass is performed [12], [13], [14], [15], [16], [17].

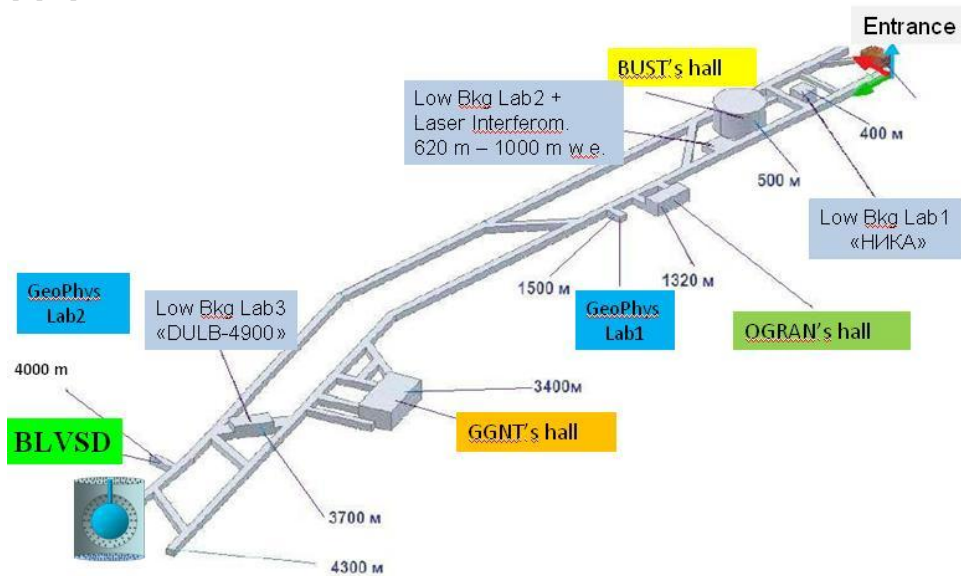


Fig1. Schematic view of the underground laboratories of the Baksan Neutrino Observatory of INR RAS.

The recent development of new experimental techniques has opened up an opportunity for a new kind of large-scale detectors capable both to detect all flavors of neutrinos and to reconstruct the supernova location. The approach exploiting the glowing track of a charged particle is under development now in INR RAS [16], [17]. A charged particle traversing a liquid scintillator induces scintillation along its track. At each point of the track the produced light is emitted isotropically. The use of suitable multi-pixel photodetectors (such as CCD or SiPM matrices) with appropriate optical collector gives, in principle, a possibility to do a snapshot of this glowing track. This technique has obvious advantages. Firstly, the snapshot of glowing track of a particle gives a possibility in principle to determine the direction of the particle. Secondly, there is a possibility to measure the energy release along the particle track. But there are some challenges with this method. One of them is that, as opposed to PMTs, each photodetector has a large number of channels. Moreover, for the precise study of detected events the target mass of the new detector should not be too large [16]. On the other hand, large target mass of the detector is needed for obtaining large statistics of neutrino events. Nevertheless, this apparent contradiction can be resolved by

creating a network of identical LLSDs, with the target mass of LLSD in the range of 2 – 5 kilotons. The Baksan Neutrino Observatory is one of the optimal sites for location of a detector of the network.

3. Detecting the QCD phase transition in the ccSN neutrino burst

Simulations of the stellar core-collapse with the QCD phase transition predict a sharp burst of electron antineutrinos several hundred milliseconds after the prompt electron neutrinos neutronization burst [1]. Observational signatures of such electron antineutrinos burst at current neutrino detectors – IceCube and Super-Kamiokande – were studied in paper [2]. It was found that signatures of the QCD phase transition can be detected for a Galactic ccSN, regardless of the neutrino oscillation scenario.

Super-Kamiokande is an imaging water Cherenkov detector containing 50.0 kilotons of pure water; but the usual fiducial mass for neutrino measurements is 22.5 kton, with the approximately 1.5×10^{33} free protons [18]. Figure 2 (taken from paper [2]) shows the reconstructed antineutrino event rates expected in Super-Kamiokande for the normal mass hierarchy in square points (blue) with statistical error bars. The range of allowed rates for other possible oscillation scenarios is shown by the shaded band (red). One can see that the QCD burst would produce approximately 60 excess events in two relevant bins. The statistics of antineutrino events allows us identifying the QCD burst even at a ccSN distance of 20 kpc. It is very important because within this distance more than 95% of expected Galactic ccSNs are contained [19].

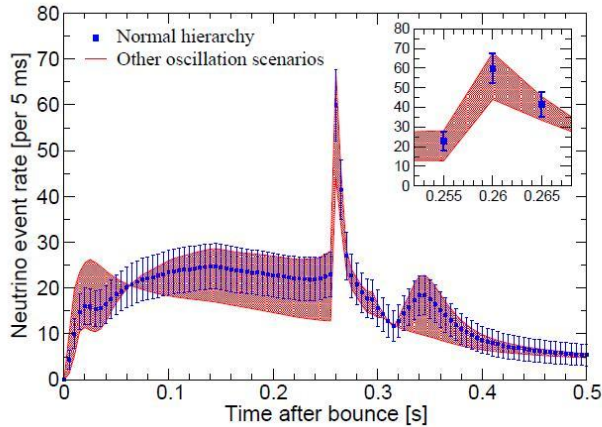


Fig2. Reconstructed antineutrino event rates at Super-Kamiokande (the inset shows the enlarged second burst). This figure is taken from paper [2] (arXiv:0912.2568v2).

The LLSD with fiducial mass of 20 kton and linear-alkyl-benzene (LAB) as a solvent contains approximately 1.49×10^{33} free protons. This means that such LLSD can recognize the QCD burst from a Galactic ccSN in the same fashion as the Super-Kamiokande detector.

4. Conclusion

The proposed large liquid scintillation neutrino detectors are acceptable to detect all flavors of neutrinos from the Galactic core-collapse supernova and to measure the total and average energy in each. Possible detection strategies to measure the total and average energy of all supernova neutrino flavors with appropriate precision are being developed [20]. The QCD phase transition during the postbounce evolution of core-collapse supernovae can be observable by LLSD with a target mass of 20 kton or more. Such LLSD can recognize the QCD burst from almost any Galactic ccSN.

Acknowledgements

This work was supported by the Russian Foundation for Basic Research (grant 14-22-03075).

References

- [1] Sagert et al. Signals of the QCD phase transition in core-collapse supernovae. *Phys. Rev. Lett.* 102, 081101, 2009. arXiv:0809.4225.
- [2] B. Dasgupta et al. Detecting the QCD phase transition in the next Galactic supernova neutrino burst. *Phys. Rev. D* 81, 103005, 2010. arXiv:0912.2568.
- [3] M. He (JUNO Collaboration). Jiangmen Underground Neutrino Observatory. arXiv:1412.4195.
- [4] Y.-F. Li. Overview of the Jiangmen Underground Neutrino Observatory (JUNO). *International Journal of Modern Physics: Conference Series*, 31, 1460300, 2014. arXiv:1402.6143.
- [5] S.-B. Kim. New results from RENO and prospects with RENO-50. arXiv:1412.2199.
- [6] M. Wurm et al. (LENA Collaboration). The next-generation liquid-scintillator neutrino observatory LENA. *Astropart.Phys.*, 35, 685, 2012. arXiv:1104.5620.
- [7] G.V. Domogatsky, V.I. Kopeikin, L.A. Mikaelyan, V.V. Sinev. Neutrino Geophysics at Baksan I: Possible Detection of Georeactor Antineutrinos. *Phys.At.Nucl.*, 68, 69, 2005. arXiv: hep-ph/0401221.
- [8] G.V. Domogatsky, V.I. Kopeikin, L.A. Mikaelyan, V.V. Sinev. Neutrino Geophysics at Baksan (Part II): Possible Studies of Antineutrino- and Radiogenic Heat Sources in Earth Interior. *Phys.At.Nucl.*, 69, 43, 2006. arXiv: hep-ph/0409069.
- [9] G.V. Domogatsky, V.I. Kopeikin, L.A. Mikaelyan, V.V. Sinev. Can Radiogenic Heat Sources Inside the Earth be located by their Antineutrino incoming Directions? *Phys.At.Nucl.*, 69, 1894, 2006; arXiv: hep-ph/0411163.
- [10] G.V. Domogatsky, V.I. Kopeikin, L.A. Mikaelyan, V.V. Sinev. On Possibilities of Studying of Supernova Neutrinos at BAKSAN. *Phys.At.Nucl.*, 70, 1081, 2007; arXiv:0705.1893.
- [11] I.R. Barabanov, G.Ya. Novikova, V.V. Sinev, E.A. Yanovich. Research of the natural neutrino fluxes by use of large volume scintillation detector at Baksan. Preprint INR 1228/2009. arXiv:0908.1466.
- [12] N.B. Lubsandorzhev, L.B. Bezrukov, B.K. Lubsandorzhev et al. Measurements of the Scintillation Decay Times of Liquid Scintillators Based on Linear Alkylbenzene and Pseudocumene and Developed for Neutrino Experiments of the Next Generation. *Instruments and Experimental Techniques*, 56, 34, 2013.
- [13] L.B. Bezrukov, N.I. Bakulina et al. Study of transparency of the of domestic growth LAB as solvent for scintillator of large volume. Preprint INR 1382/2014 (in russian).
- [14] I.R. Barabanov, L.B. Bezrukov, A.V. Veresnikova et al. Measurements of content of ^{14}C in the liquid scintillators with small volume detector inside of low-background box. Preprint INR 1393/2014 (in russian).
- [15] I.R. Barabanov, L.B. Bezrukov, A.V. Veresnikova et al. Method of purification of liquid organic scintillator on base of LAB from trace contaminants of uranium, thorium and potassium-40. Preprint INR 1397/2014 (in russian).
- [16] V.B. Petkov. Prospects of the search for neutrino bursts from Supernovae with Baksan Large Volume Scintillation Detector. arXiv:1508.01389.
- [17] I.M. Dzaparova et al. Study of the characteristics of SiPMs matrix as a photosensor for the scintillation detectors. arXiv:1512.05939.
- [18] M. Ikeda et al. (The Super-Kamiokande Collaboration). Search for supernova neutrino bursts at Super-Kamiokande. *Astrophys. J.*, 669, 519, 2007. arXiv:0706.2283.
- [19] S.M. Adams et al. Observing the Next Galactic Supernova. *Astrophys. J.*, 778, 164, 2013. arXiv:1306.0559.
- [20] R. Laha, J.F. Beacom, and S.K. Agarwalla. New Power to Measure Supernova ν_e with Large Liquid Scintillator Detectors. arXiv:1412.8425.

Current status of GW experiment and multi-messenger astronomy

V. N. Rudenko

Sternberg Astronomical Institute, Lomonosov Moscow State University, Universitetskii prospect 13, Moscow 119991, Russia; e-mail: rvn@sai.msu.ru

Abstract. A limited review of the status of advanced gravitational wave interferometers is presented. In addition, a new opto-acoustical gravitational detector OGRAN in the deep underground of BNO INR RAS is described. The second part of the paper contains a short description of the “multi-messenger astronomy” approach in the context of the GW detection. Various scenarios of such strategy proposed by different authors are discussed. Special attention is paid to the “neutrino-gravity correlation” which looks more or less realistic in respect of supernova events in the Milky Way and near-by galaxies.

Keywords: GW Detection, Multistage Collapses, Neutrino-EM-Gravity Correlations

1. Introduction

It seems that a pursuit for the Gravitational Wave Astronomy is stepped in its decisive stage: three big wide frequency band gravitational antennae (free mass laser gravitational interferometers) finished the upgrade process and at present are going through the commissioning phase [1]. They will enter a new qualitative state when the expected rate of gravitational stochastic signals can reach the average number of events up to several ones per day [2]. A distance from which these antennae are capable to register a signal is estimated by the value of few hundred Mpc, i.e. it is the cosmological scale of distance. In this talk we very briefly present the essence of the last modernization of these instruments, describe an original national OGRAN antenna of moderate sensitivity as well and finally discuss the problem of multichannel reception in searching for gravitational wave signals, so called the strategy of “multi-messenger astronomy”.

2. Sensitivity jump in advanced interferometers

In Fig.1 one can look at the noise level suppressing after transition from the old version of LIGO GW interferometers to new advanced instruments [3]. The jump of five times in the registered amplitude spectral component and more than one order of value in the signal power spectral density are demonstrated in this graph. It was achieved due to the following modernization of hardware in the three key nodes of the setup. First, the quality of seismic isolation was improved so that the noise spectral density $h = 10^{-21} \text{Hz}^{-1/2}$, which was typical for the frequency region 50 Hz in the first setup version, was shifted now to the region of 10 Hz. Second, the same shift was realized for the mirror’s Brownian noises with the typical spectral density $h = 10^{-22} \text{Hz}^{-1/2}$. Third, the photon noise reduction was realized by increasing the pump power so that at the frequency ~ 1 kHz the amplitude spectral density was evaluated from $h = 10^{-22} \text{Hz}^{-1/2}$ to the smallest level $h = 5 \cdot 10^{-23} \text{Hz}^{-1/2}$.

Advanced LIGO vs. Initial LIGO

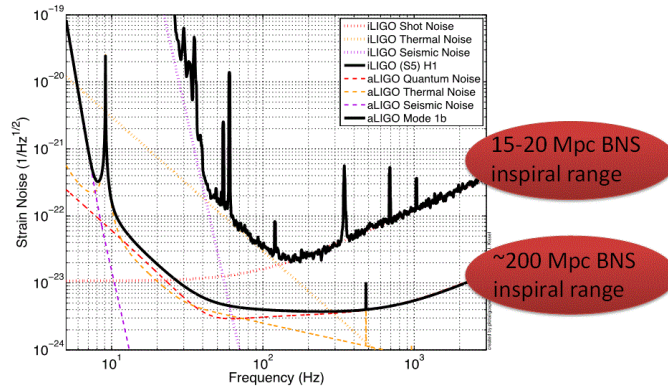


Fig1. Comparison of the initial and advance LIGO noise spectral density.

Approximately the same improvement was performed after modernization of the VIRGO setup [4] (see Fig.2). To illustrate capabilities of these instruments in solution of the problem of GW astrophysical signals detection we present Fig.3 containing the forecast of relativistic binary calescence event reliable registration from the distance 200 Mpc with the rate of events ~ 10 per day. [2, 3, 4]. Together with these extremely advanced setups the other ones – cryogenic resonance bar detectors, NAUTILUS and AURIGA, with the narrow reception frequency band in kilohertz region with sensitivity $h = 10^{-21} \text{ Hz}^{-1/2}$, – were in operation during last few years [5, 6]. It is worth mentioning here that recently a new original resonance opto-acoustical bar detector OGRAN with a moderate sensitivity was installed in the deep underground of the Baksan Neutrino Observatory [7, 8].

VIRGO sensitivity evolution

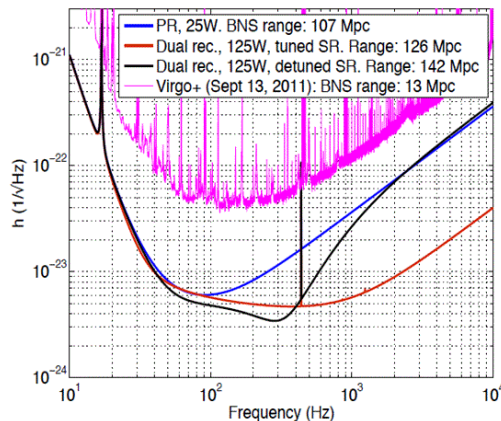
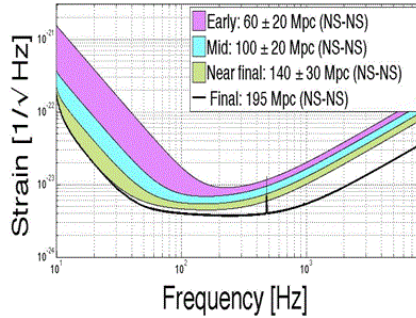


Fig2. The same comparison for VIRGO interferometer.

Detection of **Neutron Star Binaries Coalescence** LIGO program 2015 - 2022



Neutron Star Binaries:
Advanced LIGO: ~ 200 Mpc
"Detection rate" $\sim 10/\text{year}$

Class. Quant. Grav. **27**, 173001 (2010)

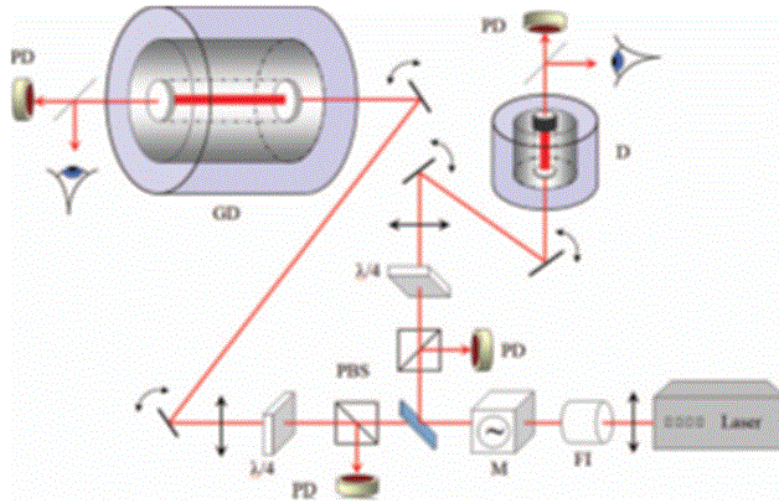
(Initial LIGO: ~ 15 Mpc, Rate
 $\sim 1/50$ years)

Fig3. Expected efficiency of reception of the GW- signal from Neutron Star Binaries coalescence for advance LIGO

3. The opto-acoustical detector in BNO INR RAS

The idea of construction of a GW detector as an acoustical resonance bar coupled with the optical FP cavity composed by mirrors attached to the bar ends was considered in [9] and [10]. A new quality was emphasized of such a combination: (a) a more complex structure of signal response, containing separately acoustical and optical parts, and (b) a possibility to get sensitivity at the level of bar Brownian noise in a relatively wide spectral frequency range due to the small back action of optical read out. The plan for implementation of this idea was reported as the OGRAN project and the first pilot model was presented in [11]. At present the full scale setup was constructed, tested and installed into underground facilities of BNO INR RAS. A perspective of the next development is associated with a cryogenic version of the opto-acoustical bar considered in [12] having a final goal sensitivity $h \sim 10^{-23} \text{ Hz}^{-1/2}$.

The principal opto-electronic scheme of the setup is given in Fig. 4. Generally, it belongs to the design type called a comparator of optical standards. It is composed of two feedback loops. The first one couples the FP cavity at the large bar (OGRAN detector) with the pump laser coercing a generated frequency to be in optical resonance with bar cavity. Thus any change of the FP optical length is converted into the pump beam frequency variation. The second loop is the measuring one. It consists of the additional FP reference cavity or a "frequency discriminator" illuminated by the same pump laser but tuned in resonance by an independent piezo-ceramic driver attached to the one of discriminator's mirror. So its output signal is proportional to the frequency difference of the pump and discriminator cavity. It means that any perturbation of the detector bar cavity is reflected in the discriminator signal. A similar scheme was tested for the AURIGA optical bar detector [13]. However, the OGRAN detector has a big FP cavity at the same scale as its acoustical resonance bar. Meanwhile the AURIGA project used a mini gap FP resonator (a kind of optical accelerometer) placed on a displacement transducer attached to one of the bar detector ends. Just this feature presents the OGRAN physical specificity: the gravitational wave interacts not only with acoustical degree of freedom (the resonance bar) but with the EM field in the cavity as well (that is why one can tell about a complex structure of signal response with optical and acoustical parts. A payment for this originality is the technical problem of constructing a large scale high finesse FP cavity rigidly coupled with the acoustical resonator without losing its high mechanical resonance quality factor Q .



The principal opto-electronic scheme of the setup OGRAN. GD - gravitational detector, PD - photo detector, D - discriminator, FI - Faraday isolator, M - modulator, and PBS - polarized beam splitter.

Fig4 Optical scheme of the OGRAN

The potential sensitivity of such a gravity gradiometer is defined by the thermal Brownian noise of fundamental acoustical mode. Under optimal filtration procedure, the minimum registered perturbation of the OGRAN optical length in the bandwidth Δf is read as $h \sim 10^{-20} (F\Delta f)^{1/2} \text{Hz}^{-1/2}$. Here the numerical factor corresponds to the OGRAN parameters: $M = 10^3 \text{ kg}$, $L = 2 \text{ m}$, $\omega_0/2\pi = 1.3 \text{ kHz}$, and $T = 300 \text{ K}$, $Q = 10^5$. The noise factor F describes the excess of optical readout fluctuation over the thermal noise level. So for the room temperature OGRAN detector, the integral potential sensitivity $h \sim 10^{-19}$ might be provided in the bandwidth $\Delta f = 100 \text{ Hz}$ if $F \sim 1$. Thus, the main technical challenge for the OGRAN construction was to provide optical readout with the noise factor $F = 1$.

Calculation of the noise factor for the optical readout associated with the Pound-Drever technique resulted in the formula $F = (2M/\tau) (G_e/G_T)^{1/2}$, where the following notations were used: a spectral density of optical fluctuations $G_e = B\omega_0^2(2h\nu_e/\eta P)(\lambda_e/2\pi N)^2$ with the parameters: $\eta \sim 0.7$ – the photodiode quantum efficiency, N – the number of reflection of FP cavity (proportional to finesse), $\tau = (1/\Delta f)$ – the time of measurement, $B = (1 - 1000)$ – the phenomenological factor of exceeding the Poissonian level of laser noise; the spectral density of the bar thermal (Brownian) fluctuations $G_T = 2kTM\omega_0/Q$; the parameter M is the effective mass was roughly equal to the half of total bar mass; τ is the measurement time (the resonance signal duration for the optimal filtration) or the inverse value of filtering bandwidth Δf . Under the maximum laser power $P = 2 \text{ W}$, the incoming luminosity for each of both FP resonators cannot exceed a half of watt. But due to losses in the light guide elements and the interference contrast $\sim 10\%$ the real value of effective power is $P = 0.01 \text{ W}$. Substituting all numerical data together with the measurement time $\tau = 0.01 \text{ s}$ leads to the resulting estimate of the required number of reflections (mirror's quality): $N = (10^3 - 10^4)$ (or better). Thus the uncooled opto-acoustical gravitational antenna was constructed for a multi-channel mode operation in the deep underground of Baksan Neutrino Observatory (look at the photo Fig.5 in parallel with Baksan Underground Scintillator Telescope (BUST) involved in the collapse searching for the program.

In the last part of this article we present also a brief prospect of the multi-channel observational strategy.



Fig5. The OGRAN detector chamber in the dust-protected box.

4. Strategy of the multi-messenger astronomy

The task of direct detection of gravitational radiation from relativistic extra terrestrial sources is very difficult due to extremely weak influence of gravitational waves (GW) on detectors and due to unpredictable nature of relativistic catastrophic events in the Universe. Up to now no reliable GW signal has been registered by available GW facilities of both types: resonance bar detectors and free-mass laser interferometers. In such a situation the idea of multichannel registration was proposed to increase the detection probability. Still, cooperative observations using different methods can, on the one hand, help to make the claims about GW detection more robust, i.e. to raise the confidence of GW detection, on the other hand, can significantly deepen our understanding of the physics related to astrophysical sources of GWs (see a brief summary in [14]).

Observations aimed at GW detection can be divided into two broad types: multi-wavelength electromagnetic (EM) and non-EM ones. The latter are mostly related to neutrino (ν)-signals. For EM observations we can also speak about two types: the follow-up observations (when registration of a GW signal serves as a trigger) and the independent observations when, for example, coincidence of two transients is derived from an off-line reduction. Below we will briefly comment on each approach, with more detailed discussion of planned observations with the OGRAN detector.

Two main sources for transient GW signals with possible counterparts are supernovae (SNe) and binary coalescence where neutron stars (NS) are involved.

There is a plethora of data related to observations of (SNe) including ν -signals [15, 16]

Unfortunately, the present-day detectors are sensitive to GW signal from an SN explosion only in a very limited volume which includes the Milky Way and close-by galaxies. The rate of core-collapse SNe

in our Galaxy is $\sim 1/30 \text{ yrs}^{-1}$. This is not very promising. In addition, in some cases we can miss the optical counterpart due to huge interstellar absorption [17]. In this case only simultaneous detection of a -burst can confirm the detection. The most optimistic scenario – two-stage collapse – was proposed and developed to explain double neutrino signal from the SN1987A.[18 – 20]

Baksan Neutrino Observatory of the Institute for Nuclear Research, Russian Academy of Science (BNO INR RAS) has two instruments for the multi-messenger GW astronomy. The first one is the Baksan Underground Scintillation Telescope (BUST) which operates in a special mode: “searching for neutrino bursts from core collapse supernovae” [21, 22]. The second one is the setup OGRAN – an opto-acoustical gravitational wave antenna which is now in the assembling stage at the underground BNO site. [23]. Both detectors have moderate sensitivity sufficient for registration of core collapse events in the Galaxy and close environment $\sim 100 \text{ kpc}$, i.e. their applications are limited by “searching for rare events”. The BUST resolution is determined by the neutrino (antineutrino) threshold energy (8 – 10) MeV registered during the time 20 sec through the secondary electrons (positrons). The OGRAN sensitivity corresponds to the threshold of spectral metric perturbations at the level 10^{-19} – $10^{-18} \text{ Hz}^{-1/2}$ in the bandwidth 1-10 Hz around the central frequency 1.3 kHz [23].

Despite moderate sensitivity, a reasonable program of two-channel (ν and GWs) search for transient signals can be proposed for these instruments. Moreover, such program was stimulated by the well-known precedent of proposed ν -GW correlation for the SN1987A event [24 – 27]. Although, later analysis of the SN1987A data did not confirm the fact of ν -GW correlation [28, 29] it has given a push for a non-standard two-stage scenario of stellar collapse (see a review in [17]). The mean neutrino energy (during the first stage) in this model is 30–40 MeV. Another mode I [30] takes into account a large-scale convection caused by non-equilibrium neutronization of matter in the central region of a proto-NS. The large-scale convection provides a high yield of high energy neutrinos from the central region of a presupernova. The average energy of neutrinos is 30–50 MeV which is larger than in the case of diffusion. A drawback of these models is related to absence of correspondent estimates for GW radiation. In fact, there is a deficit of realistic theoretical models of astrophysical sources which admit simultaneous calculation of the neutrino and gravitational radiation bursts. For this reason a strategy of data analysis in multichannel detection of relativistic catastrophic events might be based more on empirical intuition than on a reliable theoretical scenario. The first example of such strategy was given in the data processing of SN1987A phenomenon. The key point is the supposition that registration of neutrino (or an EM counterpart) event provides tic marks for the gravitational channel, i.e. GW signal is searched in the vicinity of this moment (Fig.6). Such approach to the data analysis enormously reduces the volume of stochastic data from the GW channel which has to be processed, and so we have an increase of the detection probability. The more important characteristic is the expected time delay $\Delta\tau_k$ between the registered arrival time of a neutrino burst (an astrophysical event) τ_k and the moment of the GW burst appearance t_k so that: $\tau_k = t_k + \Delta\tau_k$. It would be desirable to have a prior estimate of the time delay from theoretical understanding of internal dynamics of radiative processes in the source. If such knowledge is absent one has to accept a hypothesis of a prior homogeneous distribution for time delay inside a reasonably wide interval around t_k . In the simplest model of identical nature of multiradiation sources the time delay is taken the same for all registered neutrino (or EM) events. As the “observable variable” (or “sufficient statistics”) it is natural to choose a variable proportional to the empirical correlation function between the row of registered neutrino (or EM) events and gravitational detector noise data accounting for the supposed time delay shift. Composing the likelihood ratio for this variable one can estimate the empirical value of the time shift through the standard procedure of likelihood ratio maximization. Using this shift estimate one calculates the value of “observable variable” for comparison with the statistical threshold. The last one is calculated on the basis of an empirical record of a GW detector noise at intervals far from the moments of registered astrophysical events (neutrino or EM bursts).

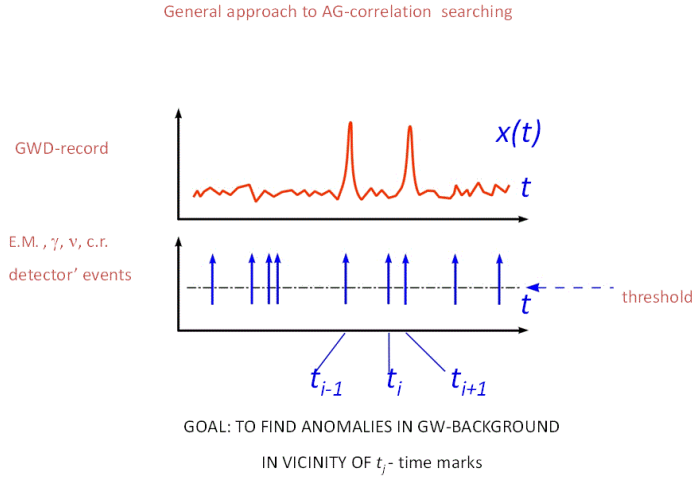


Fig6. Illustration of the strategy a search for ν -gw coincident bursts.

For LIGO/Virgo (as well as for ALIGO/adVirgo) the main sources are coalescing binaries (see a recent review in [32]). Black hole – black hole (BH) coalescence hardly can produce any (ν or EM) counterpart. But those events involving NSs are promising candidates. Many possibilities to produce a simultaneous EM burst or an afterglow have been discussed in the literature (see [33] and references therein).

Also the usage of new astronomical instruments (OpTIIX, ISS-Lobster) aboard the International Space Station (ISS) is planned to follow-up GW bursts [34], and the new wide-field X-ray instrument – NICER – is approved for installation on ISS.

One obvious task is to detect simultaneously a short GRB (SGRB) and a GW signal. The horizon for ALIGO/adVirgo is ~ 300 Mpc. SGRB are rare in such small volume, but if detected they are bright, and so their detection can be used as a tic mark to search for a GW burst in the data. Joint observations in X-rays and GWs can help to learn much more about the central engine and to determine parameters of the coalescing binary with better precision. However, less than 10% of GW bursts are expected to be accompanied by SGRB [33], and so the rate will be one in several years.

Better prospects exist for detection of an afterglow. Several mechanisms are discussed, but one of the most promising is related to the so-called “kilonova” (see recent estimates and discussion in [35] and [36] for an early proposal). In this scenario the isotropic optical emission can be generated due to radioactive decay in an ejected envelope. Emission has unique spectral characteristics, so potentially it is not very difficult to identify such a source when it is discovered. Relatively quick follow-up by wide-field instruments can provide a discovery of an optical transient. Then the source potentially can be studied in dedicated observation in optics, X-rays and other wavebands.

Problems with using a GW burst as a trigger for follow-up observations are related to poor localization of GW-sources in the sky [32]. Even three working detectors (ALIGO/andVirgo) provide multiple vast “zones” which cannot be covered on a time scale of few days with large instruments.

While the paper has been prepared to publication, information appeared about the first registration of GW from merging black holes in a binary system. See Phys. Rev. Let. 116, 061102 (2016).

References

- [1] R.X. Adhikari, Gravitational radiation detection with laser interferometry. *Rev. Mod. Phys.* vol.86, № 1, 2014
- [2] M. A. Bizouard and M. A. Papa, Searching for gravitational waves with the LIGO and Virgo interferometers. arXiv: 1304.4984 v1 17 Apr 2013
- [3] The LIGO Scientific Collaboration. *Advanced LIGO. Class.& Quantum Gravity.* vol,32 (7); 074001, 2015.
- [4] T. Accadia, F. Acernese, F. Antonucci et.al. *Class.& Quantum Gravity.* vol,32 ,020041, 2015
- [5] P. Astone, D. Babusci, L. Baggio et al., *Phys. Rev. D* 76, 102001, (2007).
- [6] M. De Rosa, L. Baggio, M. Cerdonio et al., *Class.& Quantum Gravity* vol. 19, 1919 (2002).
- [7] S.N. Bagaev, L.B. Bezrukov, N.L. Kvashnin, V.A. Krysanov, S.I. Oreshkin, A.M. Motylev, S.M. Popov, V.N. Rudenko, A.A. Samoilenko, M.N. Skvortsov, I.S. Yudin, A high frequency resonance gravity gradiometer. *Review of Scientific Instruments*, vol. 85, № 065114, c.114-1-114-8.
- [8] S.N. Bagaev, L.B. Bezrukov, N.L. Kvashnin, V.A. Krysanov, S.I. Oreshkin, A.M. Motylev, S.M. Popov, V.N. Rudenko, A.A. Samoilenko, M.N. Skvortsov, I.S. Yudin, Setup OGRAN as a high frequency resonance gravity gradiometer». arXiv: 1403.0827v1 [physics.ins det] 4 Mar 2014
- [9] A.V. Gusev, V.V. Kulagin, and V.N. Rudenko, Room-temperature gravitational bar-detector with cryogenic level of sensitivity. *Gravitation Cosmol.* 2(1), 68–70 (1996)
- [10] L. Bezrukov, S. Popov, V. Rudenko, A. Serdobolskii, and M. Skvortsov, Gravitational wave experiments and Baksan project OGRAN, in *Astrophysics and Cosmology after Gamov: Theory and Observations*, edited by G.S. Bisnovaty-Kogan et al. (Cambridge Scientific Publishers, 2007), pp. 125–138; e-print arXiv:gr-qc/0411083v1
- [11] L.B. Bezrukov, N.L. Kvashnin, A.M. Motylev, S.I. Oreshkin, S.M. Popov, V.N. Rudenko, A.A. Samoilenko, and I.S. Yudin, *Instrum. Exp. Tech.* 53(3), 423–429 (2010).
- [12] A.V. Gusev, V.N. Rudenko, S.A. Cheprasov, and M. Bassan, *Classical Quantum Gravity* 25(5), 055006 (2008).
- [13] M. De Rosa, L. Baggio, M. Cerdonio et al., *Classical Quantum Gravity* 19, 1919 (2002).
- [14] J.S. Bloom et al., ArXiv e-prints: 0902.1527 (February 2009).
- [15] S.J. Smartt, *ARA&A* 47, 63(September 2009).
- [16] K. Scholberg, *Annual Review of Nuclear and Particle Science* 62, 81(November 2012).
- [17] C.W. Stubbs, *Classical and Quantum Gravity* 25, p. 184033(September 2008).
- [18] V.S. Berezhinskii, C. Castagnoli, V. I. Dokuchaev and P. Galeotti, *Nuovo Cimento C Geophysics Space Physics* C 11, 287(June 1988).
- [19] V.S. Imshennik, *Soviet Astronomy Letters* 18, p. 194(June 1992).
- [20] V.S. Imshennik and D. K. Nadyozhin, *Soviet Astronomy Letters* 18, p. 79 (March 1992).
- [21] R.V. Novoseltseva et al., *Bulletin of the Russian Academy of Science, Phys.* 75, 419 (March 2011).
- [22] R.V. Novoseltseva et al., ArXiv e-prints: 0910.0738 (October 2009).
- [23] L.B. Bezrukov et al., *Instruments and Experimental Techniques* 53, 423 (2010).
- [24] M. Aglietta et al., *EPL (Europhysics Letters)* 3, 1315 (1987).
- [25] E.N. Alekseev, L.N. Alekseeva, V.I. Volchenko and I.V. Krivosheina, *Soviet Journal of Experimental and Theoretical Physics Letters* 45, p. 589(May 1987).
- [26] M. Aglietta, G. Badino, G. Bologna, C. Castagnoli and A. Castellina, *Nuovo Cimento C Geophysics Space*

Physics C 12, 75(February 1989).

- [27] E.N. Alexeyev, Soviet Journal of Experimental and Theoretical Physics 110, 220 (February 2010).
- [28] C.A. Dickson and B.F. Schutz, Phys. Rev. D 51, 2644(March 1995).
- [29] V.N. Rudenko, A.V. Gusev, V.K. Kravchuk and M.P. Vinogradov, Soviet Journal of Experimental and Theoretical Physics 91, 845(November 2000).
- [30] V.S. Imshennik and O.G. Ryazhskaya, Astronomy Letters 30, 14(January 2004).
- [31] I.V. Baikov, V.M. Suslin, V.M. Chechetkin, V. Bychkov and L. Stenflo, AstronomyReports 51, 274(April 2007).
- [32] N. Andersson et al., ArXiv e-prints: 1305.0816 (May 2013).
- [33] B.D. Metzger and E. Berger, ApJ 746, p. 48(February 2012).
- [34] J. Camp et al., ArXiv e-prints: 1304.3705 (April 2013).
- [35] B.D. Metzger et al, MNRAS 406, 2650(August 2010).
- [36] S. Rosswog, ApJ 634, 1202(December 2005).

Interaction of electron neutrino with LSD detector

O. G. Ryazhskaya¹, S. V. Semenov^{2,*}

¹*Institute for Nuclear Research RAS, Moscow, Russia*

²*National Investigation Centre “Kurchatov Institute”, Moscow, Russia;*

Semenov_SV@nrcki.ru

Abstract The interaction of electron neutrino flux, originating in the rotational collapse mechanism on the first stage of Supernova burst, with the LSD detector components, such as ^{56}Fe (a large amount of this metal is included in as shielding material) and liquid scintillator $\text{C}_n\text{H}_{2n+2}$, is being investigated. Both charged and neutral channels of neutrino reaction with ^{12}C and ^{56}Fe are considered. Experimental data, giving the possibility to extract information for nuclear matrix elements calculation are used. The number of signals, produced in LSD by the neutrino pulse of Supernova 1987A is determined. The obtained results are in good agreement with experimental data.

Keywords: Supernova Burst, Neutrino Signal, Charged Current and Neutral Current Interaction

1. Introduction

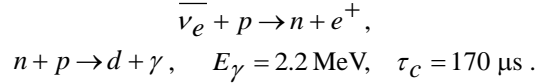
SN1987A is the first and till now the only deep space object which have been observed both in electromagnetic and neutrino light. The possibility of SN neutrino observation was considered for the first time in [1]. The neutrino signals of SN1987A were registered on February, 23, 1987 by LSD [2], Baksan [3], KII [4] and IMB [5] detectors. The review and analysis of these experimental data is presented in [6]. LSD and BUST are liquid scintillator detectors, containing, correspondingly, in their work volumes 90 and 130 tons of liquid scintillator $\text{C}_n\text{H}_{2n+2}$, $n=10$, elaborated by A.V. Voevodskiy, V.L. Dadykin, O.G. Ryazhskaya [7]. KII and IMB are the water Cherenkov detectors with work volumes of 2140 and 5000 m³.

On February, 23, 1987 LSD detected 5 neutrino events at 2.52 UT and 2 signals at 7.36 UT, BUST registered one signal at 2.52 UT and 6 signals at 7.36 UT, KII recorded 12 events at 7.35 UT and IMB – 8 signals at 7.35 UT. The two observed sets of neutrino signals with relatively large time separation of 4 h 44 min can be naturally explained on the base of the rotating mechanism of Supernova explosion [8]. In this mechanism the two-stage collapse occurs with time difference of ~ 5 h. The neutrino flux during the first burst consists of electron neutrinos with the total energy $W_{\nu_e} = 8.9 \times 10^{52}$ erg. The neutrino energy spectrum is hard with an average energy of $\sim 30\text{--}40$ MeV. The second neutrino burst corresponds to the standard collapse theory without rotation with formation of a neutrino sphere and with an equal energy distribution between all types of neutrinos [9]. Below a theoretical analysis of interaction of electron neutrino, originating from the first stage of gravitational collapse, with LSD detector is presented.

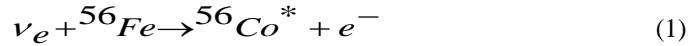
2. Neutrino Interaction

2.1. Interaction with ^{56}Fe

LSD detector contains 90 tons of scintillator for antineutrino observation by the reaction

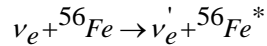


LSD could measure both particles in this reaction. Also the detector contains about 200 t of ^{56}Fe as a shielding material. Under the impact of neutrino flux electrons and gamma quanta would be produced as a result of reaction with iron nuclei and they could be registered by the detector [10]. So, the following charge-exchange reaction takes place:



Due to neutrino interaction, excitation of analog 0^+ and Gamow–Teller 1^+ giant resonances in ^{56}Co results [11], that gives rise to gamma quanta production with energies of $\sim 5 \div 10$ MeV, together with electrons emission. The cross section of reaction (1) caused by charged current was calculated in [12]. In order to compare the produced estimations with experimental data, the theoretical cross section was averaged over the muon-decay-at-rest neutrino spectrum. The corresponding value is $2.62 \cdot 10^{-40} \text{ cm}^2$, which is in agreement with the KARMEN experiment result $(2.56 \pm 1.08(\text{stat}) \pm 0.43(\text{syst})) \times 10^{-40} \text{ cm}^2$ [13]. The cross section obtained for the process (1) for $E_{\nu_e} = 40 \text{ MeV}$ equals to $4.2 \cdot 10^{-40} \text{ cm}^2$ [12].

Alongside with charged current processes, the inelastic neutrino scattering, induced by neutral current:



should be taken into account. In the neutrino energy range of interest the inelastic scattering is determined, primary, by allowed transitions. The cross section of this reaction in the case of the initial nucleus ground state has the following form [14]:

$$\sigma^{NC}(E_\nu) = \frac{G_F^2 g_A^2}{\pi(2J_i + 1)} (E_\nu - E_x)^2 \left\langle \left\| f \left\| \sum_k \boldsymbol{\sigma}(k) t_0(k) \right\| i \right\| \right\rangle^2 \quad (1)$$

Here G_F and g_A are the Fermi and axial vector coupling constants, respectively, E_ν is the energy of neutrino in the initial state, and E_x is the nucleus excitation energy. The square of the reduced matrix element

$$B(GT_0) = \frac{g_A^2 \left\langle \left\| f \left\| \sum_k \boldsymbol{\sigma}(k) t_0(k) \right\| f \right\| \right\rangle^2}{2J_i + 1}$$

governs the cross section dependence on the nuclear transition structure.

When calculating inelastic neutrino scattering on nuclei it is reasonable to deduce it in a model-independent way, basing on experimental results of nuclear structure investigations [15], for the currently available theoretical models may give substantial spread of nuclear matrix elements values. The same approach is useful in the double beta-decay theory, where information on corresponding nuclear matrix elements can be obtained from data on $\log ft$ for single beta-transitions and measurements

of characteristics of charge-exchange reactions [16]. For ^{56}Fe the allowed transitions correspond to transitions from initial 0^+ to the final 1^+ - states, therefore estimations of matrix elements can be produced with the help of data on electromagnetic $M1$ -strengths.

The processes of nuclear resonance fluorescence were investigated in [17]. Electromagnetic dipole transitions in ^{56}Fe were measured in photon-scattering experiments with a linearly polarized photon beam. In the case of $M1$ transitions the width of the excited 1^+ - state relatively to the transition on the nucleus ground state is determined by the following expression [18]:

$$\Gamma_0 = \frac{16\pi}{27} \frac{E_x^3}{\hbar^3 c^3} B(M1) \quad (2)$$

Here E_x is the excitation energy, $B(M1)$ – is the reduced probability of $M1$ -transition. $B(M1)$ is written in the following form [18,19]:

$$B(M1) = \frac{3}{4\pi} \left| \left\langle f \left\| \sum_k \mathbf{l}(k) t_0(k) + (\mu_s - 0.5) \frac{\boldsymbol{\sigma}(k)}{2} + \mu_v \boldsymbol{\sigma}(k) t_0(k) \right\| i \right\rangle \right|^2 \mu_N^2$$

Here μ_N is nuclear magneton, μ_s and μ_v are isoscalar and isovector nucleon magnetic moments, $\mu_s = 0.880$, $\mu_v = 4.706$. As follows from the expression for $B(M1)$, the isovector contribution to $B(M1)$ exceeds significantly the isoscalar part. As for the orbital term, for pf-nuclei it is concentrated at excitation energies $E_x \leq 4$ MeV, while for E_x in the range of 7-11 MeV, which is essential for neutrino registration, the determining factor is the spin contribution.

Consequently, for calculation of cross section in neutral channel $\sigma^{NC}(E_\nu)$, one can use the following relation, connecting $B(GT_0)$ and $B(M1)$:

$$B(GT_0) = \frac{4\pi g_A^2}{3\mu_v^2} \frac{B(M1)}{\mu_N^2}$$

From the values of $\mu_v = 4.706$ and $g_A = -1.2761$ it results:

$$B(GT_0) = 0.308 \frac{B(M1)}{\mu_N^2} \quad (3)$$

Here it is taken into account, that for the $^{56}\text{Fe}_{g.s.}$, $J_i = 0$. The reduced transition probabilities $B(M1)$ can be found from (2) on the base of data on the widths Γ_0 of excited states of iron-56 nucleus. If Γ_0 is measured in meV and E_x in MeV, then

$$\frac{B(M1)}{\mu_N^2} = 0.2592 \frac{\Gamma_0}{E_x^3} \quad (4)$$

As follows from (1), the cross section of inelastic neutrino-nucleus scattering is determined by the formula:

$$\sigma^{NC}(E_\nu) = 1.6862 \cdot 10^{-44} (E_\nu - E_x)^2 B(GT_0) \text{ cm}^2 \quad (5)$$

Here E_ν , E_x are measured in MeV.

The investigation of dipole excitations of ^{56}Fe for the excitation energies E_x up to 9.8 MeV was performed in [17]. Twenty 1^+ – states with the total $B(M1)$ strength $\sum B(M1) = 4.31(18) \mu_N^2$ were examined. The reduced probabilities of electromagnetic $M1$ transitions $B(M1)$ are calculated with the

help of data on the widths Γ_0 of these states, obtained in [20]. So, combining (3), (4), (5) it is possible to calculate the total cross section of inelastic neutrino scattering, caused by weak neutral current. The corresponding plot is presented in Fig. 1. Particularly, for $E_\nu=40$ MeV $\sigma^{NC} = 22 \cdot 10^{-42} \text{ cm}^2$.

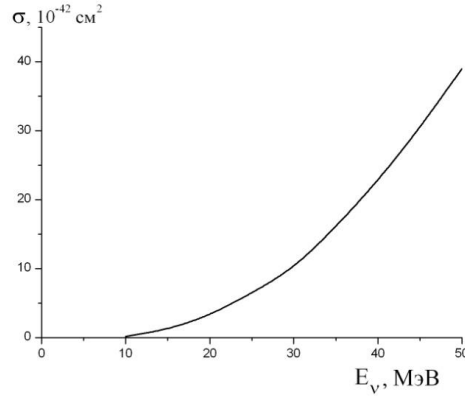
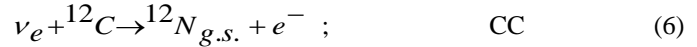


Fig1. Dependence of neutrino – ^{56}Fe inelastic scattering on neutrino energy.

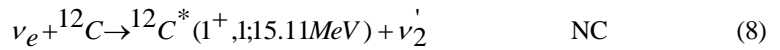
2.2. Interaction with ^{12}C

There are three channels of electron neutrino interaction with carbon, which is a part of the liquid scintillator $\text{C}_{10}\text{H}_{22}$.

Neutrino absorption, determined by charged current:



Inelastic neutrino scattering, caused by neutral current:



All these interactions lead to creation of secondary particles, electrons and gamma-quanta, which can be registered by detector as neutrino signal. With the purpose to have benchmarks of the cross section orders it is worthwhile to refer to experimental results, obtained in KARMEN experiments for neutrino muon-decay-at-rest spectrum, with characteristic neutrino energy $E_\nu \sim 35$ MeV. So, for reactions (6), (7) the experimental results are $9.1 \cdot 10^{-42} \text{ cm}^2$, $5.7 \cdot 10^{-42} \text{ cm}^2$ respectively. As for neutral current reaction (8), experimental result is a sum of cross sections both for ν_e and $\bar{\nu}_\mu$ inelastic scattering and equals to $10.1 \cdot 10^{-42} \text{ cm}^2$.

Theoretical calculations of reaction (6) cross section can be produced on the base of experimental data on $\log ft$ of ${}^{12}\text{N}_{g.s.}(\beta^+){}^{12}\text{C}_{g.s.}$ transition. Reaction (7) is considered in [21] within the continuum random phase approximation. The cross section of neutrino neutral current excitation of 15.11 MeV state in carbon can be obtained by the approach just the same as the one used for neutrino-iron inelastic scattering, taking into account the experimental rate of M1 γ -decay of 15.11 MeV state, $\Gamma_\gamma = 38.5 \text{ eV}$. The resulting sum of cross section values of (6), (7), (8) interactions equals to $20 \cdot 10^{-42} \text{ cm}^2$.

2.3. Number of Signals

In the two-stage model the first neutrino pulse from SN1987A is connected with the initial stage of the collapse. For the total neutrino power in the first phase $W_{\nu_e} = 8.9 \cdot 10^{52}$ erg, neutrino energy 40 MeV and distance from Supernova to the Earth 50 kPs, the neutrino flux at the Earth surface is $0.5 \cdot 10^{10}$ 1/cm² [12]. The calculated cross sections values lead to one interaction for neutrino-carbon reaction and five interactions for electron neutrino with ⁵⁶Fe, that together with the registration efficiency of detector gives the event numbers, which coincide with the observed number of signals

3. Conclusion

LSD is a unique detector for observing the neutrino pulse connected with the first stage of collapse in the rotational mechanism scenario [8], because it is a detector which contains a sufficient mass of proper material for detecting, namely, the electron-neutrino pulse, but not only the antineutrino one (as was expected before). As to the other detectors, including hydrogen components (e.g., IMB type), they cannot detect a pulse consisting mainly of electron neutrinos. In the same way, the number of events detected in the neutrino–electron interaction, as is in the case of the KII detector, is small because of the smallness of the cross section in the supernova neutrino energy range ($\approx 10^{-43}$ cm²) in comparison with the neutrino–⁵⁶Fe interaction.

Recently a number of works have been published [22 – 24], where the second neutrino pulse is connected with deconfinement process in compact stars. The investigations in this direction are very interesting.

On the first stage of the rotational collapse mechanism electron neutrino of high energy with $E_\nu \sim 40\text{--}50$ MeV are generated. For their registration the use of great amounts of stable isotopes with large values of neutron excess $N-Z$ is very promising.

Acknowledgements

The authors are grateful to A. Drago, V.S. Imshennik and D.K. Nadezhin for useful discussions. The work is supported by RFBR grants ofi-m-14-22-03037, 14-22-03040

References

- [1] G.V. Domogatsky and G.T. Zatsepin, On the experimental possibilities of the observation of neutrinos On the Experimental Possibilities of the Observation of Neutrinos from Collapsing Stars Proc. ICRC London ,1965, V.2, P. 1030-1031.
- [2] V.L. Dadykin et al. Detection of a rare event on 23 February 1987 by the neutrino radiation detector under Mont Blanc. JETP Letters,1987, 45, Iss10:593-5; Aglietta M., Badino G., Bologna G. et al. On the Event Observed in the Mont Blanc Underground Neutrino Observatory during the Occurrence of Supernova 1987A, Europhys. Lett. 1987, 3(12):1315-7.
- [3] E.N. Alekseev, L.N. Alekseeva, V.I. Volchenko, I.V. Krivosheina, Possible detection of a neutrino signal on 23 February 1987 at the Baksan underground scintillation telescope of the Institute of Nuclear Research, JETP Letters 1987, 45, Iss10: 589-592.
- [4] K. Hirata, T. Kajita, M. Koshiba et al. Observation of a Neutrino Burst from Supernova 1987A. Phys.Rev. Lett. 1987, 58: 1490-3.
- [5] R.M. Bionta, G. Blewitt, C.B. Brattor et al.. Observation of a Neutrino Burst in Coincidence with Supernova 1987 A in the Large Magellanic Cloud. Phys. Rev. Lett. 1987, 58: 1494-6.

- [6] V.L. Dadykin, G.T. Zatsepin, O.G. Ryazhskaya., Events detected by underground detectors on February 23, 1987. *UFN* 1989, 32: 459–468; O.G. Ryazhskaya, Neutrinos from stellar core collapses: present status of experiments. 2006, 49: 1017–1027; O.G. Ryazhskaya, On experiments in Underground Physics. *UFN* 2013, 56: 296–304.
- [7] A.V. Voevodskiy, V.L. Dadykin, O.G. Ryazhskaya, Liquid scintillators for large scintillation counters, *Pribory Tech. Eksp.* 1970, 1: 85 (in Russian).
- [8] D.K. Nadyozhin, The gravitational collapse of iron-oxygen stars with masses of 2 and 10 solar masses. II. *Astrophys. and Space Sci.* 1977, 51: 283; Imshennik V.S., Nadezhin D.K. The gravitational collapse of rotating iron-oxygen stars. *Pis'ma Astron. Zh.* 1977, 3: 353 (in Russian); V.S. Imshennik, Rotational explosion mechanism for collapsing supernovae and the two-stage neutrino signal from supernova 1987A in the Large Magellanic Cloud. *UFN* 2010; 53: 1081–1092.
- [9] V.S. Imshennik, D.K. Nadezhin, Final stages of stars evolution and supernovae bursts. *Itogi Nauki Tech., Ser. Astron. VINITI AN USSR. M.* 1982, 21: 63 (in Russian).
- [10] V.S. Imshennik, O.G. Ryazhskaya, Rotating collapsar and possible interpretation of LSD neutrino signal from SN 1987A, *Astron. Lett.* 2004, 30: 14-30.
- [11] Yu. V. Gaponov, Yu.S. Lutostansky, Possible Existence of I+ Resonance in Charge Exchange Reactions of Spherical Nuclei, *JETP Letters* 1972, 15: 120-2; Yu. V. Gaponov, Yu.S. Lutostansky, Gamow-Teller resonance and Wigner multiplet scheme. , *JETP Letters* 1973, 18: 75-7.
- [12] Yu.V. Gaponov, O.G. Ryazhskaya, and S.V. Semenov, Interaction of Electron Neutrinos with ^{56}Fe in the LSD for $E \leq 50$ MeV. *Physics of Atomic Nuclei*, 2004, 67, No. 11: 1969–1973.
- [13] B. Zenitz, KARMEN: Neutrino physics at ISIS. *Prog. Part. Nucl. Phys.*, 1994, 32: 351 -373.
- [14] T.W. Donnelly and R.P. Peccei, Nuclear structure effects in nuclei, *Phys. Rep.*, 1979, 50, 1-85.
- [15] H.C. Lee, Neutral current and the nuclear scattering of reactor antineutrinos, *Nucl. Phys.A* , 1978, 294, 473-491; K. Langanke, G. Martinez-Pinedo, P. von Neumann-Cosel, and A. Richter, Supernova Inelastic Neutrino-Nucleus Cross Sections from High-Resolution Electron Scattering Experiments and Shell-Model Calculations, *Phys. Rev. Lett.*, 2004, 93, 202501, 1-4.
- [16] A.Ya. Balysh, V.V. Khruschov, V.P. Labozin, S.V Semenov, G.O. Tsvetkov, Calculation of $2\nu 2\beta$ amplitude for ^{100}Mo and ^{150}Nd . *Proceedings 3-nd Int. Conf. "Current Problems in Nuclear Physics and Atomic Energy"*, Kyiv 2010. pp. 414-418, Kyiv.
- [17] T. Shizuma, T. Hayakawa, H. Ohgaki et al, Dipole strength distribution in ^{56}Fe , *Phys. Rev. C* 2013, 87: 024301, 1-7.
- [18] John M. Blatt and Victor F. Weisskopf, *Theoretical Nuclear Physics*. New York: Wiley; London: Chapman & Hall, 1952.
- [19] G. Morpurgo, Inhibition of $M1 \gamma$ Transitions with $\Delta T = 0$ in Self-Conjugate Nuclei, *Phys. Rev.* 1958, 110: 721-5.
- [20] F. Bauwens, J. Bryssinck, D. De Frenne et al. Dipole transitions to bound states in ^{56}Fe and ^{58}Ni . *Phys. Rev. C* 2000; 62: 024302, 1-20.
- [21] E. Kolbe and K. Langanke, S. Krewald, Neutrino-induced reactions on ^{12}C within the continuum random phase approximation. *Phys. Rev C.* 1994; 49:1122-6.
- [22] A. Drago, G. Pagliara, G. Pagliaroli, F.L. Villante and F. Vissani Formation of quark phases in compact stars and SN explosion, arXiv 0809.0518v1 [astro-ph] (2008).
- [23] G. Pagliara, M. Herzog and F. K. Röpke, Combustion of a neutron star into a strange quark star: The neutrino signal. *Phys. Rev. D*, 2013, 87: 103007, 1-8.
- [24] A. Drago and Gi. Pagliara, The scenario of two families of compact stars 2. Transition from hadronic to quark matter and explosive phenomena, arXiv 1509.02134v1 [astro-ph.SR] (2015).

Clustering of galaxies around the GRB 021004 sight-line at $z \sim 0.5$

Ilya V. Sokolov^{1,*}, Alberto J. Castro-Tirado², Oleg V. Verkhodanov³,
Olga P. Zhelenkova³ and Yuriy V. Baryshev⁴

¹*Institute of Astronomy RAS, Russia; e-mail: ilia333@land.ru*

²*Stellar Physics Department, Institute for Astrophysics of Andalucía, Granada, Spain*

³*Special Astrophysical Observatory of RAS, Nizhnij Arkhyz, Russia*

⁴*Institute of Astronomy of Saint-Petersburg State University, Saint-Petersburg, Russia*

Abstract In this report we test for reliability any signatures of field galaxies clustering in the GRB 021004 line of sight. The first signature is the BTA and Hubble GRB 021004 field photometric redshift distribution with a peak at $z \sim 0.5$ estimated from multicolor photometry. The second signature is the MgII 2796,2803 absorption doublet at $z \sim 0.5$ in the GRB 021004 afterglow spectrum. The third signature is some inhomogeneity in Plank + GRB 021004 fields. And the fourth signature may be the galaxy clustering with an effective redshift of $z = 0.5$ from the Baryon Oscillation Spectroscopic Survey (BOSS), which is a part of the Sloan Digital Sky Survey III (SDSS-III).

Keywords: Galaxy Clustering, Gamma-Ray Bursts, Multicolor Photometry

1. Introduction. Clustering of galaxies and quark phase transition in compact objects: neutrino, supernovae and gamma-ray bursts

As is well known, measurements of the surface brightness of galaxy clusters can be used to estimate the angular diameter and distance to these structures [1]. Namely, the determination of distance to sources of neutrino signals, supernovas and gamma-ray bursts resulting from quark transitions in compact objects becomes the main observational task in determining the basic parameter – an energy release related to sources of such events.

On the other hand, it is known that distribution of such sources over the sky can be anisotropic. Now this can be said with confidence at least about GRBs whose distribution correlates with nonuniformities of distribution of the cosmic microwave background (CMB) signals [2]. Paper [3] also says about anomalies in the GRB spatial distribution. A discussion on a possible clustering of neutrino signals in relation with GRBs can be seen in [4]. Observational determination of such relations directly influences the study of neutrino signals, GRBs and supernovae.

There is a mysterious connection between Gamma-Ray Bursts (GRBs) and core collapse supernovae (SNe). At least, long-duration GRBs are associated with the core collapse of very massive stars ([5] – [8]). Similarly to core collapse SNe, the most probably, in GRBs also the collapse of massive stellar iron cores results in the formation of a compact object (collapsar), accompanied by the high-velocity ejection of a large fraction of a progenitor star mass. The collapse of the massive stellar core is connected with the quark phase transition in the compact objects, which leads to neutrino and photons signals from the core collapse SNe and GRBs.

On the other hand, the sky distribution of electromagnetic and neutrino signals associated with the

core collapses can be non-isotropic [9], which can be related eventually with the clustering of galaxies in which the formation of compact objects occurs due to evolution of massive stars. The clustering of galaxies and the clustering around GRB sight-lines are detected and studied in the same manner employed with quasar spectroscopy in many papers already [10]. Galaxies that give rise to absorption line systems in gamma-ray bursts afterglow spectra have been directly imaged and investigated. So, it is possible to try to find the overdensity excess of GRB field galaxies around GRB positions by different methods – spectroscopic, photometric ones (deep images multiband photometry) plus the search for correlation with Cosmic Microwave Background (CMB) and others.

2. The Clustering of galaxies around GRB sight-lines

The Clustering of galaxies around GRB sight-lines are detected and studied in detail in many papers already since [10]. Gamma-ray Bursts (GRBs) originate at cosmological distances with energy releases of $10^{51} - 10^{53}$ ergs at a range of redshifts between ~ 0.01 and up to 10 [10]. Besides studying their host galaxies, prompt spectroscopy of the GRB afterglows has revealed (in the optical) intervening absorption systems as found in the past with quasar spectroscopy. One of such is Mg II (rest) 2800 Å which is strong and easy to detect in moderate S/N spectra. Using a large sample of GRB afterglows, it has been found [11], [12] an overdensity (the factor 2–4) of strong Mg II absorption line systems along the lines of sight. If this excess of intervening systems is real, it should be possible to find an excess of GRB field galaxies around GRB positions, although a preliminary study has revealed no anomalous clustering of galaxies (in comparison with distribution of quasar?) at the estimated median redshift ~ 0.3 around GRB line of sights [10]. Furthermore, it has been proposed that the majority of short-duration GRBs in early-type galaxies will occur in clusters and three such relationships have been already found [13]. Though the paper authors [10] are interested mostly in the GRB/quasar overdensity excess of field galaxies around sight-lines, and, in connection with this problem they made a good review (for 2013) of spectroscopic data of the 73 GRB afterglows. Intervening absorption line systems for GRB afterglows can be detected in the same manner employed with quasar spectroscopy. One such absorption line system is MgII, which is easily detected in moderate S/N spectra at $\lambda \sim 2800$ (MgII 2796,2803 doublet). As strong MgII tends to trace these galaxies, we will proceed from these spectra in our photometric study of the field galaxies around GRB 021004 line of sight.

One of these fields GRB000926 (Table 1) was already investigated and the results were published [14]. This work presents the observations of a $3.6' \times 3'$ field centered on the host galaxy of GRB000926 (J2000.0= $17^{\text{h}}04^{\text{m}}11^{\text{s}}$, J2000.0= $+51^{\circ}49.8''$). The observations were carried out on the 6-m Special Astrophysical Observatory telescope using the SCORPIO instrument. The catalog of galaxies detected in this field includes 264 objects for which the signal-to-noise ratio is larger than 5 in each photometric band. The following limiting magnitudes in the catalog correspond to this limitation: 26.6(B), 25.7(V), 25.8(R_c), and 24.5(I_c). The differential galaxy counts are in good agreement with previously published CCD observations of deep fields. Authors estimated the photometric redshifts for all of the cataloged objects and studied the color variations of the galaxies with redshift. For luminous spiral galaxies with $M(B) < 18$, authors found no evidence for any noticeable evolution of their linear sizes to $z \sim 1$.

BTA observation data are the base of our investigations. While studying other fields (Table 1) (GRB021004, GRB970508 + investigation of surroundings of radio-source RC J0311+0507), these data were supplemented with data obtained with other instruments. One of the goals of this work is to point out what is possible to obtain with 6-m telescope in these challenging and actual tasks, supplementing these studies with other instruments' data.

Table 1. BTA GRB deep fields

GRB	Filters	FWHM	T _{exp} , sec
GRB970508	BVRI	1".3	600×7, 500×4, 600×5, 400×5
GRB971214	VR	1".2	600×1, 600×1
GRB980613	BVRI	1".3	700×1, 600×1, 600×3
GRB980703	BVRI	1".3	480×1, 320×1, 300×1, 360×1
GRB990123	BVRI	1".5	600×1, 600×1, 600×1, 600×1
GRB991208	BVRI	2".1	300×6, 300×5, 180×7, 180×2
GRB000926	BVRI	1".3	500×5, 300×5, 180×25, 120×15
GRB021004	BVRI	1".5	600×6, 450×13, 180×15, 120×14

3. Method of photometry of GRB 021004 and RC J0311+0507 fields

We used the GRB021004 field, which was obtained as a part of GRB afterglow observations program (see Table 1) [15]. This field has exposure times of about one hour in each of the BVRI optical bands.

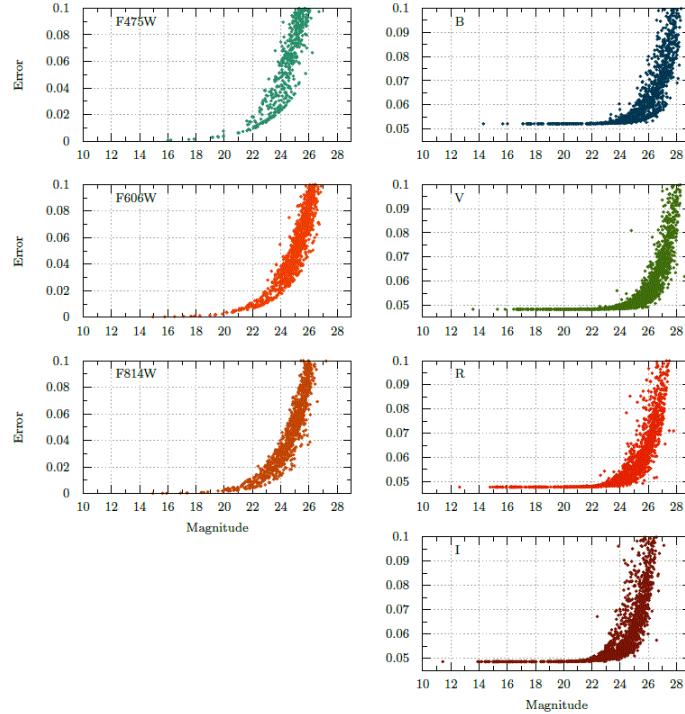


Fig1. The magnitude-error diagram for objects extracted from GRB 021004 field. Left column graphs represent data acquired with HSC ACS camera in F475W, F606W and F814W optical bands. Right column graphs represent data of BTA BVRI bands.

We used the SExtractor software package [16] to extract objects from the stacked BVRI image. The catalog of galaxies, extracted from this field of size $4' \times 4'$ includes 935 objects with the signal-to-noise ratio larger than 3. The following limiting magnitudes were achieved: 26.9 (B), 27.2 (V), 26.0 (Rc) and 25.5(I). We also made sure our results are consistent with HST ACS data (see Figure 1).

4. Photometric redshifts of GRB021004 field galaxies

The so-called photometric redshifts estimated from multicolor photometry turn out to be quite acceptable. The accuracy of these redshifts estimates is about 10%, which is high enough for statistical studies of the properties of distant objects. The main idea of the photometric redshift estimation is very simple: an object's multicolor photometry may be considered as a low-resolution spectrum that is used to estimate redshift [17] (see Figure 2). In practice, we estimated the photometric redshifts for the extended objects of our sample using the Hyperz software package [18]. The input data for Hyperz were: the apparent magnitudes of the objects in four bands, the internal extinction law (we used the law by Calzetti et al. [19] for starburst galaxies, which is most commonly used for studies similar to our own), the redshift range in which the solution is sought (we considered z from 0 to 4). The method is based on finding the best fit of template spectra (see Figure 3), so it is crucial to the initial model spectra. For ten of the brightest galaxies in the field we find that model spectra assigned to these galaxies are in good agreement to HST ACS data, which due to angular resolution of the images reveals the structure of these objects (see Figure 4). The field also contains four X-ray sources, for which we estimate redshift (see Figure 5). For spatial distribution of field galaxies we find a large inhomogeneity at $z \sim 0.57$. (see Figures 6, 7).

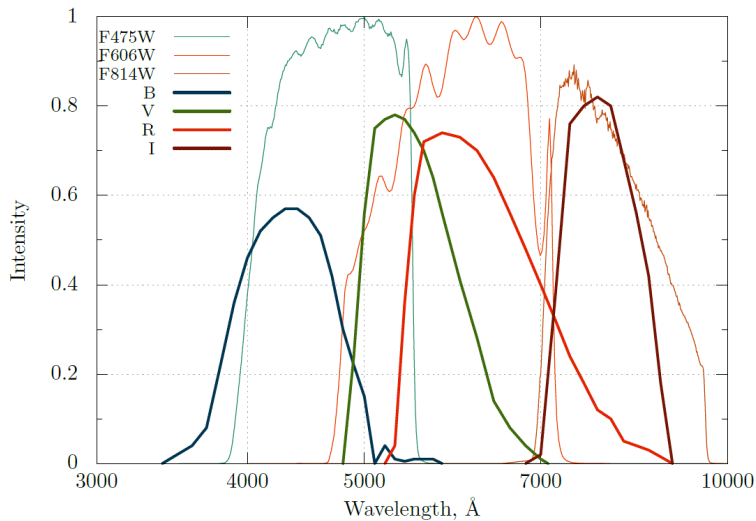


Fig2. Filter transmission curves of HST ACS optical bands F475W, F606W, F814W and BTA BVRI optical bands.

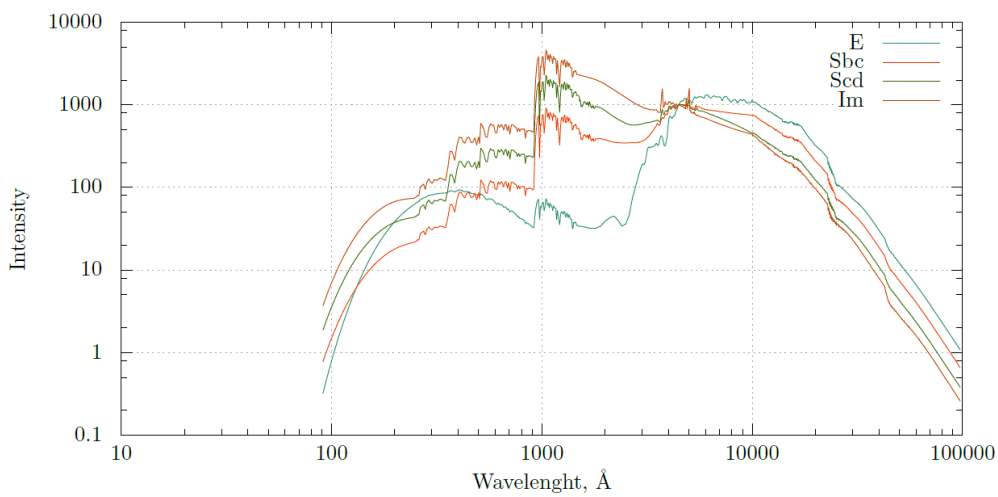


Fig3. Template spectra of various galaxy types, used in photometric redshift calculation.

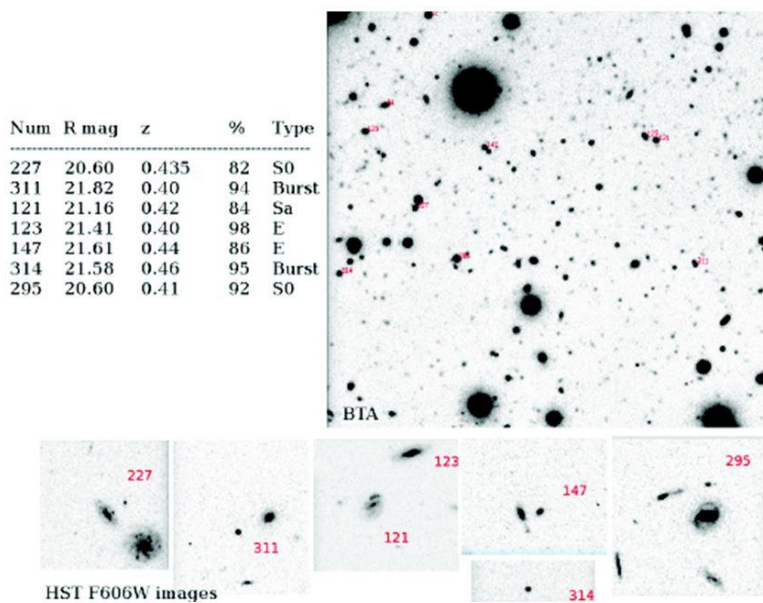


Fig4. Upper right image is GRB 021004 BTA field. The image is a stack of BVRI bands. Lower row of images are extracted from HST ACS F606W image.

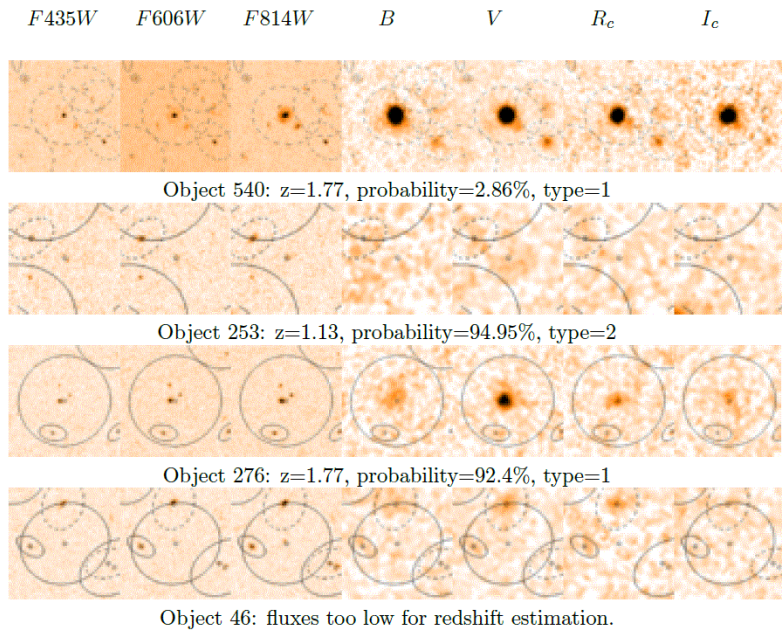


Fig5. X-ray sources in the field of GRB021004 in HST and BTA optical bands. Object numbers are from the catalog of all extracted objects in the field.

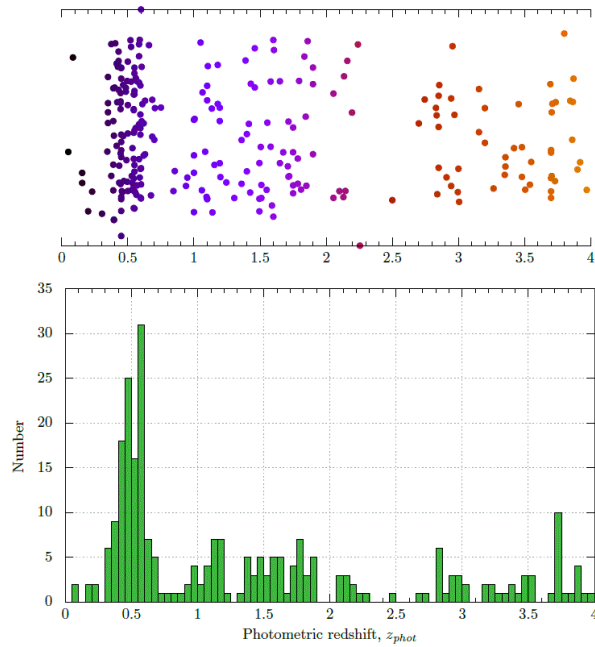


Fig6. Spatial distribution of objects (upper) along Y axis is image coordinate, and photometric redshift distribution (lower) with a well distinguished peak at $z \sim 0.57$ based on BTA data.

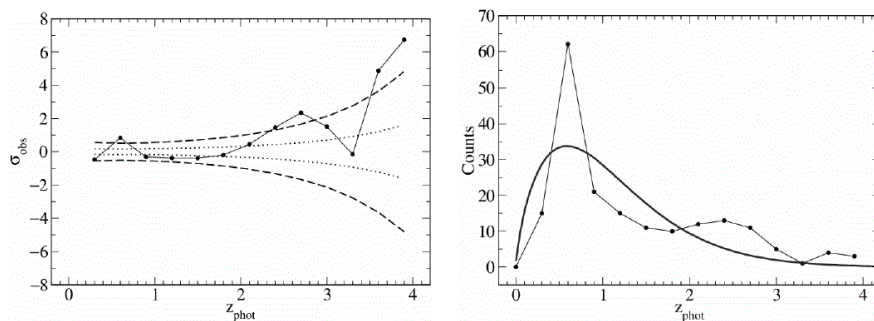


Fig7. Deviation and Poisson noise for $dz = 0.3$

The GRB 021004 afterglow spectrum has also been measured. The spectrum shows evidence of Mg II 2796/2803 redshifted at $z = 1.3820$ and $z = 1.6020$ (see Figure 8). Spectrum also has two features that could be identified as Mg II doublet redshifted at $z = 0.57$ (see Figure 9, Table 2) [12].

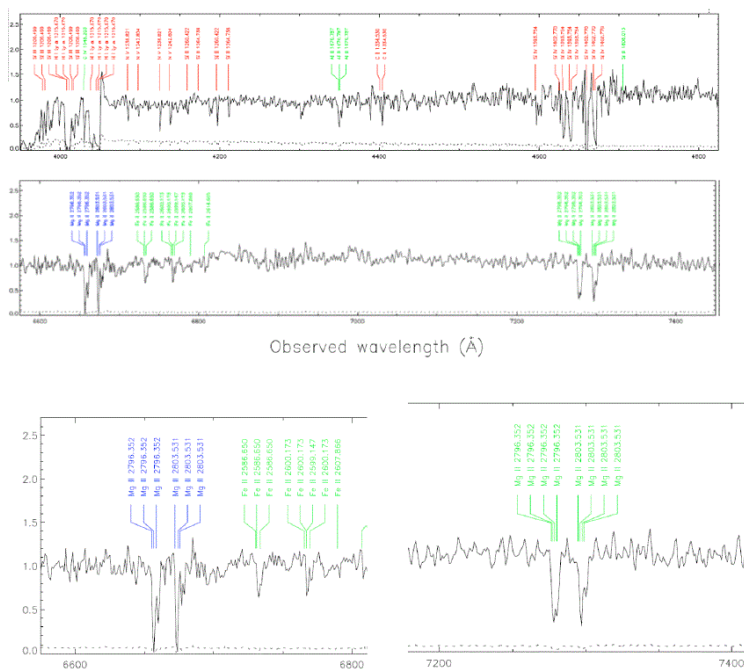


Fig8. The selected areas of VLT/UVES spectra, obtained in REF of GRB 021004 afterglow. The lines are identified with Mg II 2796/2803. Redshifted Mg II doublet at $z = 1.3820$ (left) and $z = 1.6020$ (right).

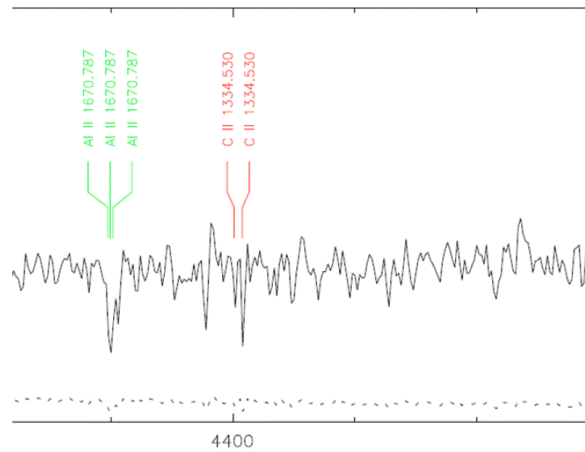


Fig9. Features of VLT/UVES spectra identified as CII could be interpreted as Mg II doublet redshifted at $z=0.57$

Table 2.

GRB	z_{GRB}	z_{abs}	$W_r(\lambda 2796) (\text{\AA})$
GRB 021004	2.3295	0.5550	0.248 ± 0.025
		1.3800	1.637 ± 0.020
		1.6026	1.407 ± 0.024
GRB 050730	3.9687	1.7732	0.927 ± 0.030
		2.2531	$< 0.783 (0.650)$
GRB 050820A	2.6147	0.6896	0.089 ± 0.007
		0.6915	2.874 ± 0.007
		1.4288	1.323 ± 0.023
		1.6204	0.277 ± 0.024

The field of GRB 021004 has two neighboring galaxy clusters at $z \sim 0.5$ at angular distances of about one degree. We examined a larger area of 3×3 degrees, which includes these two clusters, using SDSS DR12 data. SDSS survey has a limiting magnitude of about 22, and the catalog includes photometric redshift estimation as well as spectral redshifts for brighter objects. The area of 3×3 degrees is split in four regions and distribution of objects in these four regions also show peak at $z \sim 0.5$ (see Fig.10). CMB Plank data for the area of 3×3 degrees shows inhomogeneities in the areas, which could witness Sunyaev-Zeldovich effect (Fig.11).

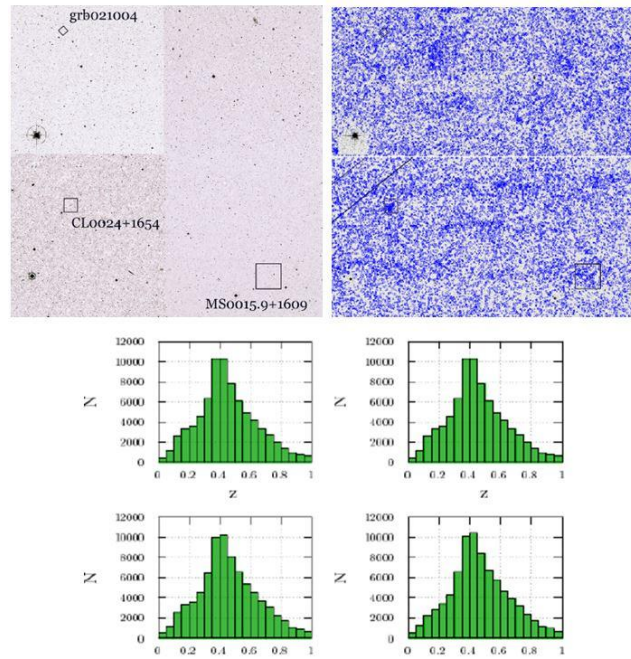


Fig10. SDSS field of 3x3 degrees. The field contains GRB 021004 field, CL 0024+1654 galaxy cluster at $z = 0.5$ and MS0015.9 galaxy cluster at $z=0.5$ (upper left), objects in the field from SDSS DR12 survey (upper right) and distribution of objects in 3x3 field divided by four regions (bottom).

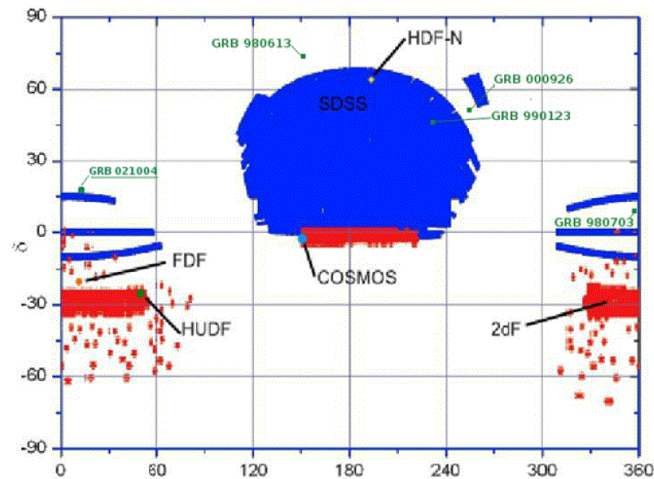


Fig11. Sky positions of GRB 021004 field, SDSS and other surveys.

Therefore, these signatures of BTA and HST data, absorption features in afterglow spectra of GRB021004, cosmic background radiation of Plank telescope and the investigation of BOSS survey, which is a part of SDSS could indicate a large structure of galaxies at $z\sim 0.5$.

References

- [1] R.F.L. Holanda, V.C. Busti, L.R. Colaço, J.S. Alcaniz, S.J. Landau, Galaxy clusters: type Ia supernovae and the fine structure constant, arXiv:1605.02578
- [2] M.L. Khabibullina, O.V. Verkhodanov, V.V. Sokolov, Statistics of the Planck CMB signal in direction of gamma-ray bursts from the BATSE and BeppoSAX catalogs, *Astrophysical Bulletin*, 2014, No 69, Vol.4 (arXiv:1406.6480)
- [3] L.G. Balazs, Z. Bagoly, J.E. Hakkila, I. Horvath, J. Kobori, I. Racz, L.V. Tóth, A giant ring-like structure at $0.78 < z < 0.86$ displayed by GRBs, arXiv:1507.00675
- [4] Daniele Fargion, UHECR and GRB neutrinos: an incomplete revolution? , arXiv:1408.0227
- [5] Hasan Yuksel and Matthew D. Kistler, arXiv:1212.4844,
- [6] Ming-Hua Li and Hai-Nan Lin, Testing the homogeneity of the Universe using gamma-ray bursts. *Astronomy & Astrophysics*, 2015, September 11 arXiv1509.0327v1
- [7] T.N. Ukwatta and P.R. Wozniak, Investigation of Redshift- and Duration-Dependent Clustering of Gamma-ray Bursts. *MNRAS* 2105, October 8. arXiv1507.07117v2
- [8] L.G. Balázs, Z. Bagoly, J.E. Hakkila, I. Horváth, J. Kóbori, I. Rácz, L.V. Tóth, A giant ring-like structure at $0.78 < z < 0.86$ displayed by GRBs *MNRAS*, 2015 July 2. arXiv 1507.00675v1
- [9] Andreja Gomboc, Unveiling the Secrets of Gamma Ray Bursts. ArXiv 1206.3127v1
- [10] V. Sudilovsky et al, Clustering of galaxies around gamma-ray burst sight-lines. *A&A* 2013 552, A143
- [11] G.E. Prochter et al, 2006, *ApJ* 648, L93;
- [12] S. Vergani et al, 2009, *A&A* 503, 771
- [13] M.-S. Shin and E. Berger, 2007, *ApJ* 660, 1146
- [14] T.A. Fatkhullin, A.A. Vasilev, V.P. Reshetnikov, A photometric study of faint galaxies in the field of GRB000926 *Astronomy Letters*, 2004, Vol.30, No.5, pp.283-292. Translated from *Pisma v Astron. Zh.*, Vol.30, No.5, 323-333 (2004)
- [15] Yu.V. Baryshev, I.V. Sokolov, A.S. Moskvitin, T.A. Fatkhullin, N.V. Nabokov and B. Kumar, Study of faint galaxies in the field of GRB021004, *Astrophysical Bulletin*, Vol. 65, No 4, pp. 327-342 (2010)
- [16] E. Bertin and S. Arnouts, *Astronom. and Astrophys. Suppl. Ser.* 117, 393 (1996)
- [17] W. Baum, *IAU Symp. 15: Problems of Extragalactic Research* (Macmillan, New York, 1963), p. 390
- [18] M. Bolzonella, J.-M. Miralles, and R. Pello, *Astron. Astrophys.* 363, 476 (2000)
- [19] D. Calzetti, L. Armus, R. C. Bohlin et al, *Astrophys. J.* 533, 682 (2000)

On the Observed Mass Distribution of Compact Stellar Remnants in Close Binary Star Systems and Possible Explanations Proposed for the Time Being

Vladimir V. Sokolov

¹*Special Astrophysical Observatory of Russian Academy of Sciences, Nizhnij Arkhyz, Russia;*

sokolov@sao.ru

Abstract It turns out that accumulation of data during 40-years observational studies just emphasized a contrast between pulsars and black hole (BH) candidates in Galactic close binary stellar systems: (1) the mass spectrum of these degenerate stellar objects (or collapsars) shows an evident absence of objects with masses within the interval from $2M_{\odot}$ (with a first peak at about $1.4M_{\odot}$) to approximately $6M_{\odot}$, (2) and in close binary stellar systems with a low-massive (about $0.6M_{\odot}$) optical companion the most probable mass value (the peak in the mass distribution of BH candidates) turned out to be close to $6.7M_{\odot}$. This puzzle of discrete mass spectra of collapsars in close binary systems demands some solution and explanation in stellar evolution scenarios in connection with the core-collapse supernovae explosion mechanism and in context of a relation between supernovae and gamma-ray bursts. The collapsar strong field – an analogue of BH in General Relativity – is investigated in a totally non-metric, dynamical model of gravitational interaction theory, in which extremely compact objects of the masses $M_Q \approx 6.7M_{\odot}$ with a quark-gluon plasma bag of radius $r^* = GM_Q/c^2 \approx 10$ km exist.

Keywords: Neutron Stars, Black Holes, Supernovae, Gamma-Ray Bursts, Dense Matter, Gravitation

1. Introduction

Compact stellar remnants in close binary systems (CBSs) have been studied systematically from the 80-th of the last century [1 – 15]. Now it is clear to everybody that there is indeed a considerable gap between masses of neutron stars (NS) and black hole (BH) candidates: the observed mass spectrum of NSs and BH candidates shows an obvious absence of compact objects with masses within the interval from $2 M_{\odot}$ to $\approx 6M_{\odot}$.

Besides, the many-year investigations led to another observational property in compact objects themselves – the BH candidates in CBSs with relativistic companions. It turned out that, like NSs, they (BH candidates) can have a selected mass value. In 16 CBSs with low-massive (about $0.6M_{\odot}$) optical companions the *most probable value* (a peak in a mass distribution of relativistic objects) is close to $6.7M_{\odot}$. So, one can speak about a *discrete mass spectrum* of compact objects in the CBSs with NSs and BH candidates.

These two problems demand some solution both in the context of the supernovae and gamma-ray bursts (GRB) relation, and in connection with the core-collapse supernovae (CCSN) explosion mechanism itself. In particular, polarized radiation of long GRBs, the black-body component in their spectra and other observational properties can be explained also by a direct manifestation of a surface in such collapsars.

So, the main purposes in this overview are to draw attention:

(1) to the discussion about the discrete mass spectrum problem of the compact objects in the stellar CBSs,

- (2) to $6.7M_{\odot}$ peak in the observed collapsar mass distributions, and
- (3) to probable interpretations the observed mass spectrum, which is rather similar to line one.

2. The Mass Spectrum of Stellar Compact Objects: Observational Properties

Though the mass distribution studies of compact remnants in binary systems have been carried out for a long time already (e.g., [1 – 12]), but astrophysicists keep discussing the mass spectrum problem of these degenerate objects for more than 20 years. Because,

On the one hand, according to General Relativity (GR), “a possibility to identify a compact object with black holes depends, in particular, on the condition that the available data allow positive asserting that the mass of an observed object is higher than the maximum permissible mass of a neutron star (or white dwarf)” (see [16], ch.9).

On the other hand, according to GR (see the same textbook by Shapiro and Teukolsky dedicated to The Physics of Compact Objects), the *mass spectrum* of compact objects (collapsars – NSs and BHs) in CBSs is likely to be continuum. (Since then nobody ever predicted that it must be discrete in GR at least.)

Though the observed mass spectrum is rather similar to the line one, see Figure 1 (a) taken from [7] and references therein. Evidently, there is a significant gap between the observed BH candidates and NSs masses.

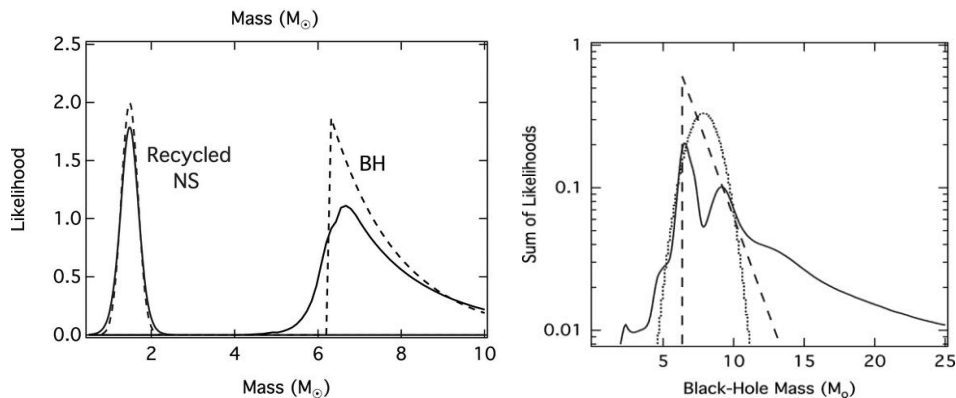


Fig1. (Taken from Özel et al. (2012,2010)[7, 8]).

(a) – The inferred mass distributions for the most massive neutron stars population (Recycled NSs) and BHs. The dashed lines correspond to the most likely values of the parameters. For the case of BHs, was used the exponential distribution with a low mass cut-off at $Mc = 6.32M_{\odot}$ and a scale of $Mscale = 1.61M_{\odot}$. The solid lines represent the weighted mass distributions for each population, for which appropriate fitting formulae are given in [7]. The distributions for the case of BHs have been scaled up by a factor of three for clarity.

(b) – Solid line shows the sum of likelihoods for the mass measurements of the 16 BHs in low-mass X-ray binaries. The dashed and dotted lines show the exponential and Gaussian distributions, respectively, with parameters that best fit the data (see [8] for details).

Bailyn et al. (1998) [3] were among the first to find evidence of a “significant gap” between the least massive BHs and a “safe” upper limit for NS masses of $3M_{\odot}$ (e.g., Kalogera & Baym (1996) [2], and see also [17] in page 3 where there are more references about this effect). Though the mass separation of the degenerate stellar objects was noticed as far as before 1990th for all CBSs including the Cygnus X-1 system (see references in [18] where one of possible interpretation of this gap is adduced for the time being). Here I say also, in particular, about of the compact object masses in 16 X-ray binary systems with faint (the low massive) optical companion stars. The tables of properties and orbital parameters for these 16 BH binaries can be found in Özel et al. (2010) [8] (and see also in Kreidberg et al. (2012) [11],

Wiktorowicz et al. (2013) [19]). For these systems with BH candidates the companion mass ratio is $q = M_{opt} / M_x \approx 0.1$.

Just these very cases of the systems (with the mass of optical star M_{opt}) with uncertainties in measurements of binary system parameters are the smallest ones now, and the mass separation between the BH candidates and NSs is seen the most clearly. It is these systems in which the BH candidate masses are concentrated near maximum in Fig.1 (a). It is seen well also in Fig.1 (b) taken from [8] for the sum of likelihoods for the mass measurements of 16 BHs in low-mass X-ray binaries.

As was specially noted in [8], this cut-off mass $M_c = 6.32M_\odot$ in the exponential distribution is well above theoretical expectations, indicating a sizable gap between NS and BH masses. Furthermore, the exponent mass scale $M_{scale} = 1.61M_\odot$ in the exponents in Fig. 1(a) and Fig. 1(b) is significantly smaller than the same theoretical expectations. I.e. *the peak* of BH masses still turns out to be *rather narrow*. In this connection, the authors [7, 8] specially emphasize that because of the high-mass wings of the individual likelihoods, the shape of their sum in Fig. 1 (a and b) is artificial at the high-mass end. (About that see also the caption of Fig. 380, ch.8, §9, volume 2 of the book by A.M. Cherepaschuk (2013) [20]: "...the shape of probability density distribution function for all BHs in the region of high mass values M_x is unreliable".) This concerns also systems with a higher ratio $q = M_{opt} / M_x > 0.1$ and heavier optical companions (including Cyg X-1).

Figure 1 (a and b) actually is a good illustration of a new property – *the peak* in the BH candidate mass distribution. Figure 2 (a) is taken from paper [11]. Here the solid line conforms to what was obtained by other authors previously (by Farr et al., 2011) [10]: "Toward the end of our analysis work, we became aware of a more recent study [8], also in a Bayesian framework, analyzing the low-mass X-ray binary sample. Our results are largely consistent with those obtained by Özel et al. [8], who examined 16 low-mass X-ray binary systems containing BHs and found a *strongly peaked distribution* at $7.8 \pm 1.0 M_\odot$."

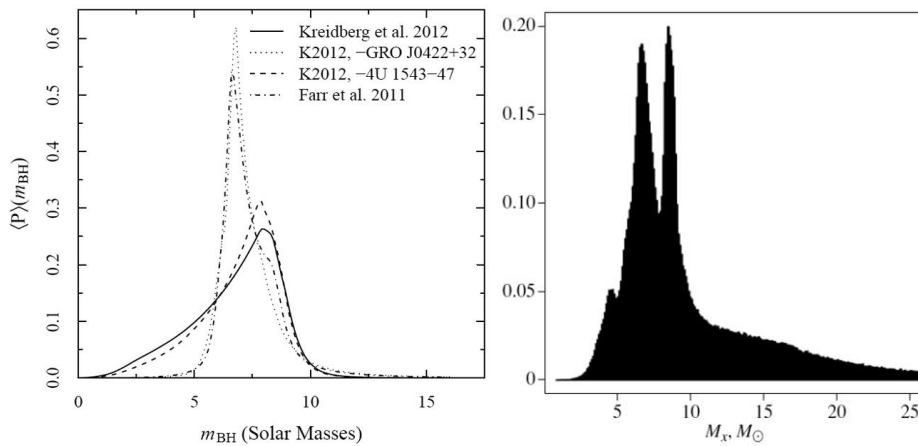


Fig2. (a) – Different versions of BH mass probability distributions calculated in the power-law model taken from [11]. The dot-dashed curve is from the power-law analysis with the using of parameters of 16 BH systems of Farr et al. [10]; the dotted curve is from analysis with the using of parameters of 16 BH binary systems of Kreidberg et al. (K2012) from [11], excluding GRO J0422+32 from the sample; the dashed curve comes from analysis with system parameters from [11], excluding 4U 1543-47 from the sample; the solid curve is from analysis using parameters of 16 BH binary systems (but including GRS 1915+105 in the sample, see the text).

(b) (taken from [13]) – Total probability density distribution of compact-object masses M_x in 20 X-ray binary systems (see the text).

For Farr et al. [10] this is the main conclusion which is well confirmed by this Fig. 2 (a) also. As was said above, from the paper by Özel et al. [8] it follows (see Fig. 1) that the parameterized probability

density distribution for 16 BHs in low-massive binary X-ray systems obtained in the exponential law is optimal (the dashed line) with a *sharp break* in the low-mass end plus the fast downfall after this peak for large masses. This fast downfall of BHs mass does not agree with theoretical expectations (or predictions) also, as well as the sizable gap between NS and BH masses – see it in the article Özel et al. [8]. Here the matter is both about 16 CBSs whose parameters are measured the most accurately and about CBSs with heavier optical components for which “...the shape of their probability density distribution function for all BHs in the region of high values of mass M_x is unreliable” [8].

And here I am interested most of all in this peak itself (and its precise value especially) in the mass distribution of objects which many people already confidently call “black holes”. Like the peak of NSs in Fig.1, the mass corresponding to *this peak* is a new observational property of real BH candidates in these CBSs.

Here astrophysicists can issue the challenge both on determination of the *minimum* mass (because there is this BH-NS gap) and on measurement of the limit mass for these objects (BH candidates), just as they do that for white dwarfs and NSs for a long time. All the more so, that now this already becomes the main observational and theoretical problem for NSs (see in Buballa et al., 2014 [21], and in this article below).

In Fig. 2 (a) from [11] the most probable value of BH candidate mass was perfectly confirmed after the strong testing of the same sample of objects and comparison of the BH mass distributions with previous results. But the main thing is this peak. And the filling of this NS-BH gap is “successful” only by taking into account the most unreliable binary system GRS 1915+105 (in which the corresponding individual probability/errors distribution in mass measurements of the compact object begins with the zero mass of the BH candidate – see Fig. 7 in [11]).

On the other hand, even with uncertainties of parameters measurements of the same 16 BH binaries introduced by GRS 1915+105 and another debatable system 4U 1543–47 (see the solid curve in Fig. 2, a), the result by Farr et al. [10] remains valid: *a strong peak* is in the sum of likelihoods distribution at $7.8 \pm 1.0 M_{\odot}$ (though with a lower maximum probability).

Recently, a SAI team [13] tested once more 20 binary X-ray systems with BH candidates by their methods and practically confirmed existence of the gap problem in the mass spectrum of the degenerate compact objects – NSs and BH candidates. The (a) and (b) images in Fig. 2 for BH mass distributions are similar, in spite of differences in the sets of binary systems, in their parameters, and in the methods (see [13] for details) of calculation of the sum probability used in these studies [11] and [13].

Thereby, calculations of probability distributions tested by four different groups ([Farr et al. [10], Özel et al. [7, 8], Kreidberg et al. [11], and Petrov et al. [13]) by different methods confirm the main thing – a peak in mass distributions for BH candidates does exist really and (one way or another) it turned out to be within the Farr et al. [10] mass interval $7.8 \pm 1.0 M_{\odot}$.

On the other hand, it is impossible to insert easily a BH in this gap in Fig.1 (a). In this mass distribution (see Fig.2 (a)) they try (see in [11] for the 1% mass quantile) to shift all 16 low-massive binary X-ray systems by only one system (4U 1543–47) just in the region where only NSs with mass not more than $\approx 2.1 M_{\odot}$ [7] are observed. But, if we look at the individual probability/errors distributions (see in [11] Fig. 7), then we see at once the strong difference of the distribution for the 4U 1543-47 system from what was obtained by Farr et al. [10] for this system before (see Fig. 1 for the individual mass distributions in [10]).

Now, returning to the upper limit of this mass gap (2–5 M_{\odot}), as was said above, it can be even higher judging from what was obtained in [11]: the most probable value for the lowest BH mass is above $6 M_{\odot}$, with a peak at $\approx 6.7 M_{\odot}$ for 16-1 X-ray binaries. This peak value was taken of directly from Fig. 2 (a). Here it is just the peak in the mass distribution that should be considered as the most probable value of the compact objects mass in these galactic CBSs. From this peak a downfall to the NSs side begins.

On the mass spectrum of BHs in the low-mass X-ray binaries: at least 16–1 of them holds the BH candidates with a mass distribution peak of $\approx 6.7 M_{\odot}$ (as the most probable value – see Fig. 2, (a)). The

authors themselves [11] wrote not a word about this peak. Though the result by Farr et al. [10] recalculated by Kreidberg et al. [11] in the scale $\langle P \rangle(m_{BH})$ in the power-law model (marked by the dash-and-dot line in Fig. 2 (a)) also turns out to be close to the maximum near $6.7M_{\odot}$. That is, nobody except Farr et al. [10] wants to notice another observational fact beside this strange mass gap.

Everyone is keen on the problem to fill it (the gap) or, at least, to understand it. In doing so, nobody wants to explain or even to notice this peak itself ($\approx 6.7M_{\odot}$) for the BH candidates. But analogous peaks (see in [7]) in NS mass distribution are explained somehow both by CBSs (+evolution) with NSs properties, and by the equation of state for these compact objects (neutron, hybrid and strange stars, see further about this).

As to peaks in mass distribution of BH candidates, here the ideological ban (“The BH mass distribution must be smooth, etc.”) hinders from the very beginning. But eventually, just this observed BH mass distribution origin (with this peak from [8] namely right near $6.7M_{\odot}$) have to be explained from standpoint of *stellar evolution* of massive stars – see Figure 2 (right panel) in [40], and a discussion therein. But even here the authors do not indicate themselves in the text the mass value corresponding to the peak near $6.7M_{\odot}$ in the BH mass function and one has to take it (the peak) directly from the image.

So, referring to the observed peaks in NSs mass distribution [7] one should pay attention to the fact that beside the strange NS and BH mass spectrum (with the characteristic lack of compact objects within mass range 2–5 M_{\odot}) the matter can be about a new observational property of compact objects – BH candidates: Like NSs, these objects can have a selected (the most frequent in these CBSs) value of mass. Also this can mean perfectly that these observed objects can have a surface and their own equation of state the same as NSs... (No ideological bans can prevent us from testing that observationally. It is necessary to measure not only mass, but the size of BH candidates also.)

2. Gravidynamics

Here I call the gravidynamics some model of gravitational interaction ([22] and references therein) in which, like for all other fields in nature, the localizability of field energy is accepted a priori as a postulate. Then, with gravitational field energy densities close or exceeding the nuclear density $\rho_{\text{nucl}} = 2.8 \cdot 10^{14} \text{ g cm}^{-3}$, completely new properties of compact gravitating stellar mass objects can be prognosticated. In particular, the understanding of the physics of phase transition to quark-gluon plasma during formation of so dense objects can be directly connected with such dynamical gravitation description. Thus, the case in point can be the direct *observational consequences* related with the gravitational energy localizability.

The compact object (collapsar) strong field – an analogue of the BH in General Relativity (GR) – is investigated in such totally non-metric, dynamical model of gravitational interaction theory. In the case of extremely strong (for gravidynamics) collapsar field a region filled by matter (“a bag”) must have a radius equal to $r^* = GM_Q/c^2 \lesssim 10 \text{ km}$ at the total collapsar mass $M_Q \lesssim 7M_{\odot}$. The article [22], dedicated to the properties of strong static field of the collapsar in gravidynamics, gives a more precise estimation of this mass and describes some properties of quark-gluon plasma inside this bag. Stability or hydrostatics of the *self-bound* quark-gluon bag based on the color forces only. Specifically, in the very centre (i.e., for distances $r \sim 1 \text{ fm} = 1 \cdot 10^{-15} \text{ m}$) of such a bag with radius $\lesssim 10 \text{ km}$ the “macroscopic” constant of the color forces will be only about 3 constants of electromagnetic interaction ($\alpha_{\text{QED}} \approx 0.0073$). For all that the density $\varepsilon(r)/c^2$ will be of the order of $5.4 \times 10^{52} \text{ g cm}^{-3}$, and the total energy (mass) in a so small sphere ($r = 1 \text{ fm}$) will be $7 \times 10^{14} \text{ g} \approx 10^{-19} M_{\odot}$. The total (*measurable*) mass of such *extremely compact* object is $M_Q \approx 6.7M_{\odot}$.

In another our article [23] dedicated to the masses of macroscopic configurations in metric and dynamic gravitation theories, a formula for calculation of the total mass of the extremely compact object

in gravidynamics is given:

$$M_Q = 6.64M_\odot \left(\frac{2\rho_{\text{nucl}}}{4B/c^2} \right)^{1/2}$$

for the bag radius $r^* = GM_Q/c^2 \approx 10 \text{ km}$ whose surface consists of a strange self-bound matter. This selected mass value $6.7M_\odot$ was obtained when we chose quite definite value of the bag constant $B = 79.925 \text{ MeV fm}^{-3}$ for some quark-gluon plasma bag model in quantum chromo-dynamics (QCD) with limiting equation of state $P_Q = 1/3(\varepsilon - 4B)$ for quark configurations, where ε is the total energy density inside the huge quark-gluon bag with the bag radius $r^* = GM_Q/c^2 \lesssim 10 \text{ km}$. And now it (the B value) is still discussed, but then it was possible to refer only to such pioneer papers as E. Witten [24] (see also the references in [23, 25]).

Thus, the gravidynamics is the model of gravitational interaction in which: (1) Gravitational field is assigned by energy and, correspondingly, quite a definite part of any gravitating object mass is the field energy like the electromagnetic mass of electron in electrodynamics. (2) All known relativistic effects of weak field (that is for $r \gg r^* = GM_Q/c^2$) are explained (see [23] and references therein), because in such cases the force is basically specified only by a *tensor part* of field, or by gravitation proper. (3) In the compact object *strong field*, when the energy density of the field itself approaches the nuclear density ρ_{nucl} (for $r \approx r^*$), the role of the *scalar component* of the field (*repulsion*) increases. (4) The total mass M_Q of such an extremely dense object – a quark star in gravidynamics – already half consists of the field only, or of its *scalar-tensor* mixture around the bag with radius r^* . Thereby, the basic *observational consequence* confirming the version of gravidynamics + QCD unification suggested here, could be indeed the existence of a selected collapsar mass value M near $6.7M_\odot$.

Relativistic effects in gravidynamics and in GR do coincide, but only in sufficiently weak fields (for $r \gg r^*$), where GR describes them in the long run only as effects of the tensor field with the spin 2 graviton in flat space-time. This is the “Feynman approach” to description of gravitation (see Feynman Lectures on Gravitation [26]). But in strong fields, when the object size is close to GM/c^2 and when the energy density of the field itself becomes comparable with the energy density of matter (and of all other fields), the consistent dynamical description of field (gravidynamics) can give quite a different result.

In gravidynamics the observational properties and all physics of the quark star – a stable configuration with extremely strong field (for $r \sim r^* = GM_Q/c^2 \approx 10 \text{ km}$) – are determined only and *uppermost* by the scalar component of the field or by “levitons” (from the word “levitation”) – “gravitons” with spin 0 [22, 23].

But then it already goes beyond the scope of the standard Feynman approach, in which “the theory with the graviton spin 0 must be rejected...” see the same Lecture 3 in [26]. So, the gravidynamics may be regarded as a certain modified or extended Feynman field approach to gravitation. In fact, in gravidynamics the most important and a critical question from the observational (experimental) point of view is the question: to which value of the gravitational field energy density in the strong field (this energy) cannot be considered non-localizable like in GR (see in [43], ch.11, § 96)?

In this article the matter is *essentially* about direct observational consequences of such consistent dynamical description of gravitation with two field components of spin 0 and 2. And here, in particular, I speak yet about a possibility to explain the second peak in the mass distribution of compact stellar objects (e.g., see Figure 1, left).

But here it should be specially said also about gravitational emission which explains secular effects in binary systems with pulsars. In gravidynamics we are to accurately account for contribution of scalar emission. Though in 1992 one attempt was already undertaken (see in [27]) for PSR 1913+16. But now modern data on binary pulsars became considerably more precise (see the references in the previous section). So far, there is a discrepancy from GR also for observed secular period changes dP/dt in these binaries. In particular, the observed dP/dt is higher and there is surely (see [28]) some unaccounted contribution, which should be taken into account carefully. It is especially important to take this into

consideration in the case of relativistic collapse of a massive stellar core in the process of formation of objects with the mass $6.7M_{\odot}$ and radius ≈ 10 km. In this case the contribution of the lepton scalar radiation becomes determinative in gravodynamics.

4. Observations of Core-Collapse Supernovae, Gamma-Ray Bursts, Possible Explanations of the Observed Collapsars Mass Spectrum and stellar evolution

In connection with observational manifestations of these compact objects origin – collapsars (NSs and the BH candidates) – one should emphasize especially the discussion on a relation between BHs and long-duration gamma-ray bursts (GRBs), since NSs and BHs formation of itself can be closely related to GRBs. Here one should inevitably say about relation between core-collapse supernovae (CCSNe) and the same GRBs since a long-duration GRB can be the beginning of CCSNe. Or at least a GRB itself can be *one of first signals* of a massive star core collapse and supernova explosion at the end of the massive star evolution (see e. g. [29], and references therein).

The masses spectrum of compact remnants in binary systems is now actively discussed just in connection with the old problem of CCSNe explosion mechanism explanation (Wong et al, 2014) [17], because the CCSN explosion mechanism has remained one of the outstanding challenges in theoretical astrophysics for decades. Among the various models that have been proposed over the years to explain CCSNe explosions [30] (Müller & Janka, 2014), see also [31] (Janka, 2014) and [32] (Adam Burrows, 2012) for an up-to-date summary. The so-called *delayed neutrino-driven mechanism* currently remains the best explored and most promising scenario (at least for CCSNe with observed explosion energies not exceeding 10^{51} ergs). Still, see the remarks in [32]: “There has been palpable progress in the development of techniques and tools to address the core-collapse problem in the last thirty years, *but* the current status of the theory for the mechanism and the systematics of core-collapse explosions is ambiguous, if not confusing. Wilson (1985) [44], in a pioneering paper and using a spherical code, obtained a *neutrino-driven explosion* after a short post-bounce delay, ...”

As was reported many times already [3, 8, 10], the problem of the “black hole mass gap” (or *paucity range*) of $2-5M_{\odot}$ demands some solution both in the context of the CCSN-GRB relation, and in connection with the CCSN explosion mechanism itself. The simplest “solution” is that the explosion energies are weaker for these stars, as it is understood by the authors in [32, 17] within the framework of their “fall-back mechanisms” in CCSNe. It is mean in hear, that some of the stellar material does not receive enough energy to escape the potential well of the newly formed NS and it falls back on to the core.

This is the fall-back which can be also connected to long-duration GRBs. At least, astrophysicists have been preoccupied with this strange “mass gap” for a long time, and *now directly* (at long last!) in connection with the SNe explosion mechanism itself, so long as one is forced to accept the fact that the details of CCSN mechanism are not fully understood. This means that it will be necessary to remember also the old *core bounce problem* in connection with SN 1987A [34]. The point is that *if a BH is formed* at once, then this “potential well” would become *infinitely deep*, and there would be *no CCSN explosion at all*. Therefore this catastrophic instability must develop before BH horizon emerges, what makes rather improbable the very accessibility of a BH configuration at the end of massive collapsing star evolution, and eventually QCD becomes incompatible with BHs [45].

Wong et al. [17] suggest their version of a model of the core collapse massive star progenitors through the core bounce, in which the essential role is played by the neutrino transport. Philosophy of their calculations is that first they form above mentioned NS (to explain the CCSN itself), and then the further “fallback” leads to BH origin. This fallback (with a posterior BH formation) plays an important role in setting compact remnant masses and is to explain some observed phenomena likes of the long-duration GRBs and a neutrino emission. But unfortunately in such a scenario the resulting BH mass *must fill* the

observed mass gap (or paucity range) 2–5 M_{\odot} right now.

At least these calculations [32, 17] indicate that such a mass gap can indeed provide constraints on the physics of CCSN explosions.

But it turns out that problems (related to the compact objects characteristic mass lack 2–5 M_{\odot}) arise already in origin explanation or *evolution* of the same CBSs with the low-mass optical companions and with $q = M_{opt}/M_x \approx 0.1$. Right in connection with the formation puzzle, the authors of [19] (Wiktorowicz, G., Belczynski, K., Maccarone, T.J. 2013) try to explain just this (observed) value q in the 19 reliably confirmed now BH Galaxy binaries or in the BH X-ray transients. The 16 of them are X-ray transients (or the BH low-mass X-ray binaries) hosting ~ 5 –10 M_{\odot} BH candidates and a Roche lobe overflowing low mass optical companion. The observed *optical companion* masses are found mostly in 0.1–1 M_{\odot} mass range, but with a *peak* at 0.6 M_{\odot} . Under such conditions none of the available common envelope models allow for the formation of the *observed* population of Galactic BH transients with masses from Figures 1 and 2 though.

That is, one cannot explain just these too small masses for the optical companions ($M_{opt} = 0.6M_{\odot}$). According to all known standard (and described in many textbooks in detail) evolution models of such CBSs, it must be 1 M_{\odot} . That is to say, the optical companion mass distribution must peak at 1 M_{\odot} also. But at least it is still in tension with the smallest measurement errors in mass measurements for these 16 binary X-ray systems.

So, the sum of all explanations of component mass ratio $q = M_{opt}/M_x$ in these 19 BH X-ray transients is as follows.

Wiktorowicz et al. [19] have reexamined the issue of donor (optical star) mass in the Galactic BH X-ray transient binaries. Since the formation scenarios involve a common envelope phase initiated by a massive BH progenitor, it is naturally expected that companion mass should not be too small as to avoid the common envelope merger. However, the donors that are found in the BH X-ray transient binaries have very low mass $\approx 0.6M_{\odot}$. Early studies have shown that stars with mass above 2 M_{\odot} are the most likely companions for Galactic BHs (CygX-1 e.g.). With the updated population synthesis code by Wiktorowicz et al. [19], they have shown that stars with mass 1 M_{\odot} are most likely companions. Despite the factor of ~ 2 improvement the predictions are still *in tension* with available (the most exact) observations.

“This failure most likely indicates that either the current evolutionary models for low mass stars are not realistic or that the intrinsic population of BHs per se (in the low-mass X-ray binaries) is quite different from the observed one” (see the remarks in [19]).

Though for the time being Wiktorowicz et al. [19] do not pay attention to the peak itself in mass distribution of the BH candidates, but they are very concerned about this “mass gap”: In the NS and BH mass spectrum the characteristic lack of compact objects is within mass range 2–5 M_{\odot} – this is close to the interval between the maximum mass of NS and minimum mass of BHs (candidates). In this connection, when speaking about the interval between the “last” peaks (Fig.1, solid lines), i.e. between the most probable values of mass of compact objects in galactic CBSs, it would be close to 1.4–6.7 M_{\odot} . I.e., the gap begins indeed with a *fast downfall* of mass of compact objects both from the NSs side (1.4 M_{\odot} peak) to BH candidates, and from the BH side (6.7 M_{\odot} peak) to NSs side.

Eventually *another* model of supernovae was suggested for the gap in the mass spectrum of compact objects [19] – this gap can be *qualitatively* explained with the specific model of CCSN explosion. But in the same model [35] (Belczynski, K., Wiktorowicz, G. et al. 2012) have to take into account the fact that the *lowest mass* BHs are above 5 M_{\odot} in correspondence with the fact that the maximal mass NSs are less than 2 M_{\odot} . “So far we have not directly commented on the associated BH mass distribution of the BH X-ray transient binaries. In all previously discussed models BH masses were found in 5–15 M_{\odot} range. This range is in agreement with the existence of mass gap and consistent with masses of BHs in the Galactic binaries” (see the remarks in [35]). At least, here the authors admit themselves the existence of a problem.

Though eventually just in this new model of CCSN explosion by Belczynski et al. [35] it also turns out that BHs (resulting from the explosions) get directly to this gap: “In this model we find that majority of BHs have mass around $3M_{\odot}$.” So, and this finding is inconsistent with the observations, since “it is hard to imagine that currently known wide spectrum of BH masses would be shifted to a very narrow range with peak at $\approx 3M_{\odot}$.” And then, peak like this for the BH candidates turns out to be at a wrong place (see in Fig.1).

Besides, it should be also taken into account that the limit mass of observed NSs is not $3,2M_{\odot}$, but is $\approx 2M_{\odot}$. I.e. there are no NSs with such limit masses ($\approx 3,2M_{\odot}$) and limit equation of state $P = \epsilon$, which was mentioned in the famous textbook by Shapiro and Teukolsky (see chapters 8.13 and 9.5 in [16]). So, the prediction based on the wrong theory of strong interaction failed here also – NSs and BHs with mass $3.2M_{\odot}$ are not observed.

4. Conclusion

As far as before 1990 it was said that a strange minimum between masses of NSs and BH candidates is outlined, but then nobody took it seriously. Accumulation of data on CBSs with the degenerate objects has been going on.

When I. M. Kopylov with me [14] were determining the mass of the first (at that time) CBS Cygnus X-1 with the relativistic companion, we concentrated then on the most precise estimation of mass of the optical star HDE 226868 – OI supergiant. It was what should be done first of all and as precisely as possible, because then it would be possible to determine reliably the *lower bound* of the degenerated star mass also. It turned out that with the mass $M_{\text{opt}} = 19.5M_{\odot}$, the mass of the BH candidate must be *not less than* $6.5M_{\odot}$.

It is this value of the mass M_{opt} in CygX-1 system that is cited in [19]. Eventually it turned out that this lower mass limit $M_x \geq 6.5M_{\odot}$ [15] of the relativistic object in CBS Cygnus X-1 is close to the low mass cut-off at $M_c = 6.32M_{\odot}$ in the exponential mass distribution as shown in Fig. 1 (a).

Now the data precision on BH candidates in the Galactic binary systems approaches to the precision of NS mass data, and they can be compared at last; there are a lot of papers about that already (see refs. at the Section 2). Certainly, they are superimposed by *individual* errors of mass determination in such binary systems and by a *real mass dispersion* of the compact objects themselves resulting from star evolution in these CBSs (see at the Section 4 of the text). But, one way or another, the peaks in mass distribution in Fig. 1 and 2 (*by definition*) are the *most probable mass values* of these degenerate objects.

So, it turns out that the accumulation of data on Galactic CBSs with degenerate stellar objects during 40 years just emphasized the *contrast* between NSs and the BH candidates. There are no compact objects with masses between $2M_{\odot}$ and $\approx 6M_{\odot}$, and what is more, – there is the peak in their mass spectrum near $6.7M_{\odot}$ (see Figs 1, 2). Thus, the previous sections concern the value of mass of a quark star (extremely compact object) in gravodynamics $M_Q \approx 6.7M_{\odot}$ [23] predicted in 1993. Besides, now it can be considered also as an independent observational confirmation of the quark-gluon plasma bag model in QCD, because the value of the bag constant $B = 79.925 \text{ MeV fm}^{-3}$ in the limiting equation of state $P_Q = 1/3(\epsilon - 4B)$ follows immediately from the value of the second peak $\approx 6.7M_{\odot}$ as the most probable value in the observed distribution of mass of degenerated objects of stellar mass in CBSs, i.e. where these masses are measured the most precisely at present.

It is not excluded that further observations will result in the fact that these compact objects (in these binary systems) can be without BH properties like singularity or event horizon. Like NSs, these degenerate objects can have their own equation of state, surface and size, determining all their observational manifestations. The absence of the pulsar effect in objects of the second peak in the mass distribution in Fig.1 does not mean that they do not have surface. This only means that these are not pulsars or NSs, at least. Therefore it is still early to say that these are BHs exactly, and BHs are discovered already. We *can* and *should* look for effects related to the surface of these objects because

many people realize that GR predictions still remain to be verified in the strong-field regime (see e. g. [41, 42, 46] and references therein).

In particular the GRBs prompt emission anisotropy, the instantaneous GRB blackbody spectra and other observed properties (e. g., well-known “Amati law”) must be a consequence some sort of compact GRB model [36] and could be explained by the direct surface manifestation of these collapsars. And strong linear polarization of some GRBs prompt emission can be also explained in principle by the direct manifestation of strong magnetic field of a collapsar resulting from an SN explosion, and may be related to radiation transfer in a medium with the strong (regular up to $\sim 10^{12}$ - 10^{16} Gauss) magnetic field on (or near) the surface of the compact object [39]. And a cyclotron feature $E_{\text{rest}} = 21.7$ (+1.9/-1.6) keV (for GRB 011211 with gravitational red-shift $z_{\text{grav}} = 0.318$) could be explained by the *direct* manifestation of the surface magnetic field of $\sim 10^{12}$ Gauss in the GRB photon gamma-ray spectrum [33] with $z_{\text{GRB}} = 2.140$.

On the other hand, the problem of a too large mass of NSs is also actively discussed now. The main point is, – what these objects consist of? See the recent discussions in [21] and NEOS2014 (The second workshop on "Nuclear Equation of State for Compact Stars and Supernovae", FIAS, Frankfurt, December 3 – 5, 2014, <http://fias.uni-frankfurt.de/~neos2014/>). And what maximum permissible mass can be reliably justified for NSs; $1.4M_{\odot}$ or $2.2M_{\odot}$? Now the equation of state is the main problem for these objects (of the first peak in the mass distribution in Fig. 1) also. Are they neutron stars? (See also [37] and references therein.) Thus, already physicists are also excited by the mass distribution (with the peak $1.48M_{\odot}$ in Fig. 1). The NSs masses near $2M_{\odot}$ are permissible in this distribution. But such objects are too heavy to be called NSs – see also the review by J. Lattimer [38] “The Nuclear Equation of State and Neutron Star Masses”.

References

- [1] Finn, L. S. 1994, Physical Review Letters, 73, 1878.
- [2] Kalogera, V., & Baym, G. 1996, Astrophys. J. (Letters), 470, L61.
- [3] Bailyn, C. D., Jain, R. K., Coppi, P., & Orosz, J. A. 1998, ApJ, 499, 367.
- [4] Thorsett, S. E., & Chakrabarty, D. 1999, ApJ, 512, 288.
- [5] Kaper, L., van der Meer, A., van Kerkwijk, M., van den Heuvel, E. 2006, The Messenger, 126, 27.
- [6] Nice, D. J., Stairs, I. H., & Kasian, L. E. 2008, in AIP Conf. Proc. Ser 983, “40 Years of Pulsars: Millisecond Pulsars, Magnetars and More”, eds C. G. Bassa, Z. Wang, A. Cumming, & V.M. Kaspi, Springer-Verlag: American Institute of Physics, 983, 453.
- [7] Özel, F., Psaltis, D., Narayan, R., & A. Santos Villarreal, 2012, ApJ, 757, 55.
- [8] Özel, F., Psaltis, D., Narayan, R. & McClintock, J. E. 2010, ApJ, 725, 1918.
- [9] Schwab, J., Podsiadlowski, P., & Rappaport, S. 2010, ApJ, 719, 722.
- [10] Farr, W. M., Sravan, N., Cantrell, A. et al. 2011, ApJ, 741, 103.
- [11] Kreidberg, L., Bailyn, C. D., Farr, W. M., & Kalogera, V. 2012, ApJ, 757, 36.
- [12] Kiziltan, B., Kottas, A., De Yoreo, M. & Thorsett, S.E. 2013, ApJ, 778, 66.
- [13] Petrov, V. S., Cherepaschuk, A. M., & Antokhina, E. A. 2014, Astronomy Reports, 58, No. 3, 113 (Original Russian Text: V. S. Petrov, A. M. Cherepashchuk, & E. A. Antokhina, *Astronomicheskii Zhurnal*, 2014, 91, No. 3, 167).
- [14] Kopylov, I. M., & Sokolov, V. V. 1984, *Pis'ma v Astronomicheskii Zhurnal*, 10, 756 (Further Evidence for Precession of the Optical Star in the Cygnus X-1 System) in Russian.

- [15] Sokolov, V. V. 1987, *Astronomicheskii Zhurnal*, 64, issue 4, 12 (On parameters of the Cygnus X-1 system) in Russian.
- [16] Shapiro, S. L., & Teukolsky, S. A., 1983, “Black Holes, White Dwarfs, and Neutron Stars“ (ch.9), John Wiley & Sons, New York.
- [17] Wong, Ts.-W., Fryer, C.L., Ellinger, C.L., Rockefeller G., & Kalogera, V. 2014, preprint, arXiv:1401.3032 [astro-ph. HE] (The Fallback Mechanisms in Core-Collapse Supernovae)
- [18] Postnov, K. A., & Cherepashchuk, A. M. 2003, *Astron. Rep.* 47, 989.
- [19] Wiktorowicz, G., Belczynski, K., Maccarone, T.J. 2013, preprint, arXiv: 1312.5924 [astro-ph. HE] (Black Hole X-ray Transients: The Formation Puzzle) .
- [20] Cherepashchuk, A. M., 2013, “*Close Binary Stars*“, FIZMATLIT, Moscow (in Russian).
- [21] Buballa, M. et al. 2014, summary of the EMMI Rapid Reaction Task Force on "Quark Matter in Compact Stars", October 7-10, 2013, FIAS, Goethe University, Frankfurt, Germany, preprint, arXiv:1402.6911 [astro-ph. HE].
- [22] Sokolov, V.V. 1992, *Astrophysics and Space Science*, 197, 179.
- [23] Sokolov, V.V., & Zharykov, S.V. 1993, *Astrophysics and Space Science*, 201, 303.
- [24] Witten, E. 1984, *Phys. Rev. D*30, 273.
- [25] Sokolov, V. V., & Zharykov, S. V. 1994, *Bulletin of the Special Astrophysical Observatory*, 37/3, 61.
- [26] Feynman, R. P., Morinigo, F. B., & Wagner, W. G. 1995, “Feynman Lectures on Gravitation”, Addison-Wesley: Caltech, Pasadena, California Sokolov, V.V. 1992, *Astrophysics and Space Science*, 198, 53.
- [27] Sokolov, V.V. 1992, *Astrophysics and Space Science*, 198, 53.
- [28] Weisberg, J. M., Nice, D. J., & Taylor, J. H. 2010, *ApJ*, 722, 1030.
- [29] Sokolov, V. V. 2013, in Proceedings of XXIXth International Workshop On High Energy Physics, “New results and actual problems in particle & astroparticle physics and cosmology” (IHEP, Protvino, Russia, June 23-28), eds R. Ryutin, V. Petrov, V. Kiselev, World Scientific: New Jersey, London, Singapore, Beijing, p. 201 (arXiv: 1310.7730 [astro-ph. HE], The gamma-ray bursts and core-collapse supernovae – global star forming rate peaks at large redshifts).
- [30] Müller, B., & Janka, H.-Th. 2014, preprint, arXiv: 1409.4783 [astro-ph. HE] (Non-Radial Instabilities and Progenitor Asphericities in Core-Collapse Supernovae).
- [31] Janka, H.-Th. 2012, *Annual Review of Nuclear and Particle Science*, 62, 407.
- [32] Burrows, A., 2012, in press (arXiv: 1210.4921 [astro-ph. HE], Perspectives on Core-Collapse Supernova Theory).
- [33] Frontera, F., Amati, L., Zand, J.J.M.in't, Lazzati, D., Konigl, A., Vietri, M., Costa, E., Feroci, M., Guidorzi, C., Montanari, E., Orlandini, M., Pian, E., Piro, L. 2004, *ApJ*, 616, 1078 (arXiv: astro-ph/0408436).
- [34] Imshennik V. S., & Nadëzhin, D. K. 1988, *Soviet Scientific Reviews, ser. E, Astrophysics and Space Physics*, vol.4, Harwood Academic Publishers, Switzerland (Original Russian text: *Uspekhi Fizicheskikh Nauk* 156, iss. 4).
- [35] Belczynski, K., Wiktorowicz, G., Fryer, C.L., Holz, D.E. & Kalogera, V. 2012, *ApJ*, 757, 91.
- [36] Sokolov, V. V., Bisnovatyi-Kogan, G. S., Kurt, V. G., Gnedin, Yu. N., Baryshev, Yu. V. 2006, *Astronomy Reports*, 50, No.8, 612 (arXiv: astro-ph/0607644).
- [37] Weber, F., Contrera, G.A., Orsaria, M. G., Spinella, W., Zubairi, O. 2014, preprint, arXiv: 1408.0079 [astro-ph. HE] (Properties of High-Density Matter in Neutron Stars).
- [38] Lattimer, J. M. 2012, *ARNPS*, 62, 485.

- [39] Mao, J., Wang, J. 2013, ApJ, in press (arXiv: 1309.5257 [astro-ph. HE], Application of Jitter Radiation: Gamma-ray Burst Prompt Polarization).
- [40] Clausen, D., Piro, L. A., & Ott, C. D. 2014, ApJ, in press (arXiv: 1406.4869 [astro-ph. HE], The Black Hole Formation Probability).
- [41] Psaltis, D. 2008, review article for Living Reviews in Relativity (arXiv: 0806.1531 [astro-ph], Probes and Tests of Strong-Field Gravity with Observations in the Electromagnetic Spectrum).
- [42] Maselli, A., Leonardo L., Pani, P., Stella, L., Ferrari, V. 2014, preprint, arXiv: 1412.3473 [astro-ph. HE] (Testing Gravity with Quasi Periodic Oscillations from accreting Black Holes).
- [43] Landau, L.D., and Lifshitz, E.M. 1973, *Theory of Fields*, Nauka, Moscow, p. 504.
- [44] Wilson, J.R., 1985, in Numerical Astrophysics, ed. J. M. Centrella, J. M. Leblanc, & R. L. Bowers, p. 422.
- [45] Royzen Ilya I., arXiv:1201.4028 [astro-ph.HE] (QCD against Black Holes of Stellar Mass).
- [46] Vladimir V. Sokolov, International Journal of Astronomy, Astrophysics and Space Science, 2015; 2(6), 51–58 (On the observed mass distribution of compact stellar remnants in close binary systems and localizability of gravitational energy)

High-Energy Neutrino Astronomy: Where do we stand, where do we go?

Christian Spiering

DESY, Zeuthen, Germany; christian.spiering@desy.de

Abstract First ideas for doing neutrino astronomy with deep-underwater detectors date back to 1960, first attempts to build such a neutrino telescope to the year 1973. It took, however, further 40 years before extraterrestrial neutrinos could be identified with the IceCube neutrino telescope in the deep Antarctic glacier. This is a real breakthrough – the opening of a new window to the Universe. The present article sketches the long path towards that discovery and summarizes the present experimental results and our present understanding of them. Much is still to be done before we can say that we have “charted the landscape of high-energy neutrinos”, and I will discuss the roadmap towards that goal.

Keywords: neutrino astronomy, cosmic rays, extraterrestrial neutrinos, multi-messenger astronomy

1. History

The march towards underwater neutrino telescopes started forty years ago at the 1973 International Cosmic Ray Conference. There, a few physicists from the USA, Japan and Russia discussed for the first time building such a device: the Deep Underwater Muon and Neutrino Detector (DUMAND). Actually, the idea for detecting the Cherenkov light of charged particles deep underwater had already been raised 13 years earlier by Moisej Markov [1]. The original DUMAND design from 1978 envisaged an array of about 20,000 photomultipliers (PMs) spread over a 1.26 cubic kilometer volume. Due to technical and financial reasons the project was terminated in 1995 [2].

Starting in 1981, Russian physicists explored Lake Baikal as the site for a “Russian DUMAND”. In 1995 the first two (atmospheric) neutrino candidates were separated from the 1994 data, taken with the 3 strings deployed at that time. NT200, with 8 strings and 196 PMs was completed in April 1998 and has been taking data since then.

In 1988, F. Halzen and J. Learned proposed to deploy a neutrino telescope in deep Polar ice. This marked the starting point for AMANDA (Antarctic Muon And Neutrino Detection Array). The array was completed in January 2000 and eventually comprised 19 strings with a total of 677 PMs, directly at the geographical South Pole. AMANDA has been switched off in April 2009, after 9 years of data taking in its full configuration. It provided 6595 atmospheric neutrinos, several important upper limits, but no clear indication of any extraterrestrial neutrino signal.

Several projects have been pursued in the Mediterranean Sea, but only one made it to a working neutrino telescope: the ANTARES neutrino telescope, consisting of 12 strings, each carrying 25 PM-triplets. With a geometrical volume of 0.01 km³ it has almost the same size as AMANDA had. ANTARES was constructed in 2002-2008. It has convincingly demonstrated that a detector with precise angular resolution can be reliably operated in the deep sea.

The breakthrough, however, came only with IceCube. This detector consists of 5160 digital optical modules (DOMs) installed on 86 strings at depths of 1450 to 2450 m. A string carries 60 DOMs. The decommissioned AMANDA was replaced by DeepCore, a high-density sub-array of eight strings at the center of IceCube. DeepCore has smaller spacing and more sensitive PMs than IceCube and sits in the clearest ice layers. This results in a threshold of about 10 GeV and opened a new venue for oscillation

physics. The first IceCube string was deployed in January 2005, the last at Dec. 18, 2010: finally, the idea of a cubic-kilometer detector became reality!

2. Detection Principles

Neutrino telescopes are large-volume arrays of “optical modules” (OMs) installed in open transparent media like water or ice, at depths that completely block the daylight. The OMs record the Cherenkov light induced by charged secondary particles produced in reactions of high-energy neutrinos in or around the instrumented volume. The neutrino energy and direction can be reconstructed from the hit pattern recorded

In detecting cosmic neutrinos, three sources of backgrounds have to be considered: (i) *atmospheric neutrinos* from cosmic-ray interactions in the atmosphere, which can be separated from cosmic neutrinos only on a statistical basis; (ii) down-going punch-through *atmospheric muons* from cosmic-ray interactions, which are suppressed by several orders of magnitude with respect to the ground level due to the large detector depths. They can be further reduced by selecting upward-going or high-energy muons or by self-veto methods sensitive to the muon entering the detector; (iii) *random backgrounds* due to photomultiplier (PMT) dark counts, ^{40}K decays (mainly in sea water) or bioluminescence (only water), which impact adversely on event recognition and reconstruction [3].

Typical event topologies in underwater/ice neutrino telescopes include *a*) tracks of muons, either generated in neutrino interactions or in air showers above the detector and *b*) contained particle cascades induced by charged or neutral current interactions of neutrinos in the geometrical volume [3]. Extraterrestrial neutrinos can be distinguished from atmospheric neutrinos by *1*) their harder spectrum (i.e. an excess at higher energies), by *2*) showing a local excess at the sky map or by *3*) coinciding locally and timely with a transient event (flare, burst) observed in electromagnetic radiation (in future also gravitational radiation!).

3. Where do we stand?

In this section, I will summarize the most important findings from searches for diffuse fluxes (*1*), for point source searches (*2*) and for transient sources (*3*).

3.1. Diffuse extraterrestrial fluxes

Atmospheric neutrino fluxes have been precisely measured with AMANDA, ANTARES and IceCube. The results are in agreement with predicted spectra – with the exception of IceCube data, which extend to energies where extraterrestrial neutrinos start dominating over atmospheric neutrinos.

The discovery of extraterrestrial neutrinos in IceCube was heralded by two cascade-like events each with about 1PeV energy, dubbed *Ernie* and *Bert* [4]. They were found in data taken in 2010 and 2011. The two events represented a – still moderate – 2.8σ excess over the expectation for atmospheric neutrinos. The sheer energy, however, made them more promising candidates for cosmic neutrinos than anything found earlier. Figure 1 shows the two events.

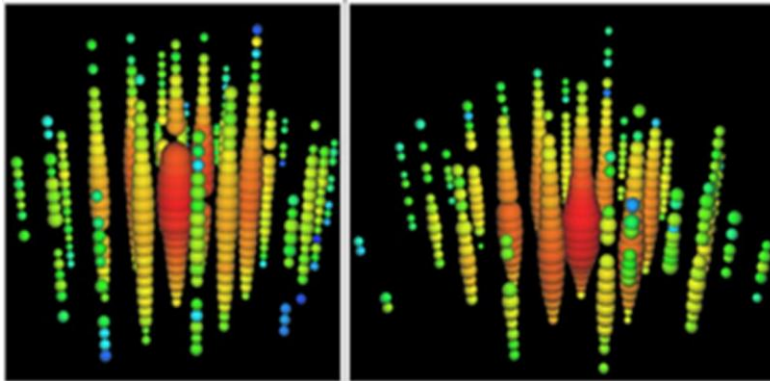


Fig1. The first two PeV events detected in IceCube. Left “Bert” (1.04 PeV), right “Ernie” (1.14 PeV). The colored spheres mark hit optical modules. Their size is proportional to the logarithm of the amount of detected light, the color indicates the time (red: early, blue: late). The diameter of the light field is more than half a kilometer, while the particle cascade itself has a cigar form with ~ 20 m length and ~ 30 cm diameter.

Motivated by this result, an alternative analysis of the same data was performed. It constrained the event to start in the inner volume of IceCube (using the outer part as veto layer), and at the same time considerably lowered the threshold compared to the first analysis, from 0.5 PeV down to 30 TeV (HESE analysis, for High Energy Starting Event). It provided 28 events, with the energies deposited in the detector ranging from ~ 30 TeV to 1.14 PeV and a significance of 4.1σ [5]. Meanwhile four years of data have been fully analyzed, resulting in 54 events, one of them a cascade event with ~ 2 PeV. A purely atmospheric origin of these events is excluded with a significance of 6.5σ . Figure 2 shows the distribution of the deposited energy, including the background and the fitted astrophysical component.

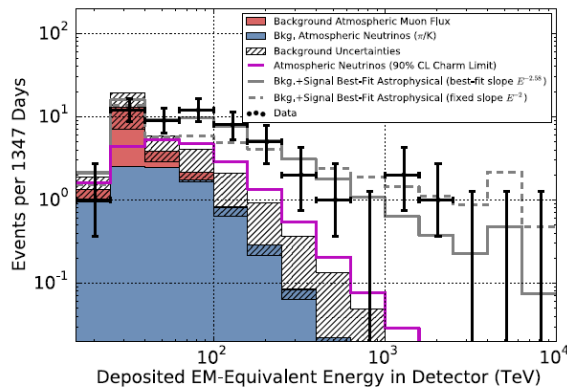


Fig2. The distribution of the energy deposited in IceCube, for the 54 HESE events (see text). The astrophysical component is best fitted with an $E^{-2.58}$ shape (solid line) while the dashed line shows the results for the canonical E^{-2} shape. About 21 events can be statistically assigned to atmospheric backgrounds (filled histograms). The dashed areas reflect the uncertainties for the flux of atmospheric neutrinos [7].

The sky-map of the 54 events shows a slight clustering about 10 degrees off the Galactic center (for IceCube: slightly above the horizon). That these events cannot be due to a quasi-point source with less than 1° extension has been demonstrated by ANTARES [6]. If the spectrum would be E^{-2} or steeper, ANTARES would have identified the source at lower energies, looking to upward moving muons (for

ANTARES the Galactic center is below the horizon).

Other searches for diffuse neutrino fluxes studied up-going muon tracks produced in neutrino interactions outside the detector and yielding up-going muons passing the detector. The most advanced of these analyses is based on two years of data and provided a 3.7σ evidence for astrophysical neutrinos. The spectral indices and the flux normalization obtained for the extraterrestrial component still differ from analysis to analysis, as shown in Fig.3 left.

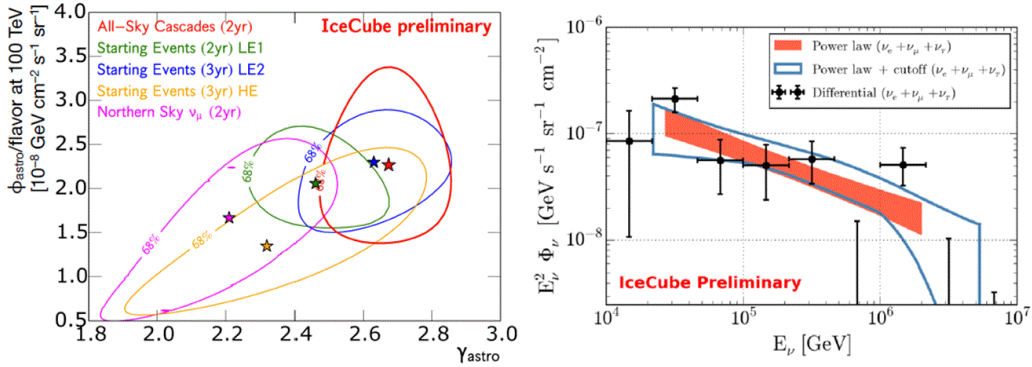


Fig.3. Left: flux normalization versus spectral index from various analyses. Right: Differential flux from various analyses, the red band with fitting a single slope, the blue contour allowing for a cut-off [8].

Figure 3 (right) shows the differential flux from different analyses, with a spectrum apparently steeper than E^{-2} . It is fitted with a single-slope unbroken spectrum and with a cut-off. More statistics and tests are needed to understand the reasons for the differences.

Definitely, a detector with different systematics would help, like KM3NeT in the Mediterranean Sea or GVD in Lake Baikal. The extraterrestrial contribution as such can be considered firm by now, but the details on spectrum and flavor composition will need to be scrutinized by independent measurements.

3.2. Search for steady point sources

Traditionally point-source searches are performed with the help of long tracks from upward-going muons which provide sufficiently good angular resolution (0.3° – 0.5° for IceCube and 0.1° – 0.2° for KM3NeT). No point sources have been found, neither by ANTARES nor by IceCube (the statistics of Baikal NT200 was much too small to compete with ANTARES). Figure 4 shows the upper limits to the flux obtained by ANTARES and IceCube as a function of the declination. The extension of IceCube's sensitivity to the Southern hemisphere is due to the fact that at very high energies the background from down-going muons can be kept sufficiently small, so that IceCube can look southwards. This possibility is mostly lost for fluxes with a high-energy cut-off (see the dashed curve). ANTARES, on the contrary, covers part of the Northern hemisphere since it is not located at the North Pole.

The somewhat disappointing picture of only upper limits might be mitigated by the fact that the remaining step to identify the predicted fluxes from some sources like the Crab nebula or sources in the Cygnus region is only a factor 2-5; therefore a detection in the next 3-5 years seems a reasonable expectation, either with IceCube itself or with KM3NeT and its superior angular resolution.

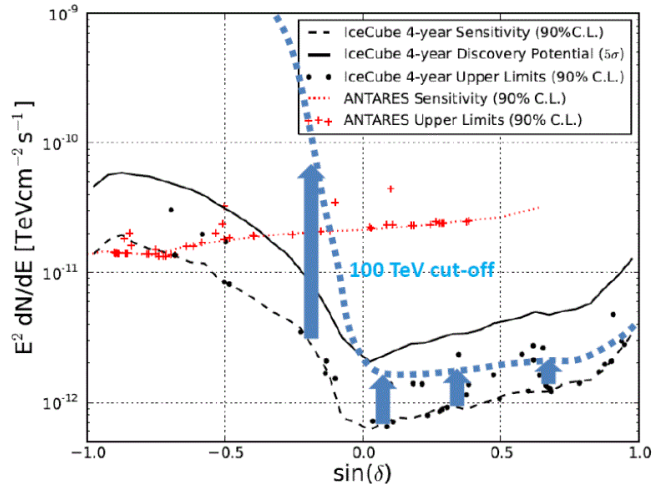


Fig4. Upper limits/sensitivities to the flux from point sources obtained with ANTARES and with IceCube (modified Figure from [9]).

3.3. Search for transient sources

Many searches for time-dependent emissions of extraterrestrial neutrinos have been performed by all four detectors, Baikal-NT200, AMANDA, ANTARES and IceCube, notably the recent target-of-opportunity programs of ANTARES and IceCube. Strong constraints on models could be set for prompt neutrino emission from Gamma-Ray Bursts using 4 years of data. For GRB searches the small spatial and temporal windows (a very few degrees and some seconds, respectively) dramatically reduce the background from atmospheric neutrinos and would make a doublet of events in coincidence with a GRB already highly significant. Figure 6 shows the constraints on a doubly broken power-law spectrum versus the first break energy ε_b and the normalization Φ_0 of the GRB flux, derived from 506 GRB and only one coincidence of a low-energy neutrino with a GRB, consistent with an atmospheric neutrino. The model of Ahlers et al. assumes that only neutrons escape from the fireball and contribute to ultra-high energy cosmic rays, the model of Waxman and Bahcall allows even all protons to escape.

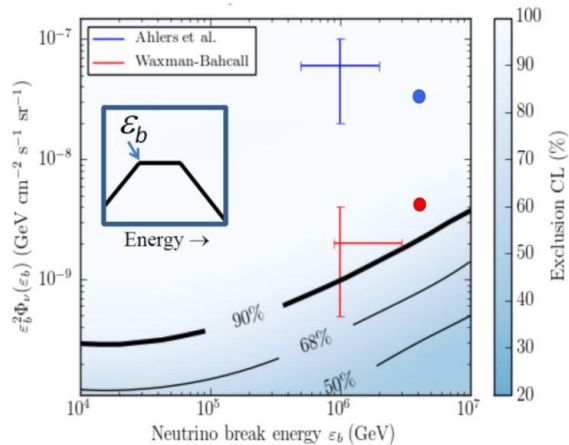


Fig5. Constraints on flux normalization and break energy of two fireball models (modified Fig. from [10]).

Follow-up programs start from alerts issued by ANTARES or IceCube [11],[12]. These alerts are distributed in real-time to Imaging Cherenkov Telescopes (Gamma Ray Follow-up), satellites (X-ray follow-up) or robotic optical telescope (Optical Follow-Up, OFU). Alerts are due to neutrino multiplets or single neutrino events of extremely high energy. This approach boosts the discovery potential for astrophysical sources and can be used to constrain models of their high-energy neutrino and gamma-ray emission. I will report here one intriguing observation made with the OFU of IceCube [13].

An alert was sent on March 20th, 2012 to satellites and optical telescopes. This alert was based on a neutrino doublet with the two events roughly one degree from each other and arriving within 1.7 seconds. In the follow-up observation performed by the Palomar Transient Factory (PTF) ten days later, a previously unknown supernova was found, only 0.14 degrees from the mean neutrino direction. Figure 6 shows the location of the two events and the supernova. However, the age of the supernova at the time when the neutrino vents arrived was already 169 days at least. Therefore the detection was classified as a coincidence and assumed that the neutrinos have no relation to the supernova. On the other hand, as I learned at this meeting, there are models able to explain such a delay between a beamed neutrino signal and the optical bursts [14].

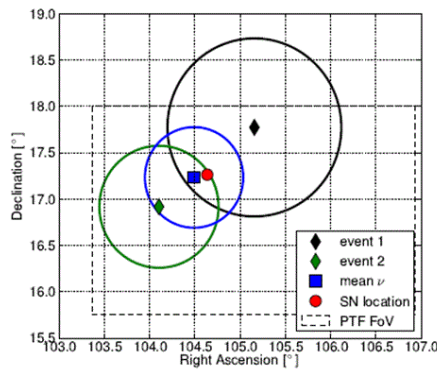


Fig6. Location of the 2 neutrinos that triggered the follow-up observation with PTF and the SN location [13].

3.4. Where do we stand and what is needed

The discovery of cosmic high-energy neutrinos with IceCube is a landmark event and a real breakthrough. Apart from this discovery, models on a number of steady and transient sources have been severely constrained or falsified – which is also an advance of knowledge. But still, not a single point source (neither steady nor transient) has been detected. Moreover, the knowledge of spectrum and flavor composition is still fuzzy. Astronomy, however, means just this: identification of individual sources, measurement of their spectrum, measurement of possible time variations; in addition coverage of the full sky.

More statistics and an incrementally improved understanding of the detector may help IceCube improving the understanding of spectrum and flavor composition, and possible even detect a first individual source. But the big leap will come only with a next generation of telescopes: KM3NeT and GVD at the Northern hemisphere and IceCube-Gen2 at the South Pole. When finished, these detector will cover 5-10 cubic kilometers of water (North) or ice (South) and will improve the sensitivity of IceCube by a factor 5-20, depending on the event signature. Moreover they will allow a full-sky observation, with a better view to the center of the Galaxy from the North. The next chapter gives a short description of the three projects.

3. Where do we go?

3.1. KM3NeT

KM3NeT comprises two deep-sea installations, the one located off-shore Toulon (France), the other at Capo Passero (Sicily), with a potential third site in Greece [15]. KM3NeT will consist of blocks with 115 strings each and 18 optical modules (OM) per string. Each OM houses 31 small photomultipliers. The diameter of the high-energy blocks (“ARCA”) is about 1 km (see Fig.7), that of the single low-energy block in France (“ORCA”) is 100 m. ARCA will address the highest energies, in the footsteps of IceCube. ORCA, with its small string spacing an efficient light collection, will have an energy threshold in the few-GeV range and will be sensitive to effects of the neutrino mass hierarchy by measuring atmospheric neutrinos having crossed the Earth.

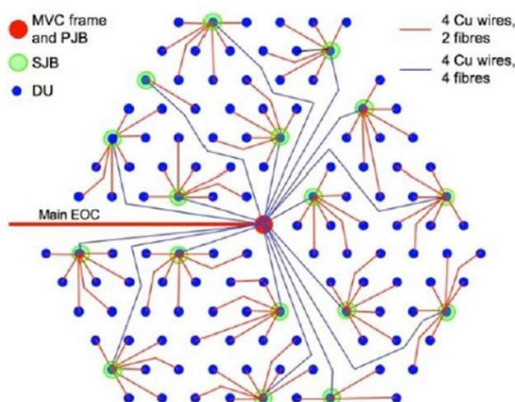


Fig7. Top view of an ARCA block, covering an area of about 1 km². DU (blue dots) stands for “Detection Unit” (i.e. a string), JB stands for “Junction Boxes” of different hierarchy levels. The main electro-optical cable (EOC) links the detector to the shore station, which is 70 km away for the Italian site.

A 24-string prototype of ARCA and a 7-string prototype of ORCA are just under construction (KM3NeT Phase-1). A second phase of KM3NeT will consist of full ORCA at the Toulon site and two ARCA blocks in Italy. ARCA Phase-2 will scrutinize the diffuse IceCube signal but also has a good chance to detect first galactic point sources. Eventually, ARCA will consist of 5 blocks, either all at the Italian site or shared between Italy and Greece.

3.2. GVD

The Baikal *Gigaton Volume Detector* (GVD) will have a modular structure with functionally independent sub-arrays. Each of these “clusters” consists of 8 strings each carrying 36 optical modules [16]. The OMs are equipped with 10-inch photomultipliers. For the first phase of GVD, 10-12 clusters are envisaged, covering ~0.4 km³ of deep water. This phase is planned to be concluded in 2020/21. In the second phase, the detector will be expanded to 27 clusters covering ~1.5 km³ of water. Figure 8 gives a top view of the 27-string phase. The distance to shore is about 3.5 km. The small box shows location and cabling of a single cluster.

After a 5-year prototyping phase, a first cluster of GVD has been completed in April 2015 and takes data since then. With 0.4 km³ volume, also GVD Phase-1 will be able to scrutinize the diffuse IceCube signal.

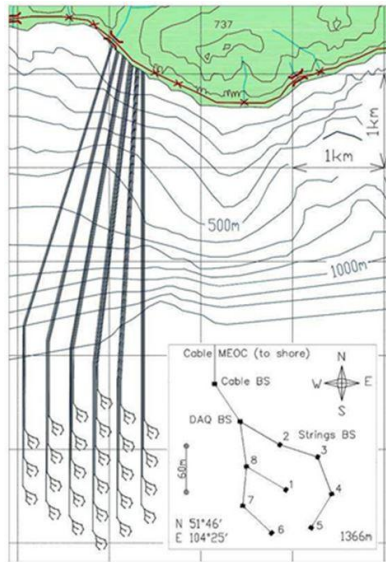


Fig8. Top view of the Baikal Gigaton Volume Detector GVD with 27 clusters. The small box sketches a single cluster.

3.3. IceCube-Gen2

IceCube is planned to be expanded w.r.t. to high-energies by an expansion of the deep-ice detector and by a huge surface detector. Oscillation physics and dark matter detection will be addressed by a high-density array, much denser than the present DeepCore array in the center of IceCube. This detector was christened PINGU. Its main goal is determining the neutrino mass hierarchy with the help of atmospheric neutrinos, similar to ORCA (see Section 3.1).

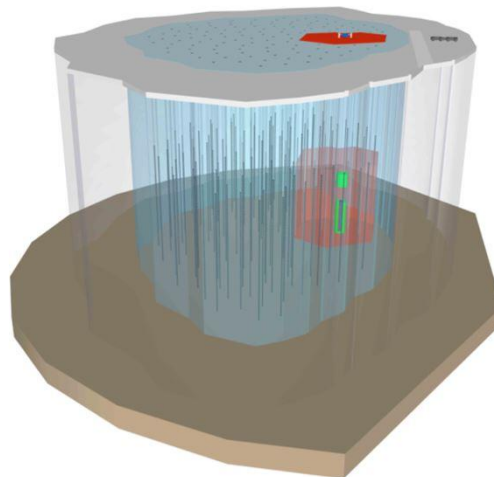


Fig9. Artists view of IceCube-Gen2. The red array is the present IceCube, including the high-density part DeepCore (the two green inner cylinders). The big blue blob is IceCube-Gen2 with its 100-140 widely spaced strings. The surface array shown in this figure has the same footprint like the deep detector (about 10 km^2). It might, however, be expanded by another order of magnitude in area, thereby increasing the acceptance of the veto against particles related to an air shower. Not shown in the figure is the extremely dense PINGU part within DeepCore.

The high-energy expansion is named IceCube-Gen2 [17]. The deep-ice detector would be enlarged to 7–10 km³, naturally with a larger spacing and consequently a much higher threshold than IceCube. The surface detector would cover an area of up to 100 km². It would allow separating muons produced by neutrinos in the ice layer between the surface and the deep detector from punch-through muons from the surface, since the latter are accompanied by an air shower detected in the surface array. This could enlarge the statistics for high-energy neutrinos from the Southern hemisphere by a factor 2–4.

Figure 9 shows an artist’s view of IceCube-Gen2. Start of construction and final configuration depend on several factors, including the outcome of the first phases of KM3NeT and GVD. A present (optimistic) plan assumes start of deployment in 2021/22.

3.4. The global view

In 2013, representatives of the collaborations ANTARES, Baikal-GVD, KM3NeT and IceCube have signed a Memorandum of Understanding for cooperation within a Global Neutrino Network (GNN). GNN aims for extended inter-collaboration exchanges, a coherent strategy planning and exploitation of the resulting synergistic effects.

The next logical step on the road towards high-energy neutrino astronomy is clear: construction of the two Northern detectors (0.4 km² in Lake Baikal and 1.0–1.5 km³ in the Mediterranean Sea), with completed detectors in 2020–22. At this point, GNN would include a total volume of 1.5–2 km³ in the North and 1 km³ in the South, the latter with a cumulated statistics of more than 10 years. 5–8 years later, one would have 4–6 km³ in the North and 7–10 km³ in the South. My personal guess is that we are already close to observing point sources and we will detect them not later than in midst of the 2020s. The case for the detectors at the end of the 2020s is even more compelling: measuring spectrum and variability of individual sources and making neutrinos a real key for understanding the non-thermal Universe!

References

- [1] Markov, M., “On high energy neutrino physics”, Proc. 10th ICHEP, Rochester (1960), 578.
- [2] Spiering, C., “Towards High-Energy Neutrino Astronomy: A Historical Review”, Eur.Phys. J. H37, 515 (2012) and arXiv:1207.4952.
- [3] Katz, u. and Spiering, C., in Review of Particle Data Group, Chin. Phys. C38 (2014) 090001.
- [4] Aartsen, M., et al. (IceCube Coll.), Phys.Rev.Lett. 111, 021103 (2013) and arXiv:1304.5356.
- [5] Aartsen, M., et al. (IceCube Coll.), Science 342, 1242856 (2013).
- [6] Adrian-Martinez, S., et al. (ANTARES Coll.), Astrophys. Journ.786, L5 (2014), arXiv:1402.6181.
- [7] Aartsen, M., et al. (IceCube Coll.), Phys. Rev. Lett. 113, 101101 (2014).
- [8] Aartsen, M., et al. (IceCube Coll.), Astrophys. Journ. 809, 98 (2015) and arXiv:1505.03991.
- [9] Aartsen, M., et al. (IceCube Coll.), Astrophys. Journ. 796,109 (2012) and arXiv:1406.6757.
- [10] Aarsten, M., et al. (IceCube Coll.) Astrophys. Journ. 805, L5 (2015) and arXiv:1412.6510.
- [11] Adrian-Martinez, S., et al. (ANTARES Coll.), arXiv:1508.01150.
- [12] Aartsen, M., et al. (IceCube Coll.) Contribution to ICRC 2015, arXiv:1510.05222, articles on 1052 and 1069 on pages 21-28 and 45-50.
- [13] Aartsen, M., et al. (IceCube Coll.) Astrophys. Journ. 811, 52 (2015) and arXiv:1506.03115.
- [14] Drago, A., private communication at this conference.
- [15] www.km3net.org
- [16] Avronin, A., et al. (Baikal Coll.), Phys. Part. Nucl. 46, 211 (2015).
- [17] Aartsen, M., et al. (IceCube-Gen2 Coll.), “IceCube-Gen2: A vision for the Future of Neutrino Astronomy in Antarctica”, arXiv:1412.5106.

Correlation between sphere distributions of gamma-ray bursts and CMB fluctuations

O. V. Verkhodanov^{1,*}, V. V. Sokolov¹, M. L. Khabibullina¹

¹*Special Astrophysical observatory, Nizhnij Arkhyz, Russia; * vo@sao.ru*

Abstract Distribution of gamma-ray bursts (GRBs) from catalogs of the BATSE and BeppoSAX space observatories relative to the cosmic microwave background (CMB) data by Planck space mission is studied. Three methods were applied for data analysis: (1) a histogram of CMB signal values in GRB directions, (2) mosaic correlation maps calculated for GRB locations and CMB distribution, (3) calculation of an average response in the area of “average GRB population” on the CMB map. A correlation between GRB locations and CMB fluctuations was detected which can be interpreted as systematic effects in the process of observations. Besides, in the averaged areas of CMB maps, a difference between the distributions of average fluctuations for short and long GRBs was detected which can be caused by different natures of these events.

Keywords: cosmic background radiation, gamma-ray bursts, statistics, data analysis

1. Introduction

The quality of sky surveys carried out in the recent decade in different wavelength ranges allows us to study matter distribution in the observable part of the Universe based on many observational effects. Apart from direct measurement of the parameters of galaxy distribution and reconstruction of the large scale structure, as was done in the SDSS survey [1], there are many effects enabling the restoration of matter distribution. Among them there are effects of the secondary CMB anisotropy: the integrated Sachs–Wolfe effect [2] caused by changes in the CMB photon frequency in the variable gravitational potential of forming galaxy clusters and prevailing on the scales greater than 10° , the Sunyaev–Zel’dovich effect [3] on the scales of less than 10° , arising in interactions between the hot electrons in galaxy clusters with the CMB photons (the inverse Compton effect), the effects of scattering during the reionization epoch, and simply obstructive factors in the form of microwave emission of radio sources and galaxy clusters. Gamma-ray bursts are also an independent sign of the Large Scale Structure (LSS) allowing us to trace matter distribution at cosmological distances. The observable uniform distribution of gamma-ray bursts projected on the celestial sphere as well as the distribution of the bulk of radio sources (except for the faintest ones related to the nearest galaxies) demonstrate the cosmological principle requiring the Universe to be uniform and isotropic irrespective of the observer’s location [4]. The observations show that the size of the largest structures is of order of 400 Mpc [5]. On lower scales, especially at low redshifts ($z < 0.1$), the matter is distributed anisotropically and inhomogeneously. However, the search for large structures continues at $z < 1$ too (see, e.g., [6, 7]). Note that integral and statistical characteristics of the CMB distribution determined from the correlation maps with the SDSS galaxy locations show the presence of certain isolated scales of $2\text{--}3^\circ$ within the redshift range $z = 0.8\text{--}2$ which corresponds to the linear scale of 60 Mpc and can be interpreted as the maximum size of a heterogeneity cell [8 – 12]. This agrees with the model of radio source activity in the range of $z \sim 1\text{--}2$ [13, 14], where the gravitational potential variations in forming clusters are expected. In this respect the comparative distribution of the CMB map extrema and GRBs on the celestial sphere is interesting as a new indicator of the LSS signature on the CMB maps at different redshifts. The uniform observable distribution of GRBs also allows us to test the cosmological principle. Besides, it is assumed

that they can be used as standard candles for the estimation of distance to objects under consideration [15, 16]. The available rather large catalogs – namely, BeppoSAX1 (Satellite per Astronomia X, “Beppo” in honor of Guiseppe Occhialini) [17] and BATSE2 (Burst and Transient Source Experiment) [18], comprising such objects – allow us studying the spatial distribution of these objects.

In recent years many authors investigated the gamma-ray distribution using various methods [19 – 26]. Among this research, paper [23] can be marked, where authors studied GRBs of short ($t < 2$ s), medium ($2 < t < 10$ s), and long ($t > 10$ s) duration from the BATSE catalog by different methods (by means of the Voronoi tessellations, minimum spanning tree, and multifractal spectrum). For the first two groups they discovered deviations from homogeneity as compared with model data. On this basis they discuss the satisfiability of the cosmological principle. In paper [26], the locations of the supernova explosions with $z < 1.4$ and gamma-ray bursts were used as the probing objects. For the supernova data a deviation from the uniform distribution on the diagram “CMB temperature in a source direction – z ” was discovered in contrast to the similar diagram for gamma-ray bursts. The authors explain this difference by the contribution of the integral Sachs–Wolfe effect.

Earlier [24, 25], we studied the statistical correlation properties of sky distribution of GRBs relative to CMB by the mosaic correlation mapping method [27, 28]. The study involved the WMAP3 (Wilkinson Microwave Anisotropy Probe) data [29], the data from the Italian-Dutch BeppoSAX satellite (the energy range 0.1–200 keV, 781 sources) and results of the BATSE experiment (20 keV – 2 MeV, 2037 sources). Each catalog was divided into two subsamples containing short (lasting $t < 2$ s) and long ($t > 2$ s) events. If we assume that GRBs are related to massive spiral (for long GRBs) or elliptic (for short bursts) galaxies and, respectively, their location is related to the large-scale structure, then one can study the statistics of CMB inhomogeneities arising due to effects of the secondary anisotropy. Thus, the GRB locations can be related to the distribution of CMB fluctuations (e.g., revealing themselves by deviations from the statistical anisotropy) in those celestial sphere regions where the GRBs were registered. Since in most cases the main problem when studying GRBs is a large size of error boxes determining the source coordinates (of about $1^\circ \times 1^\circ$), we worked with maps smoothed to 1° . Our previous work with the WMAP data resulted in the discovery of a correlation between the CMB peaks and GRB locations which, in particular, can be caused by the systematic effects. The discovered correlation between the GRB locations and the CMB distribution is sensitive to the equatorial coordinate system and can be caused, for example, by the fact that the microwave radiation of the Earth gets to far side lobes of the power beam pattern.

Here, we applied and developed our approach for data of the Planck space mission [30], specifically, for the SMICA map [31]. Below we apply several statistical approaches to study the distribution of gamma-ray bursts on the sphere (see also details in [25]). Section 2 deals with the CMB signal statistics in the region of GRBs. Section 3 investigates the mosaic correlations of CMB maps (Planck SMICA) and GRB locations. Further (Section 4) we use the averaging procedure (stacking) of CMB map fields in the direction of a gamma-ray burst to estimate the average “population” microwave signal. The obtained results are discussed in Section 5.

2. Statistics of CMB Signal in Gamma–Ray Burst Regions

The SMICA CMB map [31] of the Planck experiment was restored from the multifrequency observations obtained with the High Frequency Instrument (HFI) at the 100, 143, 217, 353, 545, 857 GHz bands and with the Low Frequency Instrument (LFI) at 30, 44, 70 GHz. Resolution of the CMB map was about 5. In spite of the fact that the Planck mission is secondary with respect to another NASA space mission – WMAP (Wilkinson Microwave Anisotropy Probe), its observational characteristics are better. Among them one can mark out a higher resolution (by 3 times), which gave an opportunity to measure the angular power spectrum to higher harmonics (i.e., to higher values of l), a higher sensitivity

(by 10 times), and 9 frequency bands, improving the procedure of separation of the background components. These Planck parameters allowed us to obtain new, practically independent (of WMAP) observational data. In this paper we used the SMICA map smoothed to $l_{\max} = 150$, and in a number of cases we applied the Mask-Ruler Minimal_2048_R1 mask [30]. To analyze the statistics of pixel values, we used the *mapcut* procedure of the GLESP package⁵ [32]. Calculations were made for the maps smoothed to the resolution of 260 ($l_{\max} = 20$), 35 ($l_{\max} = 150$), 20 ($l_{\max} = 300$), and 10 ($l_{\max} = 600$). Figure 1 shows the locations of GRBs from the subsamples of BeppoSAX and BATSE catalogs on CMB maps with the resolution 260' ($l_{\max} = 20$). The map resolution was selected in accordance with the expected scale of the Sachs–Wolfe effect manifestations and possible appearance of some features on the SMICA map.

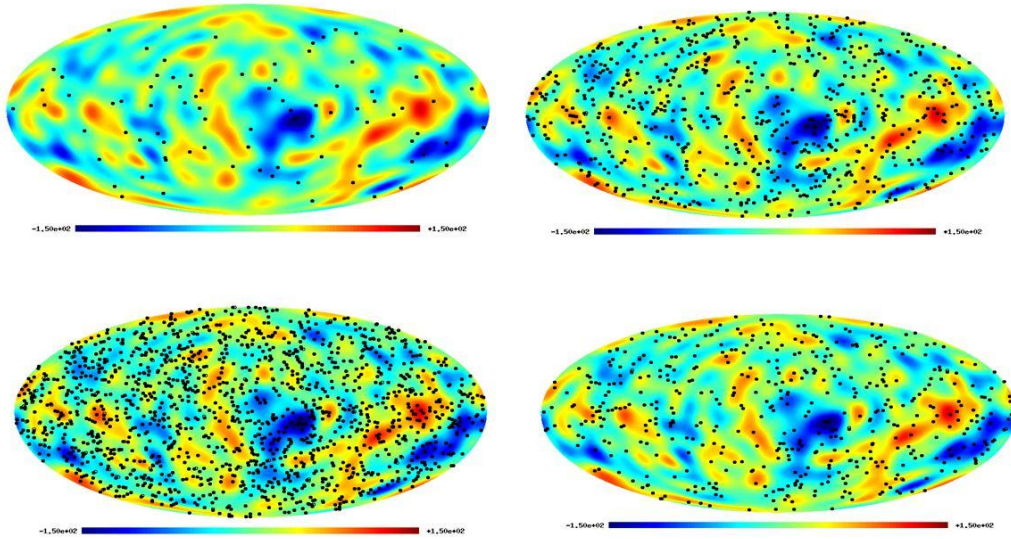


Fig1. The location of GRBs from different samples on CMB maps with the resolution $l_{\max} = 20$. The top left image shows the BeppoSAX data, $t < 2$ s. The top right image shows the BeppoSAX data, $t > 2$ s. The bottom left image presents the BATSE data, $t < 2$ s. The bottom right image is for the BATSE data, $t > 2$ s.

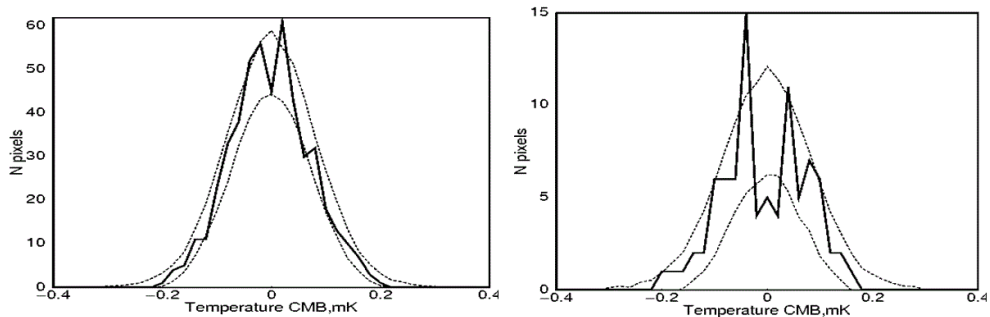


Fig2. Distribution of CMB fluctuations in the SMICA map pixels corresponding to short ($t < 2$ s) GRB locations with the map resolution $l_{\max} = 150$ for different GRB subsamples. The left diagrams show the distribution of short BATSE GRBs. The right picture gives the distribution of signals for short BeppoSAX GRBs. The dashed lines show the 1σ -dispersion of CMB values in the Λ CDM cosmological model calculated with 200 random gaussian realizations of the CMB signal.

To search for potential correlations, we counted how many GRBs get into CMB pixels with negative values of signal fluctuations, which can be due to the above mentioned effects, on CMB maps with different resolutions. We calculated the statistics of CMB pixel values in the GRB locations for subsamples of BATSE and BeppoSAX catalogs for short and long events.

Figure 2 presents diagrams of distribution of the CMB fluctuation values for four subsamples of the GRBs and the CMB maps with different resolutions. The dashed lines show the expected 1σ -dispersion of CMB values in the Λ CDM cosmological model. Earlier [24], we discovered a deviation from what was expected with the Gaussian random CMB signal in the distribution of fluctuation values with the resolution $l_{\max} = 150$ in regions of short BATSE GRBs. In the Planck data the deviations are also observed for short GRBs (see the left diagram in Fig. 2). Besides, there are small deviations from the models for long BATSE GRBs and short BeppoSAX GRBs at $l_{\max}=20$ [25], short BeppoSAX GRBs at $l_{\max} = 150$ (the right diagram in Fig. 2), long BATSE GRBs at $l_{\max} = 300$, and long BeppoSAX GRBs at $l_{\max} = 600$ [25]. To analyze the sphere distribution of those GRBs which are in the directions where the detected signal deviates from the expected one, we made pixelization with the *mappat* procedure from the GLESP software package [32]. The pixel size $700' \times 700'$ was chosen in such a way that the maximum pixel value (the number of events in a corresponding area) would not be less than 3 and a significant dynamic range for the harmonic analysis would be provided.

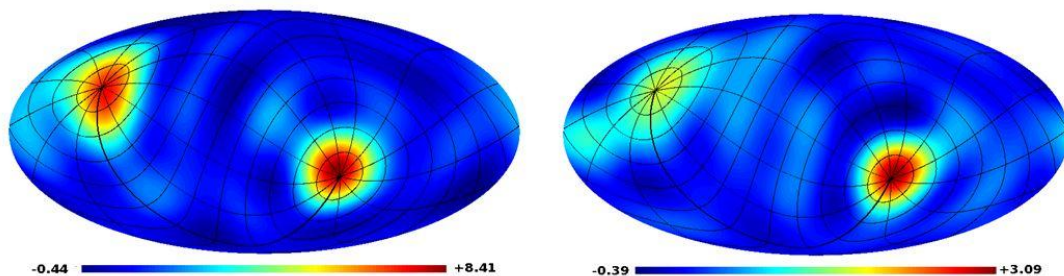


Fig3. Examples of the smoothed maps of the sky up to $l_{\max} = 7$ for different GRB subsamples. The maps were built from the CMB pixels corresponding to the direction to those GRBs which deflect the histograms from the expected ones. The equatorial coordinate system was plotted on all maps. The left image presents data for GRBs compared with CMB in the maps with resolution $l_{\max} = 20$ and long BATSE GRBs. The right plot demonstrates data of long BeppoSAX GRBs ($l_{\max} = 600$).

Fig. 3 shows examples of the GRB maps pixelized and smoothed this way. Their contribution into the histogram exceeds the expected 1σ -dispersion. The equatorial coordinate system is plotted on all maps. All images demonstrate a nonuniform sphere distribution of events, concentrated near the equatorial poles. In many cases, the hot spots are located directly on the equatorial poles. In maps with $l_{\max} = 20$ and $l_{\max} = 150$ with short BeppoSAX GRBs, we observe clusterization of hot spots in the Galaxy plane, which is more noticeable on the octupoles of these maps (see all figures in [25]). In some cases, the presence or absence of events in the pole regions markedly points to the pole regions of the equatorial coordinate system. Note that the peculiarities of CMB data of the Planck mission are identical to those of WMAP data as compared with GRB locations. Namely, the deviations in the pixel statistics are related with signal in the GRB direction oriented in the equatorial coordinate system. In [24], we estimated the probability of getting the quadrupole minima into the regions of the 5° radius around the equatorial poles. To do that, we generated 10 000 random realizations of the Gaussian signal to pixelize GLESP with 102 pixels in the equator. The probability of random hits to the pole zone is 0.0035. For a more detailed study of the correlation effects, the mosaic correlation method, presented in paper [27], was applied here.

3. Correlation maps of Distribution of Gamm-Ray Bursts and Planck SMICA Data

To study the properties of maps of the GRB locations and CMB fluctuations, we have performed the mosaic correlation of “BATSE–CMB” maps with pixels of different sizes: 500'x500', 600'x600', and 900'x900', covering the areas within which the correlation factor was calculated. To do that, first we pixelized the maps of GRB locations in all four subsamples. As in the previous stage, the pixel size 200'x200' was chosen in such a way that the maximum value (the number of events in a corresponding area) would not be less than 3. The correlation results are shown in Fig. 4. To analyze the obtained result, we calculated the angular power spectrum (2) of the map using the spherical harmonics (multipoles) expansion of the signal distributed on the sphere (1):

$$\Delta S(\theta, \phi) = \sum_{\ell=1}^{\infty} \sum_{m=-\ell}^{m=\ell} a_{\ell m} Y_{\ell m}(\theta, \phi), \quad (1)$$

$$C(\ell) = \frac{1}{2\ell + 1} \left[|a_{\ell 0}|^2 + 2 \sum_{m=1}^{\ell} |a_{\ell, m}|^2 \right] \quad (2)$$

The angular power spectrum allows us to select the harmonics contributing to the correlation map. Figure 5 shows some examples of the power spectra of the correlation factor maps, calculated by the mosaic correlation method for the BATSE and CMB data. As is shown in Figs. 4, application of the mask retains location of local maxima in the power spectra of mosaic maps. In a number of cases, the application of the mask even amplifies the amplitude of an isolated harmonic. Figure 6 demonstrates examples of such harmonics. The fourth multipole of the mosaic correlation map with the window 500'x500' calculated for the BATSE data ($t < 2s$) contains a feature – the coldest central spot in the galactic plane (Fig. 6, left top). The quadrupole of the correlation map for the BATSE data ($t > 2s$) with the window 900'x900' (Figure 6, left bottom) is sensitive to the equatorial coordinate system. Note that the

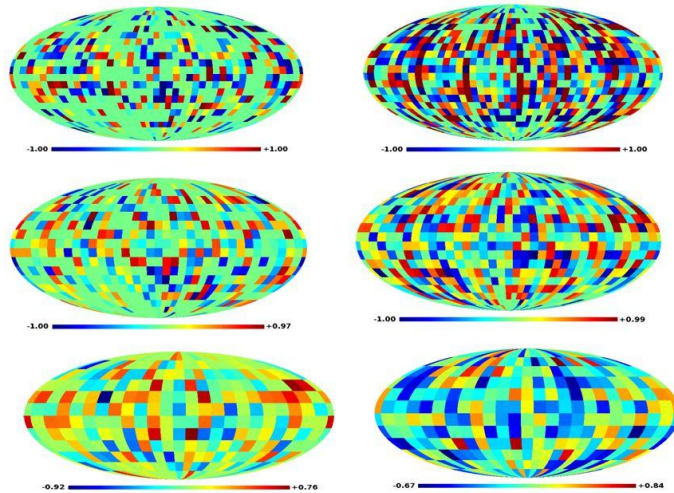


Fig4. Correlation maps of CMB and BATSE GRB locations in the galactic coordinate system. The left column presents results of the CMB and BATSE ($t < 2 s$) data correlations, and the right one is for CMB and BATSE ($t > 2 s$). The upper pair of images demonstrates maps of $l_{\max} = 26$ with the mosaic correlation pixel size $w=500'x500'$. The central pair shows the maps of $l_{\max} = 8$ with the correlation pixel size $w=600'x600'$. The lower pair is for $l_{\max} = 5$ and $w=900'x900'$.

variation of the correlation scale (namely, the size of the area in which the correlation factor is calculated and attributed to a pixel of a mosaic map) changes the power spectrum. Thus, e.g., at a transition from the pixel side size of 500 to that of 600, the harmonic $l = 4$ amplitude in the power spectrum passes from the position of a local maximum to a local minimum. This can be caused by the increase in the amount of GRB events in the area of the corresponding size.

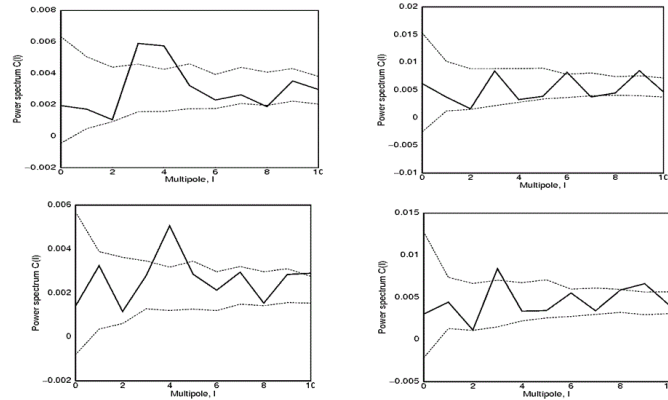


Fig5. Power spectra of the correlation factor maps (with $l_{max} = 26$) calculated for the maps of BATSE GRB locations and CMB distribution (the solid line). The correlation pixel size is $500' \times 500'$. The top left image shows the correlation spectrum of the BATSE data for $t < 2s$ and CMB not accounting for the mask. The top right image contains the correlation spectrum of the BATSE data with $t > 2s$ and CMB not accounting for the mask. The bottom left image demonstrates the correlation spectrum of the BATSE data for $t < 2s$ and CMB accounting for the mask. The bottom right image shows the correlation spectrum of the BATSE data with $t > 2s$ and CMB accounting for the mask. The images show the 1σ -dispersion obtained from results of analysis of 200 Gaussian random realizations of CMB.

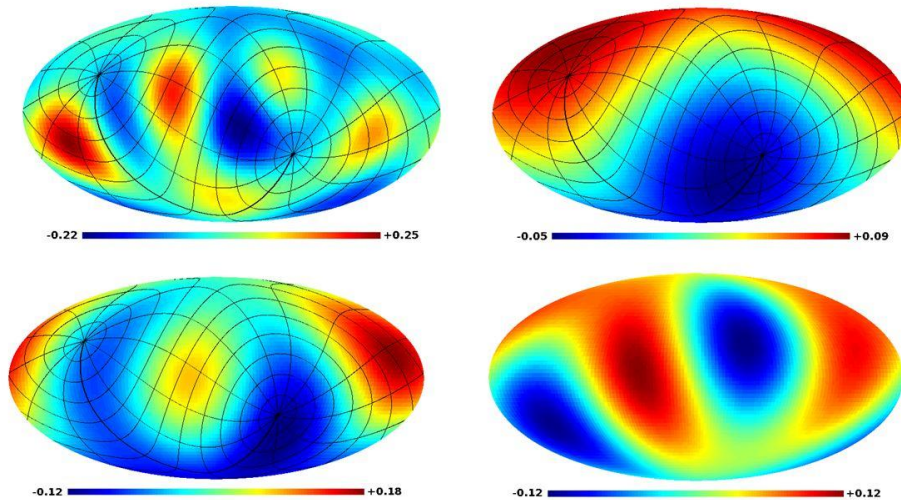


Fig6. Maps of isolated harmonics in the power spectra. The images show the multipoles of mosaic correlations of the CMB and GRB locations. Top left: the isolated harmonics $l=4$ for the correlation window $500' \times 500'$ for BATSE data ($t < 2s$); top right: the isolated harmonic $l=1$ for the correlation window 600×600 . Bottom left: the correlation map for BATSE GRBs ($t < 2s$) and CMB with the correlation window $900' \times 900'$ ($l = 2$). Bottom right: the correlation map for the BATSE GRBs ($t > 2s$) and CMB with the correlation window $900' \times 900'$ ($l = 2$). Three maps contain the overlaid equatorial coordinate grid.

4. Field Averaging

The Planck data allow us using the maps of a higher resolution than the WMAP archives. They can be used to estimate the potential signal from “an average population GRB” (the stacking procedure). To do that, areas of an identical linear or angular size around objects under investigation are selected in different directions on the celestial sphere. Then they are summed up to reveal an average signal. Because the redshift data are not available, we used the areas with identical angular sizes. To avoid the influence of a possible hard-to-consider signal of the Galaxy, we limited ourselves only to the regions around GRBs with galactic latitudes $|b| > 20^\circ$. Among BATSE and BeppoSAX samples, this range includes 338 short (68% of the initial short BATSE GRBs) and 990 (64%) long events of the BATSE catalog, and 51 short (59% of the BeppoSAX list) and 454 (65%) long sources of the BeppoSAX catalog. For every GRB from our subsample, we have chosen a field in the Planck SMICA map of size $2^\circ \times 2^\circ$ in the tangential projection (the pixel size in the area is about $80'' \times 80''$). The selected areas were averaged. Results are shown in Fig. 7. Note that the addition of data from the region $|b| < 20^\circ$ leads to the degradation (blurring) of images. The center of each averaged field in Fig. 7 gets into a local extremum region. Short BATSE and BeppoSAX GRBs are in the regions of background minima, and the long ones – in the regions of maxima. Ratios of the level of averaged fluctuation of the extremum into which a generalized GRB falls to the level of noise on the averaged maps are $dS/N = -1.65, 1.40, -1.43, 2.01$ for short and long BATSE GRBs and for short and long BeppoSAX GRBs respectively.

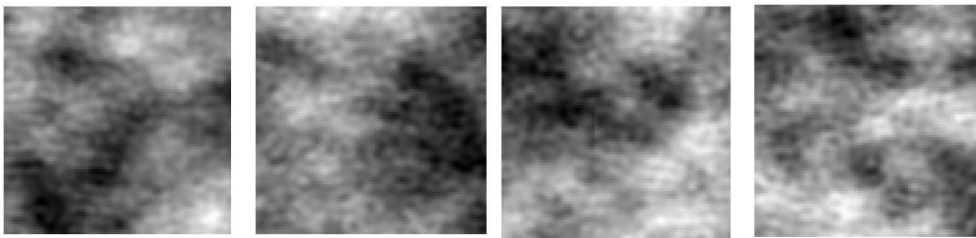


Fig.7. Results of the averaging of CMB fields, sized $2^\circ \times 2^\circ$, in GRB directions. From left to right: fields of short BATSE GRBs; long BATSE GRBs; short and long BeppoSAX GRBs.

5. Discussion

In this paper we investigated the CMB signal statistics in the direction of GRBs from the BATSE and BeppoSAX catalogs. The Planck SMICA map was used as the CMB map. We applied three approaches to study the properties of the GRB distribution on the sphere. They include: (1) the analysis of the Planck CMB signal value histogram in the direction to GRBs, (2) the study of mosaic maps built for GRB locations and CMB distribution, (3) the study of an average response on the CMB map in the region of the “average population GRB.”

The application of the first two methods demonstrates that the correlation between GRB and CMB is caused, at least partially, by a signal in the equatorial coordinate system. This agrees with the results of our work [24, 25]. This relation can be caused by the modulation of the CMB signal observed in the L2 point by the microwave radiation of the Earth through the far antenna beam lobes. Deviations in distribution of GRBs towards the equatorial system are caused by non-uniform sky sensitivity (the time of signal accumulation) of the receiving equipment of the gamma-ray satellite observatories rotating around the Earth and always directed at the opposite side from it. Then an isolated character of the equatorial coordinate system naturally appears. Note that indication to the presence of signs of the equatorial coordinate system (e.g., location of spots) in the CMB data both for WMAP and Planck maps was already discussed in a number of papers [24, 25, 33, 34]. Besides, the radiation of the Earth can be

not a single factor. Another discussed reason can be the modulation of the solar wind by the Earth magnetic field passing through the point L2. It should be added that such effects, which are not detectable by the standard analysis, could be a source of the secondary Gaussianity observed at low harmonics [35 – 39]. The third method we have applied has shown that there is an insignificant difference at the level $|S/N| > 1.4$ which can randomly occur in less than 20% cases for the Gaussian noises in the distribution of the average CMB signal in GRB directions. As this takes place, short ($t < 2s$) GRBs in an averaged field gets to a local background minimum, and long ($t > 2s$) GRBs – to a local maximum. If we assume that short GRBs occur in old elliptic galaxies formed from merging of less massive galaxies and located in the galaxy clusters, then a local minimum can be due to the Sunyaev–Zel’dovich effect [3]. The fact that long GRBs hit the local maximum in the CMB distribution could be caused by another effect. If long GRBs are related to supernova explosions, i.e., to star-forming galaxies, then even despite of location in a galaxy cluster, the proper microwave emission of a galaxy containing dust and gas would prevail over the effects of the surroundings and lead to appearance of a local maximum in the CMB maps. This effect could be tested by means of yet more sensitive data of the Planck experiment due to be published in the next release, expected in the second half of 2014.

Acknowledgements

The authors are grateful to EAS for the open access to the results of observations and processing of data in Planck Legacy Archive. For the analysis of extended emission on sphere we used the GLESP package [32, 40, 41]. M. L. Kh. and O. V. V. thank RFBR for a partial support of the project study by the RFBR grant No. 13-02-00027.

References

- [1] D. J. Eisenstein, D. H. Weinberg, E. Agol, et al., *Astron. J.* 142 , 72, 2011.
- [2] R. K. Sachs and A. M. Wolfe, *Astrophys. J.* 147, 73, 1967.
- [3] R. A. Sunyaev and Ya. B. Zel’dovich, *Astrophys. And Space Sci.* 7, 3, 1970.
- [4] P. J. E. Peebles, *Principles of Physical Cosmology* (Princeton Univ. Press, 1993).
- [5] J. A. Peacock, *Cosmological Physics* (Cambridge Univ. Press, 2000).
- [6] L. Rudnick, S. Brown, and L. R. Williams, *Astrophys. J.* 671, 40, 2007.
- [7] V. Springel, C. S. Frenk, and S. D.M. White, *Nature* 440 , 1137, 2006.
- [8] J. Yadav, S. Bharadwaj, B. Pandey, and T. R. Seshadri, *Monthly Notices Royal Astron. Soc.* 364 , 601, 2005.
- [9] P. Sarkar, J. Yadav, B. Pandey, and S. Bharadwaj, *Monthly Notices Royal Astron. Soc.* 399 , L128, 2009.
- [10] F. Sylos Labini and Y. V. Baryshev, *J. Cosmology and Astroparticle Phys.* 6, 021, 2010.
- [11] W. A. Watson, I. T. Iliev, J.M. Diego, et al., *Monthly Notices Royal Astron. Soc.* 437, 3776, 2014.
- [12] Ya. V. Naiden and O. V. Verkhodanov, *Astrophysical Bulletin* 68, 471, 2013.
- [13] J. F. Navarro, C. S. Frenk, and S. D. M. White, *Astrophys. J.* 490, 493, 1997.
- [14] M. L. Khabibullina and O. V. Verkhodanov, *Astronomy Reports* 55, 302, 2011.
- [15] L. Amati, F. Frontera; M. Tavani, et al., *Astron. and Astrophys.* 390, 81, 2002.
- [16] L. Amati, C. Guidorzi, F. Frontera, et al., *Monthly Notices Royal Astron. Soc.* 391, 577, 2008.
- [17] D. Riccia, F. Fioreb, and P. Giommia, *Nuclear Phys. B Proc. Suppl.* 69, 618, 1999.

- [18] W. S. Paciesas, C. A. Meegan, G. N. Pendleton, et al., *Astrophys. J. Suppl.* 122, 465, 1999.
- [19] R. Vavrek, et al., *AIP Conf. Proc.*, No. 662, 163, 2003.
- [20] L.L.R. Williams and N. Frey, *Astrophys. J.* 583, 594, 2003.
- [21] A. Mészáros and J. Stocek, *Astron. and Astrophys.* 403, 443, 2003.
- [22] A. Bernui, I.S. Ferreira, and C. A. Wuensche, *Astrophys. J.* 673, 968, 2008.
- [23] A. Mészáros, L.G. Balázs, Z. Bagoly, and P. Veres, *AIP Conf. Proc.*, No. 1133, 483, 2009.
- [24] O.V. Verkhodanov, V.V. Sokolov, M.L. Khabibullina, and S.V. Karpov, *Astrophysical Bulletin* 65, 238, 2010.
- [25] M.L. Khabibullina, O.V. Verkhodanov, and V.V. Sokolov, *Astrophysical Bulletin* 69, 472, 2014.
- [26] V.N. Yershov, V.V. Orlov, and A.A. Raikov, *Monthly Notices Royal Astron. Soc.* 423, 2147, 2012.
- [27] O.V. Verkhodanov, M.L. Khabibullina, and E.K. Majorova, *Astrophysical Bulletin* 64, 263, 2009.
- [28] O.V. Verkhodanov and M.L. Khabibullina, *Astrophysical Bulletin* 65, 390, 2010.
- [29] N. Jarosik, C.L. Bennett, J. Dunkley, et al., *Astrophys. J. Suppl.* 192, 14, 2011.
- [30] P.A.R. Ade et al. (Planck Collab.), arXiv:1303.5062.
- [31] P.A.R. Ade et al. (Planck Collab.), arXiv:1303.5072.
- [32] A.G. Doroshkevich, O.V. Verkhodanov, P.D. Naselsky, et al., *Int. J. Mod. Phys. D* 20, 1053, 2011.
- [33] O.V. Verkhodanov, *Astrophysical Bulletin* 69, 330, 2014.
- [34] Ya.V. Naiden and O.V. Verkhodanov, *Astrophysical Bulletin* 69, 488, 2014.
- [35] A. Rakic and D.J. Schwarz, *Phys. Rev. D* 75, 103002, 2007.
- [36] Ja. Kim and P. Naselsky, *Phys. Rev. D* 82, 063002, 2010.
- [37] O.V. Verkhodanov, *Phys. Usp.* 55, 1098, 2012.
- [38] M. Hansen, J. Kim, A.M. Frejsel, et al., *J. Cosmology and Astroparticle Phys.* 10, 059, 2012.
- [39] C.J. Copi, D. Huterer, D.J. Schwarz, and G.D. Starkman, arXiv:1311.4562.
- [40] A.G. Doroshkevich, P.D. Naselsky, O.V. Verkhodanov, et al., *Int. J. Mod. Phys. D* 14, 275, 2003.
- [41] O.V. Verkhodanov, A.G. Doroshkevich, P.D. Naselsky, et al., *Bull. Spec. Astrophys. Obs.* 58, 40, 2005.

The complex of SAO RAS optical instruments as an instrument for studying transient sources in the Universe

Vlasyuk V.V.^{1,*}, Sokolov V.V.¹

¹*Special Astrophysical Observatory of RAS, Russia; vvlas@sao.ru*

Abstract Technical facilities of Special Astrophysical Observatory of Russian Academy of Sciences (SAO RAS) and its application for studying transient sources are described. The astrophysical task related to transient sources is briefly described. Future prospects are outlined.

Keywords: Astronomical Optical Facilities, Transient Sources, Gamma-Ray Burst Afterglow

1. Introduction

The epoch of studying optical transients in Russia in 1997, when researchers of SAO RAS first succeeded in detecting a gamma-ray burst (GRB) afterglow and its identification with a host galaxy (the famous object GRB 970508).

2. Optical Facilities of SAO RAS

Optical telescopes of SAO RAS – both available and being designed ones – are a rather powerful instrument for the wide-range studying of transients sources appearing in the night sky. The observational complexes created for solution of astrophysical tasks with the basic SAO's instruments – the Big Azimuthal Telescope (BTA) with the 6-meter mirror and the 1-meter reflector Zeiss-1000 – can solve rather efficiently both the tasks of detection of such quick-changing sources and on-line determination of their most important characteristics.

From a set of scientific equipment of the SAO RAS's optical telescopes we turn our attention to the variants which are adequate to the assigned task of on-line study of transient sources. Hereinafter, from the whole variety of transient sources we will mean the variable sources of the so-called "distant space". This will allow us neglecting their motion, though at present the fulfilled reconstruction of the Zeiss-1000 telescope control system makes it possible to guide fast-moving objects of the near space.

2 variants of observations with the BTA optical telescope can be attributed to such equipment – the prime-focus optical reducers SCORPIO [1,2] and the complex for analyzing microsecond variability MANIA [3]. These complexes are installed in the telescope's prime focus in accordance with the BTA operation schedule and can be used at this time only.

The focal reducer SCORPIO are equipped with registration systems based on charge-coupled devices (CCDs), which makes them applicable in investigation of slow variations of transient characteristics. Such type of observations includes photometry in wide-, middle- and narrow-band filters, spectroscopy with long slit, photo- and spectropolarimetry. Technical parameters of the used systems restrict the temporal resolution of the investigations by tens of seconds. As is shown by statistics of exploitation of focal reducers with BTA, as a rule, their percentage is from 50 to 60% of calendar time (generally, practically all moonless and partly moon time).

On the other hand, the temporal resolution of the multimode panoramic photospectropolarimeter – the MANIA complex – is up to 10^{-6} sec, but it is used at BTA during 15-25 nights per year. This reduces

considerably the probability of its application in the study of transient sources.

The instrument facilities of the BTA telescope can be added due to application of the attached implements of the 1-meter telescope Zeiss-1000 – the UBVRI photometer with a CCD system and a large-aperture spectrograph UAGS also equipped with a CCD camera. The temporal resolution of these systems is identical to that of above-mentioned BTA focal reducers – the tens of seconds. Of course, the threshold of magnitude in these observational methods is smaller, and the study of faint objects (especially, their spectroscopy) with a small telescope will be not-too-effective. On the other hand, the field of view of a photometer of the 1-meter telescope can be extended to 10 arc minutes due to usage of a large-format CCD camera; besides, the utilization of the instrument is not too strong, which makes it possible to use it in the search of transients in the case of low precision of their coordinates.

3. Studying of transient sources

The matched operation of the 6-m and 1-m telescopes permits expecting an effective solution of the problem of detection and studying transient sources. A rather good example of such coordinated operation of the SAO's telescopes can be the story of studying of one of the first gamma-ray bursts detected and investigated with our telescopes – GRB 970508. Figure 1 shows the source of optical afterglow of this event obtained first with the 1-meter telescope in the search mode, and then its image was obtained with BTA several days later (in the inset).

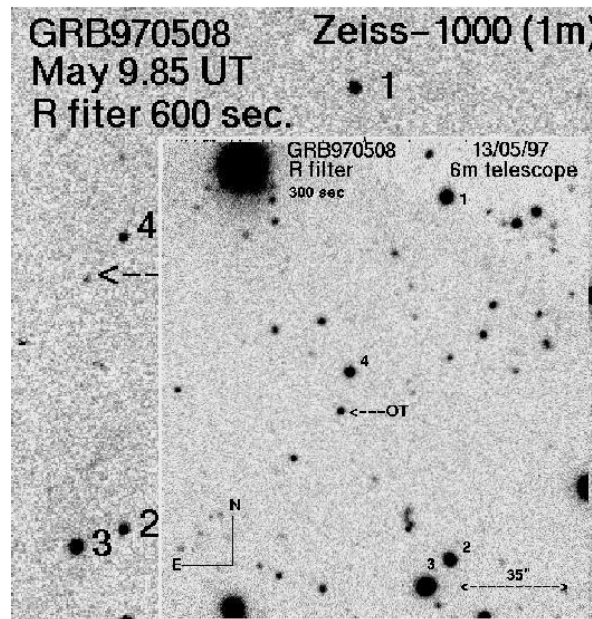


Fig. 1. Images of optical afterglow of the gamma-ray burst GRB 970508 obtained with the 1-meter telescope Zeiss-1000 at the moment of discovery and with the BTA telescope 5 days later (in the inset). Both images were obtained in the R_c band.

The next Figure 2 presents a result of joint photometry of this transient source fulfilled at both telescopes: the brightest phase was studied at the 1-me telescope, the fainter stages were accessible, naturally, only for BTA [4].

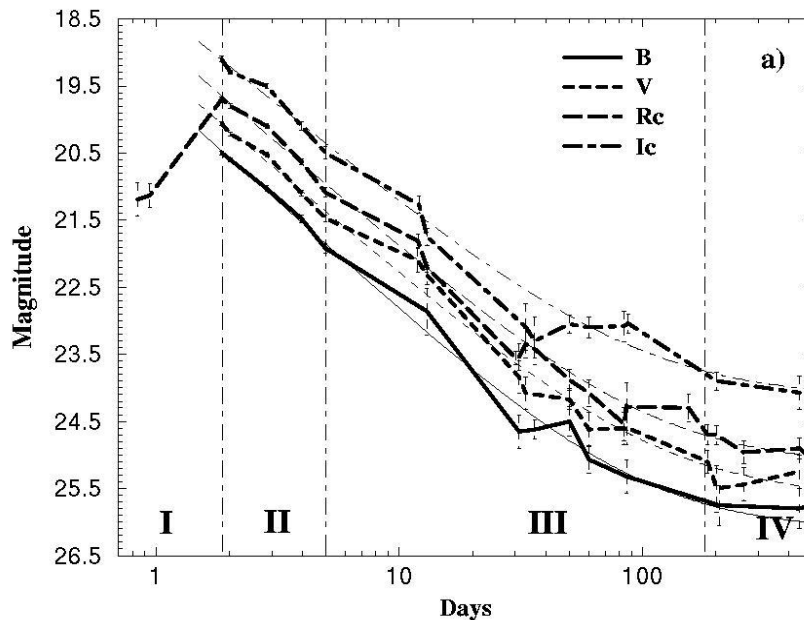


Fig.2. The combined light curve of the source GRB 970508 in the B, V, Rc, Ic bands obtained from data of the 1-m telescope Zeiss-1000 and the BTa telescope [4].

Later on, the work on identification and studying the nature of gamma-ray bursts has been fulfilled (up to the present time) in a wide international collaboration. The participants of the program, beside the SAO team, are the researchers from Spain (the 10.4-m GTC, the 4.2-m Calar Alto, etc.), France (the submm Observatory at Plateau de Bure), New Zealand, India (the 2.34-m VBT Kavalur, the 2.01-m HCT IAO, the 1.04-m ST Naini Tal).

Another example of the study of transient sources fulfilled with optical telescopes of SAO RAS is the joint program of a SAO RAS and ASC FIAN team on investigation of synchronous variability of a sample of blazars carried out at the 1-m SAO's optical telescope and the 22-m radio telescope of Crimean Astronomical Observatory. This program was started in 2002 and it includes a sample of almost 15 BL Lac type objects. In the course of the program some indications to a possible synchronism of variability of optical brightness and radio flux were detected. For example, in Figure 3 from [5] in data for a famous object AO0235+164 one can see both coinciding peaks of brightness and their total mismatch. Along with it, some indications to the presence of an intra-day variability in objects of this type were detected.

At present, the software was elaborated in SAO which provides the on-line translation of alerts about gamma-ray bursts and other transients discovered by the space missions Swift, Fermi, MAXI, INTEGRAL, etc., and with ground-based facilities. When there is an alert, an observer sees a dialog box in the monitor which, in case of the positive decision, permits to start immediate pointing to the object's coordinates. So, the reaction time of the complex is reduced to minimum.

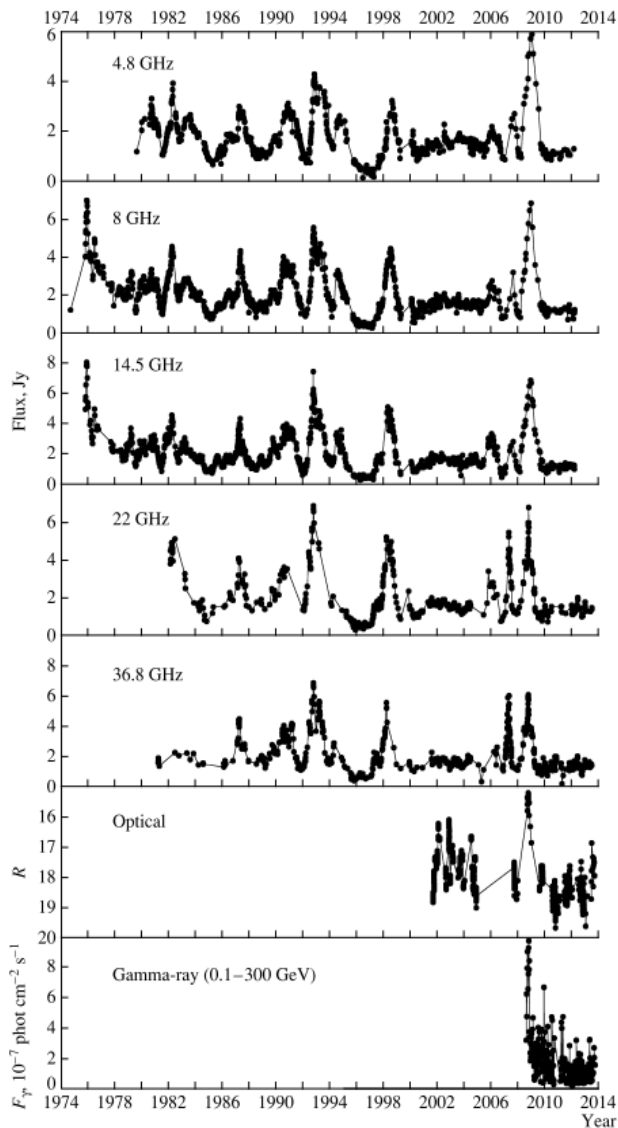


Fig. 3. The results of the long-term monitoring of variability in radio, optical and gamma-ray ranges (the lowest diagrams) of the famous BL Lac type object AO0235+164 from data of paper [5].

Beside external sources of data about transient events, SAO RAS has its own wide-field system for detection of optical events – Mini-Mega-TORTORA [6]. Its feature is the presence of a wide field of view (about 900 sq. degrees), the subsecond temporal resolution and a possibility of fast transition to the study of a detected transient by means of multi-color photometry and polarimetry. Mini-Mega-TORTORA is oriented to early detection of optical flares whose localization is unknown in advance, their on-line classification and transfer of coordinate information to other SAO RAS's telescopes.

4. Future prospects

In the nearest future SAO plans to manufacture and put into operation in the Northern Caucasus a modern wide-field telescope with a 4-meter class mirror designed to operation in optical and near infrared ranges within the field of view up to 2 degrees. Its optics should be made of astrosital with application of methods of adaptive optics and adaptation of the wave front. Such solutions will permit the new telescope to overcome BTA in investigation methods where the quality of image built by optics is crucial. The information capacity of the new instrument in which it is planned to introduce mosaic detectors of emission of the size up to $20K \times 20K$ elements will considerably overcome the BTA facilities too.

The plans include also the equipment of Nasmyth focuses of this telescope with such high-technology complexes as a panoramic spectrograph with a minute field of view, a multi-object spectrograph for several hundreds of simultaneously-studies objects, and others.

The main tasks of the new instrument will be the study of transient sources along with deep spectral surveys of the sky, the search for distant supernovae. It is planned to create such an instrument in 2017-2025.

A much cheaper and more realistic project also promoted by our specialists is the creation of a row of small telescopes of diameter 0.5 m equipped with large-size registration systems based on CCDs. With their fields of view of order of 1 degree, such systems will allow us fulfilling a mass photometry of relatively bright objects of the 15-17 st. magnitude, spectral and polarization study and, if required, getting involved to the system of studying transients.

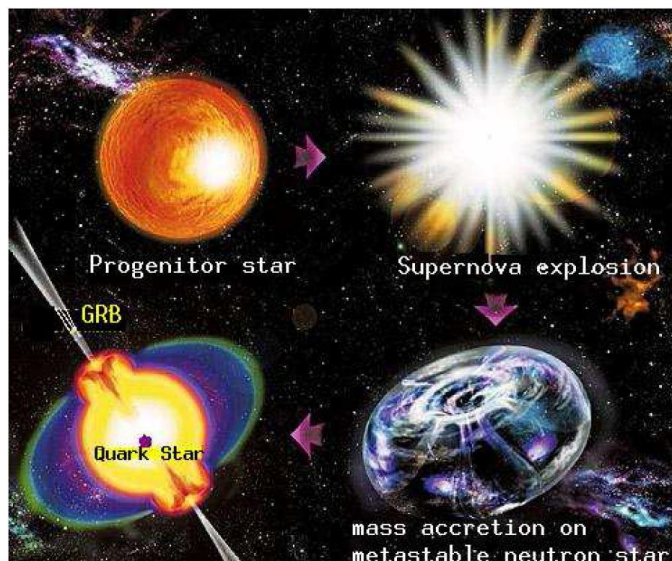


Fig. 4. (from [7]) A schematic representation of the last stages of the evolution of a massive star ($M > 8 M_{\text{sun}}$) leading to the delayed conversion of a pure hadronic star to a quark star (hybrid or strange star) and to the emission of a neutrino burst and possibly to a gamma-ray burst. Clockwise from the upper left corner of the figure: (i) nuclear burning stage of the progenitor star; (ii) supernova explosion and birth of a pure hadronic star ("neutron star"); (iii) mass accretion on the metastable hadronic star; (iv) conversion process of the hadronic star to a quark star (second "explosion") neutrino burst and gamma-ray burst.

Now quark-gluon plasma is a new direction both in the high energy physics and in the study of compact objects of the type of neutron star and collapsars (candidates in BH of stellar mass). The phase

transition in the quark-gluon state is related with the mechanism itself of core-collapse supernovae explosion (the energy of such a transition can be a source of cosmic gamma-ray bursts). Signals of transition of matter to pure quark-gluon plasma can be neutrinos that are observed with modern detectors, including our ones, e.g. Baksan Underground Scintillation Telescope (BUST). Now the equipment of the gravitational detectors LIGO/VIRGO is also customized for signals of such a transition.

Participation of astronomers in programs of the study of localization boxes of neutrino (and, possibly, gravitational) events is already being discussed in detail (e.g., see <https://wikispaces.psu.edu/display/AMON>). SAO RAS, with all its telescopes (+ other telescopes in the Northern Caucasus) can join this new international program of synchronous observations of astrophysical objects related with collapse of massive star nuclei (see Fig.4).

References

- [1] Afanasiev V.L., Moiseev A.V., *Astronomy Letters*, v.31, p.194, 2005.
- [2] Afanasiev V.L., Moiseev A.V., *Baltic Astronomy*, v.20, p. 363, 2011.
- [3] Plokhotnichenko V.L., Beskin G.M., et al. *Astrophysical Bulletin*, v. 64, p. 322, 2009.
- [4] Zharikov S.V., Sokolov V.V., Baryshev Yu.V., *A&Ap*, 1998, v.337, p.356
- [5] Bychkova V.S. et al., *Astronomy Reports*, v.59, p.851.
- [6] Biryukov A.V., Beskin G.M., Karpov S.V. et al, *Baltic Astronomy*, v.24, p.100, 2015.
- [7] I.Bombaci, D.Logoteta, I.Vidana, C.Providencia, Quark matter nucleation in neutron stars and astrophysical implications, arXiv:1601.04559

X-ray Binaries and Ultraluminous X-ray Sources

Grzegorz Wiktorowicz^{1,*}

¹*Astronomical Observatory, University of Warsaw, Poland;* **gwiktoro@astrouw.edu.pl*

Abstract Ultraluminous X-ray sources remains mysterious despite all the research which was made recently. The simplest explanation, which involves the intermediate-mass black holes, has other substantial problems. On the other hand, the super-Eddington accretion provides explanation, which aims at connecting these sources with observed X-ray binary population. We showed that powering such a source is feasible even in the most extreme case of the system ESO 243-49 HLX-1, which reaches the luminosity of $1.1 \cdot 10^{42}$ erg/s.

Keywords: X-ray binaries, mass accretion, black holes, stellar evolution

1. Introduction

Ultraluminous X-ray Sources are extremely bright ($L_X > 1 \cdot 10^{39}$ erg/s; e.g., [1]) point-like objects. Such a large luminosity exceeds the Eddington limit for a stellar mass black hole (sMBH; $M_{\text{sMBH}} \approx 10 M_{\odot}$). Up to now we discovered about 500 such objects ([2]) but none in our Galaxy (but see [3]).

For a long time it was suggested that ULXs may be the high-luminosity end of X-ray binaries (XRBs). This statement is supported both by observations and by theoretical simulations. For example, Motch [4] observed the variations in the light-curve of the irradiated companion star, which placed a $15 M_{\odot}$ upper limit on the compact object mass in the NGC 7793 P13 source. This clearly precludes the intermediate-mass black hole (IMBH) accretor. Even more striking result was acquired by Bachetti [5] who found a pulsar in an ULX (source M82 X-2).

There are also a lot of theoretical works on this subject. Feng [1] showed the formation channels for BH ULX, whereas Fragos [6] showed that the formation of ULX with NS is also possible in the light of the stellar evolution. However, there are also counter arguments against this interpretations, which favour the IMBH accretors ([7], [8]).

First, the most important characteristics of XRB population are provided (Section 2), then we move to presentation of recent results in the field of ULX (Section 3), and then we discuss the possibility in which ULXs (at least most of them) are the subgroup of XRBs (Section 4).

2. X-ray Binaries

All confirmed black holes (BH) reside in XRBs. You can find the most up-to-date list in [9]. The progenitors to compact objects are heavier than $8 M_{\odot}$ but when we include binary interactions (e.g., mass transfer) even lighter stars are potential progenitors of compact objects. Recently Sana [10] has shown that most massive stars tend to born in binaries with a possibility that even all of these stars reside in binaries with tight circular orbits.

XRB comprises a NS/BH accretor and a mass-transferring companion (Fig. 1). In the vicinity of CO the gravitational potential energy of the matter is being converted into thermal energy which results in very large temperatures in the inner part of the accretion disk. That's the place from which X-ray radiation originates.

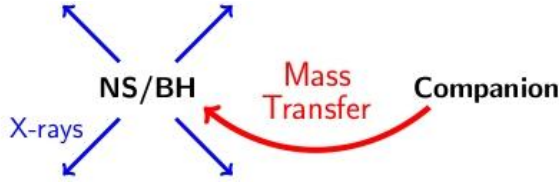


Fig 1. The schematic picture of an X-ray binary system

These systems are generally divided in two distinct groups. The first one is called Low Mass XRB (LMXB) and includes systems with companions lighter than about $1 M_{\odot}$. The mass transfer in these systems is the outcome of Roche lobe overflow (RLOF) of the secondary star. The orbital periods are in the range from a few hours to a few days. We observe them mostly in the direction of the Galaxy Center and in globular clusters. Such systems have to be born as a binary of extremely high mass ratio and with a large orbital separation.






The second group comprises high-mass XRBs (HMXBs) with companions heavier than $\sim 10 M_{\odot}$. The mass transfer occurs due to wind from the massive secondary. It is thought that HMXBs are the predecessors to Thorne-Zytkow objects and also to double compact objects.

It is important to note that there are very few systems in-between (with the companion mass $1-10 M_{\odot}$) and that all BHs reside in LMXBs (you can find collected information in Table 1).

Table 1. Parameters of low-mass X-ray binaries comprising black holes. The columns are: name of the system, companion mass, spectral type, black hole type and orbital period. For references and further information see [9] from where the table was taken.

Name	$M_{\text{comp}} [M_{\odot}]$	Spec. type	$M_{\text{BH}} [M_{\odot}]$	$P_{\text{orb}} [h]$
XTE J1118+480	0.22 ± 0.07	K7/M1V	$6.9 \div 8.2$	4.08
XTE J1550-564	0.3 ± 0.07	K2/4IV	10.5 ± 1.0	37
GS 2000+25	$0.16 \div 0.47(0.315)$	K3/6V	~ 6.55	8.26
GRO J0422+32	~ 0.45	M0/4V	~ 10.4	5.09
GRS 1009-45	~ 0.5	G5/K0V	~ 8.5	6.86 ± 0.12
GRS 1716-249	~ 1.6	K-M	$\gtrsim 4.9$	14.7
GX339-4	$0.3 \div 1.1(0.54)$	KIV	> 7	42
H1705-25	$0.15 \div 1.0$	K3/M0V	$4.9 \div 7.9$	12.55
A0620-00	0.68 ± 0.18	K2/7V	6.6 ± 0.25	7.75
XTEJ1650-50(0)	0.7	K4V	~ 5.1	7.63
XTEJ1859+226	0.7	K5V	7.7 ± 1.3	6.58 ± 0.05
GS2023+338	$0.5 \div 1.0(0.7)$	K0/3IV	12 ± 2	156
GRS 1124-68	$0.3 \div 2.5(0.8)$	K5V	6.95 ± 0.6	10.392
GRS1915+105	0.8 ± 0.5	K1/5III	12.9 ± 2.4	811.2 ± 2.4
GS 1354-64	1.03	G5IV	7.6 ± 0.7	61.07
GROJ1655-40	1.75 ± 0.25	F3/G0IV	5.31 ± 0.07	62.909 ± 0.003
4U1543-47	$2.3 \div 2.6(2.45)$	A2V	$2.7 \div 7.5$	26.8
XTEJ1819-254	$5.49 \div 8.14(6.81)$	B9III	$8.73 \div 11.70$	67.62
CygX-1	19.2 ± 1.9	O1	14.8 ± 0.1	134.4

The typical evolution leading to formation of an LMXB with a BH accretor begins with a binary with a very extreme mass ratio on ZAMS ($35 M_{\odot}$ and $1 M_{\odot}$) on a very elongated orbit ($12000 R_{\odot}$). After 5.6 Myr of evolution a common envelope (CE) phase commences which results in a significant shrinkage of the orbit. Up to that time, the primary has lost a large fraction of its envelope in the wind and has a mass of about $17 M_{\odot}$. After CE, the system consists of a helium core of the primary ($11 M_{\odot}$) and an almost unaffected secondary ($1 M_{\odot}$). It has to be stated here that CE is necessary for formation of a LMXB because we know no other process that can lead to fast and effective angular momentum loss (AML) in a wide binary.

t	Phase	M ₁		M ₂	a
0Myr	ZAMS	35 M _⊙		1 M _⊙	12000 R _⊙
5.6Myr	CE	17.5 M _⊙		1 M _⊙	4000 R _⊙
5.6Myr	postCE	11.3 M _⊙		1 M _⊙	6 R _⊙
6Myr	BH	8 M _⊙		1 M _⊙	8 R _⊙
4Gyr	RLOF	8 M _⊙		1 M _⊙	5 R _⊙

BH transient $\dot{M} \approx 10^{-10} \frac{M_{\odot}}{\text{yr}}$

Fig2. The evolution of typical predecessor to low-mass X-ray binary with a black hole accretor. See text for more information.

Just after the CE, the naked He core of the primary explodes in a supernova explosion and forms a BH ([24]) with a mass of about 8 M_⊙. The binary needed only a few Myr to shorten the orbit from 12000 R_⊙ to 8R_⊙, but needs another 4 Gyr to lose additional 5 R_⊙ due to gravitational wave emission and start MT onto BH. At that moment we acquire the XRB with a mass transfer rate of about 10⁻¹⁰ M_⊙/yr (see Fig. 2).

Although these results solve the problem of the gap in compact object distribution ([11]), a very significant problem still exists with a mass distribution of companions. A typical evolution suggests a typical donor mass of about 1M_⊙, whereas observations show 0.6 M_⊙. This problem was investigated by Wiktorowicz [9], who concentrated on the CE phase. Their conclusion was that neither CE model nor efficiency have the influence on XRB population. Therefore this problem with companion masses may be a result of systematic observational error ([12]) or the mass transfer physics is still poorly understood.

3. Ultraluminous X-ray Sources

For a long time it was believed that an accreting object cannot breach the so called Eddington limit. This constraint stems from the fact that accreted matter must overcome the radiation pressure. Increasing of the accretion also increases the emission which results in higher radiation pressure. At some point we will obtain the equality between the pressure of falling mass and the pressure of radiation.

ULXs are observed as point-like objects with luminosity far exceeding 10³⁹ erg/s (the Eddington limit for an sMBH). Their spectrum strongly resembles the XRBs' one and the other similarity is that ULXs appear to be point-like sources. What is more, their spectrum seems to agree with a multi-color disk which is an indication of disk accretion. These two facts provide two most common solutions to the problem of the nature of ULXs.

The first solution involves the hypothetical IMBH. The idea is very simple. The larger is the accretor mass the larger is the Eddington limit. Then we do not have to break it. However the problem appears during the evolution as there are no evolutionary routes that can produce IMBHs from stars. What is more, it was shown that IMBH cannot be present in all observed ULXs ([13])

The second possibility, on which we concentrate, is that the ULXs are a high-luminosity tail of the XRB distribution. There are several processes that can lead to breakage of the Eddington limit. If we assume that there is no spherization of matter, what is supported by recent detailed accretion flow calculations ([14], [15], [16]), the emission may be beamed, which will result in an apparent higher

luminosity ([17]). Another possibility is the photon bubbles ([18]). The advection may result either in a lower luminosity (the advection dominated accretion flow) or help to emit the radiation through magnetic buoyancy ([15]). The relativistic jets, observed in many systems, may result in a very high energetic radiation if observed along the axis or in a low accretion if observed perpendicularly ([19]).

4. ULX as XRB

A strong support for ULX as a part of XRB comes from the XLF (e.g., [20]). It presented no visible features near 10^{39} , where is the transition between XRBs and ULXs, but extends up to a few times 10^{40} erg/s, which includes most of the ULXs. However this argument works only for regular ULXs while the problem still exists with these with luminosities above the cut-off.

The most luminous ULXs is ESO 243-49 HLX-1 with an enormous luminosity well above the XLF cut-off (1.1×10^{42} erg/s; [21]). The outbursts, during which this luminosity is reached, are very regular (dt ~ 1 yr; [22]). It was suggested recently that this source may be a face-on version of SS433 system, which resides in our Galaxy ([3]).

The results presented in paper [23] show that it is possible to obtain the mass accretion rates high enough to powers such a source as HLX-1 in XRB system with sMBH. They presented several evolutionary channels and discussed typical evolutionary routes. What is very significant, the study showed that even NS accretors are capable of obtaining such large accretion rates.

The typical evolutionary route doesn't differ significantly from typical XRB. We start the evolution with a heavy secondary ($\sim 10 M_{\odot}$). If we omit the Eddington luminosity, the beginning of the mass transfer will give as a very large mass flow for a very short time (100-10000yr; see Fig. 3). The companion will be quickly stripped of mass and the mass transfer rate will decrease. After this extremely luminous phase the system will become a regular ULX. The conclusion of [23] is that a lot of systems evolves through the extreme ULX phase, but it is extremely short, which give us in result only few potential observations currently. Probably the case is similar for all ULXs but this thesis is being investigated in the on-going study (Wiktorowicz et al. In preparation).

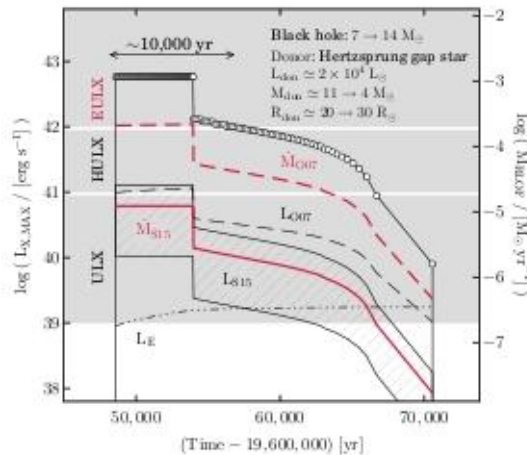


Fig3. The ULX phase. A few accretion models and parameter changes are presented. For more details see [23].

5. Conclusions

A lot of observations support the statement that ULXs are a high-energy tail of XRB population. However, the most luminous systems are still the best candidates for the elusive IMBHs. In [23] the mass transfer rates in XRBs were investigated. The disk accretion models are still under development, so the work was limited to examine the amount of available mass flow.

It was proved that we can obtain mass accretion rates high enough to power even the most luminous ULXs. Therefore if we assume that the Eddington limit may be breached by some kind of process, we are able to explain the ULX population without the need for IMBH. It appears that the ULX (extreme and possibly also regular) is just a short phase (100–10000 yr) during the evolution of a significant number (~1%) of XRB. These numbers result in a few observations that should be visible currently.

Acknowledgements

The author wants to thank the LOC for making it possible for him to attend the conference.

References

- [1] Feng H., Soria R., “Ultraluminous X-ray sources in the Chandra and XMM-Newton era”, *New Astronomy Reviews*, Vol. 55, Iss. 5, p. 166-183, 2011.
- [2] Walton D. J., Roberts T. P., Mateos S., Heard, V., “2XMM ultraluminous X-ray source candidates in nearby galaxies”, *MNRAS*, Vol. 416, Iss. 3, pp. 1844-1861, 2011.
- [3] King A., Lasota J.-P., “HLX-1 may be an SS433 system”, *MNRAS Letters*, Vol. 444, Iss. 1, p.L30-L33, 2014
- [4] Motch C., Pakull M. W., Soria R., Grisé F., Pietrzyński G., “A mass of less than 15 solar masses for the black hole in an ultraluminous X-ray source”, *Nature*, Vol. 514, Iss. 7521, pp. 198-201, 2014.
- [5] Bachetti M., Harrison F. A., Walton D. J., et al. “An ultraluminous X-ray source powered by an accreting neutron star”, *Nature*, Vol. 514, Iss. 7521, pp. 202-204, 2014.
- [6] Fragos T., Linden T., Kalogera V., Sklias P., “On the Formation of Ultraluminous X-Ray Sources with Neutron Star Accretors: The Case of M82 X-2”, *The Astrophysical Journal Letters*, Vol. 802, Iss. 1, article id. L5, 6 pp., 2015.
- [7] Colbert E.J.M., Mushotzky R.F., “The Nature of Accreting Black Holes in Nearby Galaxy Nuclei”, *The Astrophysical Journal*, Vol.519, Iss.1, pp. 89-107, 1999.
- [8] Titarchuk L., Seifina E., “Scaling of the photon index vs. mass accretion rate correlation and estimate of black hole mass in M101 ULX-1”, *Astronomy & Astrophysics*, Vol. 585, id.A94, 11 pp., 2016.
- [9] Wiktorowicz G., Belczynski K., Maccarone Th., “Black hole X-ray transients: The formation puzzle”, *Binary Systems, their Evolution and Environments, A Conference held 1-5 September, 2014 at Mongolia-Japan Centre, Ulaanbaatar, Mongolia*. Abstracts online at <http://mongolia.csp.escience.cn/>, id.37, 2014.
- [10] Sana H., Dunstall P.R., et al. “The VLT-FLAMES Tarantula Survey: Multiplicity and Dynamics of the Massive Stars in 30 Dor”, *Proceedings of a Scientific Meeting in Honor of Anthony F. J. Moffat held at Auberge du Lac Taureau, St-Michel-Des-Saints, Québec, Canada, held 11-15 July 2011*. ASP Conference Series, Vol. 465. San Francisco: Astronomical Society of the Pacific, 2012., p.284, 2012.
- [11] Belczynski K., Wiktorowicz G., Fryer Ch.L., Holz D. E., Kalogera V., “Missing Black Holes Unveil the Supernova Explosion Mechanism”, *The Astrophysical Journal*, Vol. 757, Iss. 1, article id. 91, 6 pp., 2012.
- [12] Kreidberg L., Bailyn Ch.D., Farr W.M., Kalogera V., “Mass Measurements of Black Holes in X-Ray Transients: Is There a Mass Gap?”, *The Astrophysical Journal*, Vol.757, Iss. 1, article id. 36, 17 pp., 2012.
- [13] King A.R., “Ultraluminous X-ray sources and star formation”, *MNRAS*, Vol. 347, Iss. 2, pp. L18-L20, 2004.

- [14] Ohsuga K., “Two-Dimensional Radiation-Hydrodynamic Model for Supercritical Disk Accretion Flows onto Neutron Stars”, *Publications of the Astronomical Society of Japan*, Vol.59, No.5, pp.1033—1041, 2007.
- [15] Jiang Y.-F., Stone J.M., Davis Sh.W., “A Global Three-dimensional Radiation Magneto-hydrodynamic Simulation of Super-Eddington Accretion Disks”, *The Astrophysical Journal*, Vol. 796, Iss. 2, article id. 106, 14 pp., 2014.
- [16] Sądowski A., Narayan R., “Powerful radiative jets in supercritical accretion discs around non-spinning black holes”, *MNRAS*, Vol. 453, Iss.3, p.3213-3221, 2015.
- [17] King A. R., Davies M.B., Ward M.J., Fabbiano G., Elvis M., “Ultraluminous X-Ray Sources in External Galaxies”, *The Astrophysical Journal*, Volume 552, Issue 2, pp. L109-L112, 2001.
- [18] Begelman M.C., “Photon Bubbles and the Vertical Structure of Accretion Disks”, *The Astrophysical Journal*, Vol. 643, Iss. 2, pp. 1065-1080, 2006.
- [19] Fabrika S., Karpov, S., Abolmasov P., Sholukhova O., “Properties of SS433 and ultraluminous X-ray sources in external galaxies”, *Populations of High Energy Sources in Galaxies. Proceedings of the 230th Symposium of the International Astronomical Union, Held in Dublin, Ireland 15-19 August 2005*, Edited by E. J. A. Meurs; G. Fabbiano. Cambridge: Cambridge University Press, 2006., pp.278-281, 2006.
- [20] Mineo S., Gilfanov, M., Sunyaev R., “X-ray emission from star-forming galaxies - II. Hot interstellarmedium”, *MNRAS*, Vol. 426, Iss. 3, pp. 1870-1883, 2012.
- [21] Fabbiano G., “X-Ray Emission and Extranuclear Activity in Galaxies”, *Proceedings of the ESO Workshop on Extranuclear Activity in Galaxies, held in Garching, F.R.G., May 16-18, 1989*, Followed by an informal session on Cen A, May 19, 1989. Editors, E.J.A. Meurs and R.A.E. Fosbury; Publisher, European Southern Observatory, Garching bei Munchen, F.R.G., 1989. ISBN # 3-923524-34-X. LC # QB856 .E85. P. 325, 1989.
- [22] Yan Zhen, Zhang Wenda, Soria R., Altamirano D., Yu Wenfei , “X-Ray Outbursts of ESO 243-49 HLX-1: Comparison with Galactic Low-mass X-Ray Binary Transients”, *The Astrophysical Journal*, Vol. 811, Iss. 1, article id. 23, 11 pp., 2015.
- [23] Wiktorowicz, G., Sobolewska M., Sadowski A., Belczynski K., “Nature of the Extreme Ultraluminous X-Ray Sources”, *The Astrophysical Journal*, Vol. 810, Iss. 1, article id. 20, 8 pp., 2015.
- [24] Fryer C.L., Belczynski K., Wiktorowicz G., et al. *ApJ*, 749, 91, 2012.

On some exotic properties of hybrid stars

Andrey Yudin

Institute for Theoretical and Experimental Physics, Moscow, Russia; yudin@itep.ru

Abstract We consider two “wonders” of hybrid stars, i.e. stars which contain a core made of quark matter. First, we explain the existence of a very small region on the mass–radius (M-R) diagram of hybrid stars where all of the lines representing the sequences of models with different values of the bag constant B intersect. This circumstance is shown to be a consequence of the linear dependence of pressure on energy density in the quark cores of hybrid stars. Second, we show that the unusual thermodynamic properties of matter within the region of two-phase coexistence in hybrid stars result in a change of the standard condition for beginning of convection. In particular, the thermal flux transported by convection may be directed towards the stellar center. We discuss favorable circumstances leading to such an effect of “inverse” convection and its possible influence on the thermal evolution of hybrid stars.

Keywords: Hybrid Star, Quark Matter, Convection

1. Introduction

Neutron stars, together with stellar mass black holes, develop from collapsing cores of massive stars at the final stages of their evolution. The birth of a neutron star most likely manifests itself as a supernova explosion. The major part of matter in neutron stars proves to be in an extreme state with a density exceeding the nuclear one $\rho_n \approx 2.6 \times 10^{14} \text{ g cm}^{-3}$. The possibility of phase transitions (PTs) in nuclear matter was first supposed by Gurevich [1]. Then Ivanenko & Kurdgelaidze [2] and Itoh [3] advanced hypotheses concerning stars composed of quark matter. Nowadays there exists an extensive literature on neutron stars, quark stars, and neutron stars containing quark cores (the so-called hybrid stars).

The properties of hybrid stars are of great importance for explaining the supernova explosion mechanism in the simplest case where there are no magnetic field and rotation. This is because the PT to quark matter that arises at the boundary between the core of a hybrid star and its crust can be responsible for the development of hydrodynamic instability ending with a supernova explosion.

Here we concentrate our attention on two unusual properties of hybrid stars: the existence of a “special point” on its mass-radius diagram and the “inverse” convection which can occur inside such a stars.

2. Special point

The published models of hybrid stars show a surprising peculiarity. On the mass–radius (M – R) diagram, all of the lines representing the sequences of models with different constant values of the bag constant B intersect in a very small region that we arbitrarily call a “point” here. To construct the stellar models, we use an equation of state (EOS) with the phase transition to quark matter at high densities. An approximation of the EOS from [4] is applied for the low density component of the matter. The quark component is described by the simplest version of the bag model in which the relation between pressure P and total energy per unit volume ε is linear:

$$P = \frac{1}{3}(\varepsilon - 4B), \quad (1.1)$$

where B is the quark bag constant. This approximation is widely used in modeling the properties of

quark matter and is a special case of the group of linear EOSs: $P = \alpha(\varepsilon - \varepsilon_0)$, where the dimensionless constant $0 \leq \alpha \leq 1$ means the square of the speed of sound measured in units of the speed of light, $\alpha = (c_s / c)^2$. The bag constant B is a free model parameter and, in the simplest case, is uniquely related to the density at which the phase transition begins.

The mass–radius diagram for hybrid stars calculated for our EOS is shown in Fig. 1.

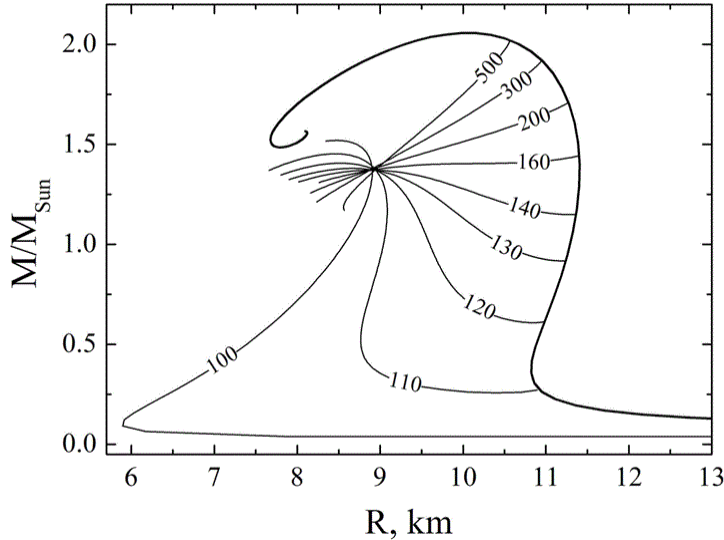


Fig1. Mass–radius diagram of hybrid stars for various values of the parameter B .

The thick line here indicates the dependence $M(R)$ for the EOS without any phase transition to quark matter. The thin lines indicate these dependences for various values of the parameter B (the values of B are indicated by the numbers in units of MeV fm^{-3}). The density at which the phase transition begins ρ_1 is uniquely related to B . For example, $B = 120$ corresponds to $\rho_1 \approx 2\rho_n$, while for $B = 145$ we have $\rho_1 \approx 3\rho_n$. The curve with $B = 100$ describes an almost pure quark star with a thin crust made of ordinary matter and, therefore, exhibits a dependence $M(R)$ typical of such stars. On the other hand, as can be seen from the figure, all stars with quark cores at $B \geq 160$ are unstable. Naturally, these specific values are unique to our model EOS.

Let us now turn to the formulation of the problem. As can be seen from Fig. 1, all curves with different B intersect in a very narrow region on the $(M-R)$ diagram (but not at a point!). This property, which is surprising per se, not only leads to some interesting consequences that we will discuss in conclusion but also undoubtedly requires an explanation. Note also that such a behavior of the curves $M(R)$ is not a unique property of precisely our EOS. The same effect can be seen, for example, in [5] – [7].

2.1. The brief explanation

Here we can only outline our explanation of this effect (for details see [8]). First, we need to compare the structures of stars near the point of intersection in Fig. 1. These stars corresponding to different values of the parameter B should have similar masses and radii. From this analysis, we see that these stars have a virtually identical crust made of ordinary matter to which a quark core is “stitched” at different depths, depending on the parameter B . Thus, when changing the parameter B , the quark matter–ordinary matter boundary is shifted, leaving the crust virtually unchanged.

We formalize this condition, starting from the stellar equilibrium equations under general relativity

conditions (the Tolman–Oppenheimer–Volkoff equations) and the phase equilibrium conditions at the boundary. After some mathematical manipulations we obtained the main equation of the problem, which must hold for “special point” property existence. To solve this equation, we use the homologous variables trick and show that our quark EOS really satisfies this conditions to some extent (i.e. not exactly, that’s why “a special point” in reality is a small domain).

The existence of “a special point” on the mass–radius diagram of hybrid stars appears to be a consequence of mostly two factors. The first one is the linearity of quark EOS (1.1). This property is characteristic of a simplest bag model of quark matter, but it also holds with very high accuracy for more realistic quark EOSs [9]. The second factor is a small value of the parameter $\alpha = 1/3$. The smaller is this parameter, the more exact is the homology property for the main equation. And inversely: at higher values of α the domain of intersection of $M(R)$ curves would be broader.

2.2. Discussion

We established that the stars at “the special point” are “masked”, hiding their true structure under the veil of observable quantities (M and R). Consider this aspect of the problem. Let us adopt the linearity of the quark EOS and assume that we know the true EOS of nuclear matter without any phase transitions that gives a thick enveloping curve on the (M – R) diagram (see Fig. 1). Then, were it not for the special point, only one measurement of the stellar mass and radius not only could say us whether such a star is a purely neutron or hybrid one (or, as a limiting case, a purely quark one) but could also point to parameters of quark matter. However, the existence of the special point changes the situation: the measuring of mass and radius of a star in its vicinity will only say us that this star contains a quark core, but neither its structure nor the parameters of quark matter will be determined. Either invoking additional information (for example, the cooling rate if the star was hot) or measuring the parameters of other hybrid stars to gain statistics and reconstruct the true curve $M(R)$ will be required.

3. Inverse convection

In a hybrid star the quark core is separated from the outer nuclear matter envelope by an intermediate layer where the PT between nuclear and quark matter occurs. Within this region of coexistence of nuclear and quark phases there is a possibility that pressure decreases as temperature increases at constant density. Such an effect was mentioned, for instance, in [10] – [12]. In single phases of quark or hadronic matter usually the opposite is the case, i.e. the pressure increases with growing temperature at constant density. According to the Clapeyron–Clausius formula (see, e.g., [13]) the temperature derivative of pressure along the PT line in the phase diagram is given by:

$$\left(\frac{\partial P}{\partial T}\right)_{\rho} = \frac{S_2 - S_1}{\frac{1}{\rho_2} - \frac{1}{\rho_1}} < 0. \quad (1.2)$$

Here $S_{1,2}$ and $\rho_{1,2}$ are the entropies per baryon and densities of phases 1 and 2 in the region of their coexistence. We consider here the simplest Maxwellian description of PT. The negative sign of the derivative in equation (1.2) thus appears because the quark phase has a higher entropy per baryon, $S_2 > S_1$ (note that $\rho_2 > \rho_1$). This also implies that to go from the low-density phase 1 to the high-density phase 2 at a fixed temperature the system absorbs the thermal energy per baryon $\Delta q = T(S_2 - S_1) > 0$. As we will show in the next section, this property ensures very unusual convection properties in the layer of phase coexistence.

3.1. The conditions for convection

Let us consider a schematic view of the phase diagram in the density–temperature plane (Fig. 2):

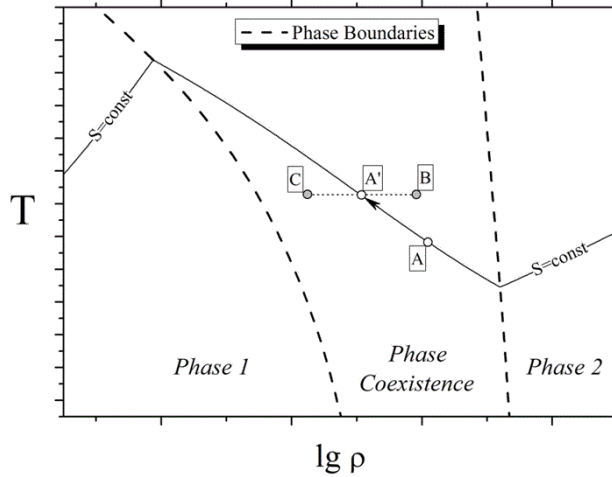


Fig2. Schematic view of a phase diagram for the transition between hadronic and quark matter.

The boundaries of the phases are shown by bold dashed lines. The region between the lines corresponds to two-phase coexistence. An isentropic curve ($S = \text{const}$) is shown by the solid line. One can observe that in the phase coexistence region the temperature begins to decrease along the isentropic curve when the density increases. Such a behavior of the PT was indicated by a number of authors (see e.g. [14]).

Consider for example a convective element that starts its adiabatic motion in the interior of a hybrid star at point A and moves outwards reaching point A' . So it keeps the initial entropy but has along its way the same pressure and hence temperature (let us remind that we consider the Maxwellian PT) as the environment. If on its way the convective element proves to be denser than the environment (point C) it will begin to sink. Such a configuration is convectively stable. On the contrary, when the state of the environment corresponds to point B , the density of the convective element is lower than that of the environment and it continues to rise – the configuration is convectively unstable. The entropy of environment in point B is higher than in point A' . Therefore the condition of appearance of convection reads

$$\frac{dS}{dr} > 0. \quad (1.3)$$

This condition has the inequality sign opposite to the common Schwarzschild criterion.

We can write the general criterion of appearance of convection in the well-known Ledoux form:

$$\left(\frac{\partial \varepsilon}{\partial S} \right)_{P,Y} \frac{dS}{dr} + \left(\frac{\partial \varepsilon}{\partial Y} \right)_{P,S} \frac{dY}{dr} > 0. \quad (1.4)$$

For simplicity we assume below $Y = \text{const}$ (chemically uniform conditions). Then the onset of convection depends on the distribution of entropy in the star (the term dS/dr in equation (1.4)) and the sign of the term $\left(\frac{\partial \varepsilon}{\partial S} \right)_{P,Y}$. In the nonrelativistic limit we have $\varepsilon \approx \rho c^2$ with c being the baryon mass density. Therefore up to a factor c^2 the multiplier in front of dS/dr is given by

$$\left(\frac{\partial \rho}{\partial S}\right)_P = -\frac{\rho^2}{\left(\frac{\partial P}{\partial T}\right)_S} = -\frac{T\rho}{P\gamma c_v} \left(\frac{\partial P}{\partial T}\right)_\rho, \quad (1.5)$$

where we introduce the adiabatic index γ and the specific heat capacity c_v . For matter under common conditions the right-hand side of equation (1.5) is obviously strictly negative and we obtain the criterion for onset of convection in the Schwarzschild form:

$$\frac{dS}{dr} < 0. \quad (1.6)$$

Hence, a negative gradient of entropy causes the onset of convection. However, within the phase-coexistence region the derivatives $\left(\frac{\partial P}{\partial T}\right)_S$ and $\left(\frac{\partial P}{\partial T}\right)_\rho$ can be negative and as a result the

Schwarzschild criterion changes its sign. The negative entropy gradient in this region ensures the convective stability while the positive one stimulates the development of a convective instability. Let us consider now the general case. One can easily show that the factor in front of dS/dr in equation (1.4) is equal to

$$\left(\frac{\partial \varepsilon}{\partial S}\right)_{P,Y} = \rho T \left[1 - \frac{\varepsilon + P}{T \left(\frac{\partial P}{\partial T}\right)_S} \right]. \quad (1.7)$$

In the non-relativistic limit the second term in square brackets is much larger than 1 and equivalent to equation (1.5). If $\left(\frac{\partial P}{\partial T}\right)_S < 0$, the sign of this term as well as the criterion of convection change again.

3.2. Discussion and conclusions

We need to emphasize that the possibility of “inverse” convection discussed here is the direct consequence of the unusual property of the deconfinement PT expressed by equation (1.2). For example, for the nuclear liquid–gas PT the condition for convection will have the ordinary form as for single phases of quark and hadronic matter.

The consequences of possible existence of the “inverse” convection zone in a hybrid star can be conceived by looking at Fig.2. In the case of well-developed convection an ascending matter element that travels from A to A' has lower entropy than the environment and thus lower heat content. Similarly, a descending element has higher heat content than the environment. Therefore in contrast to ordinary convection, within the “inverse” convection zone the heat flux is directed inwards in a star.

Currently, the neutrino-driven scenario is the favored explosion mechanism of core-collapse supernovae. In this scenario turbulence and convection are crucial to achieve sufficient neutrino heating of matter to trigger an explosion. If the “inverse” convection appeared already in the early post-bounce phase of the supernovae, in principle it could also impact the explosion dynamics. These possibilities require further investigation by detailed numerical simulations.

Acknowledgements

I would like to acknowledge my co-authors D. K. Nadyozhin, M. Hempel and T. L. Razinkova. I'm also thankful to the RFBR grant (project no. 14-22-03040 ofi-m) for financial support.

References

- [1] I. Gurevich, 1939, *Nature*, 144, 326.
- [2] D.D. Ivanenko, D.F. Kurdgelaidze, 1965, *Astrofizika*, 1, 479.
- [3] N. Itoh, 1970, *Prog. Theor. Phys.*, 44, 291.
- [4] F. Douchin and P. Haensel, *Astron. Astrophys.* 380,151 (2001).
- [5] K. Schertler, C. Greiner, J. Schaffner-Bielich, and M.H. Thoma, *Nucl. Phys. A* 677, 463 (2000).
- [6] E.S. Fraga, R.D. Pisarsi, and J. Schaffner-Bielich, *Nucl. Phys. A* 702, 217 (2002).
- [7] I. Sagert, M. Hempel, G. Pagliara, et al., *J. Phys. G* 36, 6 (2009).
- [8] A.V. Yudin, T.L. Razinkova, D.K. Nadyozhin, A.D. Dolgov. *Astron. Lett.*, 2014, 40, 4, 201.
- [9] J.L. Zdunik and P. Haensel *Astron. & Astroph.* 551, A61 (2013).
- [10] A.V. Yudin, T.L. Razinkova, D.K. Nadyozhin, 2013, *Astron. Lett.*, 39, 161.
- [11] M. Hempel, V. Dexheimer, S. Schramm, I. Iosilevskiy, 2013, *Phys. Rev. C*, 88, 1.
- [12] I. Iosilevskiy, 2014, preprint (arXiv:1403.8053).
- [13] L.D. Landau, E.M. Lifshitz, 1980, *Statistical Physics, Part 1*, 3rd edn. Pergamon Press, Oxford.
- [14] A. Steiner, M. Prakash, J.M. Lattimer, 2000, *Phys. Rev. B*, 486, 239.

Energy Injections in Gamma Ray Bursts

Y. B. Yu^{1,2}, X. F. Wu^{3,4}, Y. F. Huang^{1,2,*}, M. Xu⁵

¹*Department of Astronomy, Nanjing University, Nanjing 210046, China; *hyf@nju.edu.cn*

²*Key Laboratory of Modern Astronomy and Astrophysics (Nanjing University), Ministry of Education, China*

³*Purple Mountain Observatory, Chinese Academy of Sciences, Nanjing 210008, China*

⁴*Joint Center for Particle Nuclear Physics and Cosmology of Purple Mountain Observatory-Nanjing University, Chinese Academy of Sciences, Nanjing 210008, China*

⁵*Department of Physics, Jiangxi Science and Technology Normal University, Nanchang 330013, China*

Abstract In this study, we will introduce some special events, such as GRBs 081029, 100814A and 111209A. Unexpected features, such as multiple X-ray flares and significant optical rebrightenings, are observed in their afterglow light curves, unveiling the late-time activities of the central engines. Here, we will summarize our previous numerical results of these three bursts by using the energy injection model. Especially, we will focus on GRB 100814A, with an early-time shallow decay phase and a late-time significant rebrightening in its optical afterglow light curve. To explain the complex multi-band afterglow emission of GRB 100814A, we invoke a magnetar with spin evolution as its central engine. We argue that the optical shallow decay phase and the X-ray plateau are due to energy injection from the magnetar in its early spin-down stage, while the significant optical rebrightening observed at late time naturally comes from the spin-up process of the magnetar, which is caused by subsequent fall back accretion.

Keywords: gamma-ray bursts, jets and outflows, radiation mechanism, non-thermal

1. Introduction

Gamma-ray bursts (GRBs) are bright unpredictable flashes of gamma-rays coming from deep space (for recent review, see [1]). The external shock model is usually recognized as the standard model since it can well explain the main observed features of GRB afterglows (e.g. [2], [3]), which are generally believed to be from the interaction of the relativistic outflow with the surrounding interstellar medium (ISM) (e.g. [4]). It is generally believed that long GRBs should be connected with the collapse of massive stars (e.g. [5], [6]), while short GRBs could be due to the coalescence of two compact objects (e.g. [7] – [9]).

With the advance of new observational techniques and the launch of Swift satellite, strange events, such as GRBs 081029, 100814A, and 111209A with significant optical rebrightenings or strong flares at X-ray wavelength, are observed in GRB afterglows. To explain these unexpected features, lots of different mechanisms have been proposed, such as the two-component jet model (e.g. [10]), which is somewhat different from the density jump model (e.g. [11]), the energy injection model (e.g. [12] – [18]), and the microphysics variation mechanism ([19]), which assume that the emission comes from the same emitting region. Previously, we interpreted the unexpected afterglow light curves of GRBs 081029, 100814A and 111209A based on the energy injection model, which will be summarized in this paper.

Our paper is organized as follows. The observational facts of GRBs 081029, 100814A and 111209A are presented in Section 2. The energy injection model, including the dynamical evolution of the outflow

and the radiation process, are introduced in Section 3. In Section 4, we reproduce the unusual afterglow light curves of the above three GRBs based on different energy injection forms. In the final section, we give a brief discussion and summarize our results.

2. GRB samples

The optical afterglow light curve of GRB 081029 shows many unusual behaviors. Initially, the light curve evolved in the normal way, with the simple power-law decay as predicted by the external shock model. However, at about 3000 s after the trigger, the afterglow rebrightened sharply, interrupting the smooth temporal evolution. Subsequently, at about 8000 s, a small plateau appeared in the optical afterglow light curve. Finally, after about two days, the optical afterglow light curve became flat, which may come from the contribution of the host galaxy ([20]).

Before the significant optical rebrightening of GRB 100814A from about 2×10^4 s in all seven bands detected by the Gamma-Ray burst Optical and Near-infrared Detector (GROND), there is an initial power-law decay phase with a shallow decay index of $\alpha_{\text{opt},1} = 0.57 \pm 0.02$. After the remarkable rebrightening, the optical afterglow light curve evolved into the quick decay phase. The index of the quick decay phase in seven optical bands observed by GROND is $\alpha_{\text{opt},2} = 2.25 \pm 0.08$ ([21]). Finally, the optical afterglow light curves flatten significantly after about 10^6 s, suggesting the presence of an underlying host galaxy. As for the X-ray afterglow light curve, it follows the canonical X-ray light curves proposed by Zhang et al ([22]). Initially, there is a steep decay phase, which is usually interpreted as the curvature tail of the high latitude emission ([23], [24]). From about 630 s, the X-ray afterglow evolved into a shallow decay phase with a power law decay index of $\alpha_{\text{X},1} = 0.52 \pm 0.05$, which may be the effect of a continuous energy injection ([21]). The shallow decay phase lasts until about 10^5 s, and is followed by a steeper decay phase with an index of $\alpha_{\text{X},2} = 2.1 \pm 0.1$. Interestingly to note that, due to the contribution from a nearby source, the X-ray emission remained constant after 2×10^6 s ([21]).

The X-ray afterglow of GRB 111209A was detected by the Swift/XRT 425 s after the BAT trigger ([25]). Initially, there is a shallow decay phase in the very early X-ray afterglow light curve with a best fit decay index of $\alpha = 0.544 \pm 0.003$ ([26]). During the shallow decay evolution, a significant bump appeared, making the X-ray afterglow light curve quite unusual. At the end of the shallow decay phase, the X-ray afterglow light curve entered into the steep decay phase, which is followed by a plateau with an index of 0.5 ± 0.2 and a normal decay with decay index of 1.51 ± 0.08 ([26]).

3. Energy injection model and numerical results

To describe the dynamical evolution and calculate the radiation process of beamed GRB outflows, Huang et al developed some equations ([27], [28], [29]), which are appropriate for both radiative and adiabatic blastwaves, and the calculations can be easily extended to the deep Newtonian phase ([30]). Additionally, the lateral expansion, the cooling of electrons, and the equal arrival time surface effect were all incorporated in their equations. The differential equation of the evolution of the Lorentz factor (γ) can be expressed as

$$\frac{d\gamma}{dt} = \frac{-(\gamma^2 - 1)}{M_{ej} + \epsilon m + 2(1 - \epsilon)\gamma m},$$

where M_{ej} is the initial ejecta mass, ϵ is the radiative efficiency and m is the swept-up ISM mass.

In the standard external shock model, electrons will be accelerated by the shock as the blast wave sweeps up the surrounding medium. The multi-band afterglow emission arises from synchrotron

radiation of these shocked-accelerated electrons due to their interaction with magnetic field (e.g. [31], [32]). When considering the energy injection from the central engine, the differential equation of the evolution of the Lorentz factor should be modified accordingly. Previously, lots of energy injection forms have been studied by many authors. For example, Dai & Lu took the energy injection form as $dE_{inj}/dt \propto (1 + t/T)^{-2}$ by invoking a new-born magnetar which is losing its rotational energy through magnetic dipole radiation as the central engine of a GRB ([12]). Zhang & Mészáros argued that the general power-law energy injection form, $dE_{inj}/dt \propto t^q$, can account for many realistic cases when $q = 0$ (i.e., a constant injection power) ([33]). Especially, to explain the unusual features of multi-band afterglow light curves of GRB 070610, Kong & Huang assumed the energy injection form to be $dE_{inj}/dt = Qt^q$, for $t_{start} < t < t_{end}$, where both Q and q are constants, t_{start} and t_{end} are the beginning and ending time of the energy injection respectively ([34]). Considering the above energy injection form, the differential equation for the evolution of the Lorentz factor can be modified as,

$$\frac{d\gamma}{dt} = \frac{1}{M_{ej} + \epsilon m + 2(1 - \epsilon)\gamma m} \times \left(\frac{1}{c^2} \frac{dE_{inj}}{dt} - (\gamma^2 - 1) \frac{dm}{dt} \right).$$

As long as we know the energy injection form, we can calculate the evolution of the bulk Lorentz factor of the external shock, based on which, the synchrotron radiation of the shocked-accelerated electrons can be obtained.

3.1. Constant and GRB 081029

To explain the observed X-ray and optical afterglow light curves of GRB 081029, we assume the energy injection rate to be constant. In our model, we assumed two periods of energy injection, each with a constant injection rate. In order to account for the rapid optical rebrightening observed at about 3000 s, we resorted to the first energy injection, which starts at 2.8×10^3 s and lasts for about 2500 s, with a power of 7×10^{47} erg/s. The observed optical flat stage occurring at about 10000 s required another energy injection. The corresponding energy injection rate is 3.5×10^{47} erg/s, with the starting and ending time being 8×10^3 s and 1.3×10^4 s respectively. Additionally, contribution from a host galaxy with the magnitude of $r' \sim 25$ mag is assumed to interpret the final flat stage of the optical afterglow. Figure 1 illustrates our numerical fit to the observed optical data of GRB 081029, which are taken from Nardini et al ([20]). It is shown that the observed optical afterglow light curve, especially the significant rebrightening at about 3000 s, can be satisfactorily reproduced.

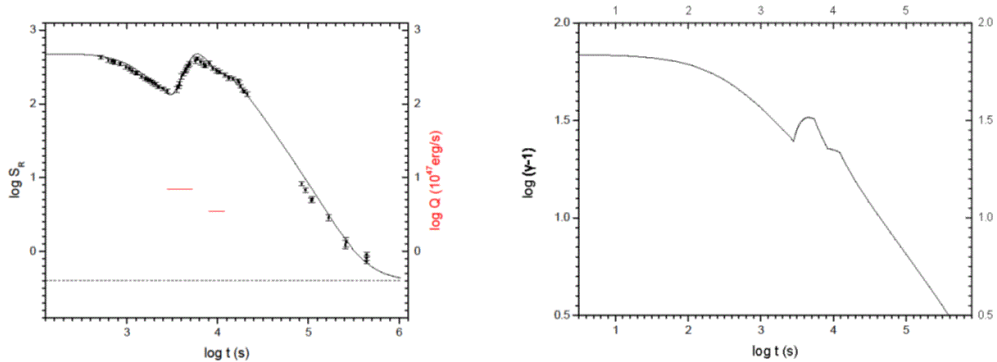


Fig1. Left: Numerical result of the optical afterglow of GRB 081029 ([16]). The observational data were taken from Nardini et al ([20]). The dashed line is the contribution from a host galaxy with the magnitude of 25 mag. The two red straight lines represent the periods of two energy injection phases. Right: The corresponding evolution of the Lorentz factor.

3.2. Fall back accretion and GRB 111209A

To explain the sharp X-ray rebrightening of GRB 121027A observed at about 10^3 s, Wu, Hou & Lei proposed a fall back accretion model ([35]). In this model, the central engine is assumed to be a BH. During the last stage evolution of the progenitor, part of the stellar envelope whose kinetic energy is less than the potential energy of the central BH will undergo fall back. When the fall back accretion is processing, the magnetic energy from the rotating BH can be extracted through the Blandford-Znajek (BZ) mechanism to power the GRB outflow, significantly increasing the X-ray brightness. According to Wu, Hou & Lei, the evolution of mass (M), and spin (a) of the BH are described as ([35])

$$\frac{dMc^2}{dt} = \dot{M}c^2 E_{ms} - \dot{E}_B,$$

$$\frac{da}{dt} = \frac{(\dot{M}L_{ms} - T_B)c}{GM^2} - 2a(\dot{M}c^2 E_{ms} - \dot{E}_B / (Mc^2)),$$

where \dot{M} is fall back accretion rate. L_{ms} and E_{ms} are the angular momentum and the specific energy respectively ([36]), while T_B is the magnetic torque and \dot{E}_B is the BZ jet power, which can be calculated as

$$\dot{E}_B = 1.7 \times 10^{50} a^2 (M/M_\odot) B_{15}^2 F(a) \text{ erg/s},$$

where $F(a)$ is a function of spin of the central BH.

As assumed by Wu, Hou & Lei, we take the spin and mass of the BH as $a = 0.9$ and $M = 3M_\odot$ respectively ([35]). Figure 2 illustrates our numerical fit to the observed X-ray afterglow light curve of GRB 111209A. The X-ray bump appearing at about 2000 s can be explained as due to the fall back accretion process and the peak accretion rate is assumed to be $\dot{M}_p = 2 \times 10^{-4} M_\odot/\text{s}$. To interpret the plateau observed after the X-ray bump, we invoke a constant energy injection with the energy injection rate being 9×10^{47} erg/s. The start and the end time of this energy injection are $t_{start} = 8 \times 10^3$ s and $t_{end} = 1.6 \times 10^4$ s respectively. The observed steep decay phase can be explained as the tail emission of the prompt phase at high-latitude, whose theoretical decay index is $2 + \beta_\chi$, where β_χ is the X-ray spectral index.

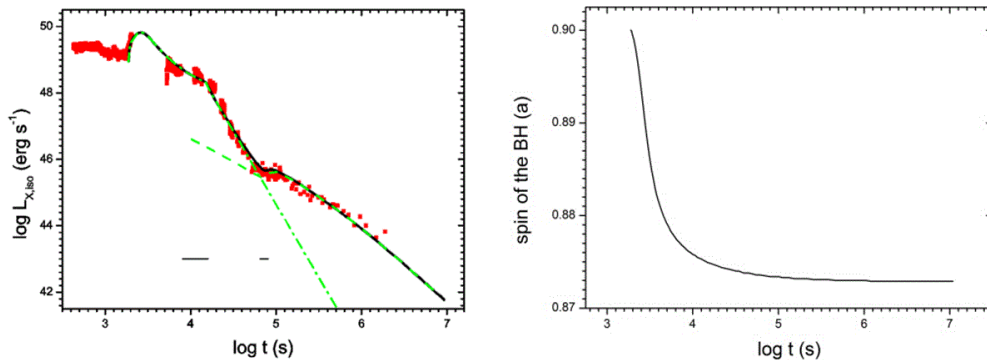


Fig2. Left: Observed X-ray afterglow light curve of GRB 111209A and our best fit ([18]). The solid points represent the observed data from Stratta et al ([37]). The two straight lines at the bottom represent the periods of two constant energy injection phases. Right: The corresponding evolution of the spin of the central BH.

3.3. Magnetar with spin evolution and GRB 100814A

Dai & Liu studied evolution of the GRB afterglow light curves by considering a newborn rapidly

rotating magnetar surrounded by a fall-back disk as the central engine ([38]). Initially, the magnetar is spinning down, losing its rotational energy through magnetic dipole radiation mechanism (e.g. [33], [39]). At late time, when the magnetospheric radius is smaller than the co-rotation radius, materials will fall back onto the surface of the central magnetar. As a result, the magnetar will spin up with the angular momentum of the fall back matter transferred to it and the magnetic dipole radiation luminosity will be increased, leading to a marked rebrightening in the afterglow light curve. They argued that this mechanism can naturally explain the observed shallow decay phase, plateaus, and significant brightenings in some GRB afterglows.

The spin evolution of the central magnetar can be expressed as,

$$\frac{d(I\Omega_s)}{dt} = \tau_{dip} + \tau_{acc},$$

Where Ω_s is the angular velocity and I is the moment of inertia. τ_{acc} and τ_{dip} are the accretion torque and the torque due to the magnetic dipole radiation respectively. During the fall back process the accretion rate initially increases with time as $\dot{M} \propto t^{1/2}$ (e.g. [40]). At late time, the accretion rate evolves with time following $\dot{M} \propto t^{-5/3}$ ([41]). Therefore, the spin evolution at early and late times can be obtained as $\Omega_s \propto t^{23/28}$ and $\Omega_s \propto t^{-5/7}$ respectively, indicating that the magnetar spins up at early times and spins down at late times during the fall back process.

In our study, the central engine of GRB 100814A is assumed to be a newly born magnetar with spin evolution surrounded by a fall-back accretion disk. The early time X-ray plateau and the optical shallow decay phase can be explained well by considering the re-energized process from the central spin-down magnetar. The optical rebrightening appearing after the shallow decay phase is due to the spin-up process, which is caused by the fall-back material from the accretion disk. Compared with the significant optical bump, the amplitude of the variation observed in X-ray band is much smaller, which also can be reproduced well by our model. The observed multi-band data of GRB 100814A and our best theoretical fit are illustrated in Figures 3.

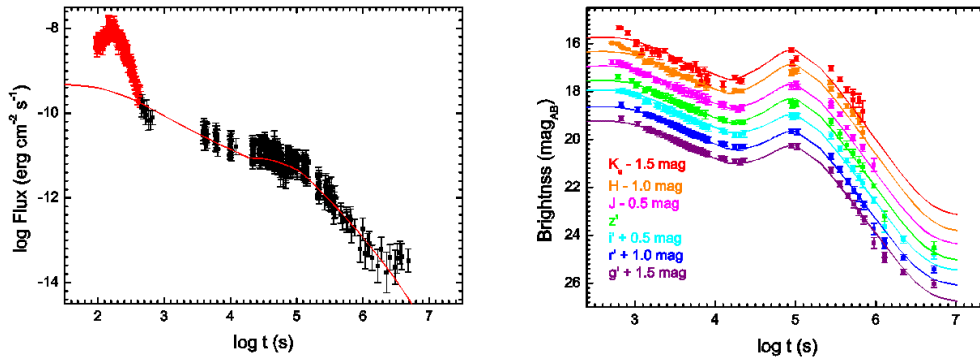


Fig3. Left: Theoretical fit to the X-ray afterglow light curve of GRB 100814A ([17]). The points correspond to the observed XRT data ([21]). Right: Numerical fit to the seven-band optical afterglow light curves of GRB 100814A ([17]). The points represent the observational data from Nardini et al ([21]). A 0.5-magnitude shift between two adjacent light curves is applied in the plot for clarity.

4. Conclusion and Discussion

In this study, we present a detailed study of the energy injection process and interpret the multi-band afterglow light curves of GRBs 081029, 100814A and 111209A. It is shown that the multi-band

afterglow light curves of the above three GRBs can be satisfactorily reproduced. Especially, the significant optical rebrightening of GRB 081029 observed at about 3000 s can be explained as due to a constant energy injection, the marked X-ray bump of GRB 111209A observed at about 2000 s after the BAT trigger is resulted from the fall back accretion process, while the observed optical and X-ray shallow decay phase of GRB 100814A can be interpreted by energy injection in the initial spin-down process of the central magnetar and the late time optical rebrightening can be reproduced quite well by the subsequent spin-up process.

As discussed by Yu & Huang, it is natural that there is an internal extinction in the host galaxies of cosmological GRBs due to the fact that the progenitors of long GRBs are associated with star forming regions ([16]). So when fitting the optical afterglow light curves of GRBs 081029, 100814A and 111209A, we take the extinction into consideration. There is a correction of 1.57 mag in the optical light curve of GRB 081029. The extinctions of the multi-band afterglow light curves of GRB 100814A were summarized in a table (for detail, see [17]).

To conclude, it is shown that our model is consistent with the observations of the above three GRBs. Especially, the optical rebrightening and the X-ray plateau or bump can be fitted quite well by assuming an energy injection process. It is argued that the energy injection process can be produced by materials that fall back onto the central compact object, which leads the accretion rate to increase and results in a strong outflow. In the future, more detailed studies on the energy injection and fall back processes will be helpful to provide important clues on the progenitors and the trigger mechanism of GRBs.

Acknowledgements

This work was supported by the National Basic Research Program of China (973 Program, Grant No. 2014CB845800) and the National Natural Science Foundation of China (Grant Nos. 11473012, 11322328 and 11203020). X. F. Wu acknowledges support by the One-Hundred-Talent Program, the Youth Innovation Promotion Association, and the Strategic Priority Research Program "The Emergence of Cosmological Structures" (Grant No. XDB09000000) of Chinese Academy of Sciences.

References

- [1] N. Gehrels, E. Ramirez-Ruiz & D. B. Fox, 2009, *ARA&A*, 47, 567
- [2] M.J. Rees and P. Mészáros, *ApJ Lett*, 1994, 430: L93-L96
- [3] T. Piran, 1999, *Phys. Rep*, 314, 575
- [4] P. Mészáros and M. Rees, *ApJ*, 1997, 476: 232-237
- [5] S.E. Woosley, *ApJ*, 1993, 405: 273-277
- [6] B. Paczyński, *ApJ Lett*, 1998, 494: L45-L48
- [7] D. Eichler, M. Livio, T. Piran & D. N. Schramm, 1989, *Nature*, 340, 126
- [8] R. Narayan, B. Paczynski, & T. Piran, 1992, *ApJ*, 395, L83
- [9] R. Perna & K. Belczynski, 2002, *ApJ*, 570, 252
- [10] Y.F. Huang, X.F. Wu, Z.G. Dai, H.T. Ma & T. Lu, 2004, *ApJ*, 605, 300
- [11] Z.G. Dai & T. Lu, 2002, *ApJ*, 565, L87
- [12] Z.G. Dai & T. Lu, 1998, *A&A*, 333, L87
- [13] M.J. Rees and P. Mészáros, 1998, *ApJ*, 496, L1

- [14] Y.F. Huang, K.S. Cheng & T.T. Gao, 2006, *ApJ*, 637, 873
- [15] J.J. Geng, X.F. Wu, Y.F. Huang & Y.B. Yu, 2013, *ApJ*, 779, 28
- [16] Y.B. Yu & Y.F. Huang, 2013, *RAA*, 13, 662
- [17] Y.B. Yu, Y.F. Huang, X.F. Wu, M. Xu & J.J. Geng, 2015, *ApJ*, 805, 88
- [18] Y.B. Yu, X.F. Wu, Y.F. Huang, D.M. Coward, G. Stratta, B. Gendre, E.J. Howell, 2015, *MNRAS*, 446, 3642
- [19] S.W. Kong, A.Y.L. Wong, Y.F. Huang & K.S. Cheng, 2010, *MNRAS*, 402, 409
- [20] M. Nardini, J. Greiner, T. Krühler et al. 2011, *A&A*, 531, A39
- [21] M. Nardini, J. Elliott, R. Filgas, et al. 2014, *A&A*, 562, A29
- [22] B. Zhang, Y.Z. Fan, J. Dyks, et al. 2006, *ApJ*, 642, 354
- [23] E.E. Fenimore, C.D. Madras & S. Nayakshin, 1996, *ApJ*, 473, 998
- [24] P. Kumar & A. Panaitescu, 2000, *ApJ*, 541, L9
- [25] E.A. Hoversten, P.A. Evans, C. Guidorzi et al. 2011, *GRB Coordinates Network*, 12632, 1
- [26] B. Gendre, G. Stratta, J.L. Atteia et al. 2013, *ApJ*, 766, 30
- [27] Y.F. Huang, Z.G. Dai & T. Lu, 1998, *A&A*, 336, L69
- [28] Y.F. Huang, Z.G. Dai & T. Lu, 1999, *MNRAS*, 309, 513
- [29] Y.F. Huang, L.J. Gou, Z.G. Dai & T. Lu, 2000, *ApJ*, 543, 90
- [30] Y.F. Huang & K.S. Cheng, 2003, *MNRAS*, 341, 263
- [31] R. Sari, T. Piran & R. Narayan, 1998, *ApJ*, 497, L17
- [32] R. Sari & T. Piran, 1999, *ApJ*, 517, L109
- [33] B. Zhang & P. Mészáros, 2001, *ApJ*, 552, L35
- [34] S.W. Kong & Y.F. Huang, 2010, *Science China-Physics, Mechanics & Astronomy*, 2010, 53(s1): 94-97
- [35] X.F. Wu, S.J. Hou & W. H. Lei, 2013, *ApJ*, 767, L36
- [36] I.D. Novikov & K.S. Thorne, 1973, *Black Holes (Les Astres Occlus)*, 343
- [37] G. Stratta, B. Gendre, J.L. Atteia et al. 2013, *ApJ*, 779, 66
- [38] Z.G. Dai & R.Y. Liu, 2012, *ApJ*, 759, 58
- [39] Z.G. Dai, 2004, *ApJ*, 606, 1000
- [40] A.I. MacFadyen, S.E. Woosley & A. Heger, 2001, *ApJ*, 550, 410
- [41] R.A. Chevalier, 1989, *ApJ*, 346, 847

Научное издание

Специальная Астрофизическая Обсерватория Российской Академии наук (САО РАН)

Труды

Международного совещания

**Кварковый фазовый переход в компактных объектах и многоволновая астрономия:
нейтринные сигналы, сверхновые и гамма-всплески**

Ответственные редакторы: В. В. Соколов, В. В. Власюк, В. Б. Петков

Компьютерная верстка: Т. Н. Соколова

Корректор: Т. Н. Соколова

Special Astrophysical Observatory of Russian Academy of Sciences (SAO RAS)

Proceedings

of the International Workshop on

**Quark Phase Transition in Compact Objects and Multimessenger Astronomy:
Neutrino Signals, Supernovae and Gamma-Ray Bursts**

Заказ №1

Подписано в печать 03.09.2016. Формат 72x104 /16. Бумага офсетная. Гарнитура Times

Печать цифровая. Усл.печ.л. 10,875. Тираж 50 экз.

ООО Издательство «СНЕГ». Россия, Ставропольский край,

357500 г. Пятигорск, ул. Делегатская, 97.

Тел.: 8 (8793) 399-000, факс: (8793) 384-062

E-mail: sneg@sneg-design.ru:

www.sneg-izdat.ru

2016 г.